SPON RESEARCH

Performace-Based Optimization of Structures

Theory and Applications

Qing Quan Liang

Performance-based Optimization of Structures

Performance-based Optimization of Structures introduces a method to bridge the gap between optimization theory and its practical application to structural engineering. The performance-based optimization (PBO) method combines modern structural optimization theory with performance-based design concepts to produce a powerful technique for use in structural design. This book provides the latest PBO techniques for achieving optimal topologies and shapes of continuum structures with stress, displacement and mean compliance constraints.

The emphasis is strongly placed on practical applications of automated PBO techniques to the strut-and-tie modeling of structural concrete, which includes reinforced and prestressed concrete structures. Basic concepts underlying the development of strut-and-tie models, design optimization procedure, and detailing of structural concrete are described in detail. The design optimization of lateral load resisting systems for multi-story steel and steel–concrete composite buildings is also presented. Numerous practical design examples are given which illustrate the nature of the load transfer mechanism of structures.

Dr Qing Quan Liang is an Australian Postdoctoral Fellow at the University of New South Wales, Australia and Guest Professor at Changsha University of Science and Technology, China. He developed the performance-based optimization (PBO) method, which is a technique for achieving optimal designs of structures and he has extensive experience in research and structural design.

Performance-based Optimization of Structures

Theory and applications

Qing Quan Liang

Spon Press
Taylor & Francis Group
LONDON AND NEW YORK

First published 2005
by Spon Press
2 Park Square, Milton Park, Abingdon, Oxon OX14 4RN

Simultaneously published in the USA and Canada
by Spon Press
270 Madison Ave, New York, NY 10016

This edition published in the Taylor & Francis e-Library, 2005.

"To purchase your own copy of this or any of Taylor & Francis or Routledge's collection of thousands of eBooks please go to www.eBookstore.tandf.co.uk."

Spon Press is an imprint of the Taylor & Francis Group

British Library Cataloguing in Publication Data
A catalogue record for this book is available from the British Library

Library of Congress Cataloging in Publication Data
A catalog record for this book has been requested

ISBN 0-203-33471-X Master e-book ISBN

ISBN 0–415–33594–9 (Print Edition)

To my wife Xiao Dan

Contents

Preface

Modern structural optimization techniques combine the finite element analysis with mathematical programming or optimality criteria methods into a single scheme to achieve optimal designs of structures. Topology optimization methods for continuum structures have achieved significant progress in the last two decades. These techniques have increasingly been used in aeronautical, mechanical and automotive industries in which the weight reduction of structures is very important. However, the potential of structural optimization techniques has not been realized by civil engineering industry. The main reason for this is that structural optimization is traditionally used as a tool for reducing the weight of engineering structures.

The purpose of this book is to introduce the theory and applications of a performance-based optimization (PBO) method for topology, shape and sizing design of structures. The PBO technique can be used not only for maximizing the performance of structures but also for automating the engineering design process. The PBO method combines modern structural optimization theory with performance-based design concepts. Performance indices and performance-based optimality criteria are incorporated into the PBO algorithms to identify the global optimum. The emphasis of the book is on the practical applications of the PBO technique to the automatic generation of optimal strut-and-tie models for the design and detailing of reinforced and prestressed concrete structures and lateral load resisting systems for multistory steel and steel–concrete composite frames. The main attractive features of the PBO method are its clarity in concepts, simplicity in mathematical formulation, ability to generate the global optimum and easy to understand.

This book is written for practicing civil and structural engineers and researchers who are interested in achieving optimal designs, particularly for concrete designers who want to apply the automated PBO technique to the generation of optimal strut-and-tie models in structural concrete. It is a comprehensive reference for undergraduate and postgraduate students in civil engineering. The materials presented in the book will also be of interests to

design engineers, academic researchers and students in aeronautical, mechanical and automotive engineering.

Chapter 1 introduces the types of structural optimization, performance-based design concepts and process, the general formulation of optimization problems and the finite element method. The PBO method for the fully stressed topology design of continuum structures with stress constraints is presented in Chapter 2. Chapter 3 describes the PBO technique for topology and shape design of continuum structures subject to displacement constraints. The PBO method for topology, shape and sizing optimization of structures with mean compliance constraints is treated in Chapter 4. Chapter 5 devotes to the applications of the automated PBO technique to the generation of optimal strut-and-tie models for the design and detailing of reinforced and prestressed concrete structures. The design and detailing of deep beams, corbels, bridge piers, shearwalls with openings, beam–column connections and prestressed concrete beams using optimal strut-and-tie models generated by the PBO technique are covered. Worked design examples in accordance with ACI 318-02 are presented. The design optimization of lateral load resisting systems for multistory steel and composite frames is described in Chapter 6. This chapter covers the strength design of double skin composite shearwalls, shear connection, simply supported and continuous composite beams in combined bending and shear, and composite columns.

Qing Quan Liang
Sydney, January 2004

Acknowledgments

The bulk of materials presented in this book are the direct result of the author and his coresearchers. The author would like to thank all those who have contributed to this work, particularly Prof Y. M. Xie and Prof G. P. Steven who offered many invaluable suggestions. The author also thanks Prof B. Uy, Prof M. A. Bradford, Prof H. D. Wright and Prof J. H. Rong for many fruitful technical discussions. Thanks are also due to Prof Y. B. Yang, Prof Y. C. Loo, Prof E. Ramm, Prof R. I. Gilbert and Dr Y. L. Pi for their support and useful communications.

The author thanks the publishers for permissions to reproduce some of the materials presented in this book. Chapter 2 includes material from the *Proceedings of the Institution of Mechanical Engineers*, Part C, 1999, 213(C8): 755–762, Liang *et al*., "Optimal selection of topologies for the minimum-weight design of continuum structures with stress constraints," with permission from the Council of the Institution of Mechanical Engineers. Chapter 3 includes material from *Computers and Structures*, 2000, 77(6): 635–644, Liang *et al*., "Optimal topology selection of continuum structures with displacement constraints," with permission from Elsevier, and material from *Structural and Multidisciplinary Optimization*, 2001, 21(5): 393–399, Liang *et al*., "A performance index for topology and shape optimization of plate bending problems with displacement constraints," with permission from Springer-Verlag. Chapter 4 includes material from *Computer Methods in Applied Mechanics and Engineering*, 2002, 191(13–14): 1471–1489, Liang and Steven, "A performance-based optimization method for topology design of continuum structures with mean compliance constraints," with permission from Elsevier. Chapter 5 includes materials from *ACI Structural Journal*, 2000, 97(2): 322–330, Liang *et al*., "Topology optimization of strut-and-tie models in reinforced concrete structures using an evolutionary procedure," 2001, 98(2): 226–232, Liang *et al*., "Generating optimal strut-and-tie models in prestressed concrete beams by performance-based optimization," 1985, 82(1): 46–56, figure 2(g), Marti, "Basic tools of reinforced concrete beams design," with permission from American Concrete Institute. Chapter 5 also includes material from

Journal of Structural Engineering, ASCE, 2002, 128(6): 815–823, Liang *et al*., "Performance-based optimization for strut–tie modeling of structural concrete," with permission from American Society of Civil Engineers (www.pubs.asce.org); and Civil-Comp Ltd, Liang *et al*., "Optimal strut-and-tie models in structural concrete members," Chapter 1, in Optimization and Control in Civil and Structural Engineering, Topping and Kumar (eds) *Proceedings of the Seventh International Conference on Civil and Structural Engineering Computing*, Paper No. 1.1, Civil-Comp Press, 1999, with permission from Civil-Comp Press, United Kingdom. Chapter 6 includes material from *Journal of Structural Engineering*, ASCE, 2000, 126(7): 823–829, Liang *et al*., "Optimal topology design of bracing systems for multistory steel frames," with permission from American Society of Civil Engineers.

Finally, the author would like to thank his wife Xiao Dan who offered great encouragement and support while suffering from his neglect over the past few months.

Notations

a	length of a plate field between stud shear connectors
a_1, a_2, a_3	dimensions of three borders in a nodal zone
A_c	cross-sectional area at one end of a strut
A_i	cross-sectional area of the ith member
ΔA_i	change in the cross-sectional area of the ith member
A_{ec}	effective shear area of concrete slab
A_n	area of a nodal zone face
A_{ps}	cross-sectional area of prestressing steel
A_{se}	total effective cross-sectional area of structural steel
A_{si}	total area of reinforcement at spacing S_i in a layer of rebars
A_{st}	total cross-sectional area of reinforcing bars
A_{sv}	cross-sectional area of longitudinal shear reinforcement
b	width of a strut or a plate
b_e	effective width of a steel plate
b_f	width of the top flange of a steel beam
c_e	strain energy of the eth element
C_e^f	filtered strain energy of the eth element
c_i	strain energy of the ith neighboring element
C	mean compliance or strain energy of a structure
C_i	strain energy of the current structure at the ith iteration
C^*	prescribed limit of the mean compliance of a structure
C^p	mean compliance of a structure under load case p
ΔC	change in strain energy of a structure due to element removal
d_a	depth of a strut or anchored depth of a tie
d_s	head diameter of a headed stud
d_w	depth of the steel web
D	depth of a structure
D_c	overall depth of a concrete slab
D_{ij}	distance between adjacent elements i and j
$[D_e]$	matrix of material elastic constants
$[D_e^s]$	matrix of scaled material elastic constants
E	Young's modulus of material

E_c	Young's modulus of concrete
E_e	current Young's modulus of the eth element
E_0	original Young's modulus of the eth element
f_c	compressive design strength of concrete
f'_c	compressive cylinder strength of concrete at 28 days
f_{ct}	tensile strength of concrete
f_{cu}	effective compressive strength of concrete in strut or nodal zone
f_{py}	yield strength of steel tendons
f_{sy}	yield strength of structural steel
$f(x)$	objective function
f_{yr}	yield strength of steel reinforcement
f_{yw}	yield strength of the web of a steel beam
F_1, F_2, F_3	force in strut
F_i	force in the ith strut or tie
$\{F_j\}$	virtual unit load vector
F_u	nominal strength of a strut, tie or nodal zone
F_{un}	nominal compressive strength of a nodal zone
F_{us}	nominal compressive strength of a strut
F_{ut}	nominal strength of a tie
F^*	design force in a strut or tie
$g_j(x)$	the jth constraint
g_j^*	limit of the jth constraint
h	height of a beam
h_c	height of a stud shear connector
h_r	rib height of profiled steel sheeting
H_i	impulse response matrix
I_c	modified moment of inertia of a composite section
I_n	moment of inertia of composite section in negative bending
I_p	moment of inertia of composite section in positive bending
k	number of constraints
k_x	critical buckling coefficient in the x direction
k_{xo}	critical buckling coefficient in the x direction under biaxial compression
k_{xy}	critical shear buckling coefficient
k_{xyo}	critical shear buckling coefficient under pure shear
k_y	critical buckling coefficient in the y direction
$[k_e]$	stiffness matrix of the eth element
$[K]$	stiffness matrix of a structure
$[\Delta K_e]$	change in stiffness matrix of the eth element
$[K^s]$	stiffness matrix of the scaled structure
$[K_r]$	stiffness matrix of the resulting structure
$[\Delta K]$	change in stiffness matrix due to element removal
l_b	length of a bearing plate

l_i	length of the ith member
l_{ij}	length of interface between adjacent elements
L	span of beam
m	total number of displacement constraints
M	number of elements connected to a node
M_{u}	ultimate moment capacity of a composite beam in combined bending and shear
M_{uo}	ultimate moment capacity of a composite section in pure bending
n	total number of elements
n_{s}	number of stud shear connectors per cross-section
n_x	total number of design variables
N_{n}	number of neighboring elements connected to the eth element
p	total number of loading cases
P	perimeter of a structure; point load
$\{P\}$	load vector
PI	performance index
$\mathrm{PI}_{\mathrm{dp}}$	performance index for bending plates with displacement constraints
$\mathrm{PI}_{\mathrm{ds}}$	performance index for plane stress structures with displacement constraints
$\mathrm{PI}_{\mathrm{ep}}$	performance index for bending plates with mean compliance constraint
$\mathrm{PI}_{\mathrm{es}}$	performance index for plane stress structure with mean compliance constraint
PI_{s}	performance index for plane stress structures with stress constraints
$\mathrm{PI}_{\mathrm{sc}}$	performance index for compression-dominant structures
$\mathrm{PI}_{\mathrm{st}}$	performance index for tension-dominant structures
Q	number of nodes in an element
$r_{\min}$	predetermined minimum member size of radius
R	element removal ratio
R_{c}	calculated cavity creation ratio
R_{u}	user-defined cavity creation ratio
R_0^{a}	initial element addition ratio
R_0^{d}	initial element deletion ratio
$R_{\mathrm{i}}^{\mathrm{a}}$	incremental element addition ratio
$R_{\mathrm{i}}^{\mathrm{d}}$	incremental element deletion ratio
R_j^{a}	element addition ratio at the jth steady state
R_j^{d}	element deletion ratio at the jth steady state
s	transverse spacing of studs
s_e	virtual strain energy of the eth element
t	thickness of element or plate

t_e	thickness of the eth element
t_e^s	scaled thickness of the eth element
T_p	pullout capacity of stud shear connectors
t_w	thickness of steel web
u_1, u_2, u_3	perimeter lengths of longitudinal shear surfaces
u_j	absolute value of the jth constrained displacement
u_j^*	prescribed limit of u_j
u_{0j}	the jth constrained displacement that is the most critical in initial design
u_{ij}	the jth constrained displacement that is the most critical in current design
u_j^l	the jth constrained displacement under load case l
u_j^{*l}	prescribed limit of u_j^l
$\{u\}$	nodal displacement vector
$\{\Delta u\}$	change in displacement vector
$\{u_e\}$	displacement vector of the eth element under real loads
$\{u_{ej}\}$	displacement vector of the eth element under the virtual unit load
$\{u_j\}$	displacement vector of a structure under virtual unit load
$\{u^s\}$	scaled displacement vector
V_i	volume of the current structure at the ith iteration
V_0	volume of the initial structure
V_L^*	longitudinal shear force
V_c	contribution of the concrete slab to shear capacity
V_o	vertical shear capacity of non-composite section
V_s	shear capacity of the web of a steel beam
V_{slab}	vertical shear strength of the concrete slab
V_u	ultimate shear capacity of composite section
V_{uo}	ultimate shear strength of composite section in pure shear
w_e	weight of the eth element
W	weight of a structure
W_0	actual weight of the initial structure
W_0^s	scaled weight of the initial structure
W_i	actual weight of the current structure at the ith iteration
W_i^s	scaled weight of the current structure at the ith iteration
x_e	design variable
X_e^s	scaled design variable
X_i^L	lower bound on the design variable x_i
X_i^U	upper bound on the design variable x_i
α_b	buckling shape factor of the buckling interaction curve

α_c	strength shape factor of strength interaction curve for plates under biaxial compression
α_m	exponent used in strength interaction formulas for composite beams
α_p	weighting factor under load case p
α_s	strength shape factor of strength interaction curve for plates under biaxial compression and shear
α_v	exponent used in strength interaction formulas for composite beams
α_w	reduction factor due to shear buckling
β	degree of shear connection
β_1	shear strength factor
β_2	shear strength factor accounting for the effect of composite action
β_j	weighting parameter
β_n	factor reflecting the degree of disruption of a nodal zone
β_s	factor reflecting the degree of disruption of a strut
ε	small positive number
ε_{mi}	mean strain of the ith member
ϕ	strength reduction factor
φ	plate aspect ratio
φ_{dp}	scaling factor for plate in bending with displacement constraints
φ_{ds}	scaling factor for plane stress structures with displacement constraints
φ_{ed}	scaling factor for plate in bending with mean compliance constraint
φ_{es}	scaling factor for plane stress structures with mean compliance constraint
γ	uniaxial strength factor
γ_e	strain energy density of the eth element
γ_e^t	change in strain energy density due to thickness reduction
γ_i^s	change in strain energy density of the ith member
η	parameter used in strength interaction formulas for plates
λ	Lagrange multiplier
θ_i	angle of the ith layer reinforcing bars to the axis of a strut
ρ	density of material
ρ_i	density of the ith element
ρ_j	density of the jth element
ρ_k	density of the element k at previous iteration
ρ^L	lower limit of element density
ρ_{min}	minimum density of element
$\{\sigma\}$	stress vector of elements
σ^e	von Mises stress of an element

σ_{cr}	critical local buckling stress
σ_o	proof or yield stress
$\{\sigma^s\}$	scaled stress vector of elements
σ^*	prescribed stress limit
$\lvert\sigma_{11,max}\rvert_0$	absolute maximum value of principal stress σ_{11} in the initial structure
$\lvert\sigma_{11,max}\rvert_i$	absolute maximum value of principal stress σ_{11} in the current structure at the ith iteration
$\lvert\sigma_{22,max}\rvert_0$	absolute maximum value of principal stress σ_{22} in the initial structure
$\lvert\sigma_{22,max}\rvert_i$	absolute maximum value of principal stress σ_{22} in the current structure at the ith iteration
$\sigma_{i,e}$	von Mises stress of the eth element at the ith iteration
σ_{max}	maximum von Mises stress of an element in a structure
$\sigma_{i,max}$	maximum von Mises stress of an element in the current design
$\sigma_{0,max}$	maximum von Mises stress of an element in the initial structure
$\sigma_{n,min}$	minimum von Mises stress of the nonboundary element
$\sigma_{b,min}$	minimum von Mises stress of the boundary element
σ_x	normal stress in x direction
σ_{xu}	ultimate strength of a steel plate in the x direction
σ_{xuo}	ultimate strength of a steel plate under biaxial compression only in the x direction
σ_y	normal stress in y direction
σ_{yu}	ultimate strength of a steel plate in the y direction
τ_0	shear yield stress
τ_{xy}	shear stress
τ_{xyu}	ultimate shear strength of steel plate
τ_{xyuo}	ultimate shear strength of steel plate under pure shear
ν	Poisson's ratio
ξ_{nd}	nodal virtual strain energy density
ξ_e	recalculated virtual strain energy density of the eth element
ψ_e	virtual strain energy density of the eth element
ψ_e^m	virtual strain energy density of the eth element under multiple constraints and load cases
ζ_e	strain energy density of the eth element
ζ_{nd}	nodal strain energy density

Chapter 1

Introduction

1.1 Background

The objective of structural optimization is to maximize the performance of a structure or structural component. Optimal structural design is driven by the limited material resources, environmental impacts and technological competition which demand lightweight, low-cost and high-performance structures. An optimal design is defined as the best feasible design that satisfies the prescribed performance criteria. Design automation is a fusion in current engineering practice and has the ultimate goal of improving productivity and enhancing design capabilities. With advances in high-speed computers, structural optimization has the potential to become an automated design tool for practicing engineers in aeronautical, mechanical, automotive and civil engineering industries.

Various structural optimization methods have been developed for the layout design of structures in the past few decades (Haftka and Gürdal 1992; Kirsch 1993). These methods can be classified into two categories, namely analytical methods and numerical methods. Analytical methods search for optimal configurations of structures using the mathematical theory of calculus and variational methods. They are suitable for studying the fundamental behavior of the material layouts of structural components and simple skeletal structures under simple loading conditions. Analytical methods cannot be used to deal with the topology optimization of complex practical problems. Numerical methods generate optimal designs automatically in an iterative manner using mathematical programming (Schmidt 1960) and optimality criteria (Rozvany 1989). Numerical methods can be used to solve large-scale practical design problems. In recent years, topology optimization of continuum structures has increasingly gained popularity in structural optimization. Many methods have been developed for the topology design of continuum structures, including the homogenization-based optimization (Hassani and Hinton 1999; Bendsøe and Sigmund 2003), evolutionary structural optimization (Xie and Steven 1997), rule-based optimization (Seireg and Rodriguez 1997) and soft-kill optimization (Mattheck 1998).

Structural optimization techniques are effective tools that can be used to improve the performance of structures in terms of the material efficiency in transferring the applied loads. However, the performance of optimized designs is often limited to the optimization methods used. It is of importance to realize that the formulation of a design problem in structural optimization significantly affects the results. Incomplete and improper problem formulation may lead to poor or meaningless designs. It is realistic to minimize the weight or cost of a structure subject to geometrical constraints and performance-based constraints, which include stress, displacement, mean compliance, frequency and buckling load constraints. This is because performance-based constraints are usually prescribed in the design codes of practice (Rozvany *et al*. 1995). Some structural optimization methods use the behavioral quantity such as the compliance as the objective function and a somewhat arbitrarily chosen material volume as the constraint to search for optimal configurations. Optimization methods based on such a problem formulation may not yield minimum weight designs.

Many books and papers on the theoretical development and practice of structural optimization have been published since 1960. Most of the publications were concerned with mathematical aspects of structural optimization rather than practical applications. There is a clear gap between the development of structural optimization theory and its practical applications to aeronautical, mechanical and civil engineering industries. The main reason for the gap between the theory and practice of structural optimization is the priority of mathematical over engineering aspects (Cohn and Dinovitzer 1994). Because of the mathematical complexity of structural optimization methods, they remained to be an academic interest. Structural optimization techniques could become more attractive to practicing civil engineers if they are developed not only for saving materials but also for automating the engineering design process (Liang 2001). It appears that the gap between structural optimization theory and its practical applications to civil engineering has not been reduced in the last two decades. The challenge in structural optimization is to transform continuum topology optimization from an exotic and fruitless academic exercise into a rational and efficient design tool for practicing civil engineers. The work presented in this textbook is to answer this challenge.

This book presents the theory and applications of a performance-based optimization (PBO) method for topology, shape and sizing design of structures. The PBO method incorporates performance-based design concepts such as performance indices and performance-based optimality criteria into modern structural optimization theory. It generates an optimal design by gradually removing inefficient material from a structure or adding efficient material to the structure until the performance of the structure is maximized. The main attractive features of the PBO technique are its

clarity in concepts, simplicity in mathematical formulation, ability to generate the global optimum and easy to understand. The PBO concept can be used to solve a wide range of topology, shape and sizing optimization problems.

Numerous examples are provided in this textbook to demonstrate the effectiveness and validity of the PBO method in producing optimal designs of continuum structures. Emphasis is placed on its practical applications to the automatic generation of optimal strut-and-tie models for the design and detailing of reinforced and prestressed concrete structures and bracing systems for multistory steel and steel–concrete composite frames, illustrating with worked practical design examples.

1.2 Types of structural optimization

The types of structural optimization can be classified into sizing, shape and topology optimization. Sizing optimization is to find the optimal cross-sectional properties of members in a truss or frame structure or the optimal thickness distribution of a plate structure. It has the goal of maximizing the performance of a structure in terms of the weight and overall stiffness or strength while the equilibrium condition and the design constraints are satisfied. The design variable is the cross-sectional area of truss members or the thickness of a plate. In sizing optimization, the design domain is fixed during the optimization process. In shape optimization, the objective is to find the optimal shape of the design domain, which maximizes its performance. The shape of the design domain is not fixed but rather is a design variable. In shape optimization, only the boundaries of the design domain are changed but not the topology of the domain. Topology optimization of continuum structures is to determine the optimal number and locations of holes within the continuum design domain. In topology optimization, both topology and shape of a structure are the design variables.

The integrated topology, shape and sizing optimization is to simultaneously optimize the topology, shape and size of a structure. It is usually called layout optimization in the literature (Rozvany *et al.* 1995). In topology optimization of continuum structures, the sizing optimization is generally not considered in most of the structural optimization methods presented in the literature. This may lead to suboptimal results as the size of a continuum structure has a significant effect on the weight and structural performance of the final design. It has been recognized that topology optimization can significantly improve the cost performance of a structure when compared with sizing and shape optimization. It should be noted that, however, the global optimum can only be achieved by using the integrated topology, shape and sizing optimization methods.

1.3 Performance-based design

1.3.1 Design concepts and criteria

The performance-based design is currently a popular design concept in the field of structural engineering. This concept describes the required and possessed performance of a structure or structural component being designed or evaluated. Structural response parameters such as stresses, strains, displacements and accelerations are employed as performance indices to evaluate the performance of structures. Many design codes of practice have been changing from the limit state design to the performance-based design. Performance-based design allows the designer to tailor the design to a specific performance level required by the owner.

The performance-based design is to design a structure or structural component that can perform physical functions in a specified manner throughout its design life. The performance-based design is defined as the methodology in which structural design criteria are expressed in terms of achieving multiple performance objectives. Performance objectives are the statements of acceptable performance of a structure. They are usually expressed by nonengineering terms, which are easily understood by the owners and the community. In performance-based earthquake engineering, the performance objectives are expressed in terms of the expected damage levels. The selection of performance objectives are made by the client who consults with the design engineers based on the consideration of his expectations, the seismic hazard exposure, economic analysis and acceptable risk (Bertero and Bertero 2002).

There are usually multiple performance objectives that must be considered by the structural designer when designing a structure. Main performance objectives can be summarized as follows:

- Functionality
- Serviceability
- Strength
- Economy.

Serviceability and strength are structural performance objectives that are related to safety. Codes and standards impose limitations on the serviceability and strength of a structure or structural component to ensure that the structure designed will perform normal functions. Functionality and economy are nonstructural performance objectives but can be used to rank alternative designs which satisfy the structural performance requirements. Performance levels can be defined by the limiting values of measurable structural response parameters, such as deflections, ductility and structural damage indices.

The cost performance (economy) of a structure is of great importance to the owner and has a significant effect on the design of the structure.

The cost of a structure includes the initial cost and the cost of maintenance, and is significantly influenced by the structural form, materials used and construction methods. As discussed in preceding section, topology optimization of structures can result in more material savings than the pure shape and sizing optimization. Therefore, to improve the cost performance of a structure, it is wiser to select a proper structural form rather than to modify the sizes of structural members.

The performance-based optimal design is to design a structure or structural component that can perform physical functions in a specified manner throughout its design life at minimum cost or weight (Liang *et al*. 2000a). The optimization problem with multiple performance objectives are usually solved by selecting only one performance of the structure as the objective function and others are considered as constraints imposed on the structure. In performance-based optimal design, the weight of a structure is usually selected as the performance objective and structural response parameters such as stresses, displacements, overall stiffness and frequency are treated as performance-based constraints.

1.3.2 The overall performance-based design process

The overall purpose of the performance-based design is to develop the best feasible structural system that satisfies the performance objectives in terms of the functionality, safety and economy. Structural design is a complex, iterative, trial and error and decision-making process. In the design process, a conceptual design is created by the designer based on his intuition, creativity and past experience. Structural analysis is then undertaken to evaluate the performance of the design. If the design does not satisfy the performance objectives, a new design is then developed. This process is repeated until the design satisfies the multiple performance objectives. The main steps of the overall performance-based design process are illustrated in Figure 1.1.

The first step in the performance-based design process is to investigate the overall design problem. The design engineers discuss the needs for the structure, its proposed function, requirements and constraints with the owner. Functionality is the ability of a structure to perform its intended non-structural use. It is one of the important performance objectives that must be achieved for a structure and affects all stages of the structural design process. The site and geotechnical investigations are then followed. The structural designers also need to study similar structures and to consult authorities from whom permissions and approvals must be obtained. Multiple performance objectives are then identified for the structure and selected by the owner who consult with the structural designers based on the consideration of his expectations, economic analysis and acceptable risk.

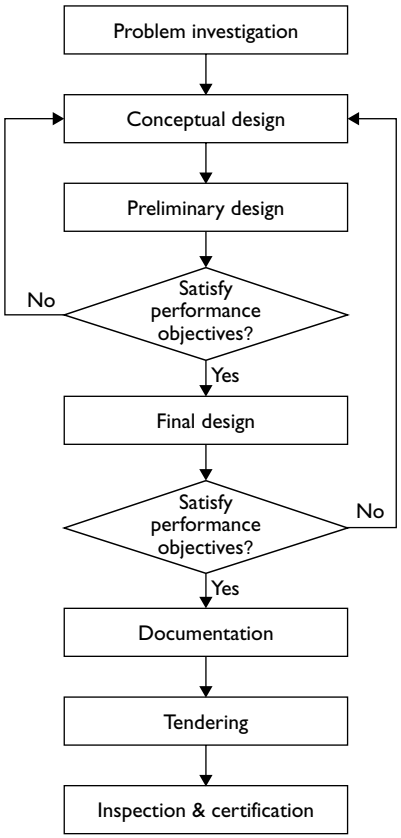

Figure 1.1 The overall performance-based design process.

In the conceptual design stage, the structural designer develops the best feasible structural systems that appear to achieve the performance objectives defined in the preceding stage. The selection of structural systems is generally iterative in nature based on the designer's creation, intuition and past experience. In order to obtain an optimal structure, a number of alternative structural systems must be invented and evaluated. The invention of structural systems is the most challenging task in structural design since it involves a large number of possibilities for the structural layouts. The traditional design process is highly time-consuming and expensive. Since the development of structural systems is an optimal topology design problem, automated topology optimization techniques such as the PBO technique can be employed in the conceptual design stage to generate optimal structures. The optimal structural system is produced by topology optimization techniques based on the

design criteria and constraints but not on the past experience. The designer also selects the materials of construction for the structure.

After the best feasible structure has been created, the preliminary design can be carried out. The design loads and load combinations applied to the structure are estimated in accordance with the loading codes. The structural analysis method or modern numerical technique such as the finite element method is then employed to analyze the structure to evaluate its structural performance. From the results of the structural analysis, structural members are preliminarily sized to satisfy the design criteria. The cost of the structure is also preliminarily estimated. If the structure does not satisfy the function, structural efficiency and cost-performance objectives, a new structural system must be developed and the design process is repeated, as depicted in Figure 1.1. It is obvious that shape and sizing optimization techniques can be applied in the preliminary design stage to achieve cost-efficient designs.

Since the structure is approximately proportioned in the preliminary design stage, it must be checked against the design criteria and objectives in the final design stage. The loads applied to the structure are recalculated and the structure is reanalyzed. The performance of the structure is then evaluated and checked with performance requirements. Any change in the member sizes may require a further reanalysis and resizing of the structure. The design and redesign process is repeated until no more modification can be made to the structure. The structure is evaluated for performance objectives such as function, serviceability, strength and cost. If these objectives are not satisfied, the structure may be modified or a new conceptual design may be generated. The design process is repeated as indicated in Figure 1.1. In the final design stage, the sizing of the structure is the main task. Therefore, sizing optimization techniques can be employed to automate the design process. It is worth noting that topology optimization techniques can also be used in the final design stage. Liang *et al.* (2000b, 2001, 2002) demonstrated that the automated PBO technique can be employed in the final design stage to generate optimal strut-and-tie models for the design and detailing of structural concrete.

After the structure is finalized, the documentation such as the detailed drawings and specifications can be prepared and tenders for construction can be called for. At the final stage the designers carry out inspection and certification during construction to ensure that all performance objectives defined are achieved in the performance-based design process.

1.4 General formulation of optimization problems

Structural optimization is to seek the minimum (or maximum) value of a function subject to design constraints. This involves the determination of

optimal design variables that minimize (or maximize) the objective function. The general formulation of an optimization problem may be expressed as

$$\text{minimize} \quad f(x) \tag{1.1}$$

$$\text{subject to} \quad g_j(x) \leq g_j^* \qquad j = 1, 2, \ldots, k \tag{1.2}$$

$$x_i^{\mathrm{L}} \leq x_i \leq x_i^{\mathrm{U}} \quad i = 1, 2, \ldots, n_x \tag{1.3}$$

where $f(x)$ is the objective function, $g_j(x)$is the jth constraint, g_j^* is the limit of the jth constraint, k is the number of constraints, x_i^{L} and x_i^{U} are the lower and upper bounds on the design variable x_i, and n_x is the total number of design variables.

The objective function can be the weight or the overall stiffness of a structure, the costs of a structure and the capacity of storage. It is difficult to construct a cost-objective function for a realistic engineering project since it depends on many factors. The weight of a structure has commonly been used as the objective function in structural optimization as it is readily quantified. The constraints can be geometrical restrictions such as the height and width of the structure or behavioral restrictions such as stresses, displacements, mean compliance, frequency and buckling loads. If the objective function and constraints are linear functions of the design variables, the optimization problem is a linear optimization problem. In contrast, if the objective function or the constraint is a nonlinear function of the design variables, the optimization problem is regarded as a nonlinear optimization problem. Structural optimization is usually a nonlinear optimization problem.

1.5 The finite element method

The finite element method (FEM) is a numerical technique for analyzing structures and continua and has been widely used by design engineers and researchers in all engineering fields. In the finite element method, a structure or structural component is discretized into finite geometrical parts (finite elements). These elements defined by their coordinates describe the shape of the component, which may be very complex. The method generates many simultaneous algebraic equations that are solved on a digital computer. One of the great advantages of the FEM is its versatility. The FEM can be applied to various physical problems with arbitrary shape, loads and support conditions and the mix elements of different types, shapes and material properties can be used. Another advantage of the FEM is that the finite element model physically represents the actual structure. With advances in digital computers, the FEM has become a computational tool in the performance-based design of engineering structures.

The PBO method presented in this textbook employs the FEM as a modeling and computational tool. From the results of the finite element

analysis (FEA), the PBO programs identify the underutilized elements that are inefficient in carrying the loads. These underutilized elements are then removed from the structure to improve its performance. The process of the FEA, performance evaluation and element removal is repeated until the optimal structure is generated.

It is beyond the scope of this textbook to describe the FEM. There are many excellent textbooks available on the concepts, formulations, procedures and applications of the FEM. For readers who want to be familiar with the FEM, the textbooks written by Zienkiewicz and Taylor (1989, 1991), Hughes (1987) and Cook *et al.* (1989) are recommended.

1.6 References

Bendsøe, M. P. and Sigmund, O. (2003) *Topology Optimization: Theory, Methods, and Applications*, Berlin: Springer-Verlag.

Bertero, R. and Bertero, V. (2002) "Performance-based seismic engineering: the need for a reliable conceptual comprehensive approach," *Earthquake Engineering and Structural Dynamics*, 31: 627–652.

Cohn, M. Z. and Dinovitzer, A. S. (1994) "Application of structural optimization," *Journal of Structural Engineering*, ASCE, 120(2): 617–650.

Cook, R. D., Malkus, D. S. and Plesha, M. E. (1989) *Concepts and Applications of Finite Elements Analysis*, 3rd edn., New York: John Wiley & Sons.

Haftka, R. T. and Gürdal, Z. (1992) *Elements of Structural Optimization*, 3rd edn., Dordrecht: Kluwer Academic Publisher.

Hassani, B. and Hinton, E. (1999) *Homogenization and Structural Topology Optimization*, Berlin: Springer-Verlag.

Hughes, T. J. R. (1987) *The Finite Element Method: Linear Static and Dynamic Finite Element Analysis*, Engelwood Cliffs, NJ: Prentice-Hall.

Kirsch, U. (1993) *Structural Optimization: Fundamentals and Applications*, Berlin: Springer-Verlag.

Liang, Q. Q. (2001) *Performance-Based Optimization Method for Structural Topology and Shape Design*, Ph.D. thesis, Victoria University of Technology, Australia.

Liang, Q. Q., Uy, B. and Steven, G. P. (2002) "Performance-based optimization for strut–tie modeling of structural concrete," *Journal of Structural Engineering*, ASCE, 128(6): 815–823.

Liang, Q. Q., Xie, Y. M. and Steven, G. P. (2000a) "Optimal topology design of bracing systems for multistory steel frames," *Journal of Structural Engineering*, ASCE, 126(7): 823–829.

Liang, Q. Q., Xie, Y. M. and Steven, G. P. (2000b) "Topology optimization of strut-and-tie models in reinforced concrete structures using an evolutionary procedure," *ACI Structural Journal*, 97(2): 322–330.

Liang, Q. Q., Xie, Y. M. and Steven, G. P. (2001) "Generating optimal strut-and-tie models in prestressed concrete beams by performance-based optimization," *ACI Structural Journal*, 98(2): 226–232.

Mattheck, C. (1998) *Design in Nature: Learning from Trees*, Berlin: Springer-Verlag.

Rozvany, G. I. N. (1989) *Structural Design via Optimality Criteria*, Dordrecht: Kluwer Academic Publisher.

Rozvany, G. I. N., Bendsøe, M. P. and Kirsch, U. (1995) "Layout optimization of structures," *Applied Mechanics Review*, 48: 41–119.

Schmidt, L. A. (1960) "Structural design by systematic synthesis," paper presented at the 2nd National Conference on Electronic Computation, ASCE, Pittsburgh, pp. 79–126.

Seireg, A. A. and Rodriguez, J. (1997) *Optimizing the Shape of Mechanical Elements and Structures*, New York: Marcel Dekker, Inc.

Xie, Y. M. and Steven, G. P. (1997) *Evolutionary Structural Optimization*, Berlin: Springer-Verlag.

Zienkiewicz, O. C. and Taylor, R. L. (1989) *The Finite Element Method*, 4th edn., Vol. 1: Basic Formulation and Linear Problems, New York: McGraw-Hill.

Zienkiewicz, O. C. and Taylor, R. L. (1991) *The Finite Element Method*, 4th edn., Vol. 2: Solid and Fluid Mechanics, Dynamics and Nonlinearity, New York: McGraw-Hill.

Chapter 2

PBO for fully stressed topology design

2.1 Introduction

In the design of aeronautical, mechanical and civil engineering structures, the engineer needs to design the exact topology of a structure for a given design space, support and loading conditions. In the absence of an efficient topology design tool, the selection of topology in current design practice usually involves a trial-and-error process based on the designer's intuition and past experience. The automation of the design process and optimal structural design are motivated by the considerations of limited material resources, technological competition and environmental issues. Topology optimization forms an important part of the performance-based design process. Topology optimization of continuum structures has recently attracted considerable attentions in the field of structural optimization. It has the potential to become an automated design tool for practicing aeronautical, mechanical and civil engineers.

The fully stressed design has traditionally been used as one of the optimality criteria (OC) for the optimal design of skeletal structures. However, the fully stressed design procedure may not lead to the minimum-weight optimal designs since no objective function is involved in the optimization algorithm. Due to its simplicity and fast convergence, the fully stressed design method is still used in other optimization procedures as a starting point for searching for optimal designs. The fully stressed design concept has been adopted in topology and shape optimization of continuum structures. Oda (1977) proposed a geometric approach to two-dimensional shape optimization by the utilization of the finite element analysis (FEA). No formal mathematical optimization algorithm is used in the geometric approach. The shape is modified based on the element stresses obtained from the results of the FEA. The cycle of FEA and shape modification is repeated until the final shape is obtained. Oda and Yamazaki (1977) extended this approach to problems of axisymmetric solids and under body forces. Rodriguez and Seireg (1985) developed a rule-based approach for topology and shape optimization of continuum structures. The objective of

this approach is to seek the optimal shape that maximizes the utilization of the material and with the most uniform stress distribution without violating the maximum allowable stress and the continuity of the shape. This is achieved by using an elimination scheme in which elements with relatively low magnitude of stress are removed from a design domain in an iterative manner after the FEA. Wu (1993) extended the rule-based approach to topology optimization of two-dimensional continuum structures under dynamic loading. The objective function is defined as the ratio of volume reduction normalized to the initial volume to the stress range normalized to the allowable stress (Seireg and Rodridguez 1997).

Stress concentrations are the main killer of structural components. Stress-based shape optimization methods are effective tools for minimizing stress concentrations and the weight of structural components. Mattheck and Burkhardt (1990) proposed a computer-aided shape optimization (CAO) method for reducing the notch stresses and lightweight design of structural components based on biological growth. The CAO seeks an optimal design with a constant von Mises stress on the surface of a growing structure (Mattheck 1998). Baumgartner *et al.* (1992) presented the soft kill option (SKO) approach to topology optimization of continuum structures by simulating the adaptive bone mineralization. In this method, the elasticity modulus is treated as a design variable. The design domain is firstly analyzed by undertaking a FEA, which provides von Mises stress distributions in the domain. The local E-modulus is then set equal to the stress computed at the particular place. This means that the more highly loaded region becomes harder, and the less loaded region becomes softer. The cycle of the FEA and E-modulus redistribution is repeated in an iterative process. Consequently, the actual load-bearing region is characterized by the variation in its modulus and the nonloadbearing region can be removed from the design domain.

The fully stressed design and element removal concepts have been adopted in the evolutionary structural optimization (ESO) method by Xie and Steven (1993) and Steven *et al.* (2002). In ESO, by slowly removing lowly stressed elements from a design domain after each FEA, the resulting structure evolves towards an optimum. Querin *et al.* (2000) proposed a bidirectional ESO method, which allows for elements to be added and removed. After elements are added to the initial design up to a specified percentage of elements, elements are removed and added simultaneously until the termination condition is satisfied. This method may not work well for practical structures with complex geometry and loading conditions. Rong *et al.* (2000) extended the ESO method to topology optimization of continuum structures under dynamic response constraints. The thermoelastic topology optimization of continuum structures with varying temperature fields using an evolutionary procedure was reported by Li *et al.* (2001). In their method, element removal criteria are based on the thermal stress level of elements.

It should be noted that stress-based continuum topology optimization methods suffer the same problem as the fully stressed design does because no performance-based optimality criteria (PBOC) are used to obtain the global optimum.

Performance indices and PBOC have been developed by Liang (2001) and Liang *et al.* (1999a,b) for stress-based topology optimization methods to guarantee a global optimal solution. This chapter presents a performance-based optimization (PBO) method for fully stressed topology designs of two-dimensional linearly elastic continuum structures with stress constraints. The PBO method combines topology and sizing optimization into a single scheme to achieve the optimal topology and thickness design of continuum structures. In the proposed methodology, the finite element method is used as a modeling and analytical tool for calculating stresses of elements. The performance objective is to seek a fully stressed topology design with the minimum consumption of material and acceptable strength performance level. The performance-based design concept is incorporated in continuum topology optimization. A stress-based performance index is employed to monitor the optimization process and used as a termination criterion. PBOC are incorporated in optimization algorithms to identify the global optimum. The effectiveness and validity of the PBO method are illustrated by several examples. Some of the results have been presented by Liang *et al.* (1999a,b).

2.2 Performance objective for structures with stress constraints

The performance-based optimal design is to design a structure or structural component that can perform physical functions in a specified manner throughout its design life at minimum cost or weight, as discussed in preceding chapter. The cost-performance objective is of practical importance, but it is usually difficult to construct an appropriate cost-objective function that depends on many parameters. Therefore, the minimum weight for required design specifications is frequently used as an objective function in structural optimization since it is readily quantified. The advantages of minimum-weight structures are low material cost, high technical performance and low environmental impact.

To be a minimum-weight design, all parts of a structure should be loaded equally and safely. This means that the design should be fully stressed within the maximum allowable stress level. Mattheck and Burkhardt (1990) reported that biological components always grow into a state of constant stress on their surface. Therefore, the performance objective of topology design for strength is to seek the fully stressed design at minimum weight while satisfying allowable stress constraints. This can be expressed in the

mathematical form as follows:

$$\text{minimize} \quad W = \sum_{e=1}^{n} w_e(t) \tag{2.1}$$

$$\text{subject to} \quad \sigma_{\max} \leq \sigma^* \tag{2.2}$$

$$t^{\mathrm{L}} \leq t \leq t^{\mathrm{U}} \tag{2.3}$$

where W is the total weight of the structure, w_e is the weight of the eth element, t is the thickness of all elements, t^{L} is the lower bound on the element thickness, t^{U} is the upper bound on the element thickness, n *is* the total number of elements, $\sigma_{\max}$ is the maximum von Mises stress of an element in the structure under applied loads and σ^* is the maximum allowable stress.

The stresses of elements are localized and highly nonlinear with respect to the changing topology in an optimization process. The maximum stress may shift from element to element in the optimization process. This leads to difficulty in imposing the maximum stress constraint on a particular element. To simplify the formulation, only the global maximum stress constraint on the von Mises stress is considered in the PBO method. In order to achieve the performance objective, underutilized elements should be removed from the discretized structure. Hence, every element in a structure is treated as a design variable. The element thickness has a significant effect on the structural weight as well as the state of stresses in elements because the stiffness matrix of a plane stress continuum structure is a linear function of its thickness. In the design of a plane stress structure, its thickness needs to be specified by the designer. Therefore, the thickness is also treated as one of the design variables. However, the simultaneous topology and sizing optimization of continuum structures will be very complicated and computationally expensive. Therefore, only the uniform sizing of element thickness is considered in the PBO method.

2.3 Element removal criteria based on stress level

Topology optimization of continuum structures is the most complicated problem in structural optimization. To solve the topology optimization problem, an initial design domain is usually used as a starting point for deriving the optimum. The design domain concept is similar to the ground structure concept used in truss topology optimization. In the design domain approach, a design domain without violating any geometric constraints is discretized into fine finite elements. Under applied loads, it is found that the stress distribution of elements in the design domain is not uniform. This means that some of the elements are not effective in transferring loads. Thus, these lowly stressed elements should be eliminated from the design domain so as to achieve the performance objective.

The equivalent stress of an element that represents its stress level in plane stress conditions can be evaluated by using the von Mises stress criteria for isotropic materials. For plane stress conditions, the von Mises stress σ^{e} is defined as

$$\sigma^{e} = \sqrt{\sigma_x^2 + \sigma_y^2 - \sigma_x \sigma_y + 3\tau_{xy}^2} \tag{2.4}$$

where σ_x and σ_y are normal stresses in x and y directions, respectively, and τ_{xy} is the shear stress.

Different element elimination criteria can be used to define the standard for elimination. In the rule-based approach by Rodriguez and Seireg (1985), elements that possess the von Mises stress values below a certain level of the average stress of elements are removed from a structure. By implying this criterion, the efficiency of a structure can be gradually improved. However, since the average stress of elements is used for elimination, the stress distribution in the final topology is still not uniform even if no more elimination is possible. Further modification is often needed in order to achieve a better design. In the PBO method, the maximum von Mises stress of elements in a continuum design domain is employed as the criteria for element removal. Element removal criteria can be expressed by

$$\sigma_{i,e} < R_j^{d} \sigma_{i,\max} \tag{2.5}$$

where $\sigma_{i,e}$ is the von Mises stress of the eth element at the ith iteration, $\sigma_{i,\max}$ is the maximum von Mises stress of an element in the structure at the ith iteration and R_j^{d} is the deletion ratio of elements at the jth steady state. All elements that satisfy Eq. (2.5) are removed from the structure. The cycle of the FEA and the element removal is repeated by using the same R_j^{d} until no more elements can be removed from the structure at the current state. In order to continue the optimization process, the element removal ratio R_j^{d} is increased by an incremental removal ratio (R_i^{d}). The element deletion ratio can be expressed by

$$R_j^{d} = R_0^{d} + (j-1)\, R_i^{d} \quad (j = 1, 2, 3, 4, \ldots) \tag{2.6}$$

where R_0^{d} is the initial deletion ratio of elements.

The optimal topology of a continuum structure under one load case is iteratively generated by using element removal criteria described in Eq. (2.5). For structures subject to multiple load cases, only those elements that satisfy Eq. (2.5) for all load cases are removed from the design domain at each iteration. This criterion for multiple loading cases generates an optimal design that can perform the required function under all load cases.

The optimal design can also be generated by gradually eliminating a small number of elements with the lowest von Mises stress from a continuum design domain. A loop is set up to count these lowly stressed elements

until they make up the prescribed amount, which is the element removal ratio times the total number of elements in the initial structure. The design is iteratively modified by removing these lowly stressed elements at each iteration until the optimum is obtained. It should be noted that the number of elements to be removed at each iteration must be sufficiently small in order to achieve a smooth solution. The elimination of a large number of elements from a design domain may cause discontinuity and the model may become singular. The initial element removal ratio (R_0^{d}) of 1 percent and the incremental removal ratio (R_i^{d}) of 1 percent are found to be typical for use in engineering practice.

2.4 Element elimination techniques

The topology design of a continuum structure is to determine the optimal layout of a given isotropic material in the design space. It needs to determine which regions should be filled with material and which regions should be void. Thus, the design problem becomes a discrete zero–one problem, to which there are no direct solutions. The methodology presented here is to search for an optimal solution by using the design/redesign scheme in an iterative manner. The structure is modified by gradually removing underutilized portions from the design domain. In the optimization algorithm, the state of an element in the model is represented by the binary integer zero or one. The integer zero represents that the element is deleted from the model while the integer one indicates that the element is remained in the model. In the structural analysis, the state of an element is represented by the Young's modulus as follows:

$$E_e = \begin{cases} E_0, & \text{if } \sigma_{i,e} \geq R_j^{\mathrm{d}}\, \sigma_{i,\max} \\ 0, & \text{if } \sigma_{i,e} < R_j^{\mathrm{d}}\, \sigma_{i,\max} \end{cases} \tag{2.7}$$

where E_e is the current Young's modulus of the eth element and E_0 is the original Young's modulus of the eth element. The elimination of an element from a design domain can be done by assigning its material property values to zero. These deleted elements are not assembled in the global stiffness of the structure in the sequent FEA. An element can also be removed by reducing its Young's modulus or thickness to a very small value as suggested by Hinton and Seinz (1995).

2.5 Stress-based performance indices

The PBO method generates many topologies in an optimization process. The performance of the resulting topology at each iteration needs to be assessed in order to obtain the optimum. In the performance-based design, the

performance of a design is quantified by using the performance index. Structural responses such as stresses and displacements are used as performance indices to evaluate the performance of a structure. However, it is not sufficient to use structural responses alone as performance indices to evaluate the performance of optimized designs. The performance objective of topology optimization is to minimize the weight of a structure while its structural responses are maintained within acceptable limits. Therefore, the minimum material that can support applied loads without violating behavioral constraints should be used as a measure of the performance of optimal designs.

A methodology for deriving performance indices for assisting the selection of the material and sectional shapes of structural components has been proposed by Ashby (1992). In his method, the performance of a structural component is expressed by the objective function, which can usually be described by the separable functional, geometric and material property functions. Design variables such as cross-sectional areas are eliminated by substituting the constraint equation into the objective function. The optimal shape design of a structural component is independent of the functional requirements and material used. Therefore, shape optimization can be undertaken without solving the whole objective function or knowing all details of functional and material parameters in advance. Minimizing the weight of a structural component is achieved by maximizing the geometric parameter function. The performance index can be derived from the group of geometric parameters. Burgess (1998a,b) has applied this method to the derivation of performance indices for simple trusses and beams under a single load. However, it is difficult to extend this approach to optimize truss structures under multiple load cases and discretized continuum structures because the objective function cannot simply be expressed by the separable functional, geometric and material parameter functions.

In the present study, a methodology based on the scaling design concept is employed to develop performance indices, which can be used to evaluate the performance of continuum structures with stress constraints. The formulation of the performance index is simple and easy to implement to optimization procedures. The scaling design concept has been used in structural optimization after each iteration to obtain the best feasible constrained design (Kirsch 1982). The advantages of scaling the design are that it can monitor the history of the reduction in the weight of a structure after each iteration and pick the most active constraints. This method can be applied to structural optimization when the stiffness matrix of a structure is a linear function of the design variables. By scaling the design, the scaled design variable is written by

$$x_e^{\mathrm{s}} = \varphi_s x_e \tag{2.8}$$

where x_e^{s} is the scaled design variable that can be the thickness of the eth element in plane stress structures, φ_{s} is a scaling factor that is same for all

elements, and x_e is the actual design variable of the eth element. The force–displacement relationship in the finite element formulation can be expressed in the matrix form as

$$\frac{1}{\varphi_s}[K^s]\{u\} = \{P\} \tag{2.9}$$

in which $[K^s]$ is the stiffness matrix of the scaled structure that is determined by the scaled design variable, x_e^s, $\{u\}$ is the displacement vector, and $\{P\}$ is the load vector. The equilibrium equation for the scaled structure can be written in terms of the scaled design variable as

$$[K^s]\{u^s\} = \{P\} \tag{2.10}$$

where $\{u^s\}$ is the scaled displacement vector. From Eqs (2.9) and (2.10), the scaled displacement vector can be obtained as

$$\{u^s\} = \frac{1}{\varphi_s}\{u\} \tag{2.11}$$

From the strain–displacement and stress–strain relations in terms of the scaled design variable, the scaled stress vector can be derived as

$$\{\sigma^s\} = \frac{1}{\varphi_s}\{\sigma\} \tag{2.12}$$

in which $\{\sigma\}$ is the stress vector of elements. Obviously, in order to satisfy the stress constraint imposed on a structure, the actual design needs to be scaled by

$$\varphi = \frac{\sigma_{\max}}{\sigma^*} \tag{2.13}$$

It is noted that the stiffness matrix of a plane stress structure is a linear function of the element thickness that is one of the design variables. By scaling the design with respect to the maximum allowable stress constraint, the scaled weight of the initial structure can be determined by

$$W_0^s = \left(\frac{\sigma_{0,\max}}{\sigma^*}\right)W_0 \tag{2.14}$$

where W_0 is the actual weight of the initial structure and $\sigma_{0,\max}$ is the maximum von Mises stress of an element in the initial structure under the applied loads. In an optimization process, the scaled weight of the current structure at the ith iteration can be expressed by

$$W_i^s = \left(\frac{\sigma_{i,\max}}{\sigma^*}\right)W_i \tag{2.15}$$

in which W_i is the actual weight of the current structure at the ith iteration and $\sigma_{i,\max}$ is the maximum von Mises stress of an element in the current structure at the ith iteration.

The performance index for evaluating the efficiency of the resulting topology at the ith iteration is determined by

$$\mathrm{PI}_s = \frac{W_0^s}{W_i^s} = \frac{(\sigma_{0,\max}/\sigma^*)\, W_0}{(\sigma_{i,\max}/\sigma^*)\, W_i} = \frac{\sigma_{0,\max}\, W_0}{\sigma_{i,\max}\, W_i} \tag{2.16}$$

If the material density is uniformly distributed within a continuum structure under consideration, the performance index can be written in terms of the volume of the structure as

$$\mathrm{PI}_s = \frac{\sigma_{0,\max}\, V_0}{\sigma_{i,\max}\, V_i} \tag{2.17}$$

in which V_0 is the volume of the initial structure and V_i is the volume of the current structure at the ith iteration.

It can be observed from Eq. (2.16) that the performance index is a dimensionless number, which measures the performance of a structural topology in terms of the material usage and the uniformity of element stresses. The performance index reflects the changes in the weight and the maximum stress levels in a structure in an optimization process. It is noted that the performance index of the initial structure is equal to unity. The performance of a structure is improved by eliminating lowly stressed elements from the structure. The performance index formula does not involve the loads and geometric parameters such as the span. This means that the optimal topology of a plane stress continuum structure is independent of the scale of the loads and the structure. The performance index measures the structural response (maximum stress) and material efficiency (the weight of a structure). Therefore, it is very convenient for the designer to use this performance index to evaluate the performance of an optimized design. The performance index can also be used to rank the performance of structural topologies produced by different structural optimization methods.

For a structure under multiple load cases, the highest values of $\sigma_{0,\max}$ and $\sigma_{i,\max}$ of an element in the initial and current structures under all load cases should be used in the calculation of the PI_s. The performance index indicates the performance of a structure in an optimization process under the most critical loading condition.

The maximum von Mises stress is used in the calculation of performance index in Eq. (2.16) since the PBO method employs the von Mises stress criterion for element elimination. For principal stress-based optimization methods, the maximum principal stress should be used in performance

index formula. Guan *et al.* (1999, 2003) presented a principal stress-based evolutionary optimization method, which employs stress-based performance indices to identify the optimal topology in an optimization process. In their method, elements with the lowest principal stresses are gradually removed from a continuum structure to improve the performance of the structure under consideration. If the tension-dominant structure is to be designed, the compression-oriented elements are removed from the design domain. On the contrary, if a compression-dominant structure is to be designed, the tension-oriented elements are eliminated.

For tension-dominant designs, the performance index at the *i*th iteration can be defined as (Guan *et al.* 2003)

$$\mathrm{PI}_{\mathrm{st}} = \frac{|\sigma_{22,\max}|_0 \, V_0}{|\sigma_{22,\max}|_i \, V_i} \tag{2.18}$$

where $|\sigma_{22,\max}|_0$ and $|\sigma_{22,\max}|_i$ are the absolute maximum values of the element principal stress σ_{22} in the initial structure and current structure at the *i*th iteration, respectively.

Similarly, for compression-dominant structures, the performance index at the *i*th iteration is

$$\mathrm{PI}_{\mathrm{sc}} = \frac{|\sigma_{11,\max}|_0 \, V_0}{|\sigma_{11,\max}|_i \, V_i} \tag{2.19}$$

where $|\sigma_{11,\max}|_0$ and $|\sigma_{11,\max}|_i$ are the absolute maximum values of the element principal stress σ_{11} in the initial structure and current structure at the *i*th iteration, respectively.

The principal stress-based topology optimization method incorporating performance indices is shown to be applicable to the form finding of cable-stayed bridges that are tension-dominant structures (Guan *et al.* 1999, 2003).

2.6 Performance-based optimality criteria

The fully stressed design has been traditionally used as an OC for optimal design of skeletal structures. The fully stressed OC is easily implemented in the optimization of skeletal structures. However, due to stress concentrations at loaded points and supports, the fully stressed designs of continuum structures can be achieved only for a few special cases. This means that a minimum-weight optimal design is not necessarily a continuum structure in which the element stress distribution is absolutely uniform. The best feasible design that can be obtained is a minimum-weight structure with an

approximately uniform stress distribution. The fully stressed condition, therefore, cannot be incorporated in continuum topology optimization algorithms as a stopping criterion for determining the optimum. To achieve the best performance of a structure, PBOC are used in the PBO method.

It is seen from Eq. (2.16) that the performance index is inversely proportional to the weight of the current structure. The performance objective of minimizing the weight of a structure with stress constraints can be achieved by maximizing the performance index in an optimization process. Therefore, the PBOC can be stated as

$$\text{maximize} \quad \text{PI}_s = \frac{\sigma_{0,\max} W_0}{\sigma_{i,\max} W_i} \tag{2.20}$$

By incorporating the PBOC into optimization algorithms, the optimal topology that corresponds to the maximum performance index can be identified from the performance index history. The higher value of the performance index means the better performance of a structural topology. The stress limit is eliminated from the performance index formulas. This indicates that the optimal topology for the minimum-weight design of a plane stress continuum structure is unique for any prescribed stress limits. The maximum allowable stress constraint is easily satisfied by uniformly scaling the thickness of elements.

The PBOC presented can be incorporated in stress-based optimization methods to identify the global optimum, such as the evolutionary structural optimization method (Xie and Steven 1993), the SKO approach (Mattheck 1998), and the rule-based optimization technique (Seireg and Rodriguez 1997). The PBOC can also be incorporated in truss topology optimization methods that employ ground structures where the cross-sectional areas of members are design variables. This is because the design can be uniformly scaled with respect to the cross-sectional area of members in an optimization process (Kirsch 1982).

2.7 Performance characteristics of structures with stress constraints

In PBO, lowly stressed elements are gradually eliminated from a continuum structure to improve the performance of the structure. The weight of a structure is thus gradually reduced due to element removal while the maximum von Mises stress of elements within the resulting structure increases accordingly. The performance characteristics of continuum structures with stress constraints can be captured by using the PBO method. Performance characteristics are expressed by the weight and maximum stress of a structure. Performance characteristics are valuable to the structural designer. They not

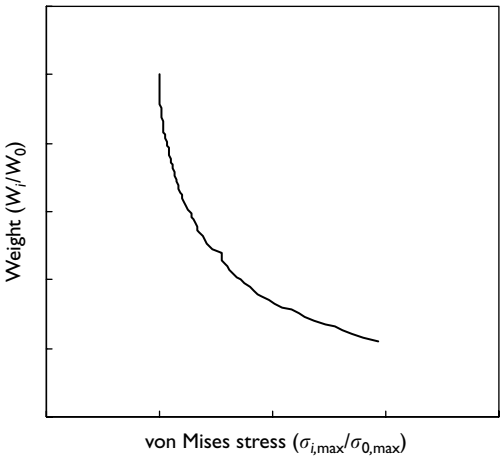

Figure 2.1 Typical performance characteristic curve for structures with stress constraints.

only indicate whether an optimized design is feasible but also measure the success of the optimized design configurations. A typical performance characteristic curve generated by the PBO technique is shown in Figure 2.1. Points on the curve are the performance response values for a prescribed performance level. A design with performance below this curve is not feasible because the design made by that amount of materials will not maintain the maximum stress within the prescribed limit. A structure with performance above this curve is obviously over-designed. Structural optimization techniques can be applied to over-designed structures to substantially improve their performance.

2.8 Performance optimization procedure

Topology optimization of continuum structures is a performance-improving process, which couples the FEA and the element elimination scheme. The performance optimization process involves the modeling of an initial design, structural analysis, performance evaluation, element elimination, checking the model connectivity and the termination criterion. A flow chart is presented in Figure 2.2 to show the main steps of the PBO procedure, which is described as follows:

1 Model an initial continuum structure with fine finite elements. The material properties, applied loads and boundary conditions are specified. Nondesign region can be specified by assigning their material property number to a different number from that of the design region.
2 Perform a linearly elastic FEA on the structure.

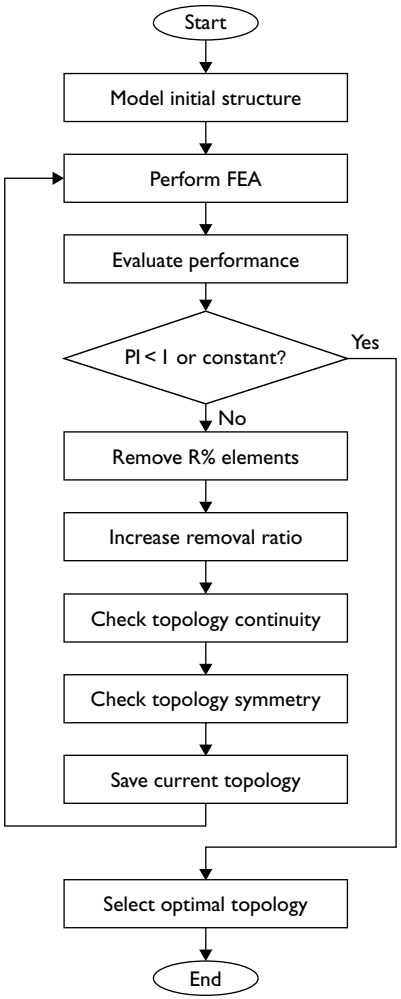

Figure 2.2 Flowchart of performance optimization procedure for fully stressed topology designs.

3 Evaluate the performance of the resulting topology using Eq. (2.16).
4 Eliminate elements that satisfy Eq. (2.5). For multiple loading cases, only elements that satisfy Eq. (2.5) for all load cases are removed from the structure at each iteration. The initial removal ratio (R_0^{d}) and the incremental removal ratio (R_i^{d}) are specified before carrying out the optimization.
5 Increase the element removal ratio (R_j^{d}) such that $R_j^{\mathrm{d}} = R_0^{\mathrm{d}} + (j-1)R_i^{\mathrm{d}}$ if a steady state is reached.

6 Check topology connectivity. It is considered that two elements are connected if they have at least one common edge. Elements that are not connected with others are treated as singular elements, which will be deleted from the model.
7 Check the symmetry of the resulting topology with an initially symmetrical condition.
8 Save current topology. The data for resulting topologies at each iteration is saved to files. This will allow all topologies obtained to be displayed at later states.
9 Repeat steps 2–8 until the performance index is kept constant or less than unity.
10 Plot the performance index history and select the optimal topology from the optimization history.

The topology of a structure is gradually modified by applying the above optimization procedure. The performance index is used to monitor the performance optimization history and as the termination criterion. When lowly stressed elements are deleted from the structure, the performance index will increase from unity to the maximum value. After the performance index reaches the peak, it may keep constant in later iterations if the topology is fully stressed. When the stress distribution in the topology is uniform, no more elements can be removed from the structure according to Eq. (2.5). However, the fully stressed designs of discretized continuum structures can only be obtained in some special cases. In most cases, elements can be continuously removed from a structure because of the non-uniformity of stresses in the structure. Consequently, the performance index in the final stage will be less than unity. If the performance index of a resulting topology is less than unity, its performance is lower than that of the initial continuum structure. Therefore, the optimization process can be terminated when the performance index is less than unity or kept constant.

2.9 Element addition and deletion schemes

2.9.1 Element addition and deletion criteria

In engineering design, the initial topology, which is selected by the design engineer based on his or her intuition and past experience for a continuum structure under given loading and support conditions, is usually over-designed and not fully stressed. To achieve a high performance structure, lowly stressed materials can be removed from an over-designed structure by applying the PBO technology. The PBO method with an element deletion capability is simple and straightforward. It allows the designer to achieve a fully stressed optimal topology by specifying an initial design domain that is big enough to cover the expected optimum and satisfies the design space

restriction. By gradually deleting lowly stressed elements from the initial design domain, the performance of the structure can be maximized.

By eliminating elements that are inefficient in carrying loads from a continuum design domain, the actual load carrying mechanism within this domain can be characterized by remaining elements. Elements in the load path are highly stressed when compared to those that have been removed. In some design situations, it is necessary to strengthen the load path by adding materials. This leads to the development of optimization techniques in which elements can be added and removed. The idea of adding and removing elements has been tried by Querin *et al.* (2000) in evolutionary optimization of continuum structures. The PBO algorithms can be easily extended to include element addition. The element deletion criterion has been given in Eq. (2.5). The element addition criterion is expressed by

$$\sigma_{i,e} > R_j^{\mathrm{a}} \sigma_{i,\max} \tag{2.21}$$

where R_j^{a} is the addition ratio of elements at the jth steady state. All potential elements that satisfy Eq. (2.21) are added to the initial structure. When no elements can satisfy either Eq. (2.5) or Eq. (2.21), a steady state reaches. In order to continue the optimization process, the deletion ratio is increased by Eq. (2.6) while the element addition ratio is increased by

$$R_j^{\mathrm{a}} = R_0^{\mathrm{a}} + (j-1)\, R_i^{\mathrm{a}} \quad (j = 1, 2, 3, 4, \ldots) \tag{2.22}$$

where R_0^{a} is the initial addition ratio of elements, and R_i^{a} is the incremental addition ratio of elements.

Potential elements can be added to the highly stressed elements on the boundary of an evolving structure if they satisfy Eq. (2.21). An element on the boundary of a structure may have more than one free edge to which potential elements can be added. Figure 2.3 shows the element addition scheme. Elements in dark color form the current structure while white color elements are potential elements with zero material property values. It is assumed that the eth element on the boundary of the structure has the highest stress level. This element is connected to the structure by one edge and its other three edges are free from connection. Therefore, three potential elements in light color around the eth element are added to the structure by assigning their material property values to those of the eth element, as shown in Figure 2.3. The added elements share the loads previously carried by the eth element. Due to element addition, the stress level of the eth element is considerably reduced so that the performance of the structure is improved.

In the optimization process, the state of element addition and deletion depends on the specified initial structure. If an initial structure occupies only a small part of the maximum design domain, the initial structure is so

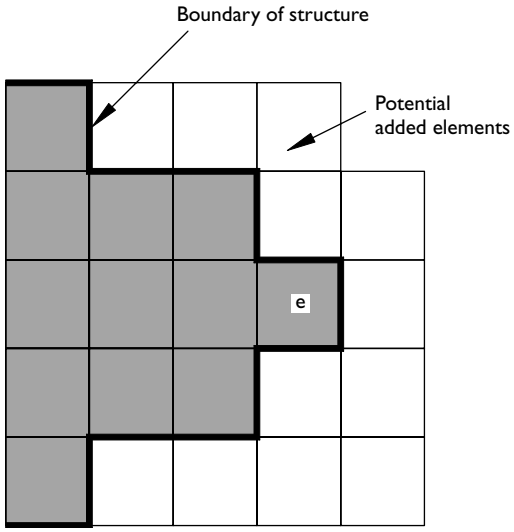

Figure 2.3 Element addition scheme.

highly stressed that potential elements need to be added to the structure to strengthen the load path. By gradual element addition, the structure is growing. If only element addition is permitted in an optimization process, the structure would eventually grow to an optimal shape with an improved stress distribution. After a continuum structure has been grown big enough, elements are simultaneously added and removed according to the element stress levels in order to generate optimal topology.

The computational efficiency of topology optimization methods with element addition and deletion schemes largely depends on the design situations. These techniques can readily apply to simple continuum structures in terms of geometry and loading conditions. Considerable savings in computational costs may be obtained when dealing with simple structures. For practical structures with complex geometry and loading conditions, however, no elements may be removed from a structure until it substantially grows to occupy nearly the maximum design domain. The PBO method with the element removal algorithm is more suitable to apply to complex design situations since it straightforwardly eliminates underutilized material from the initial structure which needs not to grow through the material addition.

2.9.2 Optimization algorithm

PBO algorithms are easily extended to include both element addition and deletion capabilities. The PBO technique automatically modify a continuum

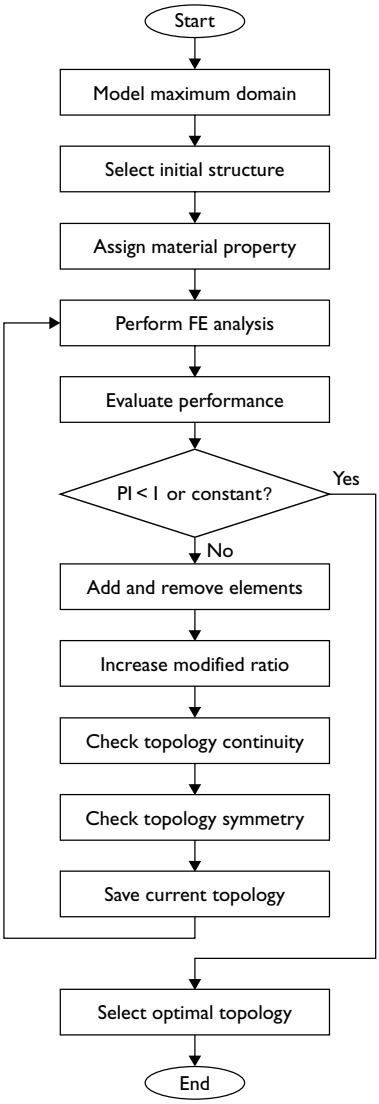

Figure 2.4 Flowchart of performance optimization procedure with element addition and deletion schemes.

structure by either adding efficient material or removing inefficient material according to the von Mises stress levels of elements. Figure 2.4 shows a flowchart of the performance optimization algorithm including element addition and deletion schemes. The main steps of the optimization

algorithm are given as follows:

1 Model a maximum design domain with fine finite elements.
2 Select an initial structure within the maximum design domain such that elements in the initial structure connect the loads to supports.
3 Assign the material property values of all elements that were not specified as the initial structure to zero.
4 Perform FEA on the structure.
5 Evaluate the performance of resulting topology using the performance index.
6 Add elements that satisfy Eq. (2.5) and remove elements that satisfy Eq. (2.21).
7 Increase the element addition and deletion ratios if a steady state has been reached.
8 Check the continuity of the resulting topology.
9 Check the symmetry of the resulting topology with an initially symmetrical condition.
10 Save model data for the current topology.
11 Repeat steps 4–10 until the performance index is less than unity.
12 Plot the performance index history and select the optimum.

2.10 Cavity controls in topology optimization

2.10.1 Concepts of cavity controls

Topology optimization of continuum structures is to create cavities in a continuum design domain by removing inefficiently used material so that the performance of the structure can be improved. When more and more material is eliminated from a design domain, a number of cavities are created and the optimal structure is achieved. Continuum topology optimization allows for inefficient material to be removed from the interior as well as the boundary of a continuum design domain. In contrast, shape optimization of continuum structures only allows material to be removed from the boundary of the design domain. No cavities are created in the shape optimization process. The optimal topology of a continuum structure depends on how many cavities are permitted to be generated. Cavity controls in topology optimization affect the optimal designs and performance of continuum structures. Without cavity controls, the PBO method would freely create a maximum number of cavities in an optimal continuum structure.

Cavity controls in topology optimization have practical applications in the design of engineering structures. In multistory building construction, reducing the story height will result in significant savings in material and construction costs. In order to achieve this cost-performance objective, cavities are often made in beams in order to pass through service equipment.

These cavities are usually called service ducts. Design engineers often face difficulty in determining the best locations of service ducts in beams without compromising the structural performance of these beams in a building. Structural optimization methods incorporating cavity control schemes can be used to determine the best locations of cavities in engineering structures.

Kim *et al.* (2000) presented an evolutionary topology optimization method for controlling the number of cavities in an optimized continuum structure. This method can control when a cavity is created during an optimization process. It employs topology and shape optimization techniques to find the optimal topology in which cavities are generated in a control manner. The shape optimization method is used to modify the existing boundaries of a continuum structure to determine the size and shape of the cavities. The topology optimization method is employed to create a cavity by removing elements from the design domain only when the program detects a need for such a cavity.

After the FEA of a continuum structure, the stress distribution within the structure is determined. The cavity creation ratio is defined as (Kim *et al.* 2000)

$$R_{\mathrm{c}} = \frac{\sigma_{n,\min}}{\sigma_{b,\min}} \tag{2.23}$$

where $\sigma_{n,\min}$ is the minimum von Mises stress of the nonboundary elements, and $\sigma_{b,\min}$ is the minimum von Mises stress of the boundary elements.

When the cavity creation ratio is less than a user-defined value R_{u}, the stress of the nonboundary elements is said to be much lower than that of the minimum boundary elements. A cavity is then created inside the design domain by applying the topology optimization algorithm that deletes a nonboundary element with the minimum stress levels. After a new cavity has been created, the shape optimization algorithm is applied to modify the shape and size of the cavity.

2.10.2 Cavity control algorithm

The PBO algorithm presented in Section 2.8 can be easily modified to incorporate the cavity control scheme. The main design optimization steps of the cavity control algorithm are similar to those of the original PBO procedure. The cavity control algorithm starts with defining an initial continuum structure and inputting the cavity creation number. A FEA is then undertaken on the initial structure to determine the von Mise stress distribution. The performance of the structure is evaluated by using the stress-based performance index. If the performance index is not less than unity, the shape of the structure is modified by removing lowly stressed boundary elements from the design domain. After a steady state reaches, the cavity

creation ratio is calculated and compared with the user-defined value. If the cavity creation ratio is less than or equal to the user-defined value, a non-boundary element with the lowest stress level is deleted from the design domain. The process of the FEA, performance evaluation, shape modification and cavity creation is repeated until the performance index is less than unity.

The main steps of the cavity control algorithm are illustrated in Figure 2.5, and are described as follows:

1 Model an initial continuum structure with fine finite elements. The material properties, applied loads, boundary conditions and the cavity creation number are specified.
2 Perform a FEA on the structure.
3 Evaluate the performance of the resulting structure using PI_s.
4 Modify the shape by removing lowly stressed elements from the boundary of the continuum design domain.
5 When a steady state is reached, calculate the cavity creation ratio R_c.
6 If the cavity creation ratio is less than the user-defined value, eliminate a nonboundary element with the minimum stress level form the structure.
7 Increase the element removal ratio if a steady state is reached.
8 Check the continuity of the resulting topology.
9 Check the symmetry of the resulting topology with an initially symmetrical condition.
10 Save model data for the current topology.
11 Repeat steps 2–10 until the performance index is less than unity.
12 Plot the performance index history and select the optimum.

The cavity control algorithm allows the designer to predefine a number of cavities as design constraints in topology optimization of continuum structures. Examples presented by Kim *et al.* (2000) show that the optimal topology generated by this optimization technique is sensitive to the user-defined cavity creation number. The values of the cavity creation number are between 0.6 and 1.0 for cavities. Further research is needed to investigate the relationship between the number of cavities and the user-defined value for the cavity creation number.

2.11 Examples

The PBO method is applied to the topology optimization problems of various continuum structures in this section. It is assumed that the strength of the structure dominates the design so that the stress constraint is considered. The magnitude of stress limits might have a significant influence on the weight of the final design but not on the optimal topology. As a result, the topology optimization process could be conveniently divided into two

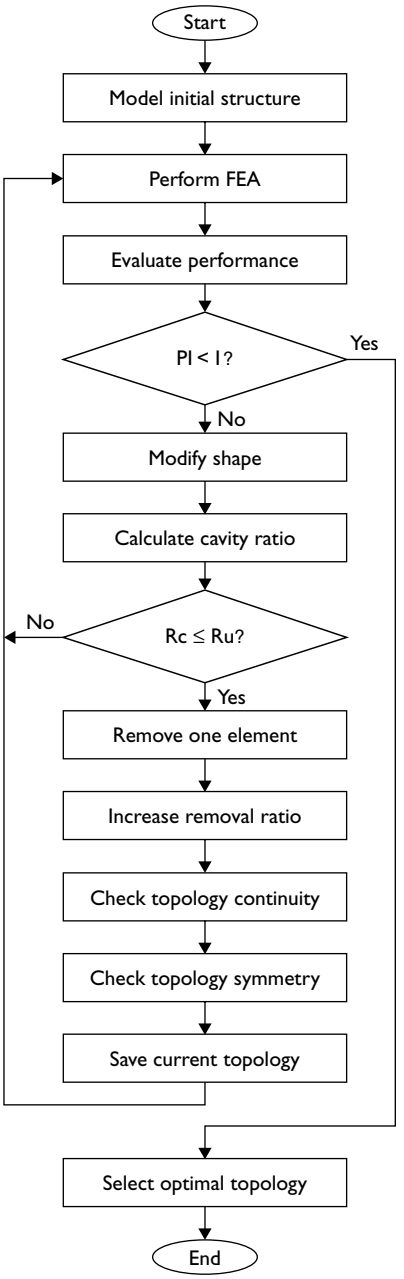

Figure 2.5 Flowchart of the performance-based cavity control algorithm.

steps. The first step is to generate the optimal topology of a continuum structure using the PBO method regardless of the magnitude of stress limit. The second step is to size the optimal topology obtained by uniformly changing the thickness of the structure in order to satisfy the stress constraint. Only the first step is considered in the following examples.

2.11.1 Two-bar frame structure

The PBO method developed is a numerical technique, which automatically generates fully stressed optimal topology designs of continuum structures in an iterative manner. It combines the modern structural optimization theory with performance-based design concepts to overcome the limitations of traditional fully stressed design methods. The PBO approach incorporates not only the performance objective function and stress constraints but also performance indices and PBOC to guarantee a global optimum. The validity and effectiveness of the PBO method is examined by a numerical example whose optimal solution can be derived by analytical methods.

A two-bar frame structure shown in Figure 2.6 was proven to be the optimum by analytical methods. The optimal height H of the two-bar frame structure can be obtained as $H = 2L$ by the analytical method if the structure is assumed to be a truss for the minimum-weight design. The PBO technique was applied to this optimization problem of this two-bar frame structure. A continuum design domain that is larger than the size of $L \times 2L$ as shown in Figure 2.7 was used as a starting point to derive the optimal two-bar frame structure. The design domain was modeled using 32×72 plane stress elements. The left side of the design domain was fixed. A point

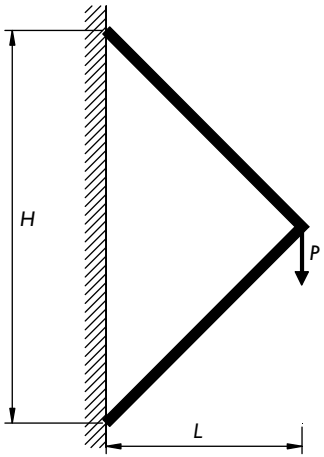

Figure 2.6 Two-bar frame structure.

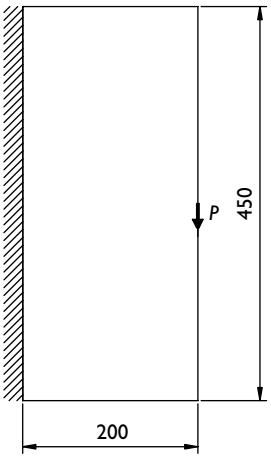

Figure 2.7 Design domain for the two-bar frame structure.

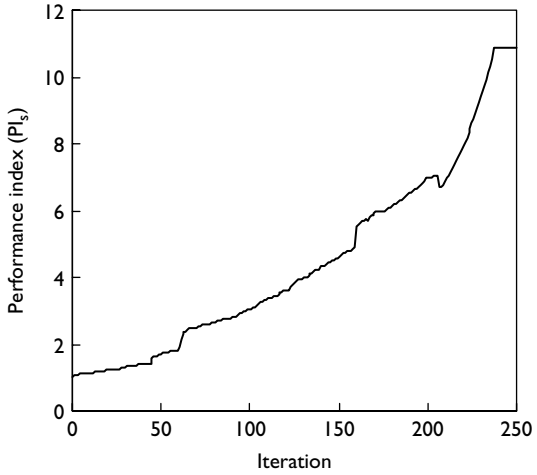

Figure 2.8 Performance index history of the two-bar frame structure.

load of 200 N was applied to the center of the free end. The Young's modulus $E = 200$ GPa, the Poisson's ratio $\nu = 0.3$ and the thickness of elements $t = 1$ mm were specified in the FEA. The plane stress condition was assumed. The initial removal ratio of 1 percent and the incremental removal ratio of 1 percent were used in the optimization process.

Figure 2.8 shows the performance index history of the structure in the optimization process. It can be observed from Figure 2.8 that the

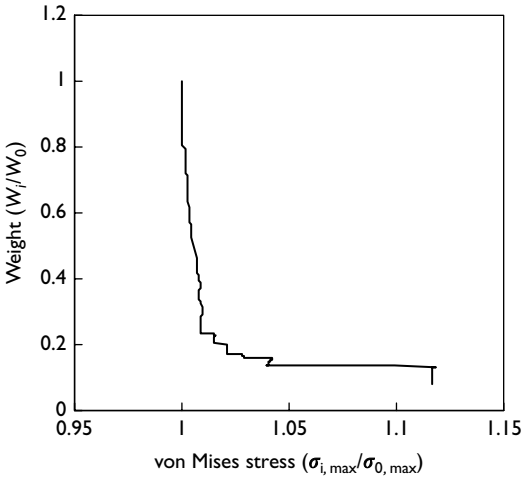

Figure 2.9 Performance characteristics of the two-bar frame structure.

performance index of the structures at the initial iteration was equal to unity because no elements were removed from the structure. By gradually eliminating lowly stressed elements from the structure, the performance index increased from unity up to the maximum value of 10.86. This means that the scaled weight of the initial structure is 10.86 times that of the optimal design obtained. It can be seen from Figure 2.8 that the maximum performance index is constant after reaching the maximum value. This indicates that the distribution of element effective stresses within the optimal topology is approximately uniform. The optimal topology generated by the PBO method is a fully stressed design at minimum weight. The performance index considering the maximum allowable stress constraint can indicate not only the optimum but also the uniformity of stresses within an optimal structure.

The performance characteristics of the structure in an optimization process predicted by the PBO technique are demonstrated in Figure 2.9. It is observed from Figure 2.9 that the weight of the structure is reduced with an increase in the maximum von Mises stress of elements. The optimal topology contains only about 8.2 percent material of the initial design domain while the maximum von Mises of an element within the structure increased only by 11.6 percent. A substantial performance improvement of the structure has been achieved by applying the PBO technique.

The topology optimization history of the two-bar frame structure is presented in Figure 2.10. The optimal topology that corresponds to the maximum performance index evolved towards a two-bar frame structure, where

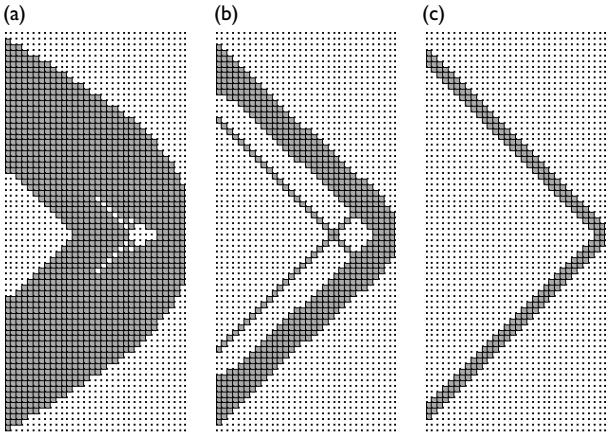

Figure 2.10 Topology optimization history of the two-bar frame structure: (a) iteration 50, (b) iteration 150 and (c) optimum.

Table 2.1 Material volumes required at different iterations for various stress limits

σ^* *(MPa)*	V_0^s *(mm^3)*	V_{50}^s *(mm^3)*	V_{150}^s *(mm^3)*	$V_{optimal}^s$ *(mm^3)*	$PI_{s,max}$
200	9428	5559	2043	868	10.86
300	6285	3706	1362	578	10.86
400	4714	2279	1022	434	10.86

its optimal height is exactly two times of its span as shown in Figure 2.10(c). This proves that the PBO method is a reliable design tool for continuum structure with stress constraints. The ability of the performance index and PBOC in identifying the optimal topology from the optimization history is demonstrated in Table 2.1, where a comparison of material volumes required for the initial structure and three topologies shown in Figure 2.10 for various stress limits is made. It appears from the Table 2.1 that material volume of the optimal topology is always less than that of other topologies obtained for each stress limits. This indicates that the topology shown in Figure 2.10(c) is the best topology, which is independent of the prescribed stress limits.

Similar solutions to this two-bar frame structure may be obtained using other optimization methods. However, no performance index and PBOC are used in other approaches to indicate the optimum. This means that the designer has to select one from hundreds of topologies generated in the

optimization process as the "optimum" for design according to his or her desire. Such a trial-and-error selection process would be cumbersome for the designer when dealing with real-world engineering design problems. Although optimization methods can be examined by comparing results with analytical solutions, such as this example, this can only be done for simple structures. For practical problems with complex geometry and loading conditions, no classical solutions would be available. Therefore, the PBOC presented are extremely useful for structural designers to assist the selection of optimal topologies in structural design.

2.11.2 Michell type structures with height constraints

In practice, the design space is often limited and significantly affects the optimal configurations of a structure. For example, the height of a beam in a building has to be limited in order to satisfy functional requirements. The designer should know how to select an initial design domain for deriving the optimal structure in a given design space. The structure generated by design domain methods is optimum in the sense of the given design domain. By applying the PBO technique to different initial design domains for the same loading and support condition, we may get different optimal topologies. The effect of geometric restrictions such as height constraints is investigated here.

The design domain for the simply supported Michell type structures with various height constraints is depicted in Figure 2.11. A point load $P = 400$ N was applied to the structure. In case (a), the initial structure with $h/L = 1/2$ was divided into 100×50 mesh using four-node plane stress elements and the initial removal ratio of 1 percent and the incremental removal ratio of 0.5 percent were employed in the PBO process. In case (b), the design domain with $h/L = 1/4$ was modeled using 100×25 elements. In case (c), the initial structure with $h/L = 1/8$ was divided into 100×13 elements. In case (d), 100×9 elements were used to model the structure with $h/L = 1/12$.

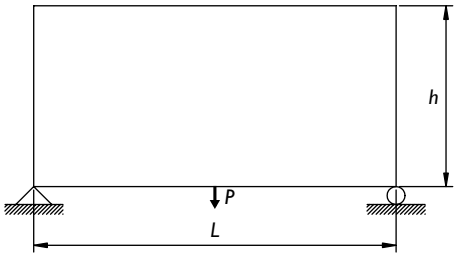

Figure 2.11 Design domain for Michell type structures with height constraints.

The Young's modulus $E = 200$ GPa, Poisson's ratio $\nu = 0.3$ and the thickness of elements $t = 2$ mm were used for all cases in the analysis. The initial removal ratio and the incremental removal ratio were 1 percent for cases (b)–(d). The plane stress condition was assumed for all cases.

The performance index history of case (a) is presented in Figure 2.12, which shows that the performance index increased with the elimination of lowly stressed elements from the structure. However, further element removal from the optimal design eventually resulted in the collapse of the structure, which is indicated by the sharp decrease of the performance index in Figure 2.12. This means that there were still lowly stressed elements in the optimal topology. However, the uniformity of stresses in the optimal design had ultimately been maximized. The stress distribution in a continuum structure is hardly uniform owing to the stress concentration in the regions of loading and supports. The objective of the proposed method is to generate an optimal topology with the most uniform stress distribution and minimum weight. This example shows that a minimum-weight design is not necessarily a fully stressed design.

The effect of height constraints on the performance index of Michell type structures is demonstrated in Figure 2.13. It is seen that the performance index increases with an increase in the height compared with the initial structures. The maximum performance indices for cases (a)–(d) were 6.8, 4.97, 1.89 and 1.44, respectively. This indicates that the performance of structural topologies can be improved by increasing the height of the initial design domain. Optimal topologies obtained for each case are shown in Figure 2.14. The optimal topologies shown in Figure 2.14(a,b) exhibit

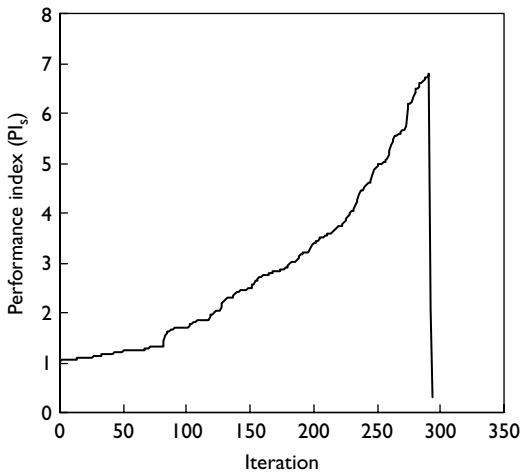

Figure 2.12 Performance index history of case (a).

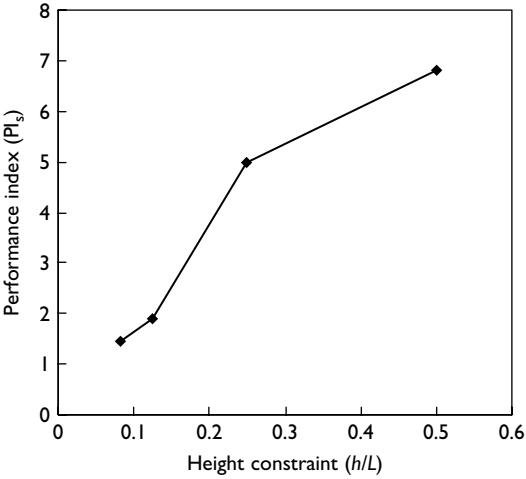

Figure 2.13 Effect of height constraints on performance index.

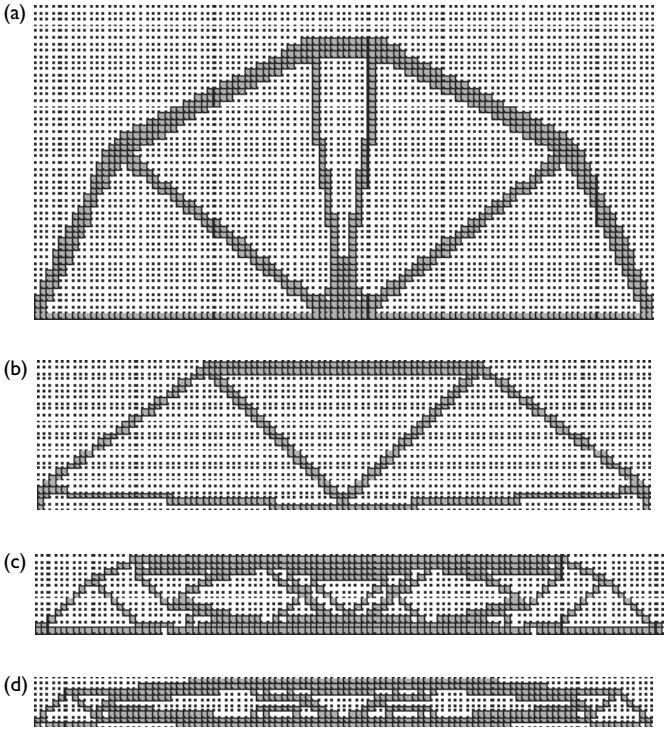

Figure 2.14 Effects of height constraints on optimal topologies: (a) $h/L = 1/2$, $PI_s = 6.8$; (b) $h/L = 1/4$, $PI_s = 4.97$; (c) $h/L = 1/8$, $PI_s = 1.89$; (d) $h/L = 1/12$, $PI_s = 1.44$.

truss-like structures that can be designed as trusses. When $h \ll L$, the optimal topology as shown in Figure 2.14(d) evolved to a continuum structure from which not much material could be removed.

2.11.3 Ranking the performance of structural topologies

Topology optimization methods are efficient tools for improving the performance of engineering structures. However, it should be noted that the performance of optimized designs depends on the methods and design optimization criteria used. It has been found that different optimization methods often lead to different final structures for the same design problem considered. It is difficult to evaluate the performance of different optimization algorithms because they usually involve different formulations. Little work has been done in this area in structural optimization. However, the efficiency of structural optimization methods can be evaluated by comparing the results produced by them. The stress-based performance index developed is used to compare the performance of structural topologies generated by different optimization methods.

A beam with fixed supports shown in Figure 2.15 was optimized by using the PBO method. The beam was subjected to a concentrated load of 400 N applied to the center of the bottom. The beam was divided into 90×30 four-node plane stress elements. The Young's modulus $E = 200$ GPa, Poisson's ratio $\nu = 0.3$ and the thickness of elements $t = 2$ mm were specified in the FEA. The initial removal ratio and incremental removal ratio were specified as 1 percent in the performance optimization process.

The performance index history of this beam is presented in Figure 2.16. It is seen from the performance index history that the performance of the structure gradually increased when lowly stressed elements were removed from the design domain. After iteration 254, a significant increase in performance was observed as shown in Figure 2.16. From iteration 261 to 300, the performance of the structure was maintained because the structure

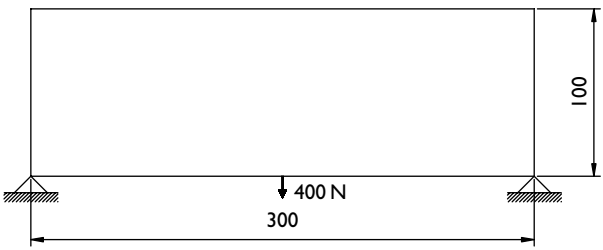

Figure 2.15 Design domain of the beam with fixed supports.

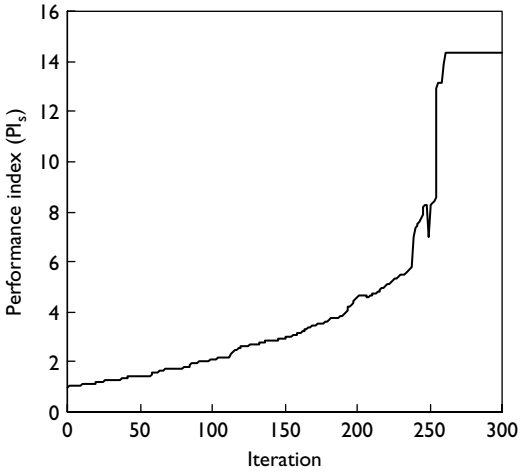

Figure 2.16 Performance index history of the beam with fixed supports.

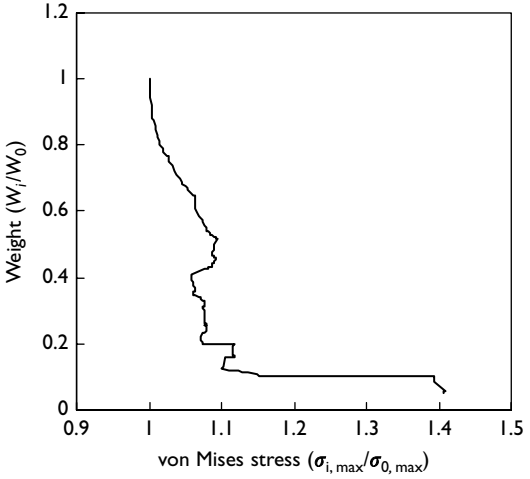

Figure 2.17 Performance characteristics of the beam with fixed supports.

reached a fully stressed state in which no more elements could be removed. The maximum performance index was obtained as 14.32. The performance characteristic curve for this evolving continuum structure is demonstrated in Figure 2.17. The optimal design has saved 95 percent material compared with the initial design domain while the maximum von Mises stress of an

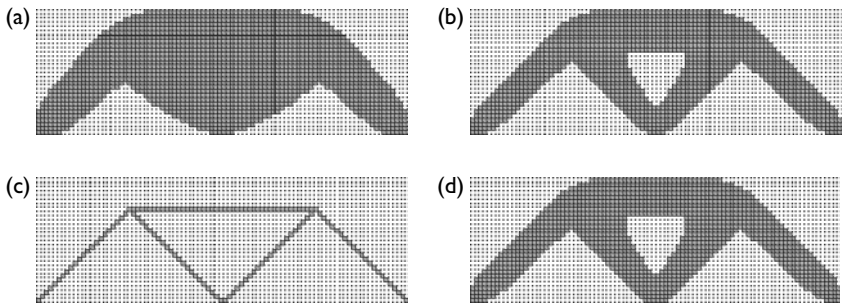

Figure 2.18 Topology optimization history of the beam with fixed supports: (a) iteration 50; (b) iteration 95; (c) optimal topology; (d) topology by Mattheck (1998).

element within the evolving structure increased by only 40.7 percent, as indicated in Figure 2.17.

The topology optimization history is shown in Figure 2.18. The optimal topology obtained was uniformly stressed, as indicated by the performance index history. Figure 2.18(d) shows the final design proposal given by Mattheck (1998) using the SKO approach. This proposal was regenerated by using the same mesh as used in the PBO. A linear FEA on the design proposal was undertaken to evaluate the performance responses. The performance index of the design proposal was calculated as 1.92, which is much less than that obtained by the PBO method. It can be observed that this final proposal obtained by Mattheck is very similar to the topology shown in Figure 2.18(b), which is far from the optimum. Therefore, it can be concluded that the proposed performance index is a useful tool for ranking the performance of structural topologies.

2.12 Conclusion

This chapter has presented the PBO method incorporating the uniform sizing of element thickness for fully stressed topology design of continuum structures with stress constraints. In PBO method, the performance objective is to seek a fully stressed topology design with minimum material consumption and acceptable strength performance level. The element removal criteria are based on the von Mises stress levels. A stress-based performance index has been derived by using the scaling design procedure for evaluating the topology performance of continuum structure in terms of the material usage and maximum strength criteria. The performance index is incorporated in PBO algorithms to monitor the optimization process and as the termination criterion. PBOC have been developed for identifying the global

optimum from an optimization history. Optimal topology of a plane stress continuum structure is achieved by gradually eliminating lowly stressed elements from a continuum design domain until its performance is maximized. Performance characteristics of a structure subject to stress constraints are expressed by the weight and maximum von Mises stress of an element in the structure. The PBO technique can fully capture the performance characteristic curves of continuum structures.

It has been shown that the proposed PBO method can generate efficient structural topologies that have been verified by analytical solutions. The performance index can indicate not only the global optimum from the optimization history but also the uniformity of stresses within an optimal continuum structure. PBOC developed overcome the limitations of traditional stress-based continuum topology optimization methods, and can be incorporated in any stress-based optimization methods for continuum and discrete structures to obtain the global optimum. Moreover, the performance index can be used to rank the performance of structural topologies produced by different structural optimization methods. It has been shown that the PBO method can be easily extended to include element addition and cavity control schemes. The PBO technique with the capabilities of element addition and deletion can be applied to the finding and strengthening of the load path in a continuum structure. The performance-based cavity control algorithm allows the designer to predefine a number of cavities as design constraints in topology optimization of continuum structures.

It is essential to specify small element removal and addition ratios to achieve smooth solutions. For the typical element removal ratio of 1 percent, it needs about 250–300 iterations to reach an optimum. By applying the PBO technology, significant material savings up to 95 percent of the initial design domain can be achieved while the maximum von Mises stress level does not increase significantly. Fortunately, two structures optimized by the PBO technique are fully stressed designs. However, it needs to be pointed out that stress-based continuum topology optimization methods are suitable for the design of structural components or structures where strength performance is the main concern.

2.13 References

Ashby, M. F. (1992) *Materials Selection in Mechanical Design*, Oxford: Pergamon Press.

Baumgartner, A., Harzheim, L. and Mattheck, C. (1992) "SKO (soft kill option): the biological way to find an optimum structure topology," *International Journal of Fatigue*, 14(6): 387–393.

Burgess, S. C. (1998a) "The ranking of efficiency of structural layouts using form factors. Part 1: design for stiffness," *Proceedings of the Institution of Mechanical Engineers, Part C, Journal of Mechanical Engineering Science*, 212(C2): 117–128.

Burgess, S. C. (1998b) "The ranking of efficiency of structural layouts using form factors. Part 2: design for strength," *Proceedings of the Institution of Mechanical Engineers, Part C, Journal of Mechanical Engineering Science*, 212(C2): 129–140.

Guan, H., Chen, Y. J., Loo, Y. C., Xie, Y. M. and Steven, G. P. (2003) "Bridge topology optimisation with stress, displacement and frequency constraints," *Computers and Structures*, 83(3): 131–145.

Guan, H., Steven, G. P. and Xie, Y. M. (1999) "Evolutionary structural optimization incorporating tension and compression materials," *Advances in Structural Engineering*, 2(4): 273–288.

Hinton, E. and Sienz, J. (1995) "Fully stressed topological design of structures using an evolutionary procedure," *Engineering Computations*, 12: 229–244.

Kim, H., Querin, O. M., Steven, G. P. and Xie, Y. M. (2000) "A method for varying the number of cavities in an optimized topology using evolutionary structural optimization," *Structural Multidisciplinary Optimization* 19: 140–147.

Kirsch, U. (1982) "Optimal design based on approximate scaling," *Journal of Structural Engineering*, ASCE, 108(ST4): 888–909.

Li, Q., Steven, G. P. and Xie, Y. M. (2001) "Thermoelastic topology optimization for problems with varying temperature fields," *Journal of Thermal Stresses*, 24(4): 347–366.

Liang, Q. Q. (2001) *Performance-Based Optimization Method for Structural Topology and Shape Design*, PhD thesis, Victoria University of Technology, Australia.

Liang, Q. Q., Xie, Y. M. and Steven, G. P. (1999a) "Optimal selection of topologies for the minimum-weight design of continuum structures with stress constraints," *Proceedings of the Institution of Mechanical Engineers, Part C, Journal of Mechanical Engineering Science*, 213(C8): 755–762.

Liang, Q. Q., Xie, Y. M. and Steven, G. P. (1999b) "Optimal topology selection of continuum structures with stress and displacement constraints," paper presented at *the Seventh East Asia-Pacific Conference on Structural Engineering and Construction*, Kochi, Japan, pp. 560–565.

Mattheck, C. (1998) *Design in Nature: Learning from Trees*, Berlin: Springer-Verlag.

Mattheck, C. and Burkhardt, S. (1990) "A new method of structural shape optimization based on biological growth," *International Journal of Fatigue*, May: 185–190.

Oda, J. (1977) "On a technique to obtain an optimum strength shape by the finite element method," *Bulletin of the JSME*, 20(140): 160–167.

Oda, J. and Yamazaki, K. (1977) "On a technique to obtain an optimum strength shape of an axisymmetric body by the finite element method," *Bulletin of the JSME*, 20(150): 1524–1532.

Querin, O. M., Young, V., Steven, G. P. and Xie, Y. M. (2000) "Computational efficiency and validation of bi-directional evolutionary structural optimization," *Computer Methods in Applied Mechanics and Engineering*, 189: 559–573.

Rodriguez, J. and Seireg, A. (1985) "Optimizing the shapes of structures via a rule-based computer program," *Computing in Mechanical Engineering*, ASME, 40(1): 20–29.

Rong, J. H., Xie, Y. M., Yang, X. Y. and Liang, Q. Q. (2000) "Topology optimization of structures under dynamic response constraints," *Journal of Sound and Vibration*, 234(2): 177–189.

Seireg, A. A. and Rodriguez, J. (1997) *Optimizing the Shape of Mechanical Elements and Structures*, New York: Marcel Dekker, Inc.

Steven, G. P., Li, Q. and Xie, Y. M. (2002) "Multicriteria optimization that minimizes maximum stress and maximizes stiffness," *Computers and Structures*, 80: 2433–2448.

Wu, C. Y. (1993) *Automatic Rule-Based Shape Optimization of Two-Dimensional Structures Subjected to Static Loading, Body Forces and Impact*, PhD thesis, University of Florida-Gainesville, USA.

Xie, Y. M. and Steven, G. P. (1993) "A simple evolutionary procedure for structural optimization," *Computers and Structures*, 49(5): 885–896.

Chapter 3

PBO for structures with displacement constraints

3.1 Introduction

The performance-based optimization (PBO) method for fully stressed topology designs of continuum structure subject to stress constraints has been presented in Chapter 2. In fully stressed topology design, element removal criteria are based on the von Mises stress levels of elements. It has been demonstrated that the PBO algorithm can generate fully stressed optimal structures. However, it should be noted that fully stressed design procedures might not lead to the stiffest structural topologies. Fully stressed design optimization methods are suitable for finding optimal topologies for the strength design of continuum structures where the system performance is not a major concern. It has wide applications in aeronautical and mechanical engineering industries.

In civil engineering, structures are often designed for required serviceability performance. For example, the maximum deflection of a steel bridge under traffic loads must be within an acceptable limit. The stiffness performance of a civil engineering structure is one of the important design criteria that need to be considered in design. To generate the stiffest structural topologies and shapes, structural optimization methods should be formulated on the basis of stiffness performance criteria. In other words, displacements should be treated as constraints. Methods for topology optimization of continuum structures subject to displacement constraints have been proposed. Atrek (1989) developed a program for topology and shape optimization of continuum structures subject to displacement constraints based on the classical optimality criteria (OC) method. This program is capable of removing material from inside the design domain as well as from immediate boundaries. Only the most critical constraint imposed on a structure is considered in a given time in deriving an optimal shape. The inefficient material is removed from a design domain to achieve a lighter design, which has a more acceptable level of structural responses compared to other feasible designs with the same material volume. The zero–one decision-making scheme has also been used for topology design by Bendsøe (1989) and Rozvany *et al.* (1992).

Chu *et al.* (1996) extended the evolutionary optimization method for optimal design of continuum structures with displacement constraints. The change of constrained displacements due to element removal is defined as a sensitivity number for element elimination. Elements with the lowest sensitivity numbers are gradually removed from a continuum design domain to achieve a maximum stiffness design. The optimization process is terminated when one of the constrained displacements reaches the prescribed limit. The only criterion used to derive the optimum is the displacement constraints. The drawback of this optimization procedure is that no criterion is used to obtain the global optimum for the given design space. Displacement constraints have also been used as the termination criterion in the density function approach by Yang (1997) to determine the optimum. However, it is worth noting that constrained displacements are significantly affected by the element thickness since the stiffness matrix of a plane stress continuum structure is a linear function of the element thickness. Prescribed displacement limits can easily be satisfied by uniformly sizing the element thickness. The result satisfying displacement constraints alone may not be the global optimum. Therefore, it is of significant importance to develop performance-based optimality criteria (PBOC) that can be incorporated in optimization algorithms to obtain the global optimum.

Liang (2001) and Liang *et al.* (2000, 2001) have developed displacement-based performance indices and PBOC for identifying a global optimal solution in an optimization process. In this chapter, the PBO method is extended to the optimal topology and shape design of continuum structures with displacement constraints. Continuum topology and shape optimization is treated as the problem of improving the performance of a continuum design domain in terms of the efficiency of material usage in resisting deformations. Two displacement-based performance indices are developed for evaluating the performance of resulting designs for plane stress continuum structures and for plates in bending in an optimization process. These performance indices are also used as termination criteria in PBO algorithms. Maximizing the performance index of a design domain is proposed as PBOC. Performance indices and PBOC can be incorporated in any continuum topology and shape optimization methods to obtain optimal designs. Some of the results have been presented recently by Liang *et al.* (1999, 2000, 2001).

3.2 Performance objective for structures with displacement constraints

Continuum topology and shape optimization is to seek the optimal material distribution within a given design domain. After the finite element analysis (FEA), it is found that some parts of the initial design domain are inefficiently used. These inefficiently used portions should be removed from a continuum design domain to achieve a better design. By gradually

eliminating underutilized material from a structure, a lighter design can be generated. The performance objective is to minimize the weight of a continuum structure while maintaining constrained displacements within acceptable limits, and can be expressed in mathematical forms as follows:

$$\text{minimize} \quad W = \sum_{e=1}^{n} w_e(t) \tag{3.1}$$

$$\text{subject to} \quad u_j \le u_j^* \qquad j = 1, \ldots, m \tag{3.2}$$

$$t^{\mathrm{L}} \le t \le t^{\mathrm{U}} \tag{3.3}$$

where W is the total weight of a structure; w_e, the weight of the eth element; t, the thickness of elements; u_j, the absolute value of the jth constrained displacement; u_j^*,the prescribed limit of u_j; m, the total number of displacement constraints and n, the total number of elements in the structure. Since the thickness of a plane continuum structure has a significant effect on the structural weight and it needs to be specified by the designer in practice, it is treated as one of the design variables. However, simultaneous topology and sizing optimization will make the optimization problem rather complicated. Moreover, in many practical design problems, the thickness of structures needs to be uniform. Therefore, only uniform sizing of the element thickness is considered in the PBO method for design of continuum structures with maximum stiffness performance.

3.3 Element removal criteria based on virtual strain energy density

In stress-based topology optimization, lowly stressed elements are systematically removed from a continuum design domain to generate a fully stressed topology design. For structures under displacement constraints, elements with the least effect on the change in constrained displacements should be listed as candidates for elimination. The resulting structure will be the stiffest design at minimum weight with respect to the specific displacements. The main point is to find out which element should be removed from the structure. This can be done by undertaking a design sensitivity analysis on the constrained displacements with respect to element removal. From the design sensitivity analysis, element removal criteria can be established for element removal and used in PBO algorithms. The derivation of the element removal criteria for continuum structures with displacement constraints is described here.

The equilibrium equation for a static structure in the FEA is expressed by

$$[K]\{u\} = \{P\} \tag{3.4}$$

If the eth element is eliminated from a structure discretized into finite elements, the stiffness and displacements of the structure will change accordingly, and Eq. (3.4) can be rewritten as

$$([K] + [\Delta K])(\{u\} + \{\Delta u\}) = \{P\} \tag{3.5}$$

in which $[\Delta K]$ is the change in the stiffness matrix and $\{\Delta u\}$, the change in the nodal displacement vector. The change in the stiffness matrix can be expressed by

$$[\Delta K] = [K_r] - [K] = -[k_e] \tag{3.6}$$

where $[K_r]$ is the stiffness matrix of the resulting structure and $[k_e]$, the stiffness matrix of the eth element. The change in displacement vector due to element elimination can be obtained approximately from Eqs (3.4) and (3.5) by neglecting the higher order terms as

$$\{\Delta u\} = -[K]^{-1}[\Delta K]\{u\} \tag{3.7}$$

It is assumed that the constraint is imposed on a specific displacement u_j. The change in the specific displacement due to an element removal needs to be evaluated. In order to extract the required displacement component, a virtual unit load is applied at u_j and acting in the direction of the displacement component. By multiplying Eq. (3.7) with the virtual unit load vector $\{F_j\}^{\mathrm{T}}$, in which only the components corresponding to the jth constrained displacement are equal to unity and all the others are equal to zero, the change in the constrained displacement can be obtained approximately as

$$\Delta u_j = -\{F_j\}^{\mathrm{T}}[K]^{-1}[\Delta K]\{u\} = -\{u_j\}^{\mathrm{T}}[\Delta K]\{u\} = \{u_{ej}\}^{\mathrm{T}}[k_e]\{u_e\} \tag{3.8}$$

where $\{u_j\}^{\mathrm{T}}$ is the nodal displacement vector of the structure under the virtual unit load; $\{u_{ej}\}^{\mathrm{T}}$, the nodal displacement vector of the eth element under the virtual unit load and $\{u_e\}$, the nodal displacement vector of the eth element under real loads. It is seen from Eq. (3.8) that the change in the constrained displacement due to the elimination of the eth element can be calculated approximately by the virtual strain energy of the eth element, which is denoted as

$$s_e = \{u_{ej}\}^{\mathrm{T}}[k_e]\{u_e\} \tag{3.9}$$

The element virtual strain energy can be calculated at the element level from the results of the FEA. To obtain the maximum stiffness design at minimum weight, it is obvious that elements with the lowest virtual strain energies should be eliminated systematically from a continuum design domain being

optimized. In other words, elements that have the least effect on the change in constrained displacements are eliminated from the design domain to achieve the performance objective.

The lowest virtual strain energies of elements are used as the element removal criteria for continuum structures, which are discretized into equal size finite elements. In design situations where a continuum structure is divided into different size elements, element weights will differ from each other. Considering two elements with the same virtual strain energy, eliminating the element with a larger weight will result in a lighter design while the changes in specific displacements are the same. Therefore, in order to obtain the most efficient design, the virtual strain energy per unit weight of an element, which is defined as the element virtual strain energy density (VSED), should be used as the element removal criteria. The VSED of the eth element is denoted as

$$\psi_e = \frac{|s_e|}{w_e} \tag{3.10}$$

where $|s_e|$ is the absolute value of s_e. If the material density is uniformly distributed in a continuum design domain, the volume of an element can be used in Eq. (3.10) for calculating the element VSED.

For a structure subject to multiple displacement constraints under multiple load cases, the VSED of the eth element can be evaluated by using the weighted average approach as

$$\psi_e^m = \sum_{l=1}^{p} \sum_{j=1}^{m} \beta_j \psi_e \tag{3.11}$$

where the weighting parameter β_j is defined as u_j^l / u_j^{l*}, which is the ratio of the jth constrained displacement to the prescribed limit under the lth load case, and p, the total number of load cases. It is noted that the absolute values of displacements are used in Eq. (3.11). If the constrained displacement is far from its prescribed limit, it will be less critical in the optimization process.

It should be noted that the VSEDs of elements are approximately evaluated by neglecting the higher order terms in the sensitivity analysis. Therefore, only a small number of elements with the lowest VSEDs are allowed to be removed from a structure at each iteration in order to obtain a sound optimal design. The element removal ratio (R) for each iteration is defined by the ratio of the number of elements to be removed to the total number of elements in the initial structure and is kept constant during the whole optimization process. The accuracy of an optimal solution is obviously improved by using a smaller element removal ratio but the computational cost will considerably be increased. The element removal ratio used

in the PBO method is similar to the step size employed in conventional OC methods (Morris 1982; Rozvany 1989).

3.4 Checkerboard patterns

3.4.1 Causes of checkerboard patterns

Checkerboard patterns are commonly present in the optimized topologies of continuum structures generated by numerical structural optimization methods. Figure 3.1 shows a typical checkerboard patterns in a continuum structure. The checkerboard material distribution patterns are not optimal structures, but are numerical anomalies, which are caused by the errors in the displacement-based finite element formulation, as shown by Díaz and Sigmund (1995), and Jog and Haber (1996). The presence of checkerboard pattern leads to difficulty in interpreting and manufacturing optimal structures. It is desirable to suppress the formation of checkerboard patterns in topology optimization of continuum structures.

Many researchers have undertaken researches into the causes of checkerboard pattern formation in topology optimization. Jog *et al.* (1994) showed that the basic functions for both displacement and material density fields have a significant effect on the solution when using the homogenization-based optimization (HBO) method. No stable solutions could be achieved if higher order elements with a low order bilinear density field were used. Díaz and Sigmund (1995) have conducted a path test of four-node elements used in the compliance optimization problem of continuum structures. Their study indicates that the checkerboard material distribution patterns are locally stiffer than any other material distribution patterns in the design domain. Jog and Haber (1996) addressed the instability problem of finite element models for topology and shape optimization. This instability problem appears in the form of checkerboard patterns. The cause of this problem is numerical rather than physical in nature.

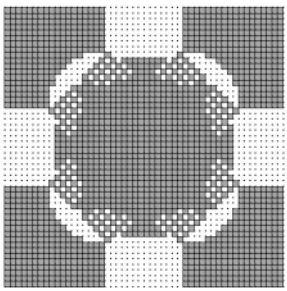

Figure 3.1 Optimal topology with checkerboard patterns.

Various methods for suppressing the formation of checkerboard patterns have been suggested. Jog and Haber (1996) suggested that either using higher order finite elements or modifying the functional of an finite element model could prevent the formation of checkerboard patterns from occurring in optimal continuum structures. However, the use of higher order elements will significantly increase the computational cost due to the increase in the degrees of freedom of the structure. The perimeter control approach has been applied to the elimination of checkerboard patterns (Beckers 1999). In this approach, a constraint on the perimeter of the boundaries of a continuum structure is introduced in the optimization problem formulation. The perimeter control method can also eliminate the mesh dependency of the optimal solutions. Sigmund and Petersson (1998) proposed a filtering technique based on the image process to prevent checkerboard patterns and mesh dependency in topology optimization. In their method, the discretized continuum design domain is treated as a digital image, and the weighted average of strain energies over neighboring elements is used to produce a checkerboard free image. Youn and Park (1997) suggested a density redistribution method which is shown to be effective in suppressing the formation of checkerboard patterns. Fujii and Kikuchi (2000) proposed a gravity control method for eliminating checkerboard patterns in topology optimization using the HBO method. Zhou *et al.* (2001) developed a density slop control algorithm for checkerboard patterns and direct minimum member size control. Some of the methods are introduced in the subsequent sections. A simple smoothing scheme in terms of the surrounding elements' reference factors was presented by Li *et al.* (2001) for suppressing checkerboard patterns in evolutionary structural optimization.

3.4.2 Perimeter control method

In the perimeter control method, the perimeter of the boundaries of a continuum structure is constrained. The boundary perimeter of a discretized structure is determined by

$$P = \sum_{ij=1}^{k} l_{ij}\left(\sqrt{(\rho_i - \rho_j)^2 + \varepsilon^2} - \varepsilon\right) \tag{3.12}$$

where l_{ij} is the length of interface between adjacent elements i and j, ρ_i and ρ_j, the density of the ith and jth elements, respectively and ε, a small positive number that ensure the differentiability of the perimeter. The density is assumed as constant in each element. This method can be applied to topology design problems with discrete variables using dual algorithms (Beckers 1999). By incorporating perimeter control, the numerical instability problems of checkerboard patterns and mesh dependence are eliminated. This method can limit the number of holes in the optimal structure but cannot control the minimum member size.

3.4.3 The filtering technique

The filtering approach is used in density-based optimization method that employs artificial material models. In this method, the material density is treated as a design variable. The optimality condition is the uniform strain energy distribution within a continuum design domain. To prevent the formation of checkerboard patterns, a weighted average approach is used in the calculation of the filtered strain energy of an element over the neighboring elements (Sigmund 1994). The filtered strain energy of the eth element is defined as

$$c_e^f = \frac{\sum_{i=1}^{N_n} H_i c_i}{\sum_{i=1}^{N_n} H_i} \tag{3.13}$$

where c_i, is the strain energy of the ith neighboring element; H_i, the impulse response matrix and N_n, the number of neighboring elements that connect to the eth element.

3.4.4 Density slop control method

As known that checkerboard patterns are caused by the poor formulation of the finite elements used in topology optimization of continuum structures where the element densities are highly discontinuous. The local gradient of the slop of element densities can be constrained to guarantee the accuracy of the finite element formulation (Petersson and Sigmund 1998). Zhou *et al.* (2001) presented an algorithm based on the density slop control concept for checkerboard and minimum member size control in continuum topology optimization. The slop constraint for general irregular element mesh is expressed by

$$|\rho_i - \rho_j| \leq (1.0 - \rho_{\min}) D_{ij} / r_{\min} \tag{3.14}$$

where $\rho_{\min}$ is the minimum density of elements, and its default value is set to 0.1 that is interpreted as void in the final solution; D_{ij}, the distance between adjacent elements i and j, and $r_{\min}$, the predetermined minimum member size of radius, $r_{\min} = d_{\min}/2$. The default value of $\rho_{\min}$ ensures that whenever an element k has the density of 1.0, the size of the member connected to this element is not less than $d_{\min}$. It is noted that if the element k is close to the boundary of the structure, the member size can be between $d_{\min}/2.$ and $d_{\min}$. To improve the computational efficiency, the adaptive lower bounds are imposed on the density as follows:

$$\rho_i \geq \max \lfloor \rho^L, \rho_k - (1.0 - \rho_{\min}) D_{ij} / r_{\min} \rfloor \tag{3.15}$$

where ρ^{L} is the lower limit of the density and ρ_k, the density of the element k at previous iteration that has the maximum value among all elements which are adjacent to the element i. An iteration scheme is implemented to achieve a clear zero–one material distribution.

3.4.5 Checkerboard suppression algorithm in PBO

Checkerboard patterns are also observed in optimal structures produced by the PBO method when four-node elements are employed in the FEA. This is mainly due to the unstable nature of the four-node elements. It is found that using higher order elements such as eight-node elements in PBO can effectively prevent the formation of checkerboard patterns. However, it will significantly increase the computational cost especially when dealing with practical structures simulated using very fine finite elements. A simple checkerboard suppression algorithm has been incorporated in the PBO method. In this algorithm, the nodal VSEDs of an element are calculated by averaging the VSEDs of the neighboring elements as follows:

$$\xi_{nd} = \frac{1}{M}\sum_{e=1}^{M} \psi_e \tag{3.16}$$

in which ξ_{nd} is the nodal VSED and M, the number of elements that connect to that node. The VSED of each element can be recalculated from the nodal strain energy densities at the nodes of the element as

$$\xi_e = \frac{1}{Q}\sum_{nd=1}^{Q} \xi_{nd} \tag{3.17}$$

where ξ_e is the recalculated VSED of the eth element and Q, the number of nodes in the element. Element removal criteria are now based on the recalculated VSED of elements. A small number of elements with the lowest values of ξ_e are deleted from the design domain in a performance optimization process.

It should be noted that the VSED (ψ_e) of an element used in Eq. (3.16) is for a single displacement constraint and load case. For structures subject to multiple displacement constraints and multiple load cases, ψ_e^{m} should be used in Eq. (3.16). This is to ensure that checkerboard is controlled before any elements are removed. This simple checkerboard control algorithm proposed here can effectively suppress the formation of checkerboard patterns as demonstrated by the examples presented in this chapter.

3.5 Displacement-based performance indices

Topology and shape optimization based on the element removal concept is a design problem of maximizing the performance of a continuum structure in

terms of the efficiency of material usage in resisting deformations. To obtain a minimum-weight optimal design, the performance of the resulting topology in an optimization process must be evaluated by using the performance index. Stress-based performance indices have been derived on the basis of a scaling design procedure in Chapter 2. The concept of the design scaling can also be applied to the formulation of displacement-based performance indices.

3.5.1 Performance index for plane stress structures

Consider a continuum structure under plane stress conditions. Since the stiffness matrix of a plane stress continuum structure is a linear function of the thickness of elements, the element thickness can be uniformly scaled to keep the critical constraint at the constraint surface. In order to satisfy the displacement constraints imposed on a structure, the actual design needs to be scaled by the following scaling factor:

$$\varphi_{\mathrm{ds}} = \frac{u_j}{u_j^*} \tag{3.18}$$

where u_j is the absolute value of the jth constrained displacement that is the most critical in the design. By scaling the initial design with respect to the most critical constrained displacement, the scaled weight of the initial structure can be represented by

$$W_0^{\mathrm{s}} = \left(\frac{u_{0j}}{u_j^*}\right) W_0 \tag{3.19}$$

where W_0 is the actual weight of the initial structure and u_{0j}, the absolute value of the most critical constrained displacement in the initial structure under applied loads. In a similar manner, the current structure can be scaled to satisfy the prescribed displacement limit at each iteration in the optimization process. The scaled weight of the current structure at the ith iteration is calculated by

$$W_i^{\mathrm{s}} = \left(\frac{u_{ij}}{u_j^*}\right) W_i \tag{3.20}$$

in which u_{ij} is the absolute value of the most critical constrained displacement in the current structure at the ith iteration under the applied loads and W_i, the actual weight of the current structure at the ith iteration.

The performance index of the resulting structure at the ith iteration is determined by

$$\mathrm{PI}_{\mathrm{ds}} = \frac{W_0^{\mathrm{s}}}{W_i^{\mathrm{s}}} = \frac{(u_{0j}/u_j^*)W_0}{(u_{ij}/u_j^*)W_i} = \frac{u_{0j}W_0}{u_{ij}W_i} \tag{3.21}$$

It can be seen from Eq. (3.21) that the performance index is a dimensionless number, which measures the performance of a structural topology or shape in terms of the material efficiency in resisting deformations. It depends on the topology or shape but not on the scale of a structure. The performance index of the initial structure is equal to unity. The performance of a structural topology or shape is gradually improved when elements with the lowest VSEDs are systematically removed from the structure. The displacement limit (u_j^*) is consequently eliminated from Eq. (3.21). This means that an optimal topology or shape for the minimum-weight design of a continuum structure is unique for any prescribed displacement limits.

For a plane stress structure subject to multiple displacement constraints and multiple load cases, the performance index of the resulting structure at each iteration can be calculated by using the most critical constrained displacement of the structure under the most critical load case in the optimization process. This is to ensure that the optimal design obtained satisfies all design constraints and will perform well in all loading environments in its design service life.

3.5.2 Performance index for plates in bending

Plate structures are commonly used as structural systems in engineering practice. Research work on the optimal topology and shape design and reinforcement of plates has been undertaken by many researchers (Olhoff, 1975; Cheng and Olhoff 1982). Their results show that there are an infinite number of fine ribs in the optimal reinforcement of plates. Atrek (1989) used a material removal procedure to generate optimal topologies of bending plates subject to displacement constraints. The HBO method has been applied to the topology optimization of plates in bending (Tenek and Hagiwara 1993).

The PBO method can also be applied to plates in bending. In the PBO method, the design objective is to seek the stiffest topology of a plate in bending at minimum weight. Unlike plane stress problems, the bending stiffness of a plate is not a linear function of the plate thickness. As a result, the performance index proposed for plane stress structures cannot be used for plates in bending. However, the scaling design concept used in deriving performance indices for plane stress structures can be adopted for plates in bending if an appropriate-scaling factor is found.

To obtain the best topology for the design of a plate in bending, the thickness of the plate is treated as one of the design variables. The plate thickness is uniformly scaled to satisfy displacement constraints. By scaling the design, the scaled thickness of the plate is represented by

$$t^{\mathrm{s}} = \varphi_{\mathrm{dp}} t \tag{3.22}$$

where φ_{dp} is the scaling factor which is the same for all elements. The material elastic constants of an element are written in matrix form as

$$[D_e] = \frac{t^3}{12}\begin{bmatrix} \frac{E}{1-\nu^2} & \frac{E\nu}{1-\nu^2} & 0 \\ \frac{E\nu}{1-\nu^2} & \frac{E}{1-\nu^2} & 0 \\ 0 & 0 & \frac{E}{2(1+\nu)} \end{bmatrix} \tag{3.23}$$

Equation (3.23) can be denoted as

$$[D_e] = t^3[C] \tag{3.24}$$

in which E is the Young's modulus and ν, Poisson's ratio. The material elastic constants of an element can be written in term of the scaled design variable as

$$[D_e] = \left(\frac{t^s}{\varphi_{dp}}\right)^3 [C] = \frac{1}{\varphi_{dp}^3}[D_e^s] \tag{3.25}$$

where $[D_e^s]$ is the scaled material elastic constant matrix of an element. The equilibrium equation for a plate can be written in the FEA as

$$\frac{1}{\varphi_{dp}^3}[K^s]\{u\} = \{P\} \tag{3.26}$$

in which $[K^s]$ is the stiffness matrix of the scaled plate that is determined by the scaled design variable t^s; $\{u\}$, the actual nodal displacement vector and $\{P\}$, the nodal load vector. The equilibrium equation for the scaled plate is expressed by

$$[K^s]\{u^s\} = \{P\} \tag{3.27}$$

From Eqs (3.26) and (3.27), the scaled displacement vector can be obtained as

$$\{u^s\} = \frac{1}{\varphi_{dp}^3}\{u\} \tag{3.28}$$

It can be seen from Eqs (3.22) and (3.28) that when the thickness of the plate is reduced by a factor φ_{dp}, the deflections will increase with a factor of $1/\varphi_{dp}^3$. In order to satisfy the displacement limit, the actual design needs

to be scaled by

$$\varphi_{\mathrm{dp}} = \left(\frac{u_j}{u_j^*}\right)^{1/3} \tag{3.29}$$

By using the above scaling factor, the design can be scaled to keep the most constrained displacement active after each iteration in the optimization process. Consequently, the best feasible constrained design can be obtained from the history of the reduction in the weight of a plate. The performance index of a plate in bending at the *i*th iteration is defined as the ratio of the scaled weight of the initial design to the scaled weight of the current design at the *i*th iteration, and is expressed by

$$\mathrm{PI}_{\mathrm{dp}} = \frac{W_0^{\mathrm{s}}}{W_i^{\mathrm{s}}} = \frac{(u_{0j}/u_j^*)^{1/3} W_0}{(u_{ij}/u_j^*)^{1/3} W_i} = \left(\frac{u_{0j}}{u_{ij}}\right)^{1/3} \frac{W_0}{W_i} \tag{3.30}$$

For a plate structure in bending under multiple displacement constraints and multiple load cases, the performance index of the resulting plate at each iteration can be calculated by using the most critical constrained displacement of the plate under the most critical load case in the optimization process. This is to ensure that the optimal plate structure obtained satisfies all design constraints and can operate in all loading environments in its design service life.

3.6 Performance-based optimality criteria

By removing a small number of elements with the lowest VSEDs from a discretized continuum structure, a more uniform distribution of element VSEDs in the resulting structure can be achieved. The uniformity of element VSEDs in skeletal structures has been used as an OC, which can be derived on the basis of the Kuhn-Tucker condition (Morris 1982; Rozvany 1989). In conventional OC methods (Rozvany 1989), the OC is derived for the dominant type of constraint imposed on a structure, and used to develop a recurrence relation. This recurrence relation is then used to update design variables so that the initial design is moved towards an optimum, which satisfies the OC.

However, the uniformity of the virtual strain energy densities of elements in a continuum structure may not be achieved in some cases even if constrained displacements are active. This means that a minimum-weight optimal design is not necessarily a design in which the distribution of the element VSEDs is absolutely uniform. This is especially true for practical design problems. Therefore, the uniformity of element VSEDs cannot be used as a termination condition in continuum topology optimization algorithms for determining optimal designs. To obtain the global optimum, new type PBOC must be developed and incorporated into continuum topology

optimization methods. PBOC that form the core of the PBO method for displacement constraints are derived in this section for the optimization problems of plane stress structures and plate structures in bending.

It is seen from the performance index formula that the performance index is inversely proportional to the weight of the current structure. Therefore, the performance objective can be achieved by maximizing the performance index in an optimization process. The PBOC for plane stress continuum structures subject to displacement constraints can be stated as

$$\text{maximize} \quad \text{PI}_{\text{ds}} = \frac{u_{0j} W_0}{u_{ij} W_i} \tag{3.31}$$

The scaling design concept allows for the structural response (displacement) to be entered into the performance index formula for plates in bending. In other words, the performance index is a measure of structural responses and the reduction in the weight of plates in an optimization process, and thus quantifies the performance of a plate in bending. Therefore, the PBOC for bending plates subject to displacement constraints can be stated as

$$\text{maximize} \quad \text{PI}_{\text{dp}} = \left(\frac{u_{0j}}{u_{ij}}\right)^{1/3} \frac{W_0}{W_i} \tag{3.32}$$

The PBOC can be achieved by gradually removing elements with the lowest VSEDs from the plate discretized into finite elements.

It is noted that uniformly changing the element thickness does not affect the topology of a continuum structure and the performance index, but significantly influences the weight of the structure and the constrained displacements. As a result, the thickness of elements is not changed in the FEA at each iteration. Displacement limits are usually set to large values in order to obtain the optimal design, which can then be sized to satisfy the actual displacement limits.

3.7 Performance characteristics of structures with displacement constraints

The PBO method for continuum structures with displacement constraints allows for lowly strained elements to be systematically removed from a continuum structure to improve its performance of the structure. The weight of the structure being optimized is gradually reduced due to element elimination while constrained displacements are increased accordingly. The PBO technique is capable of finding the performance characteristics of a continuum structure with displacement constraints. In Chapter 2, the performance characteristics of fully stressed optimal designs are represented by the weight and maximum von Mises stresses within a structure. For stiffness

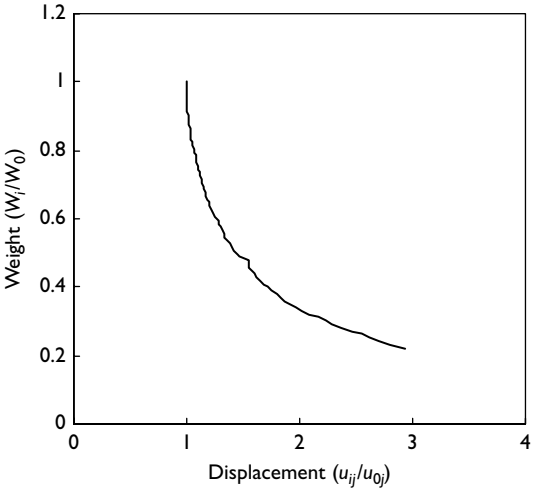

Figure 3.2 Performance characteristic curve for structures with displacement constraints.

design, the performance characteristics can be expressed by the weight of a structure and constrained displacements imposed on the structure. Performance characteristics are valuable to the structural designer. They not only indicate whether an optimized design is feasible but also measure the success of the optimized design. A typical performance characteristic curve generated by the PBO technique is shown in Figure 3.2. Points on the curve are the performance response values for a prescribed performance level. A design with performance below this curve is not feasible because the design made by that amount of materials will not maintain the constrained displacements within the prescribed limits. A structure with performance above this curve is obviously over-designed. Structural optimization techniques can be applied to over-designed structures to substantially improve their performance.

3.8 Performance optimization procedure

The performance optimization process for plane stress problems is basically the same as that for plates in bending, except that different performance indices are used in the optimization algorithms to evaluate the performance of resulting designs. The performance optimization process includes modeling of the initial design, FEA, performance evaluation, element removal, checking model connectivity and maintaining symmetry of resulting design under symmetrical conditions. A flowchart is given in Figure 3.3 to illustrate the PBO procedure for topology and shape design of continuum structures

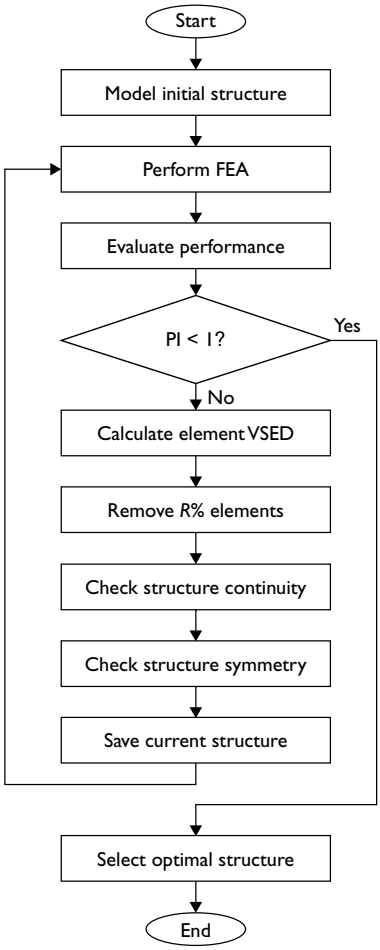

Figure 3.3 Flowchart of performance optimization procedure for structures with displacement constraints.

subject to displacement constraints. The optimization procedure is also summarized as follows:

1 Model the initial design domain with applied loads, material properties and boundary conditions. Elements around the applied loads are usually treated as the nondesign region and are not removed in the optimization process.
2 Carry out a linear elastic FEA on the structure.
3 Evaluate the performance of resulting topology or shape using Eq. (3.21) for plane stress structures and Eq. (3.30) for plates in bending. The most

critical constrained displacement of the structure under all load cases is used in the calculation of the performance index.
4 Calculate the VSEDs of elements for each loading case.
5 Eliminate a small number of elements with the lowest VSEDs from the design domain. In topology optimization, underutilized elements can be removed from the interior of a structure as well as its boundaries. However, in shape optimization, elements can only be eliminated from the boundaries of a structure.
6 Check topology/shape connectivity. It is assumed that two elements are connected together if they have at least one common edge. Any element that is not connected with other elements is considered as a singular element, and is removed from the model.
7 Maintain the symmetry of resulting structure under initially symmetrical geometry and loading conditions. It may be necessary to remove extra elements from the structure to maintain the symmetry.
8 Save model data for the current structure.
9 Repeat steps 2–8 until the performance index is less than unity.
10 Plot the performance index history and select the optimal topology or shape.

It is worth noting that the optimal design produced by the PBO method depends on the element removal ratio, which is similar to the step size used in the conventional OC method (Rozvany 1989). The smooth convergence of the performance index to the maximum value may not be guaranteed in the optimization process. The prescribed tolerance for the relative change in the performance index cannot be used as a termination criterion in an optimization procedure. If the performance index is less than unity, the performance of the corresponding structure is less than that of the initial structure. Therefore, the performance optimization process can be terminated when the performance index is less than unity. This can ensure that the optimal design that corresponds to the maximum performance index is obtained in the optimization process. It is also possible that the performance index is kept constant in later iterations. In such situations, the optimization process can be terminated. In order to continue the optimization process, displacement limits must be set to large values that allow for the performance index to be less than unity. Scaling the thickness of the optimal design obtained can easily satisfy actual displacement limits.

3.9 Element addition and deletion schemes

3.9.1 Element addition and deletion criteria

The PBO algorithm presented in previous sections has the ability to optimize a continuum structure by removing inefficient material from the structure

while the deformations of the structure are maintained within prescribed limits. The method works by specifying an initial continuum design domain that is big enough to cover the expected optimal structure. The initial design domain specified is usually over-designed for given loading and support environments. By gradually removing inefficient portions from the design domain, an innovative optimal topology or shape can be obtained. The optimal design is based on the lightweight and high stiffness performance criteria. In practice, some structures deflect excessively due to overloaded or other reasons and need to be strengthened by adding structural members. The evolutionary optimization method has been used to achieve optimal designs of continuum structures by adding and removing elements (Yang *et al.* 1998). In order to apply the PBO technique to such design situations, the PBO algorithm is modified to allow material to be added and deleted simultaneously.

The material addition and deletion criteria can be derived on the basis of design sensitivity analysis on the changes in constrained displacements with respect to material addition and deletion, as discussed in Section 3.3. Consider a continuum structure discretized into finite elements. When an element such as the eth element is deleted or added, the change in the displacement u_j at a specific node can be evaluated by

$$\Delta u_j = \pm\{u_{ej}\}^{\mathrm{T}}[K_e]\{u_e\} \tag{3.33}$$

where $\{u_{ej}\}^{\mathrm{T}}$ is the displacement vector of the eth element due to the virtual unit load that is applied at the node where the displacement constraint u_j^* is imposed; $[K_e]$, the stiffness matrix of the eth element and $\{u_e\}$, the displacement vector of the eth element under the real loads. The sign "$\pm$" is for deleted and added elements.

It is noted that the change in the specific displacement due to element addition and deletion can be calculated by the element virtual strain energies. The VSED (ψ_e) of an element, which is defined as the virtual strain energy per unit weight, is a measure of the contribution of the added or deleted element to the stiffness performance of a structure. The element deletion and addition criteria can be stated as that elements with the smallest values of ψ_e are removed from a structure while elements with the largest values of ψ_e are added to the structure to improve the performance of the structure.

To calculate the VSEDs of potential added elements, the displacements of $\{u_{ej}\}^{\mathrm{T}}$ and $\{u_e\}$ are required. A fictitious displacement field is established to extract these displacements for added elements. It is noted that a bilinear displacement function is used in four-node square elements. Figure 3.4 shows a portion of a continuum structure modeled by four-node elements. Elements in white color are potential added elements whose material property number is given a zero value. These potential added elements can be added to the boundaries of the structure as illustrated in Figure 3.4. The potential added elements are classified into three types such as E2, E3 and E4, according to

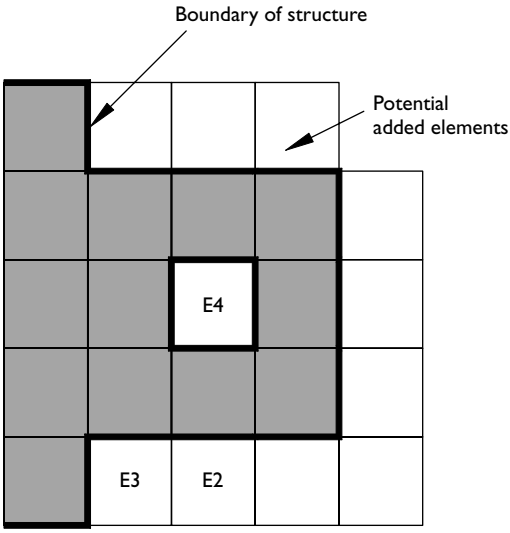

Figure 3.4 Types of potential added elements.

the number of nodes whose displacements are known. This means that the element type E2 has known displacements at two nodes. The displacement varies linearly along the edge of an element, the unknown displacements at nodes can be easily determined for element types E2 and E3.

Another way of adding elements to a structure is to attach potential elements to the free edges of the eth element with the largest values of ψ_e. Using this method, the calculation of the VSEDs for potential added elements is avoided. The added elements strengthen the existing structure to improve its stiffness performance.

The modification of a structure is based on the performance of the structure. If an initial structure selected by the user occupies only a small portion of the maximum design domain, the deformations of the initial structure will excess the displacement limits so that elements are needed to be added to the structure to strengthen the structure. The initial structure is growing bigger and bigger by gradually adding elements. After a structure occupies a certain part of the maximum design domain, elements can be added and eliminated simultaneously according to the levels of element VSEDs.

3.9.2 Optimization algorithm

The performance-based optimal design can be achieved by applying the PBO algorithms that allow efficient elements to be added to a structure and

inefficient elements to be removed from the structure. Both schemes of adding and deleting elements aim at the same goal of improving the performance of a structural topology or shape. The performance optimization algorithms are illustrated in a flowchart shown in Figure 3.5, and are

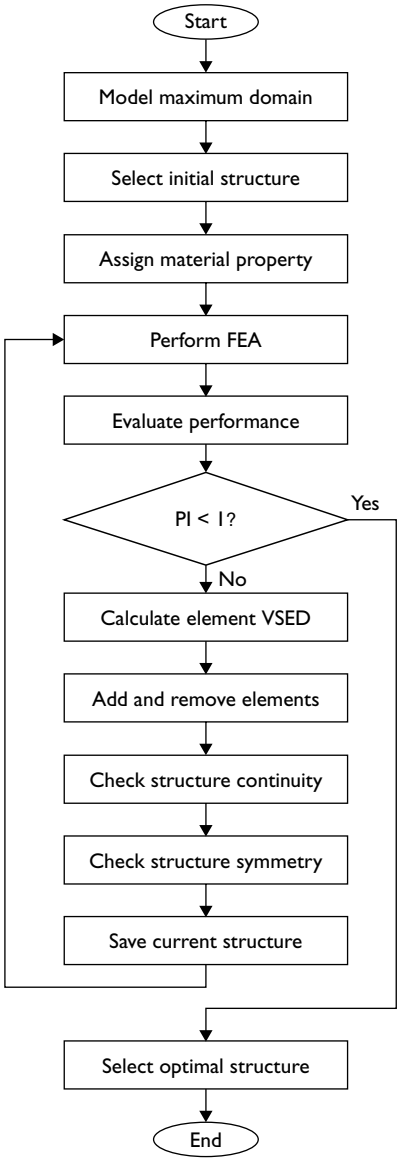

Figure 3.5 Flowchart of performance optimization procedure incorporating element addition and deletion.

summarized as follows:

1 Model a maximum design domain with fine finite elements.
2 Select the initial structure within the maximum design domain such that elements in the initial structure can connect the applied loads and the supports.
3 Assign the material property values of all elements that are not selected as the initial structure to zero.
4 Perform FEA on the structure under real loads and virtual unit loads to obtain nodal displacements.
5 Evaluate the performance of resulting structure using PI_{ds} for plane stress structures and PI_{dp} for plates in bending.
6 Identify the potential added elements of types E2, E3 and E4, and calculate their nodal displacements by linear extrapolation.
7 Calculate the VSEDs ξ_e for elements.
8 Add elements with the lowest values of ξ_e and remove element with the larger values of ξ_e.
9 Check the continuity of the resulting structure.
10 Check the symmetry of the resulting structure with an initially symmetrical condition.
11 Save model data for the current structure.
12 Repeat steps 4–11 until the performance index is less than unity.
13 Plot the performance index history and select the optimum.

3.10 Examples of plane stress structures

3.10.1 Two-bar frame structure

The PBO method for optimal topology design of continuum structures with displacement constraints is examined by solving a simple optimization problem whose optimal solution may be obtained by the analytical method. The optimization problem of a two-bar frame structure shown in Figure 3.6 is treated here for displacement constraints. If the frame structure is assumed to be a truss for the minimum-weight design, its optimal height H is obtained as $H = 2L$ using the analytical method (Rozvany 1976). This problem was considered by Suzuki and Kikuchi (1991) using the HBO method for the mean compliance minimization.

A continuum design domain that was slightly larger than the two-bar frame structure was used to derive the optimal topology of the structure as shown in Figure 3.6. A displacement constraint was imposed at the loaded point in the vertical direction, and its limit was set to a large value in order to ensure that the optimum was included in the optimization process. The design domain was divided into a 32×72 mesh using four-node plane stress elements. The left edge of the design domain was fixed. A concentrated load

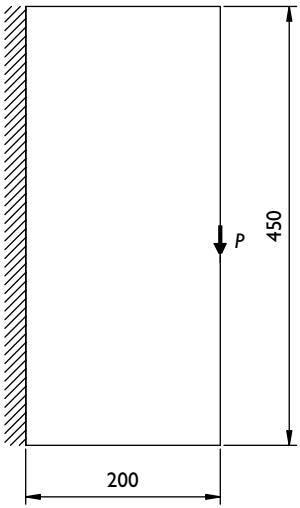

Figure 3.6 Design domain for the two-bar frame structure.

of 200 N was applied to the center of the free end. The values of Young's modulus $E = 200\,\text{GPa}$, the Poisson's ratio $\nu = 0.3$ and the thickness of elements $t = 1\,\text{mm}$ were used in the FEA. Plane stress conditions were assumed. The element removal ratio of 1 percent was adopted in the optimization process.

The performance index history of the two-bar frame structure is depicted in Figure 3.7. When elements with the lowest VSEDs were eliminated from the design domain, the performance index gradually increased from unity to the maximum value of 2.08. It is seen from Figure 3.7 that the performance index may jump in the optimization process. This is because the element removal ratio of 1 percent used in the optimization process was still high. A smoother solution could be obtained by using a smaller removal ratio such as 0.5 percent for this two-bar frame structure as shown in Figure 3.8, but the computational time was approximately double of that using a removal ratio of 1 percent. The maximum performance index of the optimal two bar frame structure produced by the PBO method employing an element removal ratio of 0.5 percent was 2.05. This indicates that these two element removal ratios do not have a significant effect on the performance of optimal topologies produced by the PBO method. Therefore, it is suggested that the element removal ratio of 1 percent can be used in the design of practical engineering optimization problems with sufficient accuracy and efficiency.

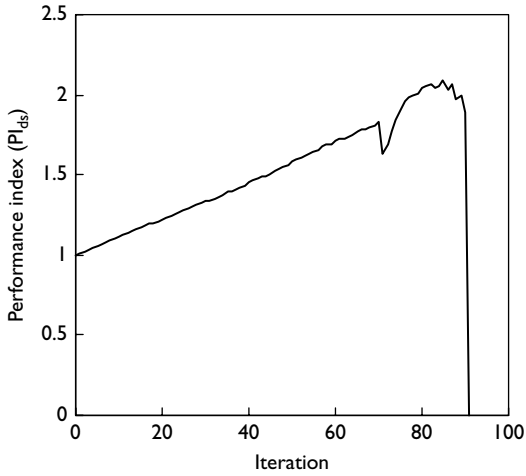

Figure 3.7 Performance index history of the two-bar frame structure ($R = 1$ percent).

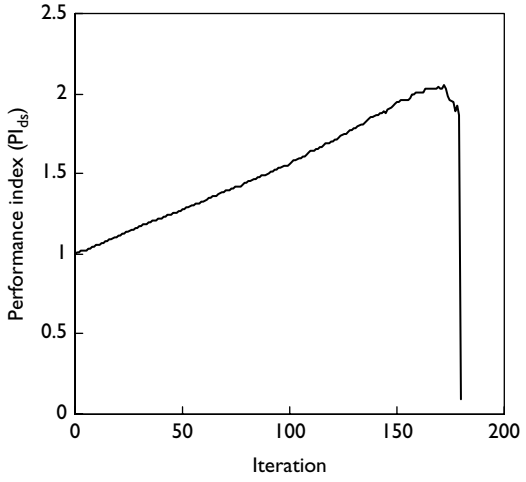

Figure 3.8 Performance index history of the two-bar frame structure ($R = 0.5$ percent).

The performance characteristic curve of the two-bar structure with a displacement constraint imposed at the loaded point in an optimization process using the removal ratio of 0.5 percent is presented in Figure 3.9. It can be observed from Figure 3.9 that the weight of the structure in an

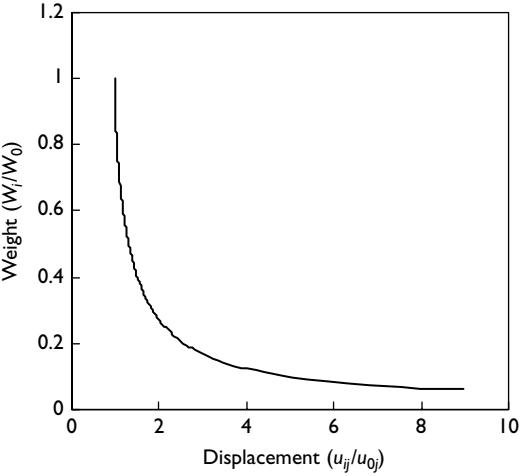

Figure 3.9 Performance characteristic curve for the two-bar frame structure.

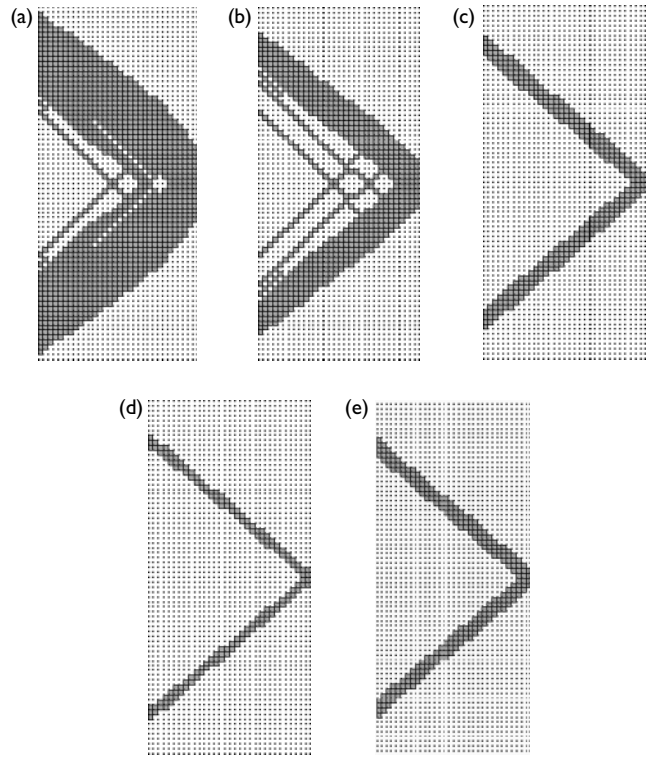

Figure 3.10 Optimization history of the deep cantilever beam: (a) at iteration 50; (b) at iteration 70; (c) optimum ($R = 1$ percent); (d) at iteration 90; (e) optimum ($R = 0.5$ percent).

Table 3.1 Material volumes required at different iterations for various displacement limits

u_j^* (mm)	V_0^s (mm^3)	V_{50}^s (mm^3)	V_{70}^s (mm^3)	V_{opt}^s (mm^3)	V_{90}^s (mm^3)	$PI_{s,max}$
1.0	370	234	203	178	195	2.08
1.5	247	156	135	119	130	2.08
2.0	185	117	102	89	98	2.08

optimization process reduced with an increase in its constrained displacement. The actual weight of the optimal structure (without scaling with respect to the displacement limit) is only 9.6 percent of that of the initial structure while its maximum deflection is 5.05 times that of the initial structure, as shown in Figure 3.9. To satisfy the same displacement limit, however, the optimal structure has resulted in material volume reduction of 51 percent in comparison with the scaled initial structure.

The topology optimization history is shown in Figure 3.10. The optimal topology evolved to a two-bar truss-like structure whose optimal height is two times of its span. Moreover, it can be observed from Figure 3.10 that optimal topologies obtained using different element removal ratios are almost the same. This proves that the PBO method can generate reliable optimal topology designs of continuum structures with displacement constraints. As discussed previously, the performance of an optimal topology does not depend on the actual values of displacement limits. This is illustrated in Table 3.1 where a comparison of material volumes required for the initial design and four topologies shown in Figure 3.10(a)–(d) for various displacement limits is made. It can be seen from the table that the volumes of optimal topologies are always less than those of other topologies. It also shows that the maximum performance indices are the same for different displacement limits.

3.10.2 Effect of geometry constraints

The design spaces of practical structures are often limited and significantly influence the performance of final optimal designs. This example is to investigate the effects of height constraints imposed on the initial design domains of Michell type structures with displacement constraints on the performance of optimal topologies. In addition, the optimal topology obtained by the PBO method is validated by the classical solution given by Michell (1904).

Figure 3.11 depicts the design domain for Michell type structures with fixed supports and various height constraints. The span of the structures

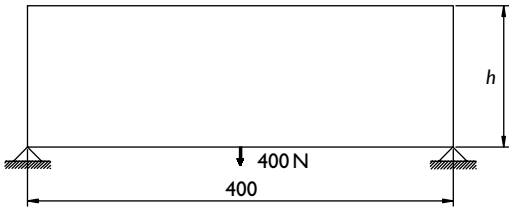

Figure 3.11 Design domain of Michell type structures with height constraints.

is 400 mm while the height of the structure is 200, 100, 50 and 33 mm, respectively. The span/height ratios of all structures are 2, 4, 8 and 12. The design domains with the span/height ratios of 2, 4, 8 and 12 were discretized into 100×50, 100×25, 100×13 and 100×9 meshes, respectively. The Young's modulus $E = 200\,\text{GPa}$, Poisson's ratio $\nu = 0.3$ and the thickness of elements $t = 2$ mm were used for all cases. A point load $P = 400$ N was applied to the structure. A displacement constraint imposed at the loaded point in the vertical direction was set to large value in the analysis. The element removal ratio of 1 percent was used in the optimization process.

Optimal topologies generated by the PBO method are shown in Figure 3.12 for four design situations. The continuum structure with a span/height ratio of 2 is the well-known Michell structure with fixed supports. The optimal topology produced by the PBO method as shown in Figure 3.12(a) agrees extremely well with the analytical solution derived by Michell (1904). The maximum performance indices of the structures with span/height ratios of 2, 4, 8 and 12 are 1.89, 1.67, 1.73 and 1.58, respectively. It is observed that increasing the height constraints imposed on the initial design domains does not necessarily increase the performance index of an optimal structure derived from them. This is because the performance index for each structure is defined by the scaled weight of the initial design and the current design at each iteration. Therefore, the performance of optimal structures with different heights cannot be ranked by comparisons with their performance indices. The suitable method is to compare their scaled weights or volumes with respect to the same displacement limit such as 1.0 mm imposed at the loaded point. A comparison of material volumes required for each optimal design while satisfying the same displacement performance level is given in Table 3.2. It is seen from the Table 3.2 that the material volume of the optimal design increases with the decrease in the height constraints. Therefore, the performance of the optimal topology of a structure can be improved by increasing the height of its initial design domain.

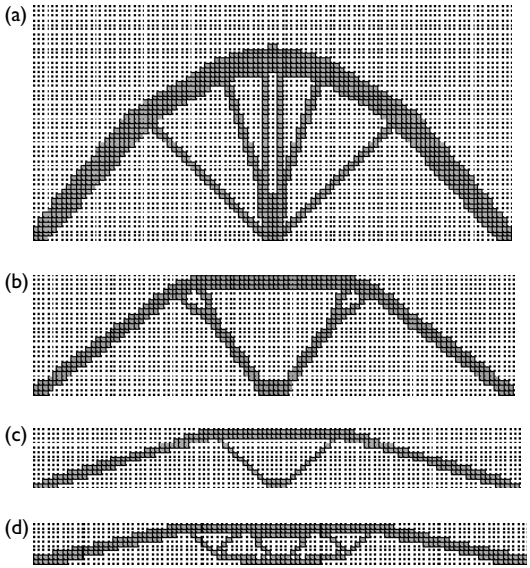

Figure 3.12 Effect of height constraints on optimal topologies: (a) $L/h = 2$, $PI_{ds} = 1.89$; (b) $L/h = 4$, $PI_{ds} = 1.67$; (c) $L/h = 8$, $PI_{ds} = 1.73$; (d) $L/h = 12$, $PI_{ds} = 1.58$.

Table 3.2 Effect of height constraints on the material volumes of optimal topologies

Height (L/h)	u_j *(mm)*	u_j^* *(mm)*	V_{opt} *(mm^3)*	V_{opt}^s *(mm^3)*
2	0.023	1.0	28 800	662
4	0.036	1.0	20 864	751
8	0.244	1.0	7138	1742
12	0.428	1.0	9125	3906

3.10.3 Multiple displacement constraints

Practical civil engineering structures are often designed for multiple displacement constraints. For example, in performance-based design, the interstory and overall drifts of a multistory building under lateral loads must be maintained within acceptable performance levels. A multistory building under lateral loads acting at each level can be treated as a structure subject to multiple displacement constraints, which are imposed at each level of the structure in the structural analysis and optimization. Moreover, engineering

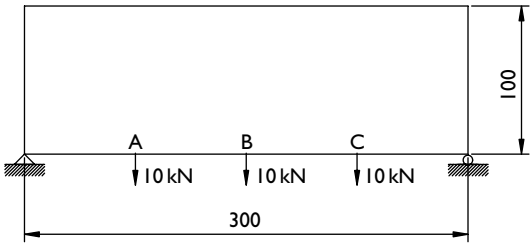

Figure 3.13 Design domain of structure with multiple displacement constraints.

structures are often subjected to many loads such as point loads. In order to generate the stiffest optimal structure, multiple displacement constraints are usually imposed at the loaded points. An example is given herein to demonstrate the effectiveness of the PBO method in dealing with continuum topology design problems subject to multiple displacement constraints.

A simply supported beam under three concentrated loads applied at points A, B and C at the same time is shown in Figure 3.13. The thickness of 5 mm was specified for the beam. The Young's modulus of material $E = 200$ GPa, and Poisson's ratio $\nu = 0.3$ were used in the analysis. Deflection constraints were imposed at point A, B and C. It was required to find an optimal structure with the minimum weight and deflections. This beam was treated as a structure with multiple displacement constraints in the performance optimization process. Three displacement constraints of the same limit were imposed at three loaded points in the vertical direction. Three virtual unit loads were also applied to the three loaded points in order to calculate the VSEDs of elements for elimination. The beam was discretized into a 96×32 mesh using four-node plane stress elements. The element removal ratio of 1 percent was used in the optimization process.

The performance characteristics of the simply supported beam subject to multiple displacement constraints are shown in Figure 3.14, where the deflection at point B was used. This characteristic curve reflects the responses of the beam in a PBO process, such as the reduction in its weight and the increase in deflections due to element removal. The actual weight of the optimal structure (without scaling to the displacement limit) is only 25.7 percent of that of the initial structure while its maximum deflection is 2.7 times that of the initial beam, as shown in Figure 3.14. The performance index history of the simply supported beam is shown in Figure 3.15. Due to symmetry, the displacements at points A and C are the same. The performance index curves shown in Figure 3.15 were obtained by using constrained displacements at points A and B in the optimization process. The maximum performance index calculated for point A was 1.46 while it was 1.43 for point B. The optimal topology that corresponds to the maximum performance index

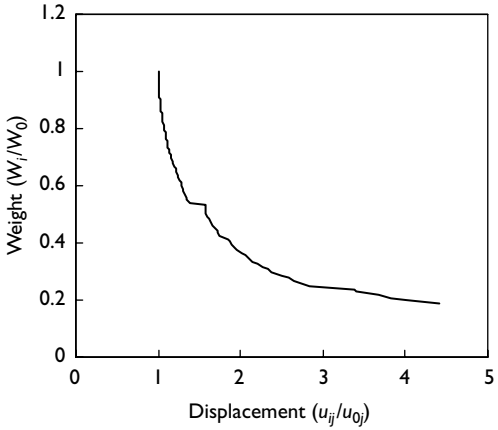

Figure 3.14 Performance characteristic curve for the structure with multiple displacement constraints.

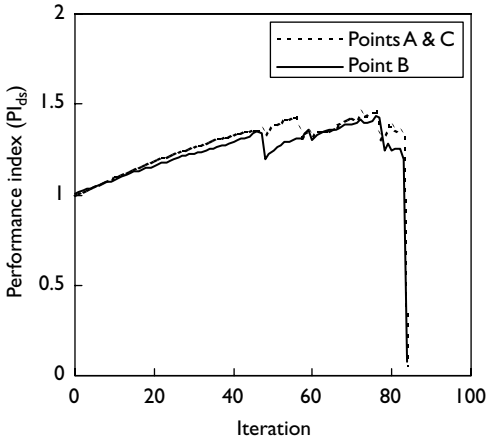

Figure 3.15 Performance index history of the structure with multiple displacement constraints.

occurred at iteration 76 for both displacement constraints. It is obvious that the material volume required for the optimal design is governed by the critical displacement constraint imposed at point B. In comparison with the scaled design of the initial structure, the PBO optimal design resulted in material volume reduction of 30 percent.

The topology optimization history of the structure subject to multiple displacement constraints is shown in Figure 3.16. The optimal topology presented in Figure 3.16(c) indicates a truss-like structure. It is observed

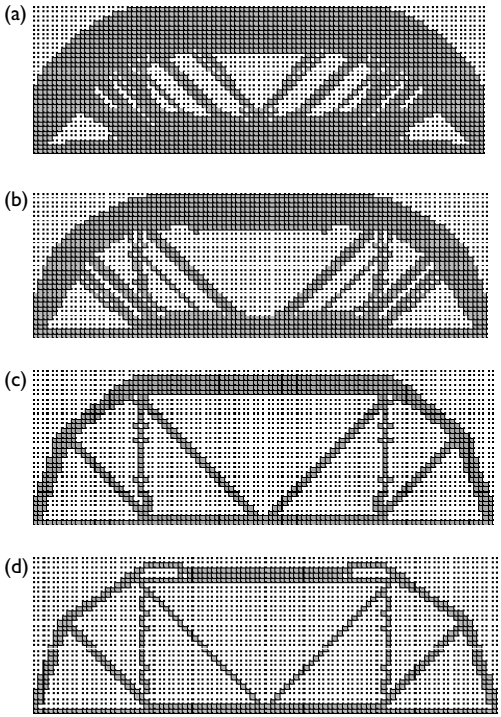

Figure 3.16 Topology optimization history of structure with multiple displacement: (a) topology at iteration 30; (b) topology at iteration 50; (c) topology at iteration 76; (d) topology at iteration 83.

that the in-plane size of members in the truss is approximately proportional to the force carried by that member since the virtual strain energy density of elements within the optimal topology is approximately uniform. The topology shown in Figure 3.16(d) is basically the same as the optimum.

3.10.4 Multiple load cases

Civil engineering structures are often subjected to different loading conditions at different times. In structural analysis, these loading conditions are treated as mutliple load cases. In current design practice, the topology of a structure under multiple load cases is selected by the designer based on his/her intuition and past experience. After undertaking a structural analysis on the structure with multiple load cases, the structure is designed for the crititcal load case. It is very difficult if not possible to obtain an optimal structure subject to multiple load cases without using automated topology optimization techniques because the load paths within the structure are extremely complicated for

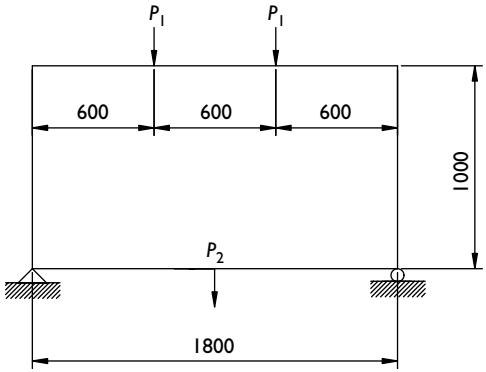

Figure 3.17 A simply supported beam under multiple load cases.

multiple load cases. The PBO technique offers an effective tool for structural designers in the design of civil engineering structures under multiple load cases. The optimal structure produced by such an optimizer can perform its normal functions in different loading environments in its service design life.

Examples are presented here to demonstrate the effectiveness of the automated PBO technique in generating optimal structures with multiple load cases. Figure 3.17 shows a simply supported continuum structure under two load cases. In load case 1, two concentrated loads (P_1) of 10 kN were applied to the top of the structure. In load case 2, a concentrated load (P_2) of 20 kN was applied at the midspan of the bottom of the structure. The span of the beam is 1.8 m while its height is 1.0 m. The beam was modeled by four-node plane stress elements and divided into a 54×30 mesh. The Young's modulus $E = 200$ GPa, Poisson's ratio $\nu = 0.3$ and the thickness of elements $t = 5$ mm were specified in the FEA. The element removal ratio of 1 percent was used in the optimization process. Displacement constraints were imposed on loaded points. The load transfer mechanism within a continuum structure varies with changes of the loading environments. To illustrate the effects of loading environments on the optimal structure, three loading situations were considered (e.g. the structure under the load case 1, the structure under load case 2 and the structure under two load cases 1 and 2).

The PBO technique was applied to the structure under three different loading environments. The performance index histories of the structure are shown in Figure 3.18. It is seen that the performance of the structure was improved by removing inefficient material from the structure under different loading conditions. The maximum performance indices of the structure under load case 1, load case 2 and the two load cases are 1.96, 1.45 and 1.46, respectively. It can be observed from Figure 3.18 that the structure under the two point loads of P_1 possesses the highest performance in terms of the material efficiency in resisting deformations than other loading conditions. The

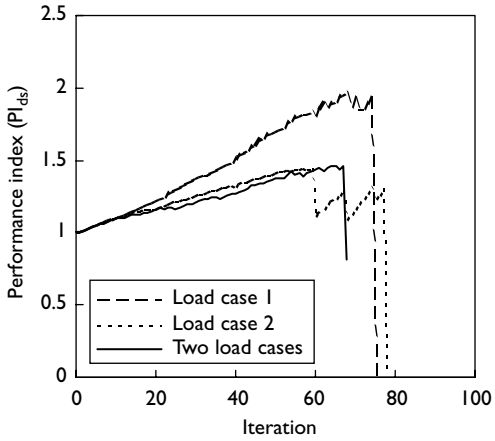

Figure 3.18 Performance index histories of the beam under multiple load cases.

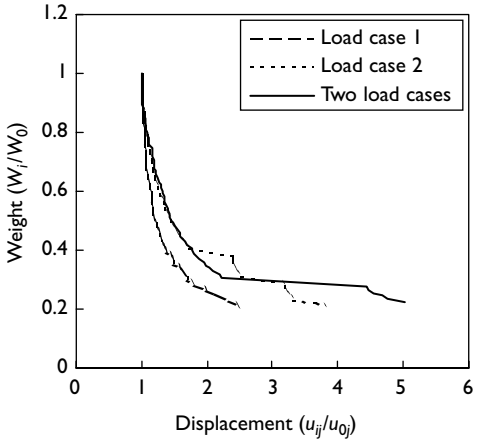

Figure 3.19 Performance characteristic curves for the beam under multiple load cases.

performance of the optimal structure under the two load cases is slightly higher than that of the optimum under only P_2. Three performance characteristic curves of the structure under three loading environments are presented in Figure 3.19. The maximum displacement at loaded points was used in the performance characteristic curves. It can be observed from Figure 3.19 that for the same material level, the structure under load case 1 has a lesser increase in deformations than the others.

The topology optimization history of the structure under three loading environments is presented in Figure 3.20. It can be observed from Figure 3.20(a)

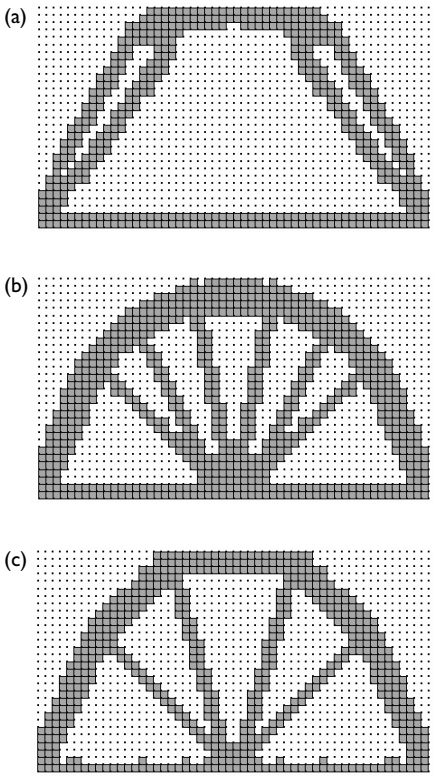

Figure 3.20 Topology optimization of structures under multiple load cases: (a) optimum under load case 1, $PI_{ds} = 1.96$; (b) optimum under load case 2, $PI_{ds} = 1.45$; (c) optimum under two load cases, $PI_{ds} = 1.46$.

that this is a simple load carrying mechanism in which the concentrated load P_1 is transferred to the supports through a direct load path. In Figure 3.20(b), the optimal structure is a tie–arch system in which the point load P_2 is transferred through the ties to the arch and then to the supports. This tie–arch load transfer mechanism is a very efficient structural system for the design situation like this example although it may be more efficient when the load is applied at the top of the structure. An optimal structure under two load cases P_1 and P_2 is shown in Figure 3.20(c). It can be observed from the figure that this optimal structure adapts to the two loading environments. It is an efficient load carrying structure for the two load cases.

3.10.5 Ranking the performance of structural topologies

Many optimization methods for the maximum stiffness topology designs of continuum structures have been developed in recent years. New developments

Figure 3.21 Design domain for the short cantilever beam.

are being undertaken in the structural and multidisciplinary optimization field. Many optimal designs have been appeared in the literature. It is worth noting that these "optimal designs" may be just local optima and are far from the global ones if they are not the worst or dangerous designs. In addition, for a same design problem, different optimization methods usually result in different final designs. The significance of a structural optimization method lies in the fact that it can produce a truly global optimal design in the sense of the best possible design. The PBO method employs displacement-based performance indices and PBOC to identify the global optimum in an optimization process. Displacement-based performance indices are used here to evaluate the quality of optimized designs produced by different continuum topology optimization methods.

A short cantilever beam is shown in Figure 3.21. A concentrated load of 3 kN was applied to the center of the free end. The thickness of the beam was 1 mm. The Young's modulus of material (E) was 207 GPa, and Poisson's ratio (ν) was 0.3. The PBO was applied to this short cantilever beam. The design domain was divided into 32×20 plane stress elements. A displacement constraint was imposed at the loaded point in the vertical direction. The element removal ratio of 2 percent was used in the optimization process.

Figure 3.22 shows the performance characteristic curve of the short cantilever beam in the performance optimization process. The actual weight of the optimal structure without scaling to the displacement limit is 49 percent of the initial design domain. However, the deflection of the optimal structure obtained is 1.69 times that of the initial design. In comparison with the scaled initial design, the optimal design generated by the PBO method resulted in a material volume saving of 17 percent.

The performance index history of this short cantilever beam is depicted in Figure 3.23. The performance index of the initial design without any element removal was equal to unity while the maximum performance index of

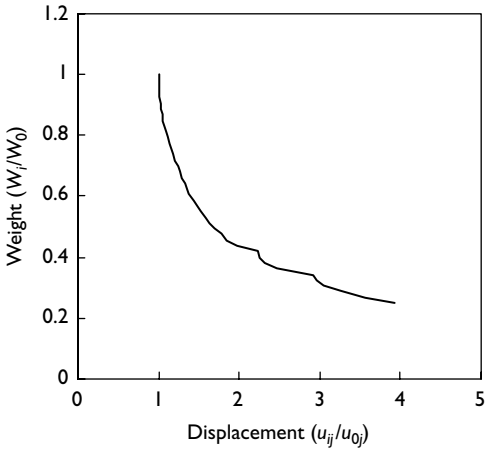

Figure 3.22 Performance characteristic curve for the short cantilever beam.

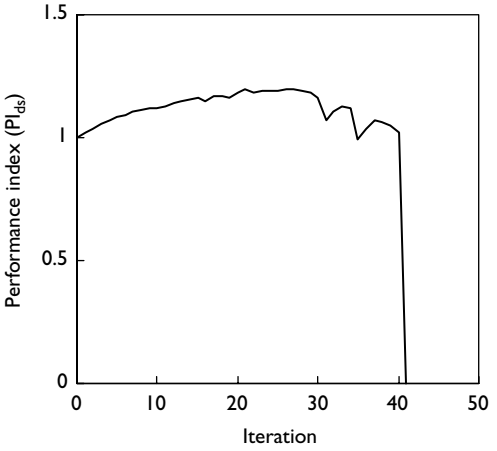

Figure 3.23 Performance index history of the short cantilever beam.

1.20 occurred at iteration 27. The optimal topology obtained by the PBO method is shown in Figure 3.24(a). The topology depicted in Figure 3.24(b) was produced by Chu *et al.* (1996). The performance index corresponding to Figure 3.24(b) was calculated as 1.11. The topology given by Zhao *et al.* (1998) is presented in Figure 3.24(c), where the model was regenerated. The performance index of the topology shown in Figure 3.24(c) was obtained as 1.18. The performance index of the topology given by Suzuki and

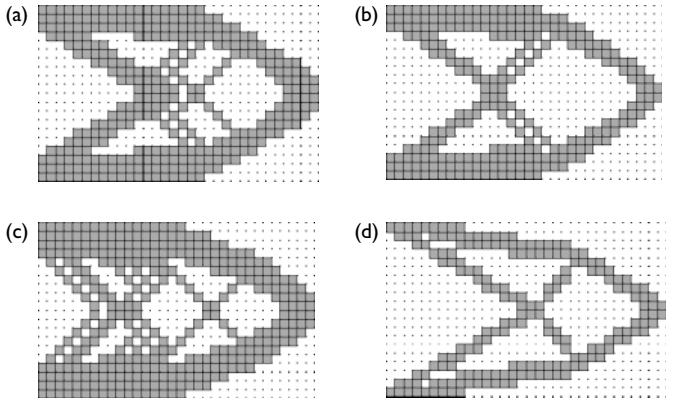

Figure 3.24 Ranking the performance of structural topologies: (a) topology by PBO, $PI_{ds} = 1.20$; (b) topology by Chu *et al.* (1996), $PI_{ds} = 1.11$; (c) topology by Zhao *et al.* (1998), $PI_{ds} = 1.18$; (d) topology by Suzuki and Kikuchi (1991), $PI_{ds} = 1.04$.

Kikuchi (1991) using the HBO method as shown in Figure 3.24(d) was found to be 1.04. It demonstrates that the performance of the optimal topology obtained by the PBO method is higher than those presented by other researchers. It can be concluded that the PBO method developed is a reliable and efficient topology optimization technique.

3.11 Examples of plates in bending

It is traditionally believed that continuum topology optimization can offer more material savings than continuum shape optimization. However, this statement may hold true only for plane stress structures, and it may not be the case for optimal designs of plates in bending. Little work has been undertaken so far to evaluate the performance of optimal plates, which are generated by using topology and shape optimization methods. Therefore, the PBO method is used to investigate the effects of topology and shape optimization techniques, loading and boundary conditions on the optimal designs of plates in bending in this section.

3.11.1 Clamped plate under concentrated loading

Figure 3.25 depicts the design domain for a clamped square plate under a concentrated load of 500 N applied to the center of the plate. The design domain was divided into 50×50 four-node plate elements. A single displacement constraint was imposed at the loaded point in the vertical direction. The

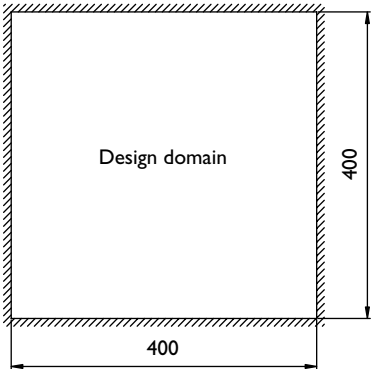

Figure 3.25 Design domain of clamped plate under concentrated loading.

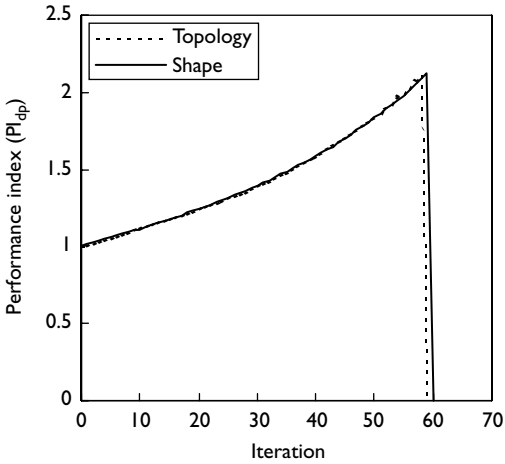

Figure 3.26 Performance index history of clamped plate under concentrated loading.

Young's modulus $E = 200$ GPa, Poisson's ratio $\nu = 0.3$ and the thickness of the plate $t = 5$ mm were specified in the FEA. Four elements around the loaded point were frozen so that this region was not removed during the optimization process. The element removal ratio of 1 percent was employed in the performance optimization process.

Figure 3.26 shows the performance index histories for topology and shape optimization of the clamped plate in bending. It is observed from Figure 3.26 that performance indices gradually increased when inefficient elements were eliminated from the plate in the optimization process. It is interesting to note that the performance indices of the topology and shape

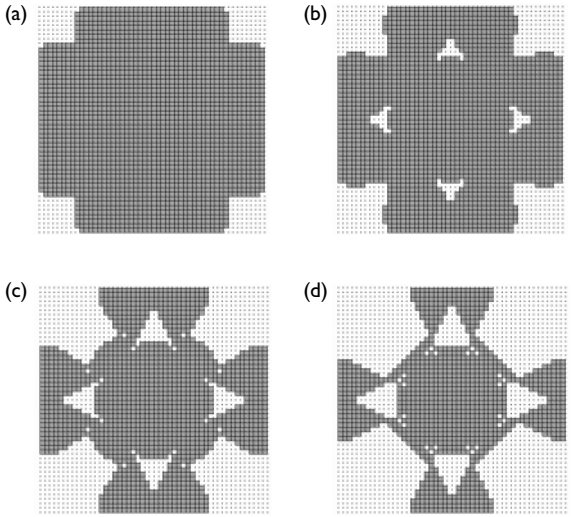

Figure 3.27 Topology optimization history of clamped plate under concentrated loading: (a) at iteration 10; (b) at iteration 20; (c) at iteration 40; (d) optimal topology.

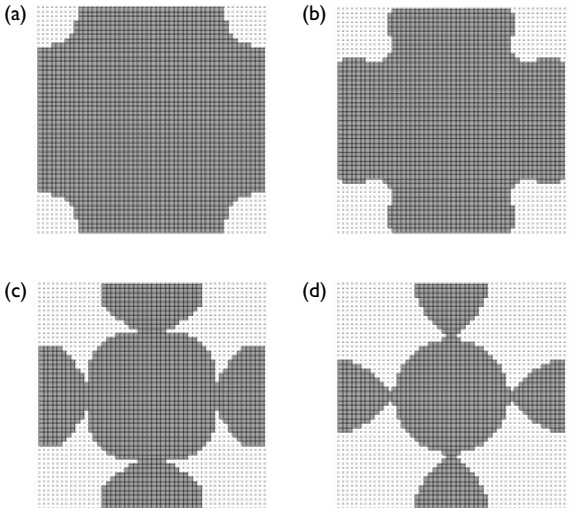

Figure 3.28 Shape optimization history of clamped plate under concentrated loading: (a) topology at iteration 10; (b) topology at iteration 20; (c) topology at iteration 40; (d) optimal topology.

were almost identical up to iteration 59. However, shape optimization provided a slightly higher performance index than topology optimization. The maximum performance index of the topology is 2.09 while the maximum performance index of the shape is 2.13. After the performance of the plate was maximized, further element removal destroyed the plate as indicated by the performance index histories shown in Figure 3.26.

The topology and shape optimization histories of the plate are shown in Figures 3.27 and 3.28. It is seen that topology optimization created cavities in the interior of the plate while no holes in the interior of the plate were generated by shape optimization. Based on the consideration of manufacture and structural performance, it is suggested that the shape optimization technique should be used to optimize plates in bending.

3.11.2 Simply supported plate under area loading

Figure 3.29 shows the design domain of a simply supported plate under a local area pressure of 0.1 MPa normal to the surface of the plate. A single displacement constraint was imposed at the center of the plate. The mesh and material properties used were the same as those used in the previous example. The loading region was frozen. The element removal ratio of 1 percent was used.

The performance index histories for topology and shape optimization are demonstrated in Figure 3.30. It is seen that performance indices were almost identical up to iteration 32 for the plate using topology and shape optimization techniques. However, the maximum performance index of the optimal shape is 1.53 while the maximum performance index of the optimal topology is only 1.34. This illustrates that shape optimization for plates in bending can generate higher performance optimal designs than topology optimization.

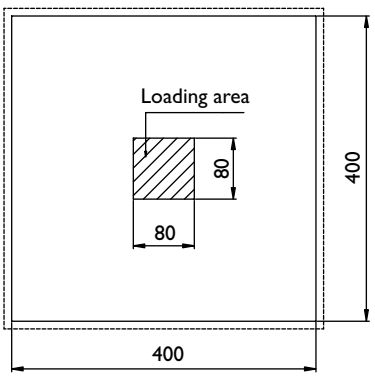

Figure 3.29 Design domain of simply supported plate under area loading.

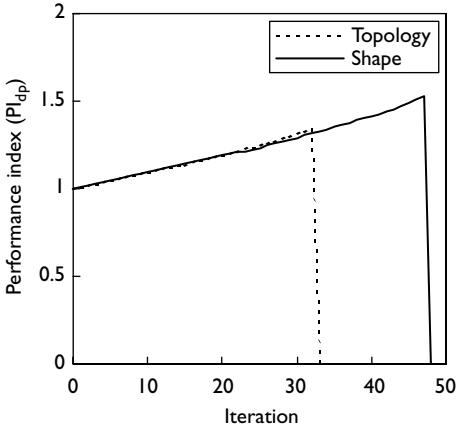

Figure 3.30 Performance index histories of simply supported plate under area loading.

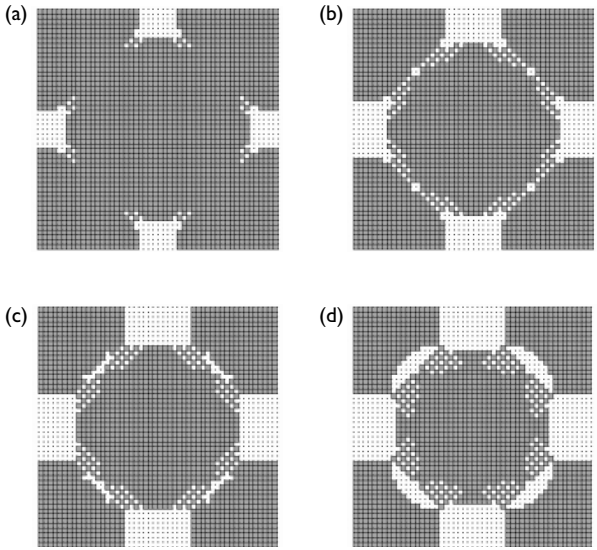

Figure 3.31 Topology optimization history of simply supported plate under area loading: (a) topology at iteration 10; (b) topology at iteration 20; (c) topology at iteration 40; (d) optimal topology.

The histories of topology and shape optimization are presented in Figures 3.31 and 3.32, respectively. It is observed that hinge lines were formed between the corners and the central region of the optimal topology using the topology optimization technique. However, no hinge lines were observed in

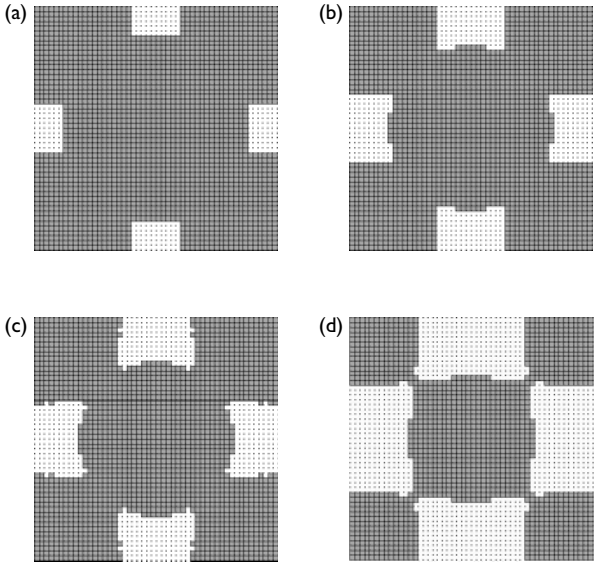

Figure 3.32 Shape optimization history of simply supported plate under area loading: (a) shape at iteration 10; (b) shape at iteration 20; (c) shape at iteration 25; (d) optimal shape.

the optimal shape because elements were only eliminated from the boundaries of the plate in shape optimization. Moreover, it is seen that checkerboard patterns appear in resulting topologies while no checkerboard pattern is present in shapes obtained. It is difficult to manufacture structures with checkerboard patterns. Although checkerboard patterns can be eliminated by incorporating an intuitive smoothing scheme into the PBO algorithms, the computational cost will be penalized. From the manufacturing, computational cost and structural performance points of view, it is suggested that shape optimization technique should be used to optimize plates in bending. The effects of boundary conditions on optimal topologies and shapes of bending plates can be seen from the example presented in Section 3.11.1 and this example.

3.11.3 Clamped plate under strip loading

The design domain of a clamped square plate under strip pressures of 0.1MPa is illustrated in Figure 3.33. A single displacement constraint imposed at the center of the plate was considered. The mesh and material properties are the same as used in previous example. Elements in the two loaded strips were frozen. The element removal ratio of 1 percent was employed in this problem. This plate was optimized using the PBO method for topology and shape optimization.

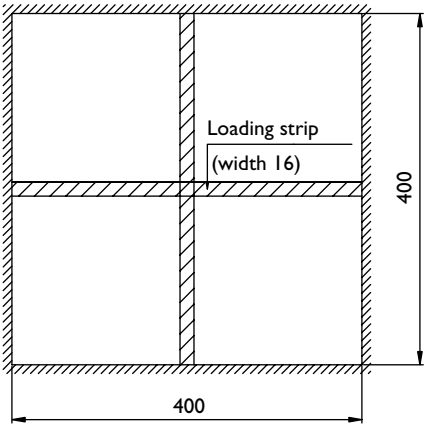

Figure 3.33 Design domain of clamped plate under strip.

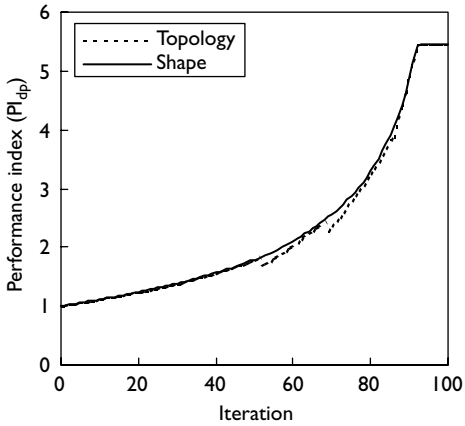

Figure 3.34 Performance index history of clamped plate under strip loading.

Figure 3.34 shows performance index histories for the topology and shape optimization of the clamped plate under a strip loading. It can be observed that the performance index curve obtained using the shape optimization method is smoother than the one generated using the topology optimization scheme. This may be the effect of holes, which were created in the interior of the plate in topology optimization process. However, it is shown that these two optimization methods provided optimal designs with the same maximum performance index of 5.44, which was constant in later iterations. This is because the loaded strips were frozen so that no elements

could be removed from loading strips after eliminating all of the unfrozen elements from the design.

The topology and shape optimization histories of the plate under the strip pressure are presented in Figures 3.35 and 3.36. It is seen from these figures

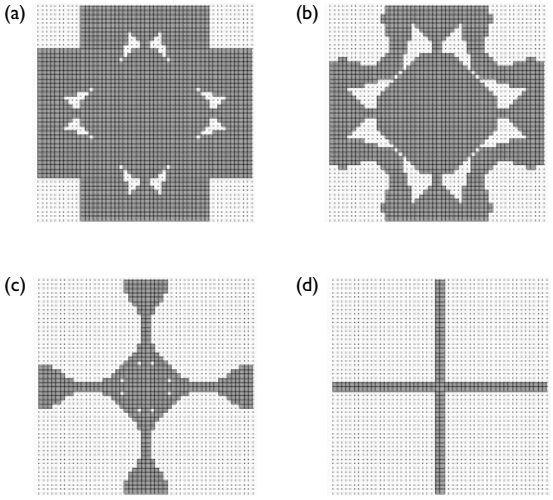

Figure 3.35 Topology optimization history of clamped plate under strip loading: (a) topology at iteration 20; (b) topology at iteration 40; (c) topology at iteration 80; (d) optimal topology.

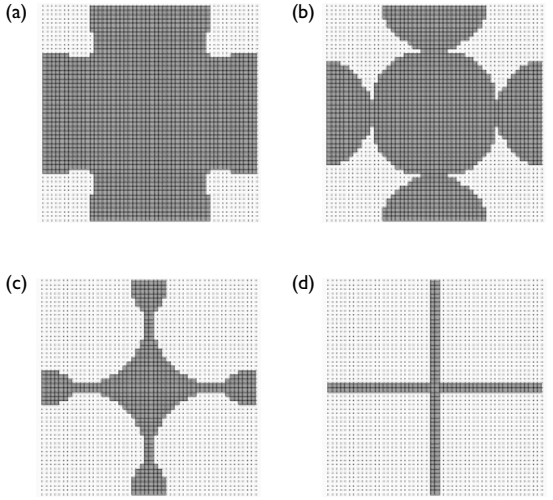

Figure 3.36 Shape optimization history of clamped plate under strip loading: (a) shape at iteration 20; (b) shape at iteration 40; (c) shape at iteration 80; (d) optimal shape.

that although the results generated at the same iteration in the performance optimization process are different using different optimization techniques, final optimal designs are the same for this plate under strip loading. The optimal shape suggests that the most efficient design can be achieved by using beams to support the strip loading.

3.12 Conclusion

In this chapter, the PBO method incorporating the uniform sizing of element thickness has been presented for the optimal topology and shape design of continuum structures subject to displacement constraints. The PBO method is formulated on the basis of displacement performance criteria. It allows for elements with the lowest VSEDs to be removed from a structure and elements with the largest values of VSEDs to be added to the structure to achieve a lightweight design with minimum deformations. In the PBO method, continuum topology and shape optimization is treated as the problem of improving the performance of a continuum design domain in terms of the material usage in effectively resisting deformations. Maximizing the performance indices in the design space is proposed as PBOC. Performance indices are used to monitor the optimization process and as a termination criterion in performance optimization algorithms. The performance characteristics of a continuum structure with displacement constraints are expressed by its weight and constrained displacement in a performance optimization process.

It has been demonstrated that the PBO method can effectively generate optimal topologies and shapes, which have been verified by analytical solutions and results produced by other optimization methods. The PBO technique is an efficient design tool that can used to solve a wide range of practical design problems for stiffness performance, such as structures under multiple displacement constraints and multiple load cases. It is shown that a smoother solution can be achieved by using a smaller element removal ratio in a performance optimization process but at the expense of a higher computational cost. It is suggested that the element removal ratio of 1 percent can be used in practical design of engineering structures. The results indicate that increasing the height of an initial design domain usually improves the efficiency of the final optimal design. The studies conducted in this chapter demonstrate that the shape optimization technique produces higher performance optimal designs of plates in bending than the topology optimization method does. From the manufacturing and efficient points of view, the shape optimization technique should be used to optimize plates in bending.

The significance of the PBO method presented lies in the fact that it can generate global optimal designs of continuum structures for maximum stiffness. The PBO method incorporates performance-based design concepts, performance indices and PBOC into optimization algorithms to ensure

a global solution to be achieved. It can capture a complete performance characteristic curve of a structure in the performance optimization process. PBOC developed can be incorporated in existing continuum topology optimization methods to guarantee success in obtaining the global optimal designs with reasonable effort. Furthermore, the proposed performance indices can be used to rank the performance of structural topologies and shapes produced by different structural optimization methods and the efficiency of continuum topology optimization methods.

3.13 References

Atrek, E. (1989) "Shape: a program for shape optimization of continuum structures," in C. A. Brebbia and S. Hernandez (eds) *Computer Aided Optimization Design of Structures: Applications*, Southampton: Computational Mechanics Publications, pp. 135–144.

Beckers, M. (1999) "Topology optimization using a dual method with discrete variables," *Structural Optimization*, 17: 14–24.

Bendsøe, M. P. (1989) "Optimal shape design as a material distribution problem," *Structural Optimization*, 1: 193–202.

Cheng, K. T. and Olhoff, N. (1982) "An investigation concerning optimal design of solid elastic plates," *International Journal of Solids and Structures*, 16: 305–323.

Chu, D. N., Xie, Y. M., Hira, A. and Steven, G. P. (1996) "Evolutionary structural optimization for problems with stiffness constraints," *Finite Elements in Analysis and Design*, 21: 239–251.

Díaz, A. R. and Sigmund, O. (1995) "Checkerboard patterns in layout optimization," *Structural Optimization*, 10: 40–45.

Fujii, D. and Kikuchi, N. (2000) "Improvement of numerical instabilities in topology optimization using the SLP method," *Structural Optimization*, 19: 113–121.

Jog, C. S. and Haber, R. B. (1996) "Stability of finite element model for distributed parameter optimization and topology design," *Computer Methods in Applied Mechanics and Engineering*, 130: 203–226.

Jog, C. S., Haber, R. B. and Bendsøe, M. P. (1994) "Topology design with optimization, self-adaptive material," *International Journal for Numerical Methods in Engineering*, 37: 1323–1350.

Li, Q., Steven, G. P. and Xie, Y. M. (2001) "A simple checkerboard suppression algorithm for evolutionary structural optimization," *Structural Multidisciplinary Optimization,* 22: 230–239.

Liang, Q. Q. (2001) *Performance-Based Optimization Method for Structural Topology and Shape Design*, PhD thesis, Victoria University of Technology, Australia.

Liang, Q. Q., Xie, Y. M. and Steven, G. P. (1999) "Optimal topology selection of continuum structures with stress and displacement constraints," paper presented at the Seventh East Asia-Pacific Conference on Structural Engineering and Construction, Kochi, Japan, September, pp. 560–565.

Liang, Q. Q., Xie, Y. M. and Steven, G. P. (2000) "Optimal topology selection of continuum structures with displacement constraints," *Computers and Structures*, 77(6): 635–644.

Liang, Q. Q., Xie, Y. M. and Steven, G. P. (2001) "A performance index for topology and shape optimization of plate bending problems with displacement constraints," *Structural and Multidisciplinary Optimization*, 21(5): 393–399.

Michell, A. G. M. (1904) "The limits of economy of material in frame-structures," *Philosophy Magazine*, 8: 589–597.

Morris, A. J. (ed.) (1982) *Foundations of Structural Optimization: A Unified Approach*, New York: John Wiley & Sons.

Olhoff, N. (1975) "On singularities, local optima and formulation of stiffeners in optimal design of plates," in A. Sawczuk and Z. Mroz (eds) *Optimization in Structural Design*, New York: Springer-Verlag, pp. 82–103.

Petersson, J. and Sigmund, O. (1998) "Slop constrained topology optimization," *International Journal for Numerical Methods in Engineering*, 41: 1417–1434.

Rozvany, G. I. N. (1976) *Optimum Design of Flexural Systems*, Oxford: Pergamon.

Rozvany, G. I. N. (1989) *Structural Design via Optimality Criteria*, Dordrecht: Kluwer.

Rozvany, G. I. N., Zhou, M. and Birker, T. (1992) "Generalized shape optimization without homogenization," *Structural Optimization*, 4: 250–252.

Sigmund, O. (1994) *Design of Material Structures Using Topology Optimization*, PhD thesis, Technical University of Denmark, Denmark.

Sigmund, O. and Petersson, J. (1998) "Numerical instabilities in topology optimization: a survey on procedures dealing with checkerboard, mesh-dependencies and local minima," *Structural Optimization*, 16: 68–75.

Suzuki, K. and Kikuchi, N. (1991) "A homogenization method for shape and topology optimization," *Computer Methods in Applied Mechanics and Engineering*, 93: 291–318.

Tenek, L. H. and Hagiwara, I. (1993) "Static and vibrational shape and topology optimization using homogenization and mathematical programming," *Computer Methods in Applied Mechanics and Engineering,* 109: 143–154.

Yang, R. J. (1997) "Multidiscipline topology optimization," *Computers and Structures*, 63(6): 1205–1212.

Yang, X. Y., Xie, Y. M., Steven, G. P. and Querin, O. M. (1998) "Bi-directional evolutionary method for stiffness optimization," paper presented at the Seventh AIAA/USAF/NASA/ISSMO Symposium on Multidisciplinary Analysis and Optimization, St Louis, USA, pp. 1449–1457.

Youn, S.-K. and Park, S.-H. (1997) "A study on the shape extraction process in the structural topology optimization using homogenized material," *Computers and Structures*, 62(3): 527–538.

Zhao, C. B., Hornby, P., Steven, G. P. and Xie, Y. M. (1998) "A generalized evolutionary method for numerical topology optimization of structures under static loading conditions," *Structural Optimization*, 15: 251–260.

Zhou, M., Shyy, Y. K. and Thomas, H. L. (2001) "Checkerboard and minimum member size control in topology optimization," *Structural and Multidisciplinary Optimization*, 21: 152–158.

Chapter 4

PBO for structures with mean compliance constraints

4.1 Introduction

The performance-based optimization (PBO) method for optimal topology and shape designs of continuum structures with displacement constraints has been presented in Chapter 3. Element removal criteria are based on the virtual strain energy densities (VSEDs) of elements. In order to calculate the VSEDs of elements, the structure has to be analyzed for the virtual unit loads, which are applied at the loaded points. An optimal design produced by the PBO method based on displacement performance criteria is in favor of the specific displacements. This means that the optimal design obtained is a maximum stiffness design at minimum weight with respect to the specific displacements. For a structure under only a few point loads, the PBO method for structures with displacement constraints is efficient in generating minimum-weight and maximum stiffness designs. When dealing with the optimization problem of a continuum structure under many concentrated loads and multiple load cases, however, many virtual unit loads have to be applied to the structure in order to calculate the VSEDs of elements and to control the system stiffness performance. This will considerably increase the computational cost. Moreover, practical structures are often designed for overall stiffness performance. To improve the computational efficiency and overall structural performance, a more general approach formulated on the basis of system performance criteria is presented in this chapter.

The shape optimization problem of continuum structures has been solved by Zienkiewicz and Campbell (1973) using a sequential programming technique. Modern continuum topology and shape optimization evolved from this earlier work. Haftka and Grandhi (1986) presented a survey on structural shape optimization in which the boundary variation method has extensively been used. The boundary variation method is implemented by using the mesh moving schemes to express the shape of a given design. The coordinates of nodal points of the finite element model are treated as design variables. Special techniques for maintaining the regularity of the

finite element model are usually required to obtain a sound optimal shape in the boundary variation method (Kikuchi *et al.* 1986). The modification of a shape is based on the sensitivity of elements. The sensitivity analysis for shape optimization has been studied by Rousselet and Haug (1983) and by Haug *et al.* (1986).

In shape optimization using the boundary variation method, the finite element model is not fixed during the optimization process so that re-meshing the model is required at each iteration. To avoid these, Bendsøe and Kikuchi (1988) proposed a homogenization-based optimization (HBO) method for topology and shape design of continuum structures using a fixed design domain. In the HBO method, topology optimization is transformed to a material redistribution problem in a continuum design domain made by composite material with microstructures. The effective material properties of the composite material are computed using the theory of homogenization. For the maximum stiffness design, the mean compliance of a structure is used as the objective function while the constraint is imposed on the material volume. Extensive studies on the HBO method have been reported in the literature (Bendsøe 1989; Suzuki and Kikuchi 1991; Hassani and Hinton 1999; Krog and Olhoff 1999; Bendsøe and Sigmund 2003). The HBO method was extended by Diaz and Bendsøe (1992) and Bendsøe *et al.* (1995) to structures under multiple loading conditions. Tenek and Hagiwara (1993) applied the HBO method to the topology optimization of plates in bending.

The density-based optimization (DBO) method has been developed as an alternative approach to the minimum compliance optimization problem (Bendsøe 1989; Mlejnek and Schirrmacher 1993; Yang and Chuang 1994; Ramm *et al.* 1994; Sigmund 2001). In the DBO method, material properties are assumed to be constant within each finite element employed to discretize the design domain and element relative densities are treated as design variables. The effective material properties are computed by the relative material density raised to some power times the material properties of the solid material. The material model described by the power law is artificial since no such physical material exists. The power law approach must be combined with perimeter constraints, gradient constraints or filtering techniques to ensure the existence of solutions (Sigmund 2001). Gea (1996) presented a microstructure-based design domain method, which employs a closed-form expression for the effective Young's modulus and shear modulus in terms of phase properties and volume fractions. Yang (1997) extended the DBO method to general topology optimization problems in which compliance, displacements and natural frequencies are treated as constraints. The DBO method can be combined with a dual approach to solve topology optimization problems with discrete design variables (Beckers 1999). In comparison with the HBO method, the DBO approach is simple to implement and can produce conceptual designs.

The difficulty associated with continuum topology optimization is to incorporate an appropriate termination criterion in optimization algorithms to obtain the global optimum. For the maximum stiffness topology design problem, the mean compliance of a structure is commonly used in most of the existing optimization methods as the objective function, and the constraint is imposed on a somewhat arbitrarily specified material volume. Based on this termination criterion, using a different percentage of the material volume as the constraint results in different designs. Obviously, appropriate criteria for identifying the global optimum are still lacking in these continuum topology optimization methods that could lead to many local optima if they are not the worst or dangerous designs. To overcome this problem, Liang (2001a,b) and Liang and Steven (2002) have developed the PBO method that employs energy-based performance indices and performance-based optimality criteria (PBOC) to achieve the global optimal designs of continuum structures with mean compliance constraints. These energy-based performance indices and PBOC can be incorporated into other optimization methods to ensure a global optimal solution to be obtained.

In this chapter, the PBO method is extended to the optimal topology, shape and sizing design problem of continuum structures with mean compliance constraints under multiple loading conditions. In the PBO method, the weight of a structure is used as the objective function and the constraint is imposed on the mean compliance of the structure. Continuum topology optimization is treated as the problem of improving the performance of a continuum design domain in terms of the efficiency of material usage and overall stiffness. Two energy-based performance indices are employed to evaluate the performance of plane stress continuum structures and plates in bending. These performance indices are also used as termination criteria in performance-based optimization algorithms. The maximization of performance indices is proposed as performance-based optimization criteria. Some of the results and optimization concepts have been presented by Liang (2001a,b) and Liang and Steven (2002).

4.2 Performance objective for structures with mean compliance constraints

The formulation of a design optimization problem is of significant importance to the success of an optimization method. A poor formulation can lead to poor designs or to prohibitive development cost. Moreover, an improper problem formulation may lead to meaningless results that cannot be used in practice. For the maximum stiffness topology design, the mean compliance of a structure has commonly been used as the objective function, and the constraint is imposed on a somewhat arbitrarily specified material volume. However, it is noteworthy that the designer usually does not know what percentage of the material volume is the minimum for supporting applied loads

in advance. Optimization methods based on such a problem formulation certainly lead to a trial-and-error design process if the designer really wants to find a minimum-weight design. The optimal material usage for a given design problem should be sought by using topology optimization methods rather than specified by the designer. The realistic optimization approaches for stiffness design are to treat the weight of a structure as the objective function and behavior quantities such as the mean compliance or displacements as constraints since limitations on behavior quantities are specified in national or international design codes (Rozvany *et al.* 1995).

In the PBO method, the weight of a structure is used as the objective function and the mean compliance is treated as the constraint. In other words, the performance objective is to minimize the weight of a continuum design domain while maintaining its overall stiffness within an acceptable performance level. The mean compliance of a structure is usually used as an inverse measure of the overall stiffness of a structure. The performance objective can be expressed in mathematical forms as follows:

$$\text{minimize } W = \sum_{e=1}^{n} w_e(t) \tag{4.1}$$

$$\text{subject to } C \leq C^* \tag{4.2}$$

$$t^{\mathrm{L}} \leq t \leq t^{\mathrm{U}} \tag{4.3}$$

where W is the total weight of a structure; w_e,the weight of the eth element, t, the thickness of elements; C, the absolute value of the mean compliance of the structure; C^*, the prescribed limit of C and n, the total number of elements in the structure; t^{L}, the lower limit of element thickness and t^{U}, the upper limit of element thickness. It should be noted that the thickness of a continuum structure has a significant effect on the weight of the structure and must be specified by the designer in practice. As a result, the element thickness is treated as one of the design variables. However, only uniform sizing of the element thickness is considered in the proposed performance-based topology optimization method to simplify the optimization problem. This can be justified by the fact that many practical civil engineering structures must be uniform thickness designs.

4.3 Element removal criteria based on strain energy density

Element removal criteria have been derived for element elimination for continuum structures with stress and displacement constraints in Chapters 2 and 3. To obtain fully stressed topology designs, lowly stressed elements are gradually removed from a discretized continuum design domain. In contrast, elements with the lowest VSEDs are gradually deleted from a design domain

in order to generate an optimal topology with the least deformations at specific locations at minimum weight. However, these element removal criteria cannot be applied to continuum structures subject to mean compliance constraints. As a result, new element removal criteria need to be derived for topology designs when considering the system performance. As presented in Chapter 3, the criteria for element removal can be developed on the basis of the design sensitivity analysis of constraints with respect to design variables. In the PBO method, the design sensitivity analysis is to investigate the effect of element removal on the change in the mean compliance of a continuum structure. Approximate concepts are employed in the design sensitivity analysis.

The equilibrium equation for a linearly elastic structure in the finite element formulation can be expressed by

$$[K]\{u\} = \{P\} \tag{4.4}$$

The element removal concept is used in the proposed topology optimization method. When the eth element is removed from a structure modeled with finite elements, the stiffness matrix and displacement vector of the structure will change accordingly. Equation (4.4) can be rewritten as

$$([K] + [\Delta K])(\{u\} + \{\Delta u\}) = \{P\} \tag{4.5}$$

where $[\Delta K]$ is the change in the stiffness matrix and $[\Delta u]$ is the change in the nodal displacements vector. It is noted that the loads applied to the structure are unchanged. Since only the eth element is removed from the structure, the change in the stiffness matrix can be derived as

$$[\Delta K] = [K_r] - [K] = -[k_e] \tag{4.6}$$

in which $[K_r]$ is the stiffness matrix of the resulting structure and $[k_e]$ is the stiffness matrix of the eth element. The change in the displacement vector due to element elimination can approximately be obtained from Eqs (4.4) and (4.5) by neglecting the higher order terms as

$$\{\Delta u\} = -[K]^{-1}[\Delta K]\{u\} \tag{4.7}$$

The mean compliance or strain energy of a structure can be determined by

$$C = \tfrac{1}{2}\{P\}^{\mathrm{T}}\{u\} \tag{4.8}$$

The change in the strain energy of a structure due to the removal of the eth element can approximately be derived as

$$\begin{aligned}\Delta C = \tfrac{1}{2}\{P\}^{\mathrm{T}}\{\Delta u\} &= -\tfrac{1}{2}\{P\}^{\mathrm{T}}[K]^{-1}[\Delta K]\{u\} \\ &= -\tfrac{1}{2}\{u\}^{\mathrm{T}}[\Delta K]\{u\} = -\tfrac{1}{2}\{u_e\}^{\mathrm{T}}[k_e]\{u_e\}\end{aligned} \tag{4.9}$$

where $\{u_e\}$ is the displacement vector of the eth element. It can be seen from Eq. (4.9) that the change in the strain energy of a structure due to the removal of the eth element can be approximately evaluated by the strain energy of the eth element. As a result, the element strain energy can be used as a measure of element contribution to the overall stiffness performance of a structure, and is denoted as

$$c_e = \tfrac{1}{2}\{u_e\}^{\mathrm{T}}[k_e]\{u_e\} \tag{4.10}$$

To achieve the maximum stiffness designs, it is obvious that a small number of elements with the lowest strain energies should be systematically removed from a structure. For continuum structures discretized into different size finite elements, the element strain energy per unit weight, which is defined as the strain energy density (SED) of an element, should be calculated for element removal. The SED of the eth element is calculated by

$$\gamma_e = \frac{|c_e|}{w_e} \tag{4.11}$$

If the material density and element thickness are uniformly distributed in a design domain, either the volume or the weight of an element can be used in Eq. (4.11) to calculate the element SED. However, if the material density varies in a continuum design domain, the element weight shall be used in Eq. (4.11).

The element removal criteria states that elements with the lowest SEDs are gradually removed from a structure to improve the performance of the structure. A loop is used to count elements with the lowest SEDs until they made up the specified amount that is the element removal ratio times the total number of elements in the initial design domain. The element removal ratio (R) for each iteration is defined as the ratio of the number of elements to be removed to the total number of elements in the initial structure. The element removal ratio is not changed in the whole optimization process.

4.4 Checkerboard suppression algorithm

Checkerboard patterns are caused by the error of the finite element formulation, as discussed in Chapter 3. The main techniques for preventing the formation of checkerboard patterns have been introduced in Chapter 3. Checkerboard patterns are also observed in optimal topologies and shapes produced by the PBO method formulated on the basis of system performance criteria when four-node elements are employed in the finite element analysis (FEA). This is mainly due to the unstable nature of the four-node elements. Using higher order elements such as eight-node elements in the PBO method can effectively eliminate the formation of checkerboard patterns. However, the computational cost will significantly increase especially for practical topology design problems in which structures are modeled with very fine finite elements.

A simple checkerboard suppression algorithm has been implemented in the PBO method based on the displacement performance criteria, as presented in Chapter 3. This algorithm can be easily modified and implemented into the PBO method for topology design with mean compliance constraints. In this algorithm, the nodal SEDs of an element are calculated by averaging the SEDs of neighboring elements as follows:

$$\zeta_{nd} = \frac{1}{M} \sum_{e=1}^{M} \gamma_e \tag{4.12}$$

in which ζ_{nd} is the nodal SED and M is the number of elements that connect to that node. The SED of each element can be recalculated from the nodal SEDs at the nodes of the element as

$$\zeta_e = \frac{1}{Q} \sum_{nd=1}^{Q} \zeta_{nd} \tag{4.13}$$

where ζ_e is the recalculated SED of the eth element and Q is the number of nodes in the element. Element removal criteria are now based on the recalculated SEDs of elements. A small number of elements with the lowest values of ζ_e can be deleted from the design domain in a performance optimization process to improve the quality of the design. It can be observed from the examples presented in this chapter that the SED redistribution scheme can effectively suppress the formation of checkerboard patterns in performance-based topology optimization.

4.5 Energy-based performance indices

In design problems with element thickness or cross-sectional design variables, an infeasible design in the optimization process can be converted into a feasible one by the scaling procedure. Due to its simplicity and efficiency, this scaling procedure has been used in conventional optimality criteria (OC) methods (Morris 1982; Kirsch 1982) for truss layout optimization. The scaling design concept has been utilized to develop performance indices in previous chapters for evaluating the performance of structural topologies and shapes with stress and displacement constraints. The scaling design procedure is also employed to derive energy-based performance indices for structures with mean compliance constraints in this section.

4.5.1 Performance index for plane stress structures

For a plane stress continuum structure, the stiffness matrix of the structure is a linear function of the element thickness. Therefore, for structures with the mean compliance constraint, the element thickness can be uniformly scaled to keep the mean compliance constraint active in the optimization

process. By scaling the initial structure with a factor of $\varphi_{es}(\varphi_{es} = C/C^*)$, the scaled weight of the initial structure can be expressed by

$$W_0^s = \left(\frac{C_0}{C^*}\right) W_0 \tag{4.14}$$

where W_0 is the actual weight of the initial structure and C_0, the absolute value of the strain energy of the initial structure under applied loads. Similarly, by scaling the current optimized structure with respect to the mean compliance limit, the scaled weight of the current structure at the ith iteration can be determined by

$$W_i^s = \left(\frac{C_i}{C^*}\right) W_i \tag{4.15}$$

in which C_i is the absolute value of the strain energy of the current structure under applied loads at the ith iteration and W_i is the actual weight of the current structure at the ith iteration.

The performance index at the ith iteration can be expressed by

$$\mathrm{PI}_{es} = \frac{W_0^s}{W_i^s} = \frac{(C_0/C^*)W_0}{(C_i/C^*)W_i} = \frac{C_0 W_0}{C_i W_i} \tag{4.16}$$

It is seen from Eq. (4.16) that the performance index is composed of the strain energy and the weight of a structure in an optimization process. This performance index is called the energy-based performance index. By systematically eliminating elements with the lowest SEDs from a continuum structure, the performance of the structure can gradually be improved. The larger value of the performance index means the higher performance of a structural topology or shape. It can be observed that the format of the performance index formula for plane stress structures with mean compliance constraint is the same as that for plane stress structures with displacement constraints.

4.5.2 Performance index for plates in bending

The performance index and PBOC for topology and shape optimization of bending plates subject to displacement constraints have been deduced by using the scaling design procedure in Chapter 3. When the thickness of a plate in bending is uniformly scaled, the displacement vector of the scaled plate can be represented by

$$\{u^s\} = \frac{1}{\varphi_{ep}^3}\{u\} \tag{4.17}$$

It can be seen from Eq. (4.8) that the mean compliance of a plate in bending is proportional to the displacement vector. When the thickness of a plate in bending is reduced by a factor φ_{ep}, the mean compliance will increase with a factor of $1/\varphi_{ep}^3$. In order to satisfy the mean compliance constraint, the plate needs to be scaled by the following factor:

$$\varphi_{ep} = \left(\frac{C}{C^*}\right)^{1/3} \tag{4.18}$$

By using the scaling design procedure, the performance index of a plate in bending at the ith iteration can be derived as follows:

$$\mathrm{PI}_{ep} = \left(\frac{C_0}{C_i}\right)^{1/3} \frac{W_0}{W_i} \tag{4.19}$$

It can be seen from Eq. (4.19) that the performance index formula is composed of the structural response (the mean compliance) and the weight of a structure in an optimization process. In other words, the performance index is a measure of structural responses and the reduction in the weight of a plate in bending in the optimization process, and thus quantifies the performance of the plate.

4.6 Performance-based optimality criteria

By gradually eliminating elements with the lowest SEDs from a design domain, the distribution of element SEDs will consequently become more and more uniform within the resulting structure. The uniform SED has been used as an optimality condition in DBO methods, and can be derived by using the Kuhn–Tucker conditions (Ramm *et al.* 1994). However, the uniform condition of element SEDs in a continuum structure may not be achieved even if the mean compliance constraint is violated. This means that a minimum-weight design with acceptable overall stiffness performance is not necessarily a structure in which the distribution of element SEDs is absolutely uniform. Therefore, as stated in the fully stressed design and design for displacement performance, the uniformity of element SEDs cannot be incorporated in continuum topology optimization methods as a termination condition for identifying the optimal topology. PBOC for plane stress structures and plates in bending are presented in this section.

To obtain the optimum, the PBOC for plane stress structures with the mean compliance constraint can be stated as

$$\text{maximize} \quad \mathrm{PI}_{es} = \frac{C_0 W_0}{C_i W_i} \tag{4.20}$$

This PBOC means that the optimal topology or shape of a continuum structure under applied loads is achieved when the product of its associated strain energy and material consumption is a minimum. The optimal structure obtained represents an efficient load carrying mechanism within the design domain. It can be observed from Eq. (4.20) that the optimal topology or shape does not depend on the mean compliance limit. Since the performance index is a dimensionless number, it is not affected by the uniform scaling of the element thickness. As a result, in the FEA and optimization process, the thickness of an initial structure can be assumed and needs not to be updated. The performance index can be employed to monitor the optimization process so that the optimum can be identified from the performance index history. After the optimal design has been obtained, its thickness can be uniformly scaled to satisfy the actual mean compliance constraint.

It is traditionally believed that the optimization problems of minimizing the mean compliance for a somewhat arbitrarily specified material volume constraint and minimizing the weight of a structure for a prescribed mean compliance constraint result in equivalent solutions. However, it can be seen from Eq. (4.20) that this statement holds true only when the specified material volume is the minimum value, which maximizes the performance index in Eq. (4.16). In practice, the minimum material usage is difficult to be determined a priori by the design engineer. Therefore, the applications of structural optimization methods formulated with an objective of minimizing the mean compliance for a somewhat arbitrarily chosen material volume are limited.

Similarly, to obtain an optimal design, the PBOC for plates in bending with an overall stiffness constraint can be stated as

$$\text{maximize} \quad \text{PI}_{\text{ep}} = \left(\frac{C_0}{C_i}\right)\frac{W_0}{W_i} \tag{4.21}$$

It can be observed that the optimal topology or shape of a plate in bending is independent of the mean compliance limit. In order to obtain the global optimum, the mean compliance limit is usually set to a large value in an optimization process. The initial thickness of a plate is assumed and needs not to be updated in the FEA and optimization process. The performance index is a dimensionless number, which is not affected by the uniform scaling of plate thickness. Therefore, the performance index can be employed in optimization algorithms to evaluate the performance of a plate in the optimization process. The optimal topology or shape of the plate can be identified from the performance index history.

4.7 Performance characteristics of structures with mean compliance constraints

The PBO method proposed allows for lowly strained elements to be gradually removed from a continuum structure to improve the performance

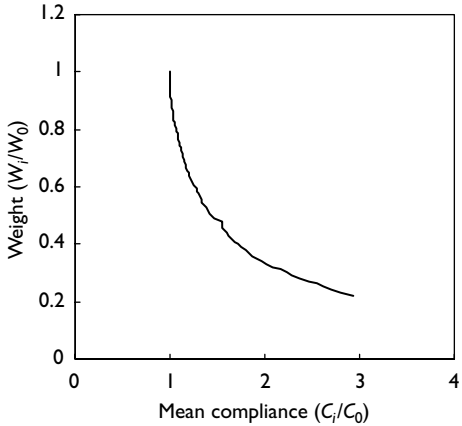

Figure 4.1 Performance characteristic curve for structures with mean compliance constraints.

of the structure. The weight of a structure in an optimization process is gradually reduced due to element removal while the mean compliance of the structure increases accordingly. The performance characteristics of a structure can be expressed by the weight and the strain energy of the structure in an optimization process. The PBO technique can fully capture the performance characteristic curve of a structure in an optimization process. Performance characteristics provide valuable information for the structural designer. They not only indicate whether an optimized design is feasible but also measure the success of the optimized design for stiffness. A typical performance characteristic curve generated by the PBO technique is shown in Figure 4.1. A structure with performance below this curve is not feasible because the structure made by that amount of material will violate the mean compliance constraint. A structure with performance above this curve is obviously over-designed. Structural optimization techniques can be applied to the over-designed structure to improve its performance.

4.8 Optimal design for multiple load cases

Civil engineering structures are often subjected to multiple loading conditions in their design service life. All possible loading conditions must be considered in the design stage of these structures. In practice, structures with fixed topologies selected by the designer are usually designed for the worst combination of all load cases so that they can perform physical functions in their design service life. The optimal topology design of a continuum structure under multiple load cases is much more complicated than the one under

only a single load case. The topology design of continuum structures under multiple load cases is better to be done by computer-based optimization tools. The optimal topology design problem for multiple load cases is addressed in this section.

4.8.1 Optimization problem formulation

A weighted average approach is used to define the objective function in the HBO method presented by Díaz and Bendsøe (1992) and Bendsøe *et al.* (1995) for the compliance minimization problem under multiple loading conditions. In the HBO method, the optimization problem for multiple load cases is stated as

$$\text{minimize} \quad f(C^p) = \sum_{p=1}^{\text{NL}} \alpha_p C^p \tag{4.22}$$

$$\text{subject to} \quad V \leq V^* \tag{4.23}$$

where α_p is the weighting factor under the load case p, C^p is the mean compliance of the structure under load case p, NL is the total number of load cases, and V^* is the specified volume limit. The weighting factor is defined as

$$\sum_{p=1}^{\text{NL}} \alpha_p = 1 \quad (\alpha_p > 0) \tag{4.24}$$

Since it is difficult to determine the weighting factor for each load case, the same weighting factor (α_p = 1/NL) is usually used for all load cases (Díaz and Bendsøe 1992). This implies that the importance of each load case is not ranked in an optimization process, which may result in local optima for complex design situations.

The PBO algorithm can easily be modified to deal with the topology and shape design problems with multiple load cases. The performance objective for multiple load cases is to minimize the weight of a structure for a prescribed system performance level. For topology and uniform thickness sizing design, the performance objective can be stated as follows:

$$\text{minimize} \quad W = \sum_{e=1}^{n} w_e(t) \tag{4.25}$$

$$\text{subject to} \quad C^p \leq C^* \quad (p = 1, 2, \ldots, \text{NL}) \tag{4.26}$$

$$t^{\text{L}} \leq t \leq t^{\text{U}} \tag{4.27}$$

It is noted that the mean compliance (C^p) of an optimal structure under each load case must be within the prescribed limit (C^*).

4.8.2 Two-level control scheme

A two-level control scheme is implemented in the PBO algorithm to guarantee the success in achieving the global optimum based on the performance-based design criteria. The first-level control is in the element removal stage. The SEDs of elements are calculated for each load case. A Logical AND condition is employed in the optimization algorithm to take account of the effects of multiple loading conditions on optimal designs. In the Logical AND condition, an element is eliminated from the design domain only if its SED is the lowest for all load cases. The resulting structure will be stiffest with respect to the worst loading condition.

The second-level control is in the performance evaluation stage for the resulting structure. The performance index of the resulting structure at each iteration is calculated by using the strain energy of the structure under the most critical load case in the optimization process. The strain energy of the structure is usually largest under the most critical load case. The two-level control schemes are consistent with the performance-based optimal design concepts, which require that the overall stiffness performance of an optimal design must be maintained within the prescribed performance level for all loading conditions.

4.9 Performance optimization procedure

The PBO technique utilizes the FEA method as the modeling and computational tool. Based on the information obtained from the results of the FEA, the SEDs of elements can be calculated. Elements with the lowest values of SEDs are listed as inefficient elements for elimination. The performance of a structure can then be improved by gradually eliminating these inefficient elements from the structure. The process of FEA and performance improvement is repeated until the performance of the structure is maximized. The main steps of the performance optimization procedure are illustrated in the flowchart given in Figure 4.2. The optimization procedure is also summarized as follows:

1 Model the initial structure with fine finite elements. Applied loads, material properties and support environments are specified. Design and nondesign regions within the structure can be specified by assigning different material property numbers to elements. Nondesign regions are not removed in an optimization process even if their SEDs are lowest.

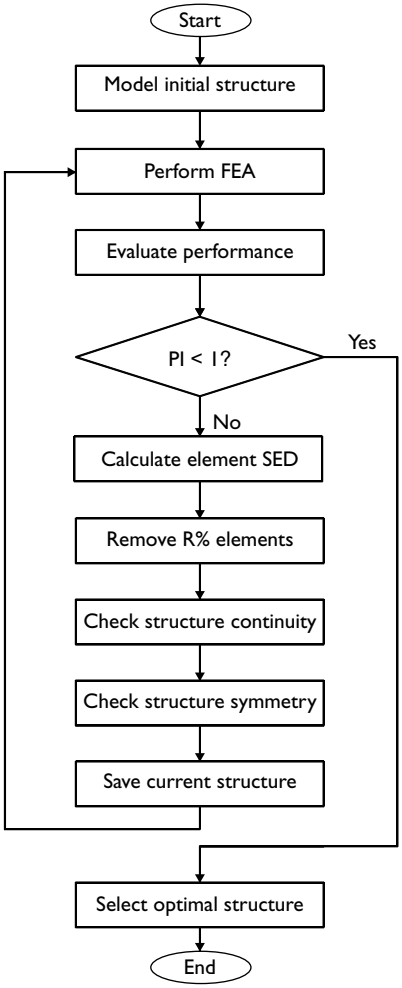

Figure 4.2 Flowchart of performance optimization procedure for structures with mean compliance constraints.

2 Perform a linear elastic FEA on the structure.
3 Evaluate the performance of the resulting structure using PI_{es} for plane stress structures and PI_{ep} for plates in bending.
4 Calculate the SEDs of elements under each load case.
5 Remove a small number of elements with the lowest SEDs from the design regions.

6 Check the continuity of the resulting structure. The continuity constraint affects resulting topologies in an optimization process. Implementing the continuity scheme in optimization algorithms will prevent the discontinuity of the design domain from occurring. It is assumed that two elements are connected together if they have at least one common edge. Any element that is not connected with other elements is considered as a singular element, which is removed from the model.
7 Check the symmetry of the resulting structure in the optimization process. The symmetrical condition of the initial design domain is specified before performing the FEA and optimization. Numerical errors may occur in the calculation of element SEDs since approximate concepts are adopted. This may result in an unsymmetrical structure even if the initial structure has a symmetrical geometry, loading and support condition. A scheme for checking the symmetry of resulting structures is incorporated in the optimization algorithm. Extra elements are removed from the structure to maintain the symmetry of the resulting structure under an initially symmetrical condition.
8 Save model data for the current structure.
9 Repeat steps 2–8 until the performance index is less than unity.
10 Plot the performance index history and select the optimum, which corresponds to the maximum performance index.

4.10 Element addition and deletion schemes

In the PBO method presented in previous sections, an initial continuum structure that is big enough to cover the expected optimal shape is chosen. The initial structure specified is usually over-designed and contains inefficient material. By gradually removing inefficient material from an over-designed structure, the optimal design can be obtained on the basis of the lightweight and high stiffness performance criteria. As discussed in Chapter 3, some structures deflect excessively due to overloaded or other reasons and need to be strengthened by adding material. In order to apply the PBO technique to such design situations, the PBO algorithm is modified to allow elements to be added as well as deleted.

4.10.1 Element addition and deletion criteria

The element addition and deletion criteria can be derived on the basis of design sensitivity analysis on the change in the mean compliance of a structure with respect to material addition and deletion, as discussed in Section 4.3. When an element such as the eth element is deleted or added, the change in the mean compliance of the structure can be evaluated by

$$\Delta C = \pm\{u_e\}^{\mathrm{T}}[k_e]\{u_e\} \tag{4.28}$$

where $\{u_e\}^T$ and $\{u_e\}$ are the displacement vectors of the eth element due to the virtual unit load and real loads, respectively, and $[k_e]$ is the stiffness matrix of the eth element. The sign $\pm$ is for deleted and added elements.

It is noted that the change in the mean compliance of a structure due to element addition and deletion can be calculated by the element strain energy. The SED (γ_e) of an element, which is defined as the strain energy per unit weight, is a measure of the contribution of the added or deleted element to the overall stiffness performance of a structure. The element deletion and addition criteria can be stated as that elements with the smallest values of γ_e are removed from a structure while potential elements with the largest values of SEDs are added to the structure to improve the performance of the structure.

To calculate the SEDs of potential added elements, the displacements $\{u_e\}$ are required. A fictitious displacement field can be established to extract these displacements for added elements. It is noted that a bilinear displacement function is used in four-node square elements. Figure 3.4 shows a portion of a continuum structure modeled by four-node elements. Elements in white color are potential added elements whose material property number is given a zero value. These potential added elements can be added to the boundaries of the structure as illustrated in Figure 3.4. The potential added elements are classified into three types such as E2, E3 and E4, according to the number of nodes whose displacements are known. This means that the element type E2 has known displacements at two nodes. The displacement varies linearly along the edge of an element, the unknown displacements at nodes can be easily determined for element types E2 and E3.

Another way of adding elements to a structure is to attach potential elements to the free edges of the eth element with the largest values of SEDs. Using this method, the calculation of the SEDs for potential added elements is avoided. The added elements strengthen the existing structure to improve its stiffness performance.

The modification of a structure is based on the performance of the structure. If an initial structure selected by the user occupies only a small portion of the maximum design domain, the mean compliance of the initial structure will excess the limit so that elements are needed to be added to the structure to strengthen the structure. The initial structure is growing bigger and bigger by gradually adding elements. After a structure occupies a certain part of the maximum design domain, elements can be added and eliminated simultaneously according to the levels of element SEDs.

4.10.2 Optimization algorithm

The performance-based optimal design can be achieved by applying the PBO algorithms that allow efficient elements to be added to a structure and

inefficient elements to be removed from the structure. Both schemes of adding and deleting elements aim at the same goal of improving the performance of a structural topology or shape. The performance optimization procedure is summarized as follows:

1 Model a maximum design domain with fine finite elements.
2 Select the initial structure within the maximum design domain such that elements in the initial structure can connect the applied loads and the supports.
3 Assign the material property values of all elements that are not selected as the initial structure to zero.
4 Perform the FEA on the structure.
5 Evaluate the performance of resulting structure using PI_{es} for plane stress structures and PI_{ep} for plates in bending.
6 Identify the potential added elements of types E2, E3 and E4 and calculate their nodal displacements by linear extrapolation.
7 Calculate the SEDs for elements.
8 Remove a small number of elements with the lowest values of SEDs and add a small number of elements with the largest values of SEDs.
9 Check the continuity of the resulting structure.
10 Check the symmetry of the resulting structure with an initially symmetrical condition.
11 Save model data for the current structure.
12 Repeat steps 4–11 until the performance index is less than unity.
13 Plot the performance index history and select the optimum.

4.11 Sizing optimization of continuum structures

Sizing optimization of structures has traditionally been a research topic in optimal structural designs. In sizing optimization, design variables are the cross-sectional areas of a truss member or the thickness of a plate. The PBO method presented in previous sections can be used for simultaneous topology and uniform sizing optimization of continuum structures. In certain design situations, design variables must be selected from a set of discrete values such as the plate thickness that is available from manufacturers. The sizing optimization problem with discrete design variables is usually much more difficult to solve than a similar problem with continuous design variables. Therefore, this optimization problem is usually solved using continuous design variables. The rounding-off method is employed to obtain a discrete solution from the continuous one. Structural optimization methods employ the zero–one decision-making scheme are capable of dealing with the sizing optimization of continuum structures with discrete design variables (Chu *et al.* 1998; Steven *et al.* 2002). The performance-based

optimization method for optimal sizing design of continuum structures with discrete design variables for system performance is briefly described in this section.

4.11.1 Thickness design problem formulation

The sizing optimization of a continuum structure is to seek the optimal distribution of element thickness that minimizes the weight of the structure while satisfying the requirement on the overall stiffness performance. The topology of a structure is fixed in a sizing optimization process. In the proposed method, the weight of a continuum structure is treated as the objective function and the constraint is imposed on the mean compliance of the structure. The optimal thickness design problem under multiple load cases can be stated as follows:

$$\text{minimize} \quad W = \sum_{e=1}^{n} w_e(t_e) \tag{4.29}$$

$$\text{subject to} \quad C^p \leq C^* \quad (p = 1, 2, \ldots, \text{NL}) \tag{4.30}$$

$$t^{\text{L}} \leq t_e \leq t^{\text{U}} \tag{4.31}$$

where t_e is the thickness of the eth element. It is noted that the thickness of every element within a structure is a discrete design variable, which can only be selected from a set of discrete values. The upper and lower bounds are imposed on the thickness of elements.

4.11.2 Element thickness reduction criteria

In sizing optimization of a continuum structure modeled with finite elements, elements cannot be removed from the structure. The only way to achieve the performance objective is to reduce the thickness of elements by selecting the smaller values from a prescribed set. The effect of element thickness reduction on the mean compliance of a structure can be evaluated by the design sensitivity analysis, as presented in precious section for topology optimization.

When the thickness of the eth element is reduced from t_e to the next lower value $(t_e - \Delta t_e)$, the stiffness matrix and mean compliance of the structure will change accordingly. The change in the stiffness matrix of the structure is

$$[\Delta K] = [\Delta K_e] = [K_e(t_e - \Delta t_e) - K_e(t_e)] \tag{4.32}$$

where $K_e(t_e)$ and $K_e(t_e - \Delta t_e)$ are the stiffness matrices of the eth element for the thickness t_e and $(t_e - \Delta t_e)$, respectively. According to Eq. (4.9), the

change in the mean compliance of the structure can be evaluated as

$$\Delta C = -\tfrac{1}{2}\{u_e\}^{\mathrm{T}}[\Delta K_e]\{u_e\} \tag{4.33}$$

The above equation indicates that the change in the mean compliance of a structure due to the thickness reduction of the eth element is equal to the change in the strain energy of that element. The change in SED of the eth element due to its thickness reduction is denoted as

$$\gamma_e^{\mathrm{t}} = \frac{|\Delta C|}{w_e} \tag{4.34}$$

The change in the SEDs of elements is a measure of the contribution to the overall stiffness performance of a structure. It is obvious that reducing the thickness of an element with the lowest value of γ_e^{t} will result in a minimum change in the mean compliance of the structure. Therefore, the element thickness reduction criteria state that the thickness of an element with a minimum change in its SED due to thickness reduction is modified.

The SED redistribution method presented in the previous section is also employed to suppress the formation of checkerboard patterns in the sizing optimization of continuum structures including plane stress structures and plates in bending. The two-level control scheme is adopted in the sizing optimization of structures under multiple loading conditions.

4.11.3 Performance-based sizing optimization algorithm

The main steps of the performance optimization procedure for optimal thickness design of continuum structures with mean compliance constraints are illustrated in Figure 4.3 and are summarized as follows:

1 Model the initial continuum structure with fine finite elements.
2 Perform a linearly elastic FEA on the structure.
3 Evaluate the performance of the resulting structure by using Eq. (4.16) for plane stress structures and Eq. (4.19) for plates in bending.
4 Calculate the changes in the SEDs of elements due to thickness reduction.
5 Reduce the thickness of a small number of elements with the smallest changes in SEDs.
6 Check the symmetry of the thickness distribution within the structure with an initially symmetrical condition.
7 Save model data for the current structure.
8 Repeat steps 2–7 until the performance index is maximized.
9 Plot the performance index history and select the optimal design.

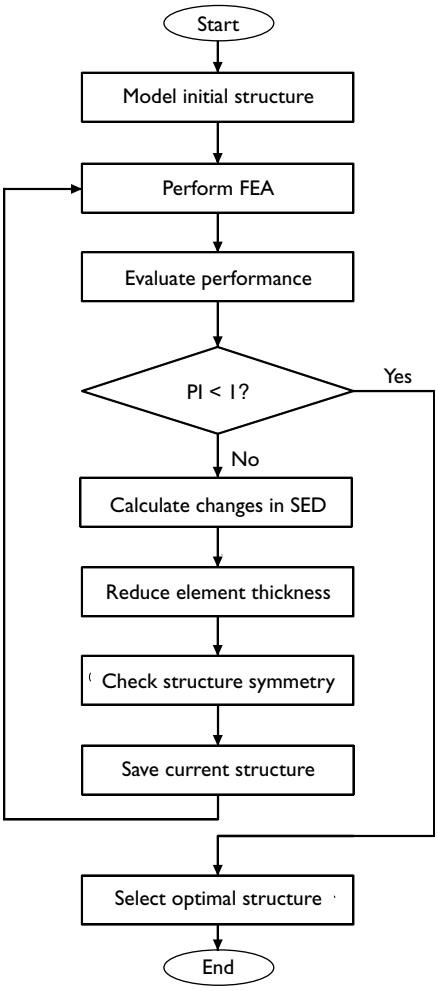

Figure 4.3 Flowchart of performance-based sizing optimization procedure.

4.12 Integrated topology, shape and sizing optimization

The traditional engineering design process is a design/redesign process based on the designer's intuition and past experience, as described in Chapter 1. The engineering design process usually starts with a conceptual design suggested by the designer. This model is then analyzed by using

the FEA software to determine structural responses such as stresses and displacements. Based on the structural responses obtained from the FEA, the design is modified in order to improve its structural performance. This interactive process of design, analysis and redesign is continued until a satisfactory design is achieved. The traditional engineering design process is time-consuming and costly. To significantly reduce the development time and cost of new products and to achieve high-performance innovative designs, integrated topology, shape and sizing optimization techniques must be employed in the engineering design process.

The PBO technology presented in preceding sections has been developed for simultaneous topology and sizing optimization, shape and sizing optimization and pure sizing optimization of continuum structures. In topology and sizing optimization, material can be removed from the boundaries and the interior of a structure so that both topology and shape of the structure are modified in an optimization process. Topology and sizing optimization generally produces very-high-performance optimal structures that can be used in conceptual design. In some design cases, however, further improvement on the optimal topology obtained may be necessary in order to meet design criteria on stresses, displacements and manufacture. In such design situations, shape and sizing optimization technique can be employed. It is nature to combine topology, shape and sizing optimization techniques into a single optimization system. The performance-based integrated topology, shape and sizing optimization procedure is described here.

The procedures for topology optimization and shape optimization are basically same, except that topology optimization allows elements to be removed from any parts of a design domain while shape optimization allows elements to be removed only from the boundaries of the design domain. The flowchart of an integrated topology, shape and sizing optimization procedure is shown in Figure 4.4. The main steps of the procedure are described as follows:

1 Model the initial continuum structure with fine finite elements. Material properties, loading and supported conditions are defined. Nondesign regions are assigned a special material property number.
2 Perform a linearly elastic FEA on the structure.
3 Evaluate the performance of the resulting topology by using Eq. (4.16) for plane stress structures and Eq. (4.19) for plates in bending.
4 Carry out topology optimization.
5 Repeat steps 2–4 until the performance index is less than unity.
6 Plot the performance index history and select the optimal topology.
7 Perform a linearly elastic FEA on the optimal topology obtained in step 6.
8 Evaluate the performance of the resulting shape by using PI_{es} for plane stress structures and PI_{ep} for plates in bending.
9 Carry out shape optimization.

10 Repeat steps 7–9 until the performance index is less than unity.
11 Plot the performance index history and select the optimal shape.

In the integrated topology, shape and sizing optimization, only uniform sizing of element thickness is considered. In steps 4 and 9, topology and shape can be modified by either deleting elements or adding elements.

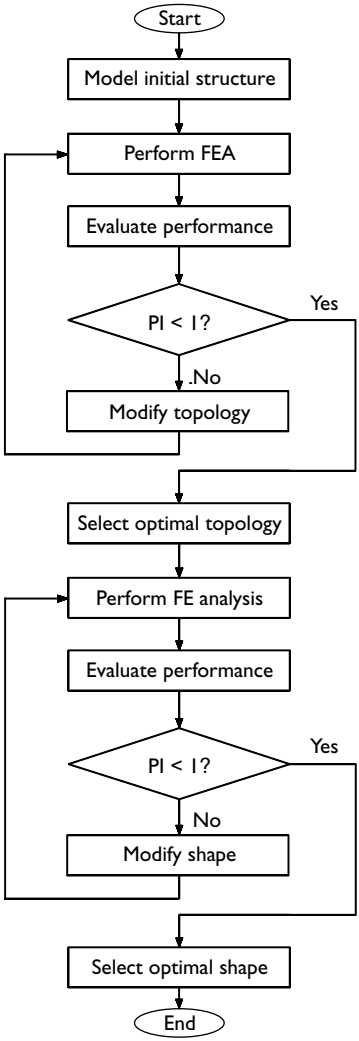

Figure 4.4 Flowchart of the integrated topology, shape and sizing optimization procedure.

Conventional boundary variation methods (Haftka and Grandhi 1986) can also be incorporated in step 9 to modify the shape. However, the boundaries of the initial shape need to be defined before carrying out the shape optimization process.

4.13 Examples

Benchmark examples are provided in this section to demonstrate the effectiveness and validity of the PBO method developed for optimal topology and shape design of continuum structures with mean compliance constraints. First, the PBO method is verified by the well-known analytical solution of the Michell structure. In Section 4.13.2, the PBO technique is used to find the best layout of a bridge structure. Topology optimization of a structure under multiple load cases is treated in Section 4.13.3. In Section 4.13.4, the optimal shape design is presented. The characteristics of the performance index for plates in bending are investigated in Section 4.13.5. Finally, the effects of mesh discretization on optimal designs are investigated in Section 4.13.6.

4.13.1 Michell structure

Figure 4.5 shows the optimal solution of a Michell truss, which was derived by Michell (1904) using the analytical method. This example is to demonstrate that whether the PBO method incorporating the uniform sizing of element thickness for the optimal topology design of continuum structures with mean compliance constraints can reproduce the Michell truss. A continuum structure shown in Figure 4.6 was used as the initial structure for deriving the Michell truss (Bendsøe *et al.* 1993). The initial structure was discretized into 110×80 four-node plane stress elements. The circular non-design domain was modeled approximately by rectangular elements and was treated as the fixed support. A tip load was applied to the center of the free end as illustrated in Figure 4.6. The Young's modulus of material

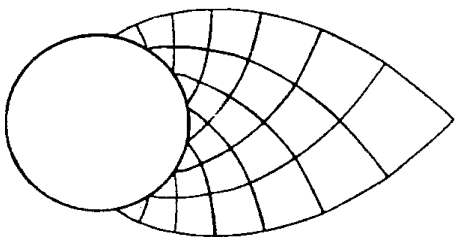

Figure 4.5 Michell truss.

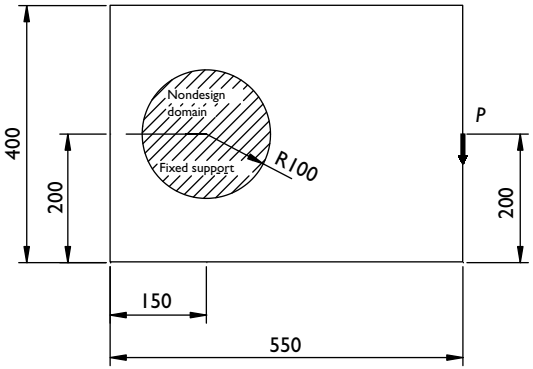

Figure 4.6 Design domain for the Michell structure.

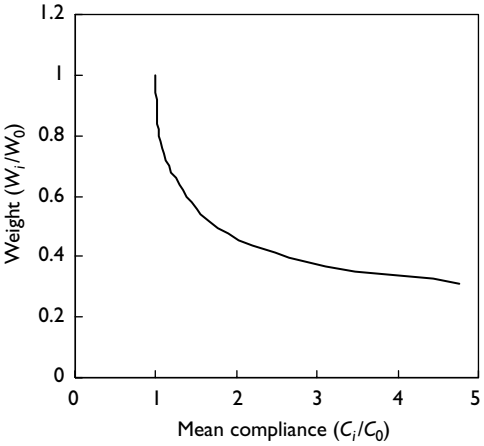

Figure 4.7 Performance characteristic curve for the Michell structure.

$E = 200\,\text{GPa}$, Poisson's ratio $\nu = 0.3$, and thickness of elements $t = 5\,\text{mm}$ were specified in the FEA. The element removal ratio of 2 percent was used in the optimization process.

The performance characteristic curve for the Michell structure in the performance optimization process is presented in Figure 4.7. It can be observed from the dimensionless weight–compliance curve that the weight of the Michell structure reduces with an increase in the mean compliance. In addition, this curve indicates the variation rate of the weight and mean compliance in the optimization process. The performance index history of the Michell type structure is presented in Figure 4.8. It is seen that the performance of

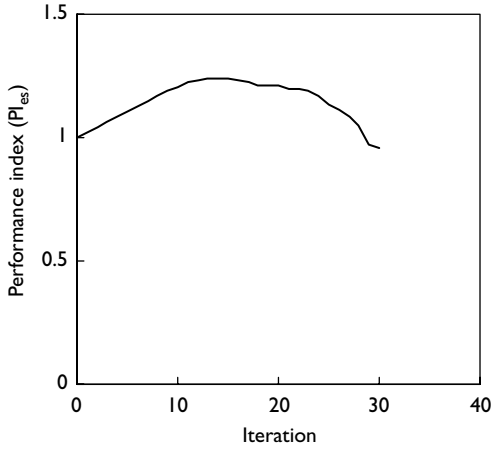

Figure 4.8 Performance index history of the Michell structure.

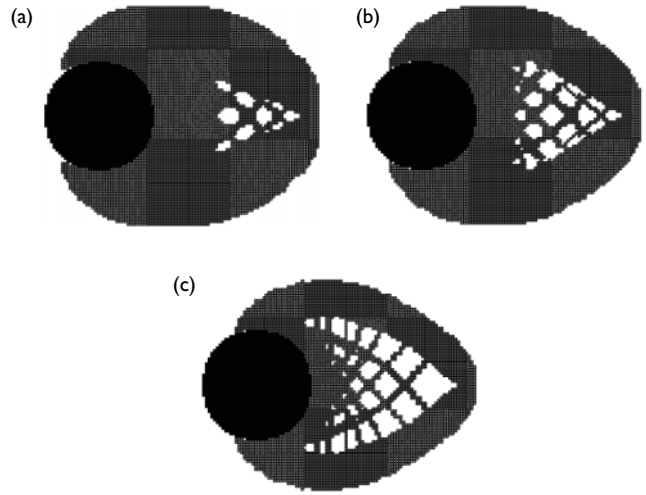

Figure 4.9 Topology optimization history of the Michell structure: (a) at iteration 14, $PI_{es} = 1.24$; (b) at iteration 17, $PI_{es} = 1.22$; (c) at iteration 23, $PI_{es} = 1.19$.

resulting topologies in the optimization process was gradually improved by eliminating elements with the lowest SEDs from the design domain. The maximum performance index was 1.24, which occurred at iteration 14.

The optimal topology corresponding to the maximum performance index is shown in Figure 4.9(a) based on the PBOC. It is observed that the optimal topology obtained is a continuum structure rather than a Michell truss.

It is noted that continuum topology optimization is a more general approach than the truss topology optimization method, and may or may not result in truss-like structures. In order to generate a truss-like structure, the optimization process was continued. The resulting topologies at iterations 17 and 23 are presented in Figure 4.9(b,c). It can be seen that when more and more elements were removed from the design domain, the resulting topology gradually evolved towards a Michell truss. If the resulting structure is to be designed as a truss, the topology shown in Figure 4.9(c) agrees extremely well with the Michell truss depicted in Figure 4.5 and solutions produced by the HBO method (Suzuki and Kikuchi 1991; Bendsøe *et al*. 1993).

It appears from Figure 4.9 that the performance of resulting topology at iterations 14–23 decreased only slightly. This indicates that the material volume that is needed to construct these structures is almost the same while maintaining their overall stiffness performance within the same level. In other words, the structure can be designed by selecting one of these topologies shown in Figure 4.9. When compared with the scaled initial structure, topologies shown in Figure 4.9(a)–(c) result in material volume reduction of 19.3, 18.7 and 16 percent, respectively. After iteration 23, the interior of the topology obtained was broken up. As a result, the performance of the resulting topologies decreased considerably as indicated by the performance index history. Continuum topology optimization is the selection of the best configurations for the design of continuum structures. The performance index is a useful tool for assisting the selection of the best topology in structural design when considering the structural performance, esthetic and construction constraints. The importance of the system performance should be ranked the first since it relates to the safety of the design.

4.13.2 Form optimization of bridge structures

In this example, the PBO method was used to find the best layout of a bridge structure under uniformly distributed traffic loading. The design domain, loading and support conditions of a bridge structure are depicted in Figure 4.10. The bottom supports of the bridge were fixed. The continuum design domain was discretized into 90×30 four-node plane stress finite elements. The bridge deck was modeled by two rows of elements below the loading level and treated as the nondesign domain. The uniformly distributed loading was simulated by applying a 500 kN point load per node. The Young's modulus of material $E = 200$ GPa, Poisson's ratio $\nu = 0.3$ and the thickness of elements $t = 300$ mm were specified in the FEA. The element deletion ratio of 1 percent was employed in the optimization process.

The performance index history of the bridge structure obtained by the PBO method is provided in Figure 4.11. When underutilized elements were eliminated from the design domain, the performance index of the

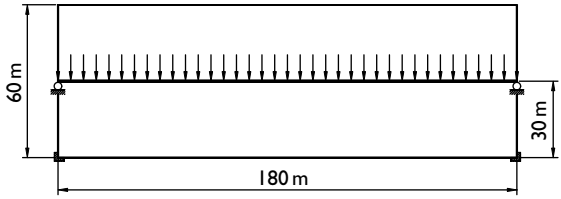

Figure 4.10 Design domain for a bridge structure.

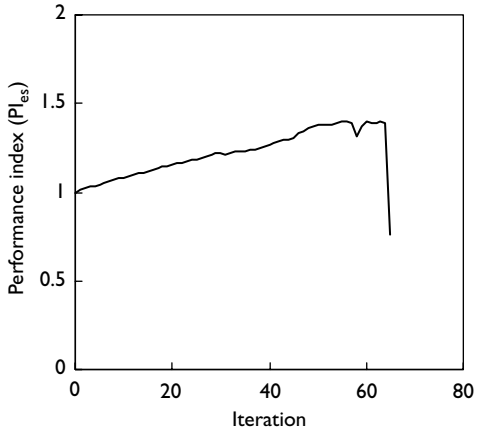

Figure 4.11 Performance index history of the bridge structure.

bridge structure increased from unity to the maximum value of 1.4, which corresponded to the iteration 56. After iteration 64, the performance index dropped sharply and this indicated that the load-carrying mechanism was destroyed by further element elimination. The increase in strain energy and the reduction in the weight of the bridge structure are characterized by the performance characteristic curve shown in Figure 4.12. After 69 percent material was removed from the bridge structure, the mean compliance increased to 2.3 times the value of the initial structure. Further material removal led to a significant increase in the mean compliance of the bridge as shown in Figure 4.12. Therefore, the topologies obtained after iteration 64 are not recommended as the final design.

Figure 4.13 depicts the topology optimization history of the bridge structure. It can be seen from the topology optimization history that the part below the bridge deck was systematically eliminated because they were inefficient in transferring the loads. The optimal topology generated by the PBO technique is shown in Figure 4.13(c), which indicates a well-known

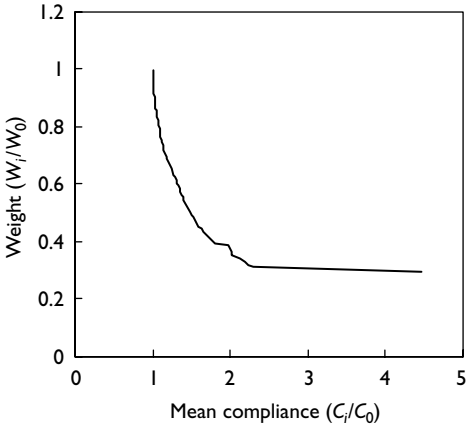

Figure 4.12 Performance characteristic curve for the bridge structure.

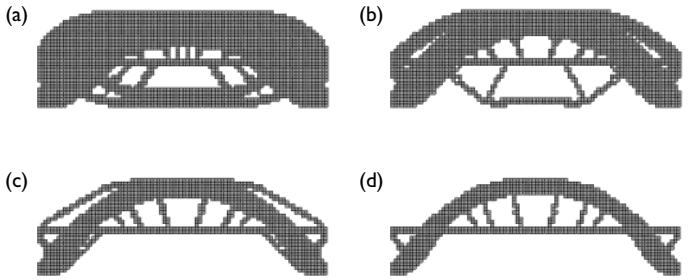

Figure 4.13 Form optimization of a tie–arch bridge structure: (a) topology at iteration 20; (b) topology at iteration 40; (c) optimal topology at iteration 56; (d) topology at iteration 64.

tie–arch bridge structural system that has commonly been used in bridge engineering. In the design of bridge structures, multiple performance objectives need to be considered, including functionality, economy, esthetic and construction constraints. The esthetic issue may weight over the economic aspects if the beauty of a bridge is of importance to the surrounding environment. The performance index can be used to assist the selection of a bridge form that has not only a good looking but also high structural performance. It can be observed from Figure 4.13 that the performance of the topology obtained at iteration 64 is the same as that of the optimum. However, the bridge form shown in Figure 4.13(d) looks better than that of the optimum. Therefore, the topology presented in Figure 4.13(d) shall be

used as the final form for the bridge. The optimized design shown in Figure 4.13(d) has resulted in material volume reduction of 28 percent in comparison with the scaled initial structure. The arch of the bridge can be constructed by using either reinforced concrete or steel trusses, which were the construction form used in the Sydney Harbor Bridge.

4.13.3 Multiple load cases

Structures or structural members are designed to carry applied loads. Different structural topologies must be developed for different loading environments in which they will operate. Optimal topology design for multiple load cases is to find the best load carrying structure in a given design domain, which can safely operate in all loading conditions. This example is to investigate the effects of various loading conditions including multiple load cases on optimal structures by using the PBO technique. A simply supported beam under multiple load cases is shown in Figure 4.14. The thickness of the beam was 10 mm. In load case 1, a concentrated load $P_1 = 40\,\text{kN}$ was applied at the top of the beam. In load case 2, two concentrated loads with a magnitude $P_2 = 20\,\text{kN}$ were applied to the bottom of the beam as shown in Figure 4.15. The beam was modeled using 60×30 four-node plane stress elements. The Young's modulus $E = 200\,\text{GPa}$ and Poisson's ratio $\nu = 0.3$ were used in the FEA. The element removal ratio of 1 percent was employed in the optimization process for all cases.

It was assumed that this simply supported beam was subjected to various loading conditions, such as load case 1 alone, load case 2 alone, two load cases applied at a different time, and all loads acting simultaneously. The performance index histories of the beam under various loading conditions are shown in Figure 4.15. It is interesting to note that the performance of

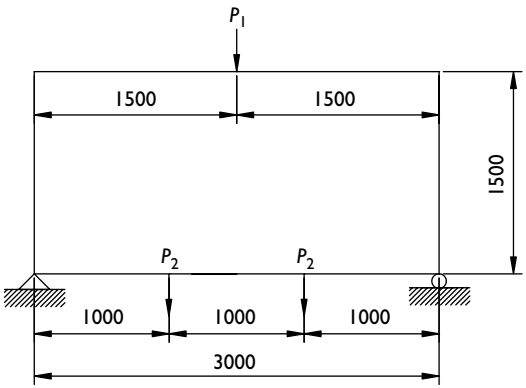

Figure 4.14 Simply supported beam under multiple load cases.

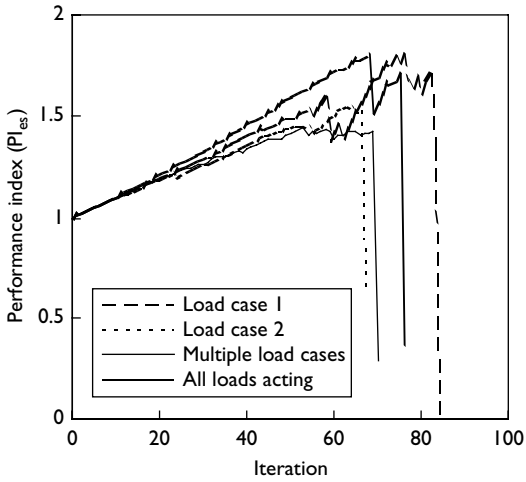

Figure 4.15 Performance index histories of the beam under multiple load cases.

the optimal design under load case 1 alone is the same as that of the optimum under all loads acting simultaneously. These two optimal structures have a maximum performance index of 1.8, which is the highest in all cases considered. The optimal design under multiple load cases in which load cases 1 and 2 were applied at different times has the lowest performance in comparison with other loading conditions. Its performance index is only 1.44. The maximum performance index was determined as 1.55 for the optimal structure subject to load case 2 alone. It is shown that the optimal structure under multiple load cases usually needs more material to construct than the one under a single load case for the same design space and supported condition. This can be justified by the fact that an optimal structure under a single loading condition can transmit the applied loads to the supports more directly than the one under multiple loading conditions. The direct load paths lead to significant material savings and high performance structures. The performance characteristic curves of the beam under various loading conditions are presented in Figure 4.16. These curves represent the actual performance responses of the beam in the optimization processes. It can be observed from Figure 4.16 that the beam under multiple load cases is heaviest for the same system performance level.

Optimal designs produced by PBO for the beam under various loading conditions are shown in Figure 4.17. It is seen from Figure 4.17 that the optimal topology of the beam subject to load case 1 is the simplest. It transfers the point load from the top of the beam to two supports through two direct load paths. When the two point loads P_2 are applied at the bottom of

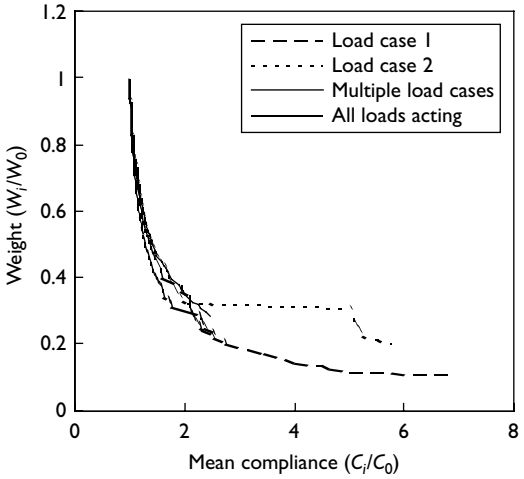

Figure 4.16 Performance characteristic curves for the beam under multiple load cases.

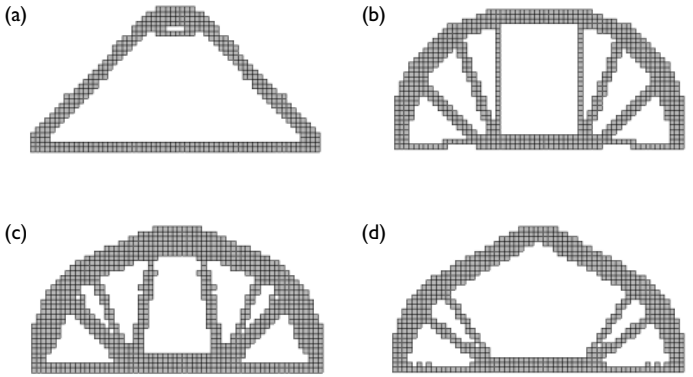

Figure 4.17 Optimal designs for various loading conditions: (a) load case 1, $PI_{es} = 1.8$; (b) load cases 2, $PI_{es} = 1.55$; (c) multiple load cases, $PI_{es} = 1.44$; (d) all loads acting, $PI_{es} = 1.8$.

the beam, the loads are transferred to the arch through ties and than to the supports. A complex load carrying system is formed, as shown in Figure 4.17(b). When multiple load cases are applied to the beam, the ties and arch shown in Figure 4.17(c) are adjusted to transfer the loads P_1 and P_2. The optimal structure obtained for the beam with the loads P_1 and P_2 acting simultaneously is presented in Figure 4.17(d). This structure is simpler than that under multiple load cases. When compared with the scaled

initial structure, optimal designs presented in Figure 4.17(a)–(d) have resulted in material volume reduction by 44.4, 35.5 and 30.6 percent, respectively.

It can also be observed from Figure 4.17 that applying the loads at the top of the beam results in a simpler and higher performance load carrying mechanism than hanging them at its bottom. This addresses another optimal design problem, which is how to define the initial structure that can result in the best performance design. Optimal structural design is really a challenging design task. It needs the creativity of the designer although the PBO method offers him or her an efficient, automated tool for achieving lightweight, high-performance and innovative structures in given design spaces.

4.13.4 Optimal shape design

Topology optimization generally yields higher performance designs than shape optimization, except for some special cases such as plates in bending, as demonstrated in Chapter 3. In certain design situations, a structure or structural component is not allowed to have cavities within the structure or structural component. For such design situations, the performance-based shape optimization technique with a uniform thickness-sizing scheme should be used. In shape optimization, material can only be removed from the boundaries of a continuum structure. In the PBO method, boundary elements with the lowest SEDs are gradually eliminated from a structure so that the performance of the structure can be maximized. An example is presented here to demonstrate the ability of the PBO method to produce the optimal shape of a continuum structure with mean compliance constraints.

The continuum design domain for a short cantilever beam is shown in Figure 4.18. The left side of the beam was fixed. A point load of 3 kN was applied to the tip of the beam. It was required to find the optimal shape of

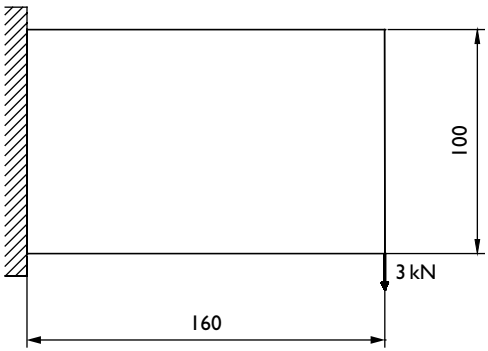

Figure 4.18 Design domain for the short cantilever beam.

this short cantilever beam with the maximum overall stiffness performance and minimum weight. Material could be removed from any boundaries of the beam. The beam was discretized into 48×30 four-node plane stress elements. The thickness of elements was 1 mm. The Young's modulus $E = 207$ GPa and Poisson's ratio $\nu = 0.3$ were assumed in the FEA. The element removal ratio of 2 percent was specified in the optimization process.

The performance index history of the cantilever beam in the optimization process is shown in Figure 4.19. The energy-based performance index increased from 1.0 to the maximum value of 1.16 when boundary elements with the lowest SEDs were systematically deleted from the model. The performance characteristics of the cantilever beam predicted by PBO are demonstrated in Figure 4.20. It is seen that shape optimization produced a smooth weight–compliance curve since elements were removed only from the boundaries of the beam. The performance of the cantilever beam was maximized when 35 percent elements were eliminated from the boundaries. This led to an increase in the mean compliance by 32.5 percent. In comparison with the initial design, the optimal shape obtained results in 14 percent material saving for any required stiffness performance level.

The shape optimization history of the cantilever beam is presented in Figure 4.21. It can be observed from this figure that elements were gradually removed from two boundary regions of the beam. No internal cavities were created within the resulting shapes. The optimal shape shown in Figure 4.21(d) is a continuum structure rather than a truss-like structure. If the elements at the left boundary of the initial design are specified as the nondesign domain, the reader can imagine what the optimal shape will look like.

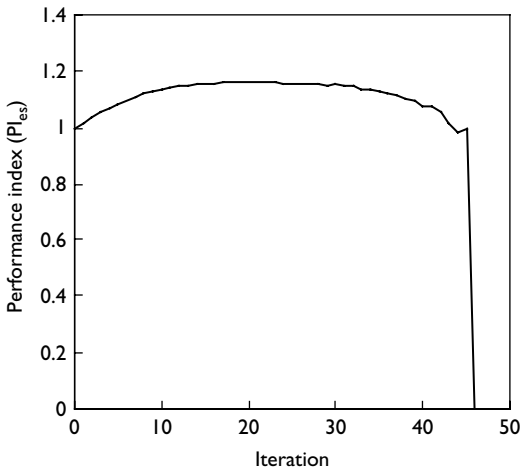

Figure 4.19 Performance index history of the short cantilever beam.

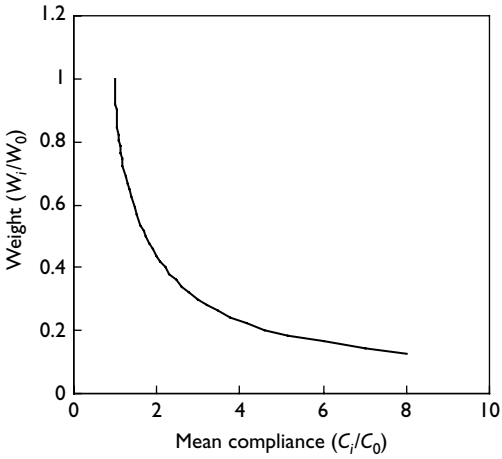

Figure 4.20 Performance characteristic curve for the short cantilever beam.

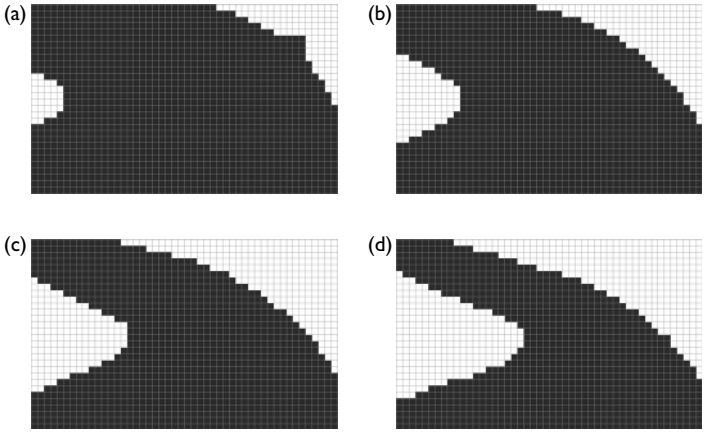

Figure 4.21 Shape optimization history of the short cantilever beam: (a) shape at iteration 5; (b) shape at iteration 10; (c) shape at iteration 15; (d) optimum at iteration 20.

4.13.5 Plates in bending

For a structure under a concentrated load, both of the PBO techniques for structures with displacement constraints and mean compliance constraints are equally efficient and shall produce a same solution for the same design problem. This example is to investigate whether the PBO methods with

different formulations can produce the same optimal topology for a plate in bending. The clamped plate under a concentrated load applied at its center presented in Section 3.11.1 was optimized using the PBO method for overall stiffness performance. The design and optimization parameters given in Section 3.11.1 were adopted, except that the overall stiffness constraint instead of a displacement constraint was considered.

Figure 4.22 shows the history of the performance index calculated using Eq. (4.19). The performance index curve shown in Figure 4.22 is similar to that presented in Figure 3.26. This is because for a structure under a single point load, the performance index calculated using Eq. (3.30) based on the displacement under the point load is the same as that calculated using Eq. (4.19) based on the mean compliance of the structure. The maximum performance index by the PBO method for structures with displacement constraints was 2.09 while it was 2.13 by the PBO method for structures with overall stiffness constraint. It is shown that the PBO method based on the overall stiffness performance criteria provides higher performance topologies than that based on displacement performance criteria. The performance characteristics of the plate in bending in the optimization process are demonstrated in Figure 4.23.

The topology optimization history of the plate in bending is presented in Figure 4.24. The topology obtained at iteration 10 as shown in Figure 4.24(a) is identical to that presented in Figure 3.27(a). The slight differences between topologies obtained by the two PBO techniques are observed at iteration 20, 40 and the optimum. These differences may be caused by the element removal criteria adopted in the optimization algorithms since the VSEDs and SEDs are approximately calculated for element elimination

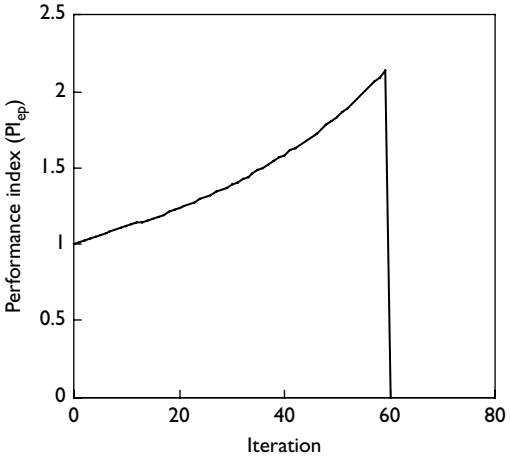

Figure 4.22 Performance index history of clamed plate in bending.

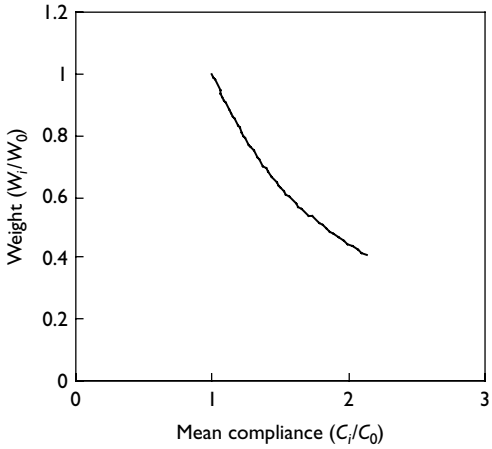

Figure 4.23 Performance characteristic curve for the plate in bending.

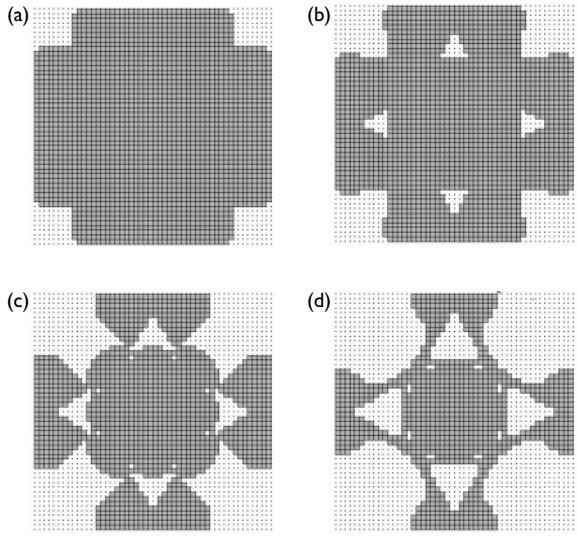

Figure 4.24 Topology optimization history of the plate with mean compliance constraint: (a) topology at iteration 10; (b) topology at iteration 20; (c) topology at iteration 40; (d) optimal at iteration 59.

in both methods. The weight of the optimal topology shown in Figure 4.24 is 47 percent of that of the scaled initial plate for the same stiffness performance. The optimal design produced by PBO thus saves 53 percent material in comparison with the initial plate design.

4.13.6 *Effects of finite element meshes*

It has commonly been observed that optimal designs depend on the refinement of finite element meshes in topology optimization of continuum structures. This problem is referred to mesh dependency in the literature. Similar to the checkerboard pattern problem, mesh dependency is also caused by the error of the finite element formulation. This example is to investigate the effects of finite element meshes on the optimal topologies of continuum structures optimized by the PBO method while other conditions are fixed. The Michell type structure with a simply supported condition was used as the test example.

The design domain for the simply supported Michell structure under a concentrated load of $P = 100$ kN is depicted in Figure 4.25. The design domain was divided into 70×35, 100×50 and 120×60 meshes using four-node plane stress elements. The Young's modulus $E = 200$ GPa, Poisson's ratio $\nu = 0.3$ and the thickness of all elements $t = 10$ mm were specified in the FEA. The structure was assumed to be in plane stress conditions. The element removal ratio of 1 percent was used for all cases in order to eliminate the effect of the element removal ratio on optimal solutions. The PBO technique was applied to the structure modeled with three different finite element meshes.

The performance index histories of the Michell structure modeled with three different finite element meshes are depicted in Figure 4.26. The results show that the discrepancies of the performance index value between different mesh increase with an increase in the iteration numbers. The finer the mesh used to model the structure, the higher the performance of the optimal topology obtained. The performance indices of optimal topologies obtained using meshes 70×35, 100×50 and 120×60 were 1.53, 1.60 and 1.67, respectively. Performance indices were maximized at different

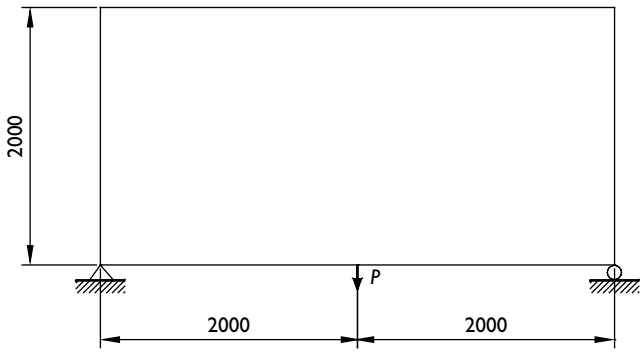

Figure 4.25 Design domain for simply supported Michell type structure.

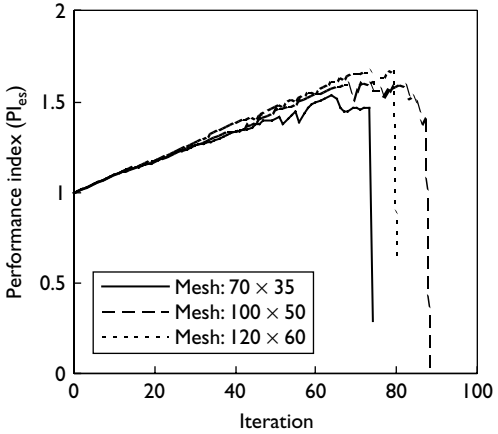

Figure 4.26 Effects of finite element meshes on performance indices.

iterations for the structure modeled using different meshes for the same element removal ratio. It is also observed that performance indices decreased and finally dropped very sharply after they reached the peak. The performance index histories indicate that more iteration is usually needed for a structure modeled with a finer mesh to obtain the optimum.

Figure 4.27 shows optimal topologies obtained using three different finite element meshes. The optimal topology obtained using 70×35 finite elements is a truss-like structure as shown in Figure 4.27(a). It can be observed that the in-plane member size of the truss is approximately proportional to the axial force carried by that member. The distribution of element SEDs within this optimal topology was approximately uniform because underutilized elements were systematically eliminated from the structure. Figure 4.27(b) presents the optimal topology obtained by using a 100×50 mesh. It is observed from Figure 4.27(a,b) that the topologies of these two optimal designs are almost identical. However, the in-plane member size of the optimal design with a finer mesh discretization is smaller than that of the design modeled with a coarse mesh.

The optimal structure obtained by Michell (1904) using the analytical method is a pin-jointed truss with finite members. It was assumed that the strain field in the Michell truss was linearized. Furthermore, compression and tension members were subjected to the same allowable stress. The Michell truss is theoretical optimum and is not necessarily a practical design. A more accurate solution can be achieved by using a finer mesh in the FEA. To see whether the optimal design can approach the Michell truss, the structure was divided into a 120×60 mesh. Figure 4.27(c) depicts the

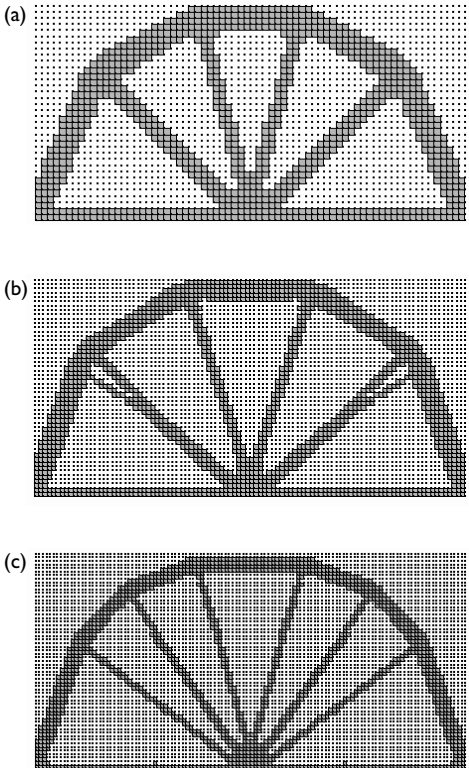

Figure 4.27 Mesh effects on optimal topologies of Michell structure: (a) 70×35, $PI_{es} = 1.53$; (b) 100×50, $PI_{es} = 1.60$; (c) 120×60, $PI_{es} = 1.67$.

optimal topology obtained by the PBO method using 120×60 elements. The optimum obtained by using the finer elements agrees well with the optimal solution of the Michell truss. If elements were refined infinitely, the optimal structure would be towards the Michell truss.

It can be concluded that the optimal structure converges to the theoretical optimum as sufficiently finer mesh is used in the finite element model. Even coarse mesh can produce a rough idea of the optimal structure. In the conceptual design stage, if the PBO method is used to produce the primary layout of a structural system, a coarse mesh can be used to solve the optimization problem. After the structural system has been generated, shape and sizing optimization techniques can be employed to further improve its performance.

4.14 Conclusion

The PBO method formulated on the basis of system performance criteria for optimal topology design of continuum structures under multiple loading conditions has been presented in this chapter. In the proposed approach, element removal criteria are based on the SEDs of elements. By gradually deleting elements with the lowest SEDs from a structure or adding elements with the largest values of SEDs to the structure, the optimal topology or shape of the structure with maximum stiffness at minimum weight can be generated. Two energy-based performance indices have been derived using the scaling design concept for evaluating the topology performance of plane stress structures and of plates in bending. Performance indices are used as the termination criteria in the PBO algorithms. Maximization of performance indices is proposed as PBOC. The PBO algorithm is easily extended to the sizing optimization of continuum structures with overall stiffness constraints and discrete design variables. Benchmark examples have been provided to demonstrate the effectiveness and validity of the PBO method for maximum stiffness topology design of continuum structures.

Based on the study presented in this chapter, the following conclusions are drawn:

- The PBO method is a realistic structural optimization approach, in which the performance objective is to minimize the weight of a structure while maintaining its mean compliance within an acceptable performance level.
- The sensitivity analysis shows that the element SED is a measure of the element contribution to the overall stiffness performance of a structure, and thus can be used as element removal criteria in continuum topology optimization. The maximum stiffness topology design at minimum weight can be obtained by removing elements with the lowest SEDs from a structure or adding potential elements with the highest SEDs to the structure.
- Performance indices presented are dimensionless and can be used to evaluate the performance of structural topologies and shapes in terms of the mass and overall stiffness efficiency.
- Energy-based performance indices are extremely useful tools in continuum topology optimization. They can be used to monitor the optimization process and as termination criteria.
- PBOC can be incorporated in stiffness-based continuum topology optimization methods to obtain the global optimum. For example, they can be incorporated in the HBO method and the DBO method.
- Continuum topology optimization is a generalized shape optimization approach. It has been shown that continuum topology optimization methods may or may not result in truss-like structures, they are in this

sense more general than the truss topology optimization based on the ground structure approach.
- The optimal topology produced by continuum topology optimization methods is not necessarily the one that meets the construction requirements. As a result, performance indices can be used to assist the selection of the best design in terms of the structural performance, esthetics and constructability.
- For a structure under multiple loading conditions, a logical AND scheme is employed in the optimization method to take account of the effects of multiple load cases on the optimal design. The performance index at each iteration is determined by using the strain energy of the resulting structure under the most critical loading case.
- It has been shown that the finer the mesh used to model a structure, the higher the performance of the optimal topology obtained.
- More iteration is usually needed for a structure modeled using a finer mesh to obtain the optimum.

Chapters 2–4 were concerned with the theoretical development and verification of the PBO method for the layout design of continuum structures for strength, displacement and overall stiffness performance. Examples presented in these chapters were mainly used to verify the proposed methods from theoretical aspects rather than practical application. However, in order to develop continuum topology optimization methods into practical design tools for practicing design engineers, the PBO method for structures with displacement and overall stiffness constraints are extended to solve real-world civil engineering problems in Chapters 5 and 6. In Chapter 5, the PBO method will be proposed as an automated design tool for generating optimal strut-and-tie models in structural concrete. In Chapter 6, the PBO method formulated on the basis of system performance criteria will be developed for the conceptual design of lateral load resisting systems for multistory building frames.

4.15 References

Beckers, M. (1999) "Topology optimization using a dual method with discrete variables," *Structural Optimization*, 17: 14–24.

Bendsøe, M. P. (1989) "Optimal shape design as a material distribution problem," *Structural Optimization*, 1: 193–202.

Bendsøe, M. P. and Kikuchi, N. (1988) "Generating optimal topologies in structural design using a homogenization method," *Computer Methods in Applied Mechanics and Engineering*, 71: 197–224.

Bendsøe, M. P. and Sigmund, O. (2003) *Topology Optimization: Theory, Methods, and Applications*, Berlin: Springer-Verlag.

Bendsøe, M. P., Díaz, A. R. and Kikuchi, N. (1993) "Topology and generalization layout optimization of elastic structures," in M. P. Bendsøe and C. A. Mota Soares (eds)

Topology Design of Structures, Dordrecht: Kluwer Academic Publishers, pp. 159–206.

Bendsøe, M. P., Díaz, A. R., Lipton, R. and Taylor, J. E. (1995) "Optimal design of material properties and material distribution for multiple loading conditions," *International Journal for Numerical Methods in Engineering*, 35: 1449–1170.

Chu, D. N., Xie, Y. M. and Steven, G. P. (1998) "An evolutionary structural optimization method for sizing problems with discrete design variables," *Computers and Structures*, 68: 419–431.

Díaz, A. R. and Bendsøe, M. P. (1992) "Shape optimization of structures for multiple loading condition using a homogenization method," *Structural Optimization*, 4: 17–22.

Gea, H. C. (1996) "Topology optimization: a new microstructure-based design domain method," *Computers and Structures*, 61(5): 781–788.

Haftka, R. T. and Grandhi, R. V. (1986) "Structural shape optimization – a survey," *Computer Methods in Applied Mechanics and Engineering*, 57(1): 91–106.

Hassani, B. and Hinton, E. (1999) *Homogenization and Structural Topology Optimization*, Berlin: Springer-Verlag.

Haug, E. J., Choi, K. K. and Komkov, V. (1986) *Design Sensitivity Analysis of Structural Systems*, New York: Academic Press.

Kikuchi, N., Chung, K. Y., Torigaki, T. and Taylor, J. E. (1986) "Adaptive finite element methods for shape optimization of linear elastic structures," *Computer Methods in Applied Mechanics and Engineering*, 57(1): 67–91.

Kirsch, U. (1982) "Optimal design based on approximate scaling," *Journal of Structural Engineering*, ASCE, 108(ST4): 888–909.

Krog, L. A. and Olhoff, N. (1999) "Optimum topology and reinforcement design of disk and plate structures with multiple stiffness and eigenfrequency objectives," *Computers and Structures*, 72: 535–563.

Liang, Q. Q. (2001a) *Performance-Based Optimization Method for Structural Topology and Shape Design*, PhD thesis, Victoria University of Technology, Australia.

Liang, Q. Q. (2001b) "Performance-based optimization method in civil and structural engineering," paper presented at the Australasian Structural Engineering Conference, Gold Coast, Australia, pp. 37–44.

Liang, Q. Q. and Steven, G. P. (2002) "A performance-based optimization method for topology design of continuum structures with mean compliance constraints," *Computer Methods in Applied Mechanics and Engineering*, 191(13–14): 1471–1489.

Michell, A. G. M. (1904) "The limits of economy of material in frame-structures," *Philosophy Magazine*, 8: 589–597.

Mlejnek, H. P. and Schirrmacher, R. (1993) "An engineer's approach to optimal material distribution and shape finding," *Computer Methods in Applied Mechanics and Engineering*, 106: 1–26.

Morris, A. J. (ed.) (1982). *Foundations of Structural Optimization: A Unified Approach*, New York: John Wiley & Sons.

Ramm, E., Bletzinger, K. U., Reitinger, R. and Maute, K. (1994) "The challenge of structural optimization," in B. H. V. Topping and M. Papadrakakis (eds) *Advances in Structural Optimization*, Scotland: Civil-Comp Press pp. 27–52.

Rousselet, B. and Haug, E. J. (1983) "Design sensitivity analysis in structural mechanics, III. Effects of shape variation," *Journal of Structural Mechanics*, ASCE, 10(3): 273–310.

Rozvany, G. I. N., Bendsøe, M. P. and Kirsch, U. (1995) "Layout optimization of structures," *Applied Mechanics Review*, 48: 41–119.

Sigmund, O. (2001) "A 99 line topology optimization code written in Metlab," *Structural and Multidisciplinary Optimization*, 21: 120–127.

Steven, G. P., Li, Q. and Xie, Y. M. (2002) "Multicriteria optimization that minimizes maximum stress and maximizes stiffness," *Computers and Structures*, 80(27–39): 2433–2488.

Suzuki, K. and Kikuchi, N. (1991) "A homogenization method for shape and topology optimization," *Computer Methods in Applied Mechanics and Engineering*, 93: 291–318.

Tenek, L. H. and Hagiwara, I. (1993) "Static and vibrational shape and topology optimization using homogenization and mathematical programming," *Computer Methods in Applied Mechanics and Engineering*, 109: 143–154.

Yang, R. J. (1997) "Multidiscipline topology optimization," *Computers and Structures*, 63(6): 1205–1212.

Yang, R. J. and Chuang, C. H. (1994) "Optimal topology design using linear programming," *Computers and Structures*, 52(2): 265–275.

Zienkiewicz, O. C. and Campbell, J. S. (1973) "Shape optimization and sequential linear programming," in R. H. Gallagher and O. C. Zienkiewicz (eds) *Optimum Structural Design*, New York: Wiley, pp. 109–126.

Chapter 5

Automatic generation of strut-and-tie models in structural concrete

5.1 Introduction

Despite extensive experimental work has been carried out on shear in structural concrete, the shear design problem of structural concrete members has not been solved fully due to its complexity. The load transfer mechanism of a structural concrete member is not the function of a single variable and it depends on the geometry, loading and support conditions of the member. Empirical equations adopted in current concrete model codes lead to complex design procedures for shear and generally yield shear strength predictions, which deviate considerably from experimental results. In addition, empirical equations need to be continuously evaluated for new materials. Design procedures based on test results, rules of thumb, guess work and past experience have been one of the main reasons for the poor structural performance and failure of concrete structures. These highlight the limitations of empirical equations and the need for a rational approach to structural concrete.

It has been recognized that the simple strut-and-tie model approach provides a better understanding of the behavior of structural concrete under combined actions of bending, shear and torsion (ASCE-ACI Committee 445 on Shear and Torsion 1998). The strut-and-tie model is primarily used to represent the load transfer mechanism in a cracked structural concrete member at its ultimate limit state. Traditional methods are not efficient in developing strut-and-tie models in structural concrete since they involve a trial-and-error process. The strut-and-tie models obtained by trial-and-error methods vary greatly with the designer's intuition and past experience. On the other hand, it is time-consuming and difficult for the structural designer to find an appropriate strut-and-tie model for a structural concrete member with complex geometry and loading conditions. Therefore, it becomes apparent that the development of an efficient and reliable technique for strut-and-tie modeling of structural concrete is of significant importance.

As described in the preceding chapters, topology optimization of continuum structures has achieved significant progress in the past two decades. Many structural optimization algorithms have been developed for topology design of continuum structures. It should be noted that, however, most of the existing topology optimization methods focus mainly on mathematical aspects rather than practical applications. Moreover, no performance-based optimality criteria (PBOC) are used in these methods to obtain the global optimum. The gap between the progress of continuum topology optimization theory and its applications to civil engineering does not appear to have been reduced during the last two decades (Cohn and Dinovitzer 1994). The work presented in this chapter is an attempt to reduce the gap between the theoretical development of continuum topology optimization and its practical applications to structural engineering.

In this chapter, the performance-based optimization (PBO) method formulated on the basis of displacement and overall stiffness performance criteria is extended to the automatic generation of optimal strut-and-tie models in reinforced and prestressed concrete structures. In the proposed methodology, developing strut-and-tie models in structural concrete is transformed to an optimal topology design problem of continuum structures. Fundamental concepts underlining the development of strut-and-tie models are introduced. The optimal strut-and-tie model in a cracked structural concrete member is generated by gradually removing regions that are ineffective in carrying loads from the member based on the overall stiffness performance criteria. An integrated design optimization procedure is proposed for strut-and-tie design. Optimal strut-and-tie models in reinforced and prestressed concrete structures are investigated by using the automated PBO technology. Some of the findings have been reported by Liang *et al.* (1999a,b, 2000, 2001, 2002) and Liang (2001a,b).

5.2 Historical development of strut-and-tie model approach

The truss model was originally developed by Ritter (1899) for the analysis and design of reinforced concrete beams under shear in 1899. Ritter found that a reinforced concrete beam after cracking due to diagonal tensile stresses could be idealized as a parallel chord truss with compressive diagonals inclined at 45° with respect to the longitudinal axis of the beam. Mörsch (1920, 1922) extended the truss models to the design of reinforced concrete members under torsion. The truss analogy method was refined and expanded by Kupfer (1964) and Leonhardt (1965). The truss model with diagonals having a variable angle of inclination was considered as a viable model for design of reinforced and prestressed concrete beams under shear

and torsion (Kupfer 1964; Lampert and Thürlimann 1971; Thürlimann *et al*. 1983). Collins and Mitchell (1980) proposed the truss model approach considering deformations for the design of reinforced and prestressed concrete. The truss analogy method provides a rational mean for the design of reinforced concrete beams in shear. The location and quantities of steel reinforcement can be determined on the basis of static equilibrium conditions without the use of empirical equations.

Standard truss models, however, can only be used to design the regions of a concrete structure where the Bernoulli hypothesis of plane strain distribution is assumed valid. At regions where the strain distribution is significantly nonlinear such as point loads, corbels, deep beams, beam–column connections and openings, the truss model theory is not applicable. The strut-and-tie model, which is a generalization of the truss analogy method for beams, has been proposed for design of the disturbed regions of structural concrete. Marti (1985) applied the strut-and-tie model approach with consistent equilibrium and ultimate strength considerations to the design of reinforced concrete beams. The determination of the ultimate strength of a strut-and-tie model is based on the lower-bound plastic theory. Struts, ties, nodes, fans and arches were proposed as basic tools for the design and detailing of reinforced concrete beams.

Schlaich *et al*. (1987) and Schlaich and Schäfer (1991) extended the truss model theory for beams to a consistent strut-and-tie model approach for the design and detailing of structural concrete including reinforced and prestressed concrete structures. This consistent design approach allows any part of a concrete structure to be designed and detailed using strut-and-tie systems. The concept of B- and D-regions was introduced by Schlaich *et al*. The distribution of strains in B-regions (where B stands for beam or Bernoulli) is linear whereas the distribution of strains in D-regions (where D stands for discontinuity or disturbance) is nonlinear. More often, a concrete structure can be divided into B- and D-regions. The B-regions can be designed on the basis of standard truss models or sectional methods. Specific strut-and-tie models have to be developed for D-regions where standard truss models are not applicable. Schlaich *et al*., suggested that prestressing forces could be treated as external loads in the development of strut-and-tie models.

Ramirez and Breen (1991) suggested that the modified truss model approach that considers a variable angle of inclination diagonals and a concrete contribution could be used for the design of reinforced and prestressed concrete beams. Ramirez (1994) proposed some guidelines for the strut-and-tie design of pretensioned concrete members. Experimental and analytical study on the use of strut-and-tie models for the design of posttensioned anchorage zones has been conducted by Sanders and Breen (1997). The strut-and-tie model approach and related theories for the design of structural concrete were summarized in the state-of-the-art report by the ASCE-ACI Committee 445 on Shear and Torsion (1998). Modern concrete model codes

and standards rely on the strut-and-tie model approach as the basis for the design and detailing of reinforced and prestressed concrete structures (CEB 1987; AS 3600 (1994); ACI 318-02 (2002)).

5.3 Traditional methods for developing strut-and-tie models

The elastic stress distribution method can be used to develop strut-and-tie models in structural concrete, as suggested by Schlaich *et al*. (1987). In the elastic stress distribution method, a strut-and-tie model is constructed by orientating struts and ties to the mean direction of principal stress trajectories, which are obtained by performing a linear elastic finite element analysis (FEA) on an uncracked homogenization concrete member. However, due to the uncracked assumption of concrete in the linear elastic FEA, the strut-and-tie model obtained by this approach may differ from the actual load transfer mechanism at the ultimate limit states, as reported by Schlaich and Schäfer (1991). It is often required to adjust the strut-and-tie model obtained on the basis of the elastic stress analysis in order to realize the real behavior of cracked structural concrete.

The load path method can also be used to develop strut-and-tie models in structural concrete. The first step in the load path method is to determine all loads and reactions acting on the member or a D-region in a structure for the outer equilibrium. The load paths are then traced by following the center of gravity of the corresponding stress diagrams. The principle to be followed is that the loads transfer through the paths with minimum deformations. After plotting all load paths in the direction of applied loads, further struts and ties must be added for transverse equilibrium between nodes. However, it is difficult to find the correct models in structural concrete members with complex loading and geometry conditions using these conventional methods, which usually involve a trial-and-error process. It is also a difficult task for the designer to select the correct strut-and-tie models from many possible equilibrium configurations for complex design situations using traditional drawing board methods.

Marti (1985) realized the limitations of conventional methods for developing strut-and-tie models and suggested that interactive computer programs should be developed for strut-and-tie modeling of structural concrete. Attempts to develop computer programs with graphical input and output routines for strut-and-tie modeling have been made by several researchers. Kumar (1978) applied the truss topology optimization theory to find the load transfer mechanism in reinforced concrete deep beams. A continuum concrete structure with specified geometry and loading conditions was modeled by using a highly indeterminate truss (ground structure). The best truss used as a basis for the design of reinforced concrete beams is the one with the maximum stiffness. In other words, the minimum strain energy

principle was used as the optimal design criterion for trusses. The linear programming technique was employed to solve the truss topology optimization problem. The truss topology optimization technique has also been used by Biondini *et al.* (1998) and Ali and White (2001) to find optimal truss models in structural concrete members based on the ground structure approach. These methods offer an automatic search for strut-and-tie models in reinforced concrete members in an iterative process. Since the ground structure grid has a significant effect on the optimal topology of a structure, the chosen ground structure may not adequately simulate the nature of a continuum concrete structure. In other words, the load paths are restricted to the chosen ground structure grid.

Ramm and Maute (1994) and Ramm *et al.* (1997) applied the density-based topology optimization method to the generation of strut-and-tie models in concrete structures. The strut-and-tie model is generated by maximizing the stiffness of a plain concrete member for a given mass constraint in the design space. The linear elastic behavior of concrete is considered in the development of strut-and-tie models. The fundamental changes in the structural performance due to concrete cracking are not considered. The strut-and-tie model produced by this approach depends on the material mass constraint. Different mass constraints lead to different strut-and-tie models and different layouts of steel reinforcement for the same structural concrete member.

Computer graphics have been used as a design aid for the strut-and-tie modeling of structural concrete (Alshegeir and Ramirez 1992; Mish 1994; Yun 2000). In these computer graphical methods, FEA packages are used in the construction of a strut-and-tie model. After a continuum finite element model of the structural concrete member is created and analyzed, the load paths in the structure may be visualized by locating the maximum principal stresses and the direction of these principal stresses. The equivalent force resultant in the member is obtained by the summation of stresses. These computer graphical methods are useful design aids for developing strut-and-tie models in structural concrete. The success of these methods, however, relies on the designer's ability to sketch appropriate strut-and-tie models for structural concrete members with complex loading and geometry conditions. It appears that it is necessary to develop stiffness-based optimization techniques with computer graphical input and output for strut-and-tie modeling of structural concrete.

5.4 Key features of strut-and-tie modeling

Strut-and-tie modeling is considered as the basic tool in the design and detailing of structural concrete under shear and torsion. The strut-and-tie model approach is justified by the fact that the loads applied to a structural

concrete member are transferred through a set of compressive stress fields that are distributed and interconnected by tension ties. The flow of compressive stresses is idealized using compression members called struts while tensile stress fields are idealized using tension members called ties. Tension ties can be reinforcing bars or prestressed tendons or concrete tensile stress fields. Figure 5.1 indicates the key features of a strut-and-tie model, which consists of struts, ties and nodal zones. Bottle-shaped struts can be idealized as prismatic struts, provided that they are reinforced with additional reinforcement to sustain transverse tensile stresses.

The strut-and-tie model developed is employed to investigate the equilibrium between the loads, the reactions and the internal forces in the concrete struts and in the reinforcement (Marti 1985). The actual load carried by the strut-and-tie model is treated as a lower bound ultimate load for the structural concrete member based on the lower bound theorem of plasticity. This simple approach provides a clear understanding of the behavior of structural concrete. The advantages of using strut-and-tie modeling are summarized as follows:

- The designer can easily idealize the flow of internal forces in a structural concrete member.
- The influence of shear and moment can be accounted for simultaneously and directly in one model.
- The designer can give special attentions to the potential weak spots indicated by the strut-and-tie model.
- It offers a unified, rational and safe design procedure for structural concrete.

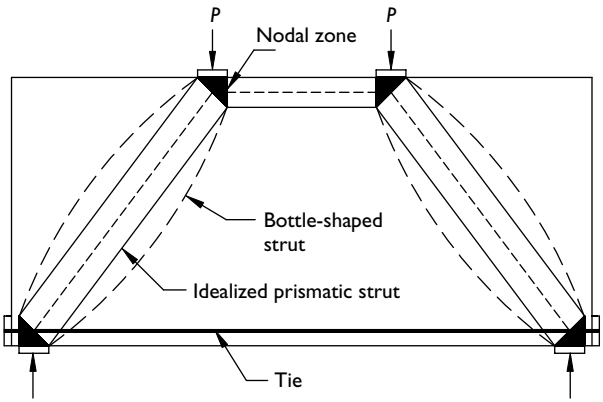

Figure 5.1 Key features of a strut-and-tie model.

5.5 B- and D-regions in concrete structures

Strut-and-tie models are particularly useful for the analysis and design of disturbed regions or D-regions where the simple flexural beam theory is not applicable. These D-regions are sometimes called non-flexural regions. The D-regions in a concrete structure are characterized by a complex stress distribution due to the presence of concentrated loads or abrupt changes in the geometry of a member or reactions. The assumptions of flexural beam theory, such that plane sections remain plane or that the shear stresses are uniformly distributed over the depth of the member, are not appropriate for D-regions.

Stress distribution patterns in D-regions are complex compared to a quite smooth stress pattern in B-regions. The FEA indicates that stress intensities decrease with an increase in the distance from the center of the stress concentration. These characteristics can be used to identify the B- and D-regions in a concrete structure. The advantage of dividing a concrete structure into B- and D-regions is that the designer can focus his or her attentions on the D-regions, which are the potential weak spots that need special considerations in design and detailing. It is important to ensure that the D-regions are properly reinforced and have adequate strength performance.

The B- and D-regions in a simply supported beam with web opening are shown in Figure 5.2. It can be seen that the D-regions are near the supports. The point load, web opening and change in the depth of the beam create D-regions in the beam. In a continuous reinforced concrete beam under uniform distributed loads, the midspan regions are B-regions while the D-regions are formed near the supports. It is obvious that the entire deep beam should be treated as a D-region.

Figure 5.3 shows the B- and D-regions in a reinforced concrete frame. The beam–column connections are regarded as D-regions since the flow of internal forces in the frame corners is complex. The corbels on the columns create D-regions because the loads applied to the corbels cause complex stress patterns in those regions. The mid-regions of the columns are identified as B-regions. Due to geometrical discontinuities between the columns and footings, the bottom regions of the columns are classified as D-regions.

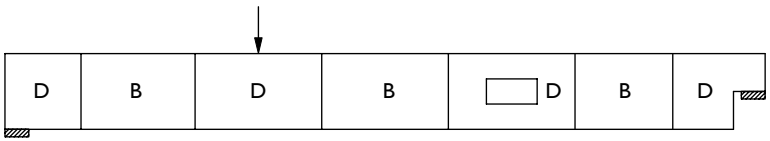

Figure 5.2 B- and D-regions in a beam with web opening.

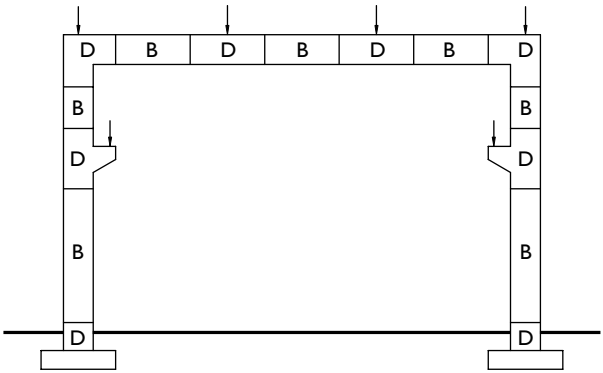

Figure 5.3 B- and D-regions in a reinforced concrete frame.

5.6 Strut-and-tie modeling as a topology optimization problem

Since concrete permits only limited plastic deformations, the strut-and-tie model in a structural concrete member has to be selected so that the structural system has the least deformations. Based on the principle of the minimum strain energy for the linear elastic behavior of struts and ties after cracking, Schlaich *et al.* (1987) proposed the following equation for assisting the selection of strut-and-tie models as

$$\sum_{i=1}^{N} F_i l_i \varepsilon_{\mathrm{m}i} = \text{minimum} \tag{5.1}$$

where F_i is the force in the ith strut or tie, l_i is the length of the ith member and $\varepsilon_{\mathrm{m}i}$ is the mean strain of the ith member and N is the total number of members in a strut-and-tie system. This equation is helpful for selecting a better strut-and-tie model from several possible ones. However, it will be cumbersome to find the optimal strut-and-tie model using this method since there are a large number of possibilities for the equilibrium configurations of a structure.

Strut-and-tie models are used to idealize the load transfer mechanism in a cracked structural concrete member at the ultimate limit states. The design task is mainly to identify the load transfer mechanism in a structural concrete member and reinforce the member such that this load path will safely transfer the applied loads to the supports. Obviously, some regions of a structural concrete member are not as effective in carrying loads as others. By eliminating these underutilized portions from a structural concrete

member, the actual load transfer mechanism in the cracked concrete member can be found. The PBO method has the ability to identify the underutilized portions of a structure and remove them from the structure to improve its performance. Developing an appropriate strut-and-tie model in a structural concrete member can be transformed to a topology optimization problem of a continuum structure. The optimal topology of a plane stress continuum structure produced by the PBO method is often a truss-like structure. Therefore, it is appropriate to apply this technology to the automatic generation of strut-and-tie models in concrete structures.

In nature, loads are transmitted by the principle of the minimum strain energy (Kumar 1978). This suggests that the strut-and-tie system in structural concrete should be developed on the basis of system performance criteria (overall stiffness) rather than component performance criteria (strength). Component performance criteria can be easily satisfied by dimensioning the component. Based on these design criteria, the PBO methods for continuum structures with displacement constraints and with mean compliance constraint are modified and tailored for generating strut-and-tie models for the design and detailing of structural concrete. The performance objective of strut-and-tie model optimization is to minimize the weight of a concrete structure while maintaining its overall stiffness within an acceptable performance level. The performance objective can be expressed in mathematical forms as follows:

$$\text{minimize} \quad W = \sum_{e=1}^{n} w_e(t) \tag{5.2}$$

$$\text{subject to} \quad u_j \leq u_j^* \qquad j = 1, 2, \ldots, m \tag{5.3}$$

$$\text{or} \quad C \leq C^* \tag{5.4}$$

If the PBO method for structures with displacement constraints is used to develop strut-and-tie models in structural concrete, sufficient displacement constraints have to be specified in order to generate the stiffest strut-and-tie models. Only uniform sizing of the element thickness (or the width of the member) is considered in the optimization process. By means of systematically removing elements from the discretized concrete member, the actual load paths within the cracked structural concrete member can be gradually characterized by the remaining elements.

5.7 Limit analysis and finite element modeling

Topology optimization theory is rarely applied to the special and important field of reinforced and prestressed concrete due to the difficulty in modeling the nonlinear behavior of structural concrete for optimization. Concrete has a considerable strength in compression, but a very low strength in

tension. Moreover, reinforced concrete is a composite material. The nonlinear behavior of reinforced concrete is characterized by the cracking of concrete and the yielding of steel reinforcement. The behavior can be well approximated by the uncracked linear, cracked linear and limit analysis (Marti 1999).

The shrinkage and temperature may have significant effects on the load-deformation response of reinforced concrete. However, neither the stresses induced by them nor associated deformations can be determined accurately in practice. If a sufficiently ductile behavior is ensured, the ultimate strength of a structural concrete member is not affected by the loading history including the effects of shrinkage and temperature (Marti 1999). Therefore, the ultimate strength based on the limit analysis will be reliable if a structural concrete member is designed with adequate ductility and detailing.

The limit analysis has been discussed in the IABSE state-of-the-art report (1979) and the book by Nielsen (1984). The limit analysis can be classified into lower bound and upper bound methods. In lower bound methods, a concrete structure is usually designed by strengthening its load transfer mechanism. Lower bound methods are particularly suitable for designing new concrete structures. In contrast, upper bound methods allow for quick checks for the ultimate strength, dimensions and the details of existing structures. They are suitable for the performance evaluation of existing concrete structures. For example, the nonlinear FEA developed for reinforced concrete is an upper bound method, which is suitable for the evaluation of load-deformation response, but rarely used in designing new structures in practice. Strut-and-tie modeling corresponds to the lower bound limit analysis. Strut-and-tie models can indicate the necessary amount, the correct location and the required detailing of the steel reinforcement. Moreover, they allow for checking of critical nodal zones. It is apparent that strut-and-tie modeling is a rational method for the design and detailing of structural concrete.

After extensive cracking of concrete, the loads applied to a reinforced concrete member are mainly carried by the concrete struts and steel reinforcement. The failure of a reinforced concrete member is mainly caused by the breakdown of the load transfer mechanism, such as the yielding of steel reinforcement in ductile structural concrete members, rather by that the tensile stress attains the tensile strength of concrete (ASCE-ACI Committee 445 on Shear and Torsion 1998). It should be noted that the locations of tension ties and the amounts of steel reinforcement are not known before designing a non-flexural structural concrete member. Actually, the design task is to develop an appropriate strut-and-tie model for the structural concrete member in order to reinforce it. Therefore, the stiffness of reinforcing steel and the nonlinear behavior of reinforced concrete cannot be taken into account in the finite element model for the development of strut-and-tie systems.

In the PBO method, plain concrete members are treated as homogenization continuum structures, and modeled using plane stress elements. The linear elastic behavior of cracked concrete is assumed in the FEA. Since tension ties in the strut-and-tie model obtained will be reinforced with steel reinforcement in a reinforced concrete structure, the effect of cracking due to stresses attaining the tensile strength of concrete is not considered. However, the progressive cracking of a concrete member is simulated by gradually removing elements from the member, which is fully cracked at the optimum. The goal of the proposed method is to find a strut-and-tie system as stiff as possible. The strength of struts, ties and nodes can be treated when dimensioning the strut-and-tie model obtained.

It is proposed here to develop strut-and-tie models in structural concrete based on the linear elastic theory of cracked concrete for system performance criteria (overall stiffness) and to design the concrete structure based on the theory of plasticity for component performance criteria (strength). It is worth noting that the load–deformation response of a concrete member in an optimization process is highly nonlinear due to the change in the topology of the structure at each iteration.

5.8 Optimization criteria for strut-and-tie models

Strut-and-tie models in structural concrete are load-carrying structural systems that transfer the applied loads to the supports. To generate the stiffest strut-and-tie systems, the PBO technique for continuum structures with displacement constraints or mean compliance constraints can be used. Since stress-based topology optimization method may not produce the stiffest optimal structures, they should not be used for the strut-and-tie modeling of structural concrete. Optimization criteria for strut-and-tie models are briefly described in this section.

5.8.1 Element removal criteria

In the PBO method formulated on the basis of displacement performance criteria, the objective is to maximize the performance of an initial continuum structure in terms of the efficiency of material usage in resisting deformations. The element removal criteria are based on the virtual strain energy densities (VSEDs) of elements. For concrete structures, an optimal strut-and-tie model can be generated by gradually eliminating a small number of elements with the lowest VSEDs from a discretized concrete member. The VSED of the eth element is approximately calculated by

$$\psi_e = \frac{|\{u_{ej}\}^{\mathrm{T}}[k_e]\{u_e\}|}{w_e} \tag{5.5}$$

For a concrete structure under multiple displacement constraints, the weighted average approach is used to calculate the VSEDs of elements for elimination. The VSED of the eth element for multiple displacement constraints is determined by

$$\psi_e^m = \sum_{j=1}^{m} \beta_j \psi_e \tag{5.6}$$

Similarly, in the PBO method formulated on the basis of overall stiffness performance criteria, element removal criteria are based on the strain energy densities (SEDs) of elements. For concrete structures, the optimal strut-and-tie model can be generated by gradually eliminating a small number of elements with the lowest SEDs from a discretized concrete structure. The SED of the eth element is approximately evaluated by

$$\gamma_e = \frac{|\{u_e\}^{\mathrm{T}}[k_e]\{u_e\}|}{2w_e} \tag{5.7}$$

By systematically removing elements with the lowest VSED or SED from a concrete structure, the maximum stiffness topology design at minimum weight can be obtained. It is possible to select the best one from resulting topologies in the optimization process as the strut-and-tie model for a structural concrete member. These two stiffness-based optimization techniques can be used to develop strut-and-tie models in structural concrete.

5.8.2 Performance-based optimality criteria

In order to obtain the optimal strut-and-tie model, the performance of the resulting system in a performance optimization process must be quantitatively evaluated by using performance indices. It is proposed to treat optimal topologies generated by the PBO technique as optimal strut-and-tie models in structural concrete members. When applying the PBO method based on displacement performance criteria to concrete structures, the PBOC for strut-and-tie models can be stated as

$$\text{maximize} \quad \mathrm{PI}_{\mathrm{ds}} = \frac{u_{0j} W_0}{u_{ij} W_i} \tag{5.8}$$

Similarly, when applying the PBO technique based on system performance criteria to concrete structures, the PBOC can be stated as

$$\text{maximize} \quad \mathrm{PI}_{\mathrm{es}} = \frac{C_0 W_0}{C_i W_i} \tag{5.9}$$

The optimal topology identified by the PBOC represents the load-carrying mechanism of a structural concrete member at its ultimate limit state. The physical meaning of the PBOC is that the optimal strut-and-tie model transfers loads in a way such that the product of its associated strain energy (or critical displacement) and material consumption is a minimum. As demonstrated in preceding chapters, the optimal topology adapts to the geometry, loading and support conditions of the structural concrete member.

It is worth noting that changing the width of a structural concrete member under a plane stress condition has no effect on the topology of the structure or on the performance index, but it has a significant influence on the weight of the structure and structural responses. As a result, it is not necessary to change the width of a concrete member in the finite element model at each iteration. Performance indices can be employed to evaluate the performance of the resulting topology at each iteration and to identify the optimum, which can then be sized by adjusting the width of the structure in order to satisfy actual displacement or overall stiffness requirements.

5.9 Design optimization procedure

The design of a concrete structure by using the strut-and-tie model approach usually involves the estimation of an initial size, developing an appropriate strut-and-tie model and dimensioning struts, ties and nodal zones. Developing an appropriate strut-and-tie model for a concrete structure with complex geometry and loading conditions is the most challenging task in the design process. Afterwards, dimensioning the strut-and-tie model is straightforward according to codes of practice. The main steps of the automated design optimization procedure are illustrated in Figure 5.4, and explained as follows:

1 Model the two-dimensional plain concrete member in a concrete structure using the finite element method (FEM). The initial size of the structural concrete member should be estimated on the basis of serviceability performance criteria. The loads, support conditions and openings are specified. The material properties of concrete such as the Young's modulus (E_c) and Poisson's ratio (ν) must be input for the linear elastic analysis. The values of Poisson's ratio for concrete are between 0.11 and 0.21. It is suggested that the value of 0.15 should be used in the optimization of strut-and-tie models. Prestressing forces are treated as external loads.
2 Perform a linear elastic FEA on the structural concrete member. If the PBO technique for structures with displacement constraints is used, the concrete must also be analyzed for virtual unit loads. The FEA provides element stresses and nodal displacements.

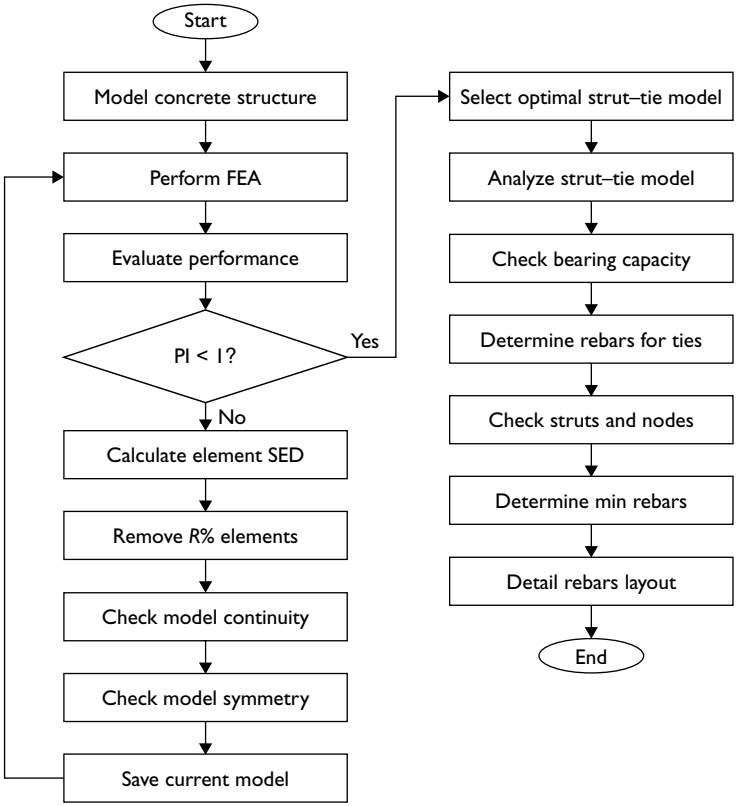

Figure 5.4 Flowchart of design optimization procedure for strut-and-tie modeling of structural concrete.

3 Evaluate the performance of the resulting system by using the displacement-based performance index (PI_{ds}) or energy-based performance index (PI_{es}) for plane stress structures.
4 Calculate the VSEDs or SEDs of elements.
5 Remove a small number of elements with the lowest VSEDs or SEDs from the concrete structure. It is suggested that the element removal ratio of 1 or 2 percent should be used in engineering practice.
6 Check model continuity. This is to ensure that the strut-and-tie model generated by the PBO technique must be a continuous model and satisfies the equilibrium condition.
7 Check model symmetry for a structural concrete member with an initial symmetrical loading, geometry and support condition.
8 Save current model.

9 Repeat steps 2–8 until the performance index is less than unity.
10 Select the optimal topology which corresponds to the maximum performance index.
11 Transform the optimal topology to a discrete strut-and-tie model. The discrete strut-and-tie model is an idealization of the optimal topology. It may be necessary to make some modifications to the discrete strut-and-tie model for practical purposes.
12 Analyze the discrete strut-and-tie model. Axial forces in struts and ties are determined.
13 Check the bearing capacity of loading points and supports.
14 Determine steel reinforcement for tension ties.
15 Check the capacity of struts and nodal zones.
16 Determine minimum steel reinforcement for crack control.
17 Detail the layout of steel reinforcement based on the strut-and-tie model obtained.

5.10 Dimensioning struts, ties and nodal zones

Dimensioning struts, ties and nodal zones is of significant importance to the overall structural performance of a concrete structure. Dimensioning a strut-and-tie model includes not only sizing the struts and reinforcing the ties based on the forces they carry, but also checking the capacity of nodal zones for safe transfer of the loads. The detailing of nodal zones directly affects the strength performance of concrete struts connected to the nodal zones and of the ties anchored in the nodal zones. Moreover, the details of nodal zones influence the flow of internal forces in a concrete structure. The key importance is to ensure that the optimal strut-and-tie model generated by the PBO technique can be realized at its ultimate limit state after detailing. It should be noted that the optimal strut-and-tie model produced by the PBO technique indicates the locations of struts, ties and nodes but not necessarily their exact dimensions. This is because the model is developed on the basis of the overall stiffness performance criteria without consideration of the strength performance criteria. Dimensioning strut-and-tie models must be based on the strength requirements and bearing conditions.

5.10.1 Strength performance requirement

In the design of struts, ties and nodal zones, the strength performance requirement is:

$$F^* \leq \phi F_u \tag{5.10}$$

where F^* is the force in a strut or tie, or the force acting on one face of a nodal zone under the factored loads; F_u, the nominal strength of the strut,

tie or nodal zone and ø, the strength reduction factor. In ACI 318-02 (2002), the strength reduction factor is taken as 0.75 for struts, tie and nodal zones. The forces in struts, ties and nodal zones are determined by applying the factored loads to the strut-and-tie model.

5.10.2 Concrete struts

The nominal compressive strength of a strut can be determined by the effective compressive stress of concrete in the strut and the cross-sectional area at the ends of the strut. In some design situations, the capacity of a strut needs to be increased to carry the internal force. This can be achieved by providing longitudinal reinforcing bars parallel to the axis of the strut within the concrete strut. Closed ties are usually used to prevent these longitudinal bars from buckling. In general, the nominal compressive strength of a strut can be calculated by

$$F_{us} = f_{cu}A_c + f_{yr}A_{st} \tag{5.11}$$

where A_c is the cross-sectional area at one end of the strut; f_{yr}, the yield stress of the longitudinal bars; A_{st}, the cross-sectional area of longitudinal steel reinforcement and f_{cu}, the lesser value of the effective compressive strengths of concrete in the strut and in the nodal zone at the same end of the strut. If no longitudinal reinforcing bars are provided within the strut A_{st} should be taken as zero. The cross-sectional area A_c of a strut is calculated using the smaller depth at the ends of the strut. The depth of a concrete strut is measured perpendicularly to the axis of the strut.

The state of stresses, cracks and the arrangement of steel reinforcement influence the compressive strength of concrete in struts. The transverse compression considerably improves the compressive strength of concrete. This may be provided by the transverse reinforcement that confines the concrete. Transverse tensile stresses and cracks induced by tensile stresses detrimentally reduce the compressive strength of concrete. If steel reinforcement is not provided to carry these tensile stresses, the concrete may fail at below its cylinder compressive strength. The compressive strength of concrete in struts is also reduced by cracks that are not parallel to compressive stresses. For safety, the effective compressive strength of concrete should be used in the design of struts.

Marti (1985) suggested that the effective compressive strength of concrete (f_{cu}) in struts should be taken as $0.6f'_c$, whereas Ramirez and Breen (1991) suggested a value of $2.5\sqrt{f'_c}$ (MPa). Schlaich *et al.* (1987) suggested that different values of the effective compressive strength of concrete should be used in the design of struts, depending on the state of stress, crack patterns and the arrangement of steel reinforcement in the structural concrete

member. Foster and Gilbert (1996) proposed efficiency factors for normal- and high-strength concrete used in non-flexural members.

The strut-and-tie model approach has been incorporated in ACI 318-02 (2002) for the design and detailing of non-flexural members or disturbed regions in a concrete structure. In ACI 318-02, the effective compressive strengths of concrete in struts is determined by

$$f_{cu} = 0.85\beta_s f'_c \tag{5.12}$$

where β_s is equal to 1.0 for prismatic struts in compression zones, 0.75 for bottle-shaped struts with crack control reinforcement, 0.6 for bottle-shaped struts without crack control reinforcement, 0.4 for struts in tension members and 0.6 for all other cases.

In some design situations, the point loads are transferred through the bottle-shaped stress fields where transverse tensile stresses develop due to the spreading of compressive stresses (Schlaich *et al*. 1987). These tensile stresses can be idealized using the tension ties in a refined strut-and-tie model. In a simpler model, the concrete struts can be idealized as straight members, provided that additional reinforcement is provided to control cracking. To control concrete cracking, a minimum amount of reinforcement must be provided in both transverse and longitudinal directions. These reinforcing bars also prevent the spalling of concrete and enhance the overall structural performance of the strut-and-tie system as well as the structural concrete member. In ACI 318-02 (2002), the minimum reinforcement requirement for crack control is

$$\sum \frac{A_{si}}{bs_i} \sin\theta_i \geq 0.003 \tag{5.13}$$

where A_{si} is the total area of reinforcement at spacing s_i in a layer of reinforcing bars with an angle θ_i to the axis of the strut, and b is the width of the strut.

In AS 3600 (1994), the effects of transverse stresses, cracking and the arrangement of steel reinforcement are not taken into account in the determination of the effective compressive strength of concrete in struts. In AS 3600, the effective compressive strength of concrete in struts is calculated by

$$f_{cu} = \left(0.8 - \frac{f'_c}{200}\right) f'_c \tag{5.14}$$

The effective width of a concrete strut should be determined by three-dimensional conditions in the regions. It should not be greater than the width of any adjacent bearing plates or supports. The effective depth of a concrete strut measured perpendicular to the longitudinal axis of the strut

depends on the geometry of end nodes. Figure 5.6 shows the depths of struts and the anchorage depths of ties in CCT and CCC nodes.

5.10.3 Ties

Tension ties in a strut-and-tie model can be reinforcing bars, prestressing tendons or concrete tensile stress fields. Reinforcing steel should be provided to carry tensile forces in ties. The nominal strength of a tie reinforced by steel reinforcing bars and prestressing tendons can be determined by

$$F_{ut} = A_{st} f_{yr} + A_{ps} f_{py} \tag{5.15}$$

where A_{st} is the total cross-sectional area of reinforcing bars; A_{ps}, the cross-sectional area of prestressing steel and f_{py}, the effective yield strength of prestressing steel for the tensile tie. Since part of the strength of the prestressed steel has been utilized by prestressing, only the rest is effective in resisting tensile forces. The effective yield strength of prestressing steel is used in the calculation of the strength of the tensile tie.

Sufficient anchorage of reinforcing bars must be provided to ensure that the stress in reinforcing bars could be developed to their yield strength before concrete crushing. The bar anchorage length measured from the innermost boundary of the strut or nodal zone should not be less than the stress development length of the bar. In ACI 318-02 (2002), the anchorage length of reinforcement in a tension tie is measured from the point where the centroid of the tie reinforcement leaves the extended nodal zone. The extended nodal zone is defined by either the extension of the bearing area or the assumed prismatic outlines of the struts anchored by the nodal zone, whichever is larger. Figure 5.5 illustrates the anchorage length for reinforcement in ties and the extended nodal zone. If the space is not available for anchorage, cogs, bends, U-bars and anchor plates should be used.

5.10.4 Nodal zones

Nodal zones are the interaction regions of three or more struts and ties in a strut-and-tie model. The flow of forces changes its direction at a nodal zone. The compressive strength of nodal zones depends on the tensile straining from the tensile ties, and confinement provided by compressive stresses and transverse reinforcement. Nodal zones may be classified according to the number of connecting elements and their types. Some of the possible combinations of nodal zones are CCC, CCT, CTT, TTT, CCCC, CCCT, CTTT, CCCCC and TTTTTTT. The C refers to a compression strut and the T refers to a tension tie. Some of the nodes are shown in Figure 5.6. The CCT and CCC nodal zones can be found in the

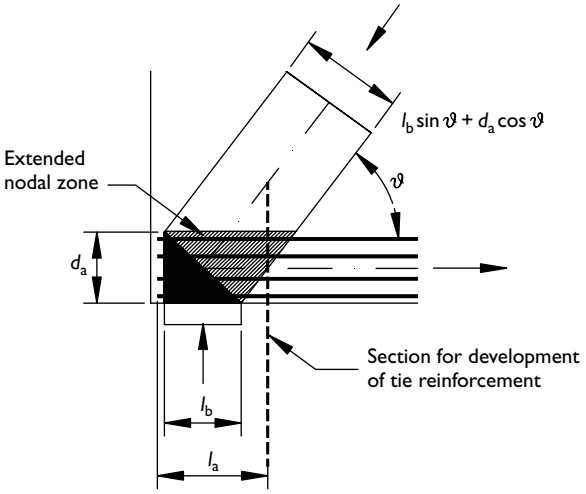

Figure 5.5 Extended nodal zone and anchorage length for reinforcement.

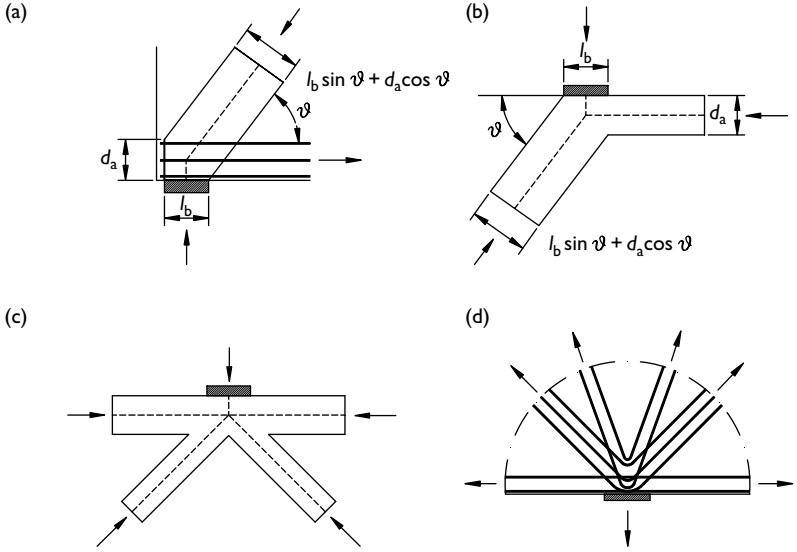

Figure 5.6 Types of nodes: (a) CCT; (b) CCC; (c) CCCCC; (d) TTTTTTT.

strut-and-tie model in a deep beam under two point loads. The tension nodal zone shown in Figure 5.6(d) consists of ties only. This type of nodal zones can be formed in simply supported deep beam when the load is applied to the bottom of the beam.

The nominal compressive strength of a nodal zone can be calculated by

$$F_{un} = f_{cu}A_n \tag{5.16}$$

where A_n is the area of the nodal zone face on which that the axial force F^* acts, and f_{cu} is the effective compressive strength of concrete in the nodal zone. In ACI 318-02 (2002), the effective compressive strength of concrete in nodal zone is determined by

$$f_{cu} = 0.85\beta_n f'_c \tag{5.17}$$

where β_n is equal to 1.0 when the nodal zone is bounded by struts and/or bearing areas, 0.8 when the nodal zone anchors only one tie and 0.6 when the nodal zone anchors more than one tie. The factor β_n reflects the degree of disruption of the nodal zone due to the incompatibility of the tension strains in the ties and compression strains in the struts.

The sizes of struts are likely to be governed by the shapes and sizes of adjacent nodal zones. Therefore, AS 3600 (1994) requires that the sizes of struts and ties shall not be larger than the capacity of nodal zones in order to safely transfer forces between struts and ties in a strut-and-tie model. For a nodal zone consisting of three concrete struts, the borders of the nodal zone can be designed in a way such that they are perpendicular to the longitudinal axis of the struts. If the effective compressive strength of concrete is the same in all three struts, the dimensions of the three borders (a_1, a_2, a_3) can be proportioned to the forces in the struts (Schlaich *et al.* 1987), such as:

$$a_1 : a_2 : a_3 = F_1 : F_2 : F_3 \tag{5.18}$$

For nodal zones consisting of tension ties, the dimensions of nodal zones are governed by the sizes of any anchor plates for reinforcing bars as well as the concrete cover to the bars.

5.11 Multiple load cases

As discussed in preceding sections, the strut-and-tie model in a structural concrete member adapts to the geometry, loading and support conditions of the member. Different loading conditions lead to different strut-and-tie models and different layouts of steel reinforcement in the member. Although the PBO technique is capable of generating optimal topologies of continuum structures under multiple load cases as demonstrated in Chapter 4, it is not recommended to be used for developing a single strut-and-tie model for a structural concrete member under multiple loading conditions. Different strut-and-tie models must be developed for a structural concrete

member under different load cases. Attempt to use one strut-and-tie model for the design and detailing of a structural concrete member under multiple load cases may lead to cracking and significant reduction in the strength performance of the member. The design must be checked for each strut-and-tie model for the corresponding load case.

5.12 Optimal strut-and-tie models in reinforced concrete

The proposed method for developing optimal strut-and-tie models in structural concrete is based on a very simple engineering design concept that by gradually removing lowly strained elements from a discretized concrete structure, the actual load transfer mechanism of the structure can be found. In this section, numerical examples are provided to demonstrate the effectiveness and validity of the automated PBO technique in generating optimal strut-and-tie models in reinforced concrete structures. The design and detailing of deep beams with openings continuous beams, beams with various span-to-depth ratios, corbels, bridge piers, shearwall with openings and beam–column connections are covered. The accuracy of the PBO techniques in generating optimal strut-and-tie models in structural concrete is established by comparison with experimental observation as well as existing analytical solutions.

5.12.1 Verification by experimental evidence

To verify the performance-based design optimization theory developed for generating optimal strut-and-tie models in structural concrete, the automated PBO method formulated on the basis of displacement performance criteria was employed to investigate the strut-and-tie model in two deep beams with web openings, and the results are compared with experimental observations.

5.12.1.1 Verification I

A simply supported deep beam with two web openings based on the test specimen (O-O.3/3) conducted by Kong and Sharp (1977) is shown in Figure 5.7. The width of the deep beam was 100 mm. In the tested specimen, one 20-mm diameter deformed bar of 430 MPa yield strength was used as the bottom longitudinal steel reinforcement anchored by the external steel plates at the ends. No web reinforcement was provided in the beam. The cylinder compressive strength of concrete used in the tested specimen was 35.5 MPa. The two-point loading was used to test the deep beam

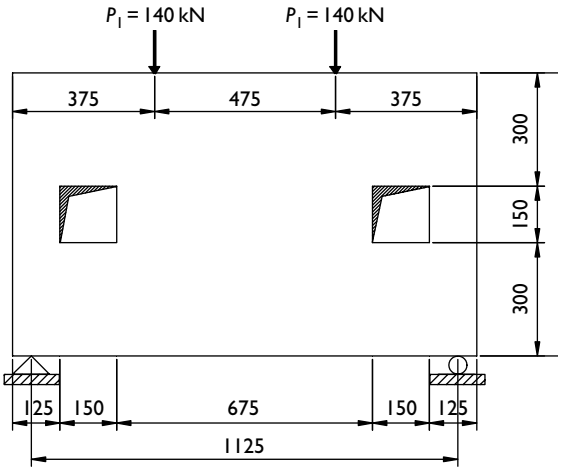

Figure 5.7 Deep beam with web openings.

to failure. The ultimate load of the beam obtained from the experiment was 280 kN. The two-point loads of $P_1 = 140$ kN were applied to the top of the beam in the FEA. By neglecting the effect of the bottom longitudinal steel reinforcement, the plain concrete beam was modeled using 25-mm square, four-node plane stress elements. The displacement constraints of the same limit were imposed at the two loaded points in the vertical direction. The Young's modulus of concrete $E_c = 30\,088$ MPa and Poisson's ratio $\nu = 0.15$ and the thickness of elements $t = 100$ mm were specified in the analysis. Plane stress conditions were assumed. The element removal ratio of 1 percent was specified in the optimization process.

The performance index history of the deep beam with web openings generated by the PBO technique is presented in Figure 5.8. The maximum performance index of the deep beam is 1.58. The strut-and-tie model optimization history is depicted in Figure 5.9, which shows that the load transfer mechanism of the deep beam was gradually manifested by the remaining elements in the deep beam. Since the portions of concrete that were ineffective in carrying loads were gradually removed from the deep beam, the beam was fully cracked in the optimization process as indicated in Figure 5.9(c). This means that the loads are mainly carried by the resulting structural system in the deep beam at a fully cracked state under the ultimate condition. The optimal topology shown in Figure 5.9(c) was interpreted as the optimal strut-and-tie model in the deep beam as shown in Figure 5.9(d), where the solid bold lines represent concrete struts and the dashed lines represent tension ties.

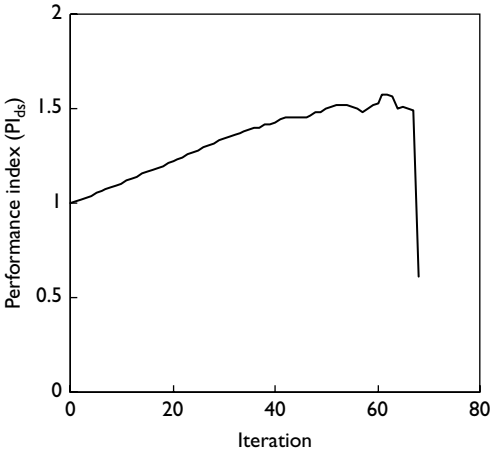

Figure 5.8 Performance index history of the deep beam with web openings.

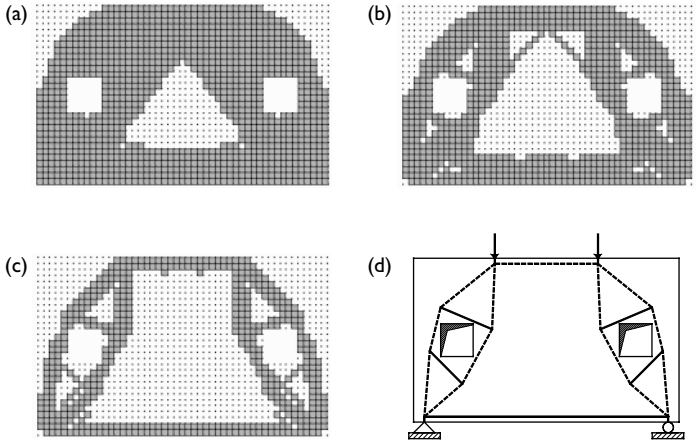

Figure 5.9 Optimization history of strut-and-tie model in the deep beam with web openings: (a) topology at iteration 20; (b) topology at iteration 40; (c) optimal topology; (d) optimal strut-and-tie model.

In nature, the loads are transmitted along the shortest natural load paths between the loading and support points to minimize the associated strain energy of the load-carrying system. If the opening intercepts the natural load path, the load is to be re-routed around the opening (Kumar 1978). This is confirmed by the optimal strut-and-tie model depicted in Figure 5.9(d). The

optimal strut-and-tie model shows that the point loads are transferred to the supports by the upper and lower concrete struts around the opening. The test conducted by Kong and Sharp (1977) showed that diagonal cracking occurred at above and below the opening. It is clear that tensile stresses developed across the corners of the openings. The two inclined tension ties that connect the upper and lower struts around the opening shown in Figure 5.9(d) are confirmed by experimental observations. The optimal strut-and-tie model obtained clearly indicates the location of struts, ties and nodal zones. In dimensioning the optimal strut-and-tie model, inclined web reinforcement should be provided to carry inclined tensile forces. Inclined web reinforcement has been proved to be the most effective in increasing the ultimate strength and for crack control of such deep beams with web openings (Kong and Sharp 1973, 1977).

5.12.1.2 Verification II

A further verification of the PBO method was conducted on a simply supported lightweight-concrete deep beam with two web openings located below the axis of the depth of the beam as shown in Figure 5.10. This deep beam is based on the test specimen (O-O.3/16) presented by Kong and Sharp (1977). In the tested specimen, one 20-mm diameter deformed bar was placed at the bottom of the beam as the longitudinal tensile steel reinforcement. No web reinforcement was provided in the tested specimen. The width of the tested beam was 100 mm. The cylinder compressive strength of concrete used in the deep beam was 37.6 MPa. The measured ultimate jack load was 195 kN. In this study, two concentrated loads of $P_1 = 97.5$ kN

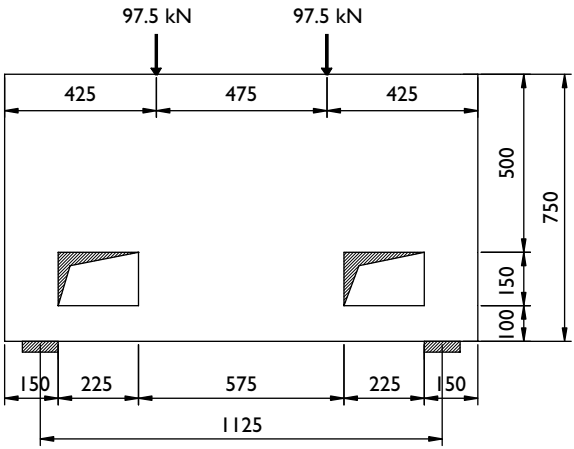

Figure 5.10 Simply supported deep beam with web openings.

were thus applied to the top of the beam. The Young's modulus of concrete E_c = 30 966 MPa, Poisson's ratio ν = 0.15 and the thickness of elements t = 100 mm were specified in the FEA. The plain concrete beam was modeled using 25-mm square, four-node plane stress elements. The displacement constraints of the same limit were imposed at the two loaded points in the vertical direction. The element removal ratio of 1 percent was used in the optimization process.

Figure 5.11 depicts the performance index history of this deep beam in the performance optimization process. It appears from Figure 5.11 that the performance index increased from unity to the maximum value of 1.52 when inefficient elements were gradually deleted from the model. The optimal strut-and-tie model in the deep beam under the given geometry and loading conditions was generated while the performance index was maximized. Topologies obtained at iterations 20, 40 and 50 are presented in Figure 5.12. It can be observed from Figure 5.12 that the load transfer mechanism in the cracked concrete deep beam could be identified by gradually removing elements with the least contribution to the stiffness performance of the beam from the finite element model.

The optimal topology shown in Figure 5.12(c) was idealized to the optimal strut-and-tie model presented in Figure 5.12(d). By comparison of the optimal strut-and-tie model with the tested specimen (Kong and Sharp 1977), it can be observed that the tension ties in the strut-and-tie model exactly indicate the patterns and locations of cracks in the tested specimen. This strongly proves that the proposed PBO method can predict extremely well the actual load transfer mechanism of cracked structural concrete members at the ultimate limit states. Therefore, it is appropriate to develop

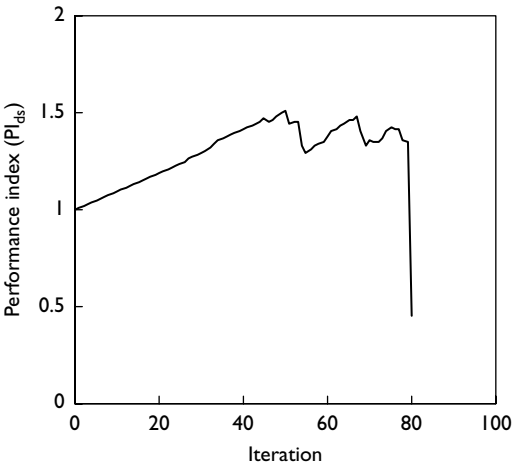

Figure 5.11 Performance index history of the deep beam with web openings.

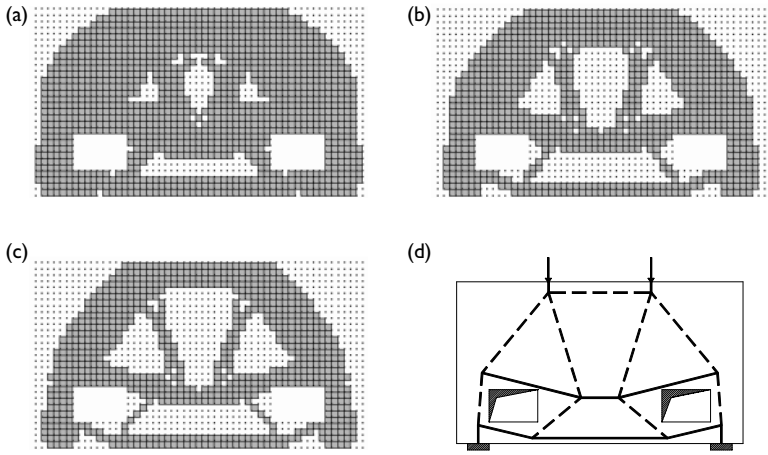

Figure 5.12 Optimization history of strut-and-tie model in deep beam with openings: (a) topology at iteration 20; (b) topology at iteration 40; (c) optimum at iteration 50; (d) strut-and-tie model.

strut-and-tie models in structural concrete based on the linear elastic theory of cracked concrete for system performance criteria, and to design concrete structures based on the theory of plasticity for strength performance criteria, as pointed out previously.

5.12.2 Deep beam with a large hole

Deep beams are used in multistory buildings to transfer the loads from one or more columns to the adjacent columns to achieve column-free space in the lower stories. These deep beams are usually designed as one story height. When the span of a beam is considerably greater than its depth, the beam displays flexural behavior and is called a slender beam. When the span of a beam approaches its depth, however, the simple beam theory is not applicable since the strain distribution over the depth of the beam is significantly nonlinear. Traditionally, the span-to-depth ratios of beams have been used to distinguish slender beams and deep beams in design codes. In AS 3600 (1994), different limiting values of the clear span to overall depth ratios are used to define deep beams with different support conditions. A cantilever is regarded as a deep beam if its span-to-depth ratio is less than 1.5. This limiting span–depth ratio is 3.0 for simply supported beams and 4.0 for continuous beams. In CEB Model Code (1990), beams with a slenderness ratio L_0/D of less than 2.0 are defined as deep beams, where L_0 is the distance between the points of contraflexure. It should be noted that

this simple rule of span–depth ratios used to classify deep beams is misleading. The identification of the B- and D-regions is a rational method to classify structures based on their geometry, loading and support conditions (Schlaich *et al*. 1987).

Web openings create disturbed regions in a deep beam and complicate the design process as the entire deep beam may be a D-region itself. Traditionally, the design of deep beams is based on experimental observations and empirical equations derived from limited test data. The empirical equations obviously lead to unsatisfactory strength predictions for deep beams and cannot explain the observed behavior. On the contrast, the simple strut-and-tie model theory can fully explain the experimental behavior of deep beams. Strut-and-tie modeling is particularly suited to the design of deep beams. This example is to demonstrate the reliability and efficiency of the automated PBO technology for the strut-and-tie modeling of a deep beam with a large hole.

The optimal strut-and-tie model in a simply supported deep beam with a large hole shown in Figure 5.13 was developed by using the PBO method based on the displacement performance criteria, and compared with the analytical solution given by Schlaich *et al*. (1987). This deep beam was subjected to a factored point load of 3 MN applied to the top of the beam. The compressive design strength of concrete (f_c) was 17 MPa. The concrete beam was discretized by using 100-mm square, four-node plane stress elements. A displacement constraint was imposed at the loaded point in the vertical direction. The Young's modulus of concrete E_c = 20 820 MPa and Poisson's ratio ν = 0.15 were specified in the FEA. The width of the beam

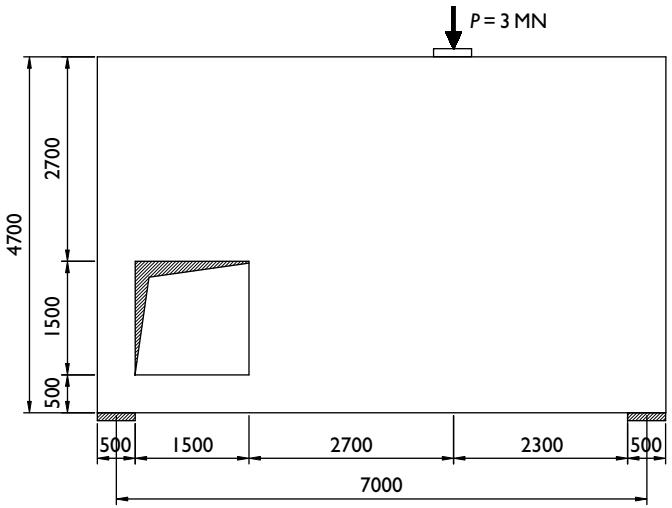

Figure 5.13 Deep beam with a large hole.

b = 400 mm was assumed in the analysis. The element removal ratio of 1 percent was used in the optimization process.

Figure 5.14 shows the performance index history of the deep beam with a large hole in the optimization process. It is observed from the figure that the performance index dropped sharply after reaching the peak value. This was caused by the breakdown of the load transfer mechanism in the deep beam due to element removal. The maximum performance index was obtained as 1.65. The topology optimization history is presented in Figure 5.15. It is seen that the point load is transferred to the supports by three load paths. The right-side load path is a straight strut connecting the load point and support. Because of the large hole, the left-side load path is to be re-routed around the hole. The inclined tension tie developed to transfer the load from the middle load path to the left-side strut and the right-side support. The inclined tension tie across the upper right corner of the opening, which will tend to crack under the applied load. The basic layout of the load transfer system is clearly shown by the topology obtained at iteration 40, as presented in Figure 5.15(b). Further element removal only sized the model. The two internal concrete struts joined together at iteration 40, but departed from each other at the optimum shown in Figure 5.15(c). This might be caused by the checkerboard patterns.

The optimal strut-and-tie model interpreted from the optimal topology is depicted in Figure 5.15(d), where the two internal struts have been joined together. The optimal strut-and-tie model obtained by the present study is similar to the model given by Schlaich *et al.* (1987). However, the optimal strut-and-tie model predicted by the PBO technique consists of the tension tie below the hole. This tension tie is needed to transfer the load to the

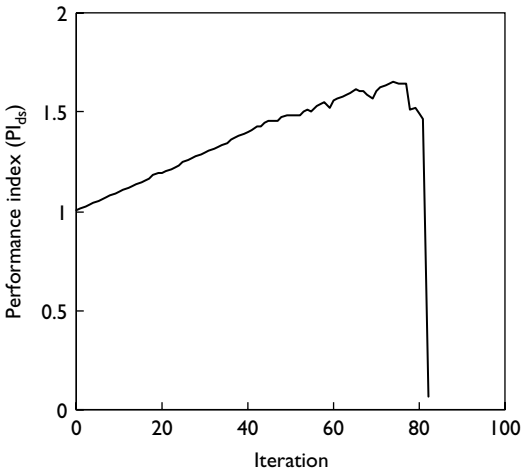

Figure 5.14 Performance index history of the deep beam with a large hole.

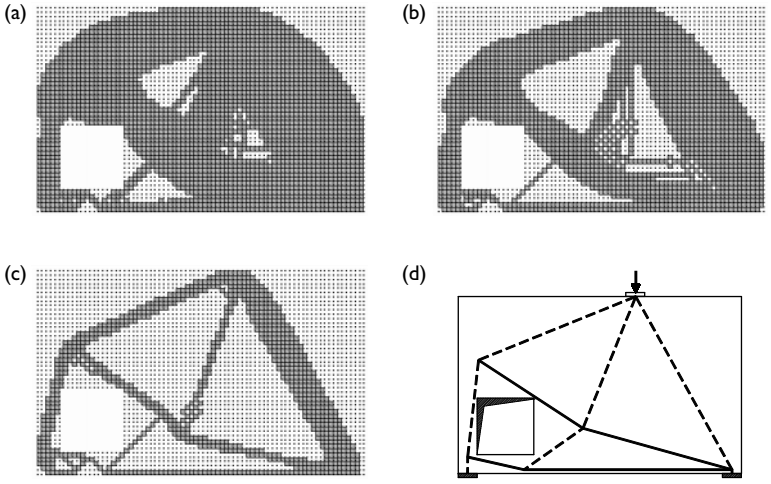

Figure 5.15 Optimization history of strut-and-tie model in the deep beam with a large hole. (a) Topology at iteration 20; (b) topology at iteration 40; (c) optimal topology; (d) optimal strut-and-tie model.

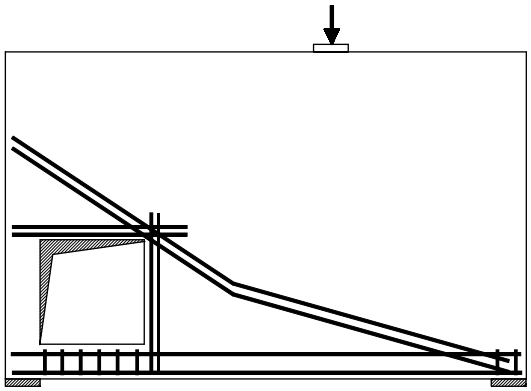

Figure 5.16 Main steel reinforcement in the deep beam with a large hole.

supports. The layout of main steel reinforcement for this deep beam is illustrated in Figure 5.16. Vertical stirrups are used in the regions below the hole to resist tensile stresses and to control cracking. This region is a potential weak spot. It is worth noting that minimum web reinforcement should be provided to the deep beam for crack control in accordance with codes of practice.

5.12.3 Effects of span-to-depth ratios

As discussed in preceding sections, the load transfer mechanism in a concrete structure depends on the geometry, loading and support conditions of the structure. The span-to-depth ratios are used in international concrete model codes to classify slender beams and deep beams, as discussed in the previous section. This classification is not rational as it reflects only the effect of geometry on the behavior of concrete beams. This example is to investigate the effects of span-to-depth ratios on optimal strut-and-tie models in reinforced concrete beams when other conditions are fixed. Simply supported concrete beams under a concentrated load applied to the midspan of the beams as shown in Figure 5.17 were considered. The depth of the beams D is 1000 mm for all cases while the span-to-depth ratio for cases (a)–(d) is 2, 3, 4 and 5 (Figure 5.18). The applied point load $P = 1200$ kN and the initial width of 250 mm were assumed for all beams. The concrete beams were modeled using 50-mm square four-node plane stress elements. A displacement constraint imposed at the loaded point in the vertical direction was considered. The compressive cylinder strength of concrete $f'_c = 32$ MPa, Young's modulus of concrete $E_c = 28\,567$ MPa, Poisson's ratio $\nu = 0.15$ were specified in the FEA for all cases. The element removal ratio of 1 percent was employed in the optimization process.

The maximum performance indices obtained for cases (a)–(d) are 1.88, 1.3, 1.23 and 1.21, respectively. Figure 5.18 depicts the optimal topology and corresponding strut-and-tie model for the beams with various span-to-depth ratios. It is demonstrated that the strut-and-tie model in the concrete beams changes with the changes in the span-to-depth ratio. When the span-to-depth ratio of the beam is equal to 2, the load is transferred from the loaded point to the supports through straight struts. For beams with a span-to-depth ratio of greater than 2, inclined tension ties connecting compressive concrete struts are necessary to form the strut-and-tie model as shown in Figure 5.18(b)–(d). In detailing, some of the bottom steel

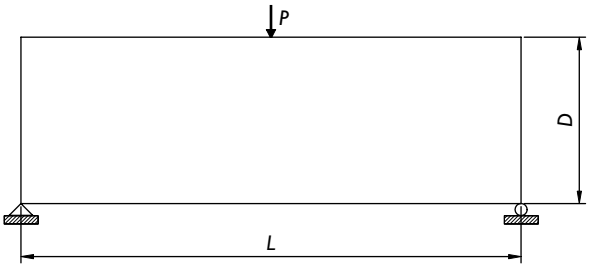

Figure 5.17 Simply supported beams with various span-to-depth ratios.

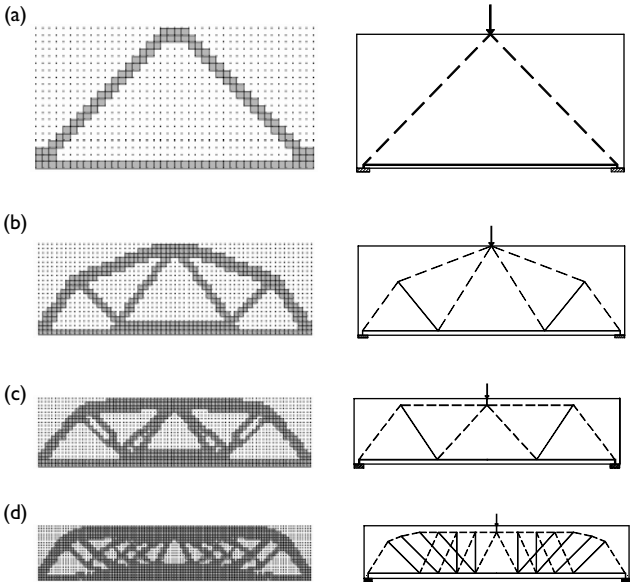

Figure 5.18 Optimal topologies and corresponding strut-and-tie models showing the transition from deep beams to slender beams: (a) $L/D = 2$; (b) $L/D = 3$; (c) $L/D = 4$; (d) $L/D = 5$.

bars may be bent up to carry the forces in inclined tension ties. For very slender beams, optimal topologies obtained by the PBO method are continuum-like structures, in which strut-and-tie actions are difficult to be identified, such as that shown in Figure 5.18(d). The sectional method or standard truss models may be used to design these slender concrete beams.

In developing strut-and-tie models in concrete structures using trial-and-error methods, the strut angle must be limited to achieve efficient strut-and-tie models and to avoid dangerous ones. The CEB Model Code (1987) limits the strut angle between 31° and 59° based on experimental observations. The optimal strut-and-tie models shown in Figure 5.18 indicate that the angles between the compressive concrete struts and longitudinal ties are equal to or greater than 45°. Therefore, it is suggested that the strut angle with respect to the longitudinal ties should not be less than 45° to be efficient in transferring loads.

It is clearly demonstrated that the load transfer mechanism in a structural concrete member adapts to its geometry such as the span-to-depth ratios of the beams. Without modification, a strut-and-tie system developed for a specific structural concrete member cannot be used in the design of members with different geometry, loading and support conditions.

5.12.4 Continuous deep beams

Continuous reinforced concrete deep beams are sometimes used in building construction. More efforts are usually needed to develop strut-and-tie models in continuous concrete beams than in single span beams if conventional methods are used. This example is to show the efficiency of the PBO technique in dealing with the strut-and-tie modeling of continuous concrete beams.

The PBO technique based on displacement performance criteria was used to develop the optimal strut-and-tie model in a continuous concrete beam under two point loads of $P_1 = 1000$ kN and $P_2 = 550$ kN, as shown in Figure 5.19. The compressive cylinder strength of concrete (f'_c) was 32 MPa. The Young's modulus of concrete $E_c = 28\,600$ MPa, and Poisson's ratio $\nu = 0.15$ were specified in the FEA. The continuous plain concrete beam was divided into 50-mm square, four-node plane stress elements in the FEA. An initial width of 200 mm was selected for the beam. The same deflection limit was imposed at the two loaded points A and B in the vertical direction. Two virtual unit point loads were applied to points A and B. The element elimination ratio of 1 percent was employed in the performance optimization process.

Figure 5.20 shows the performance index history curves for the continuous beam. The performance indices were calculated using the displacements at points A and B. It can be observed from Figure 5.20 that the performance index determined using the displacement at point A is less than that computed using the displacement at point B up to iteration 55. This is because the deflection is more critical at point A than at point B. After iteration 55, however, the performance index at point B dropped sharply since further element removal caused the large deflection at point B, which becomes the most critical displacement. It is apparent that the performance of the continuous beam was maximized at iteration 55.

The optimization history of the strut-and-tie model in this continuous deep beam is shown in Figure 5.21. The optimal strut-and-tie model presented in Figure 5.21(d) indicates a very complex load-carrying system. It is difficult to find the optimal load paths in this continuous beam using conventional trial-and-error methods. It can be observed that the loads are

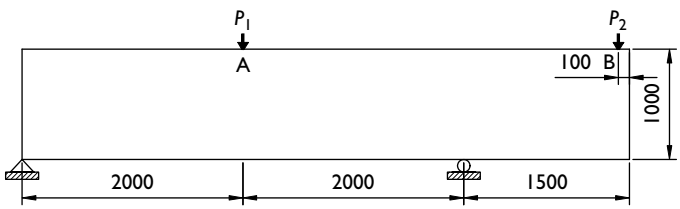

Figure 5.19 Continuous deep beam.

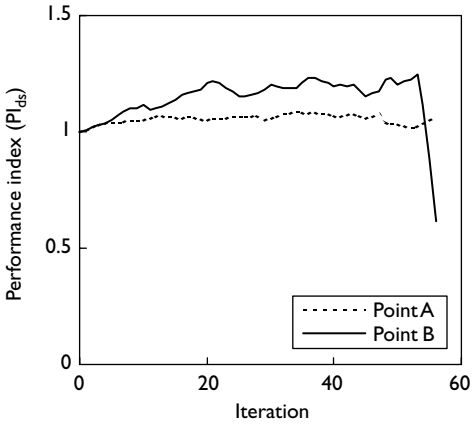

Figure 5.20 Performance index history of the continuous deep beam.

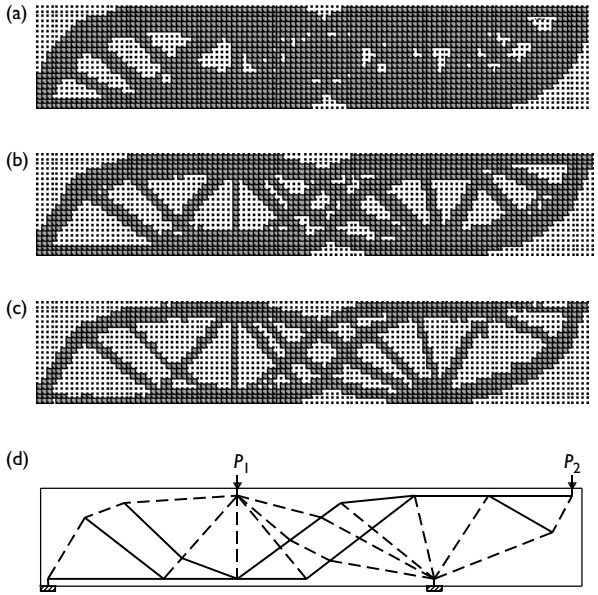

Figure 5.21 Optimization history of strut-and-tie model in the continuous beam: (a) topology at iteration 20; (b) topology at iteration 40; (c) optimal topology at iteration 55; (d) optimal strut-and-tie model.

transferred through struts and ties to the supports. The point load P_1 creates a disturbed region where the concentrated load is transferred by six struts. The interior support is in compression and withstands compression forces from six struts. Inclined tension ties develop in shear spans, as shown

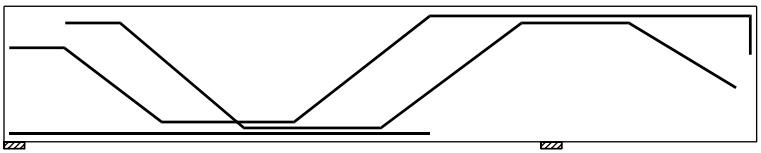

Figure 5.22 Layout of main steel reinforcement in the continuous beam.

in Figure 5.21(d). This optimal strut-and-tie model suggests that the inclined reinforcement bent up from the bottom steel reinforcing bars should be used to resist tensile forces developed in the shear spans and extended to the end of the cantilever to carry tensile forces induced by the point load P_2. A layout arrangement of the main steel reinforcement in the continuous beam is illustrated in Figure 5.22. It should be noted that steel reinforcement in the bottom or the top of the beam could be in one layer if they can fit in.

5.12.5 Corbels

Corbels are used to transfer large concentrated loads from beams to the columns at intermediate floor levels. The concentrated load leads the entire corbel into a disturbed region. Strut-and-tie models can indicate the locations of internal forces induced in the corbel by the external load and also the failure modes to be expected. In many cases, the failure of corbels was caused by the poor detailing. Strut-and-tie modeling is an effective tool for the design and detailing of corbels. However, special attentions must be given to the support conditions of corbels when developing strut-and-tie models for the corbels. Different support conditions lead to different strut-and-tie models and different reinforcement layouts in the corbels. This section is devoted to the development of strut-and-tie models for the design and detailing of corbels with different support conditions by using the automated PBO technique.

5.12.5.1 Corbel mounted on a column

A corbel mounted on a column as shown in Figure 5.23 is to be designed to carry a point load of 500 kN. The column is fixed at both ends. The width of the column and corbel is 300 mm. It is required to develop a strut-and-tie model for the design and detailing of the corbel. To look at how the load is transferred from the corbel to the column, the corbel and column were treated as a whole in the development of the strut-and-tie system. In the FEA, this structure was discretized into finite elements using 25-mm square,

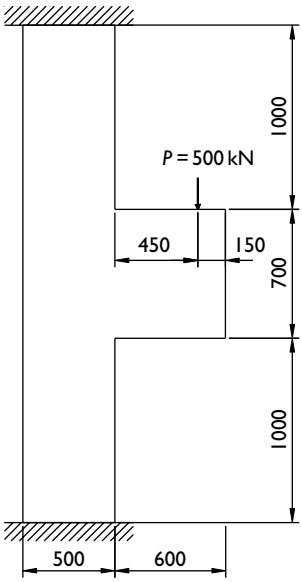

Figure 5.23 Corbel mounted on a column.

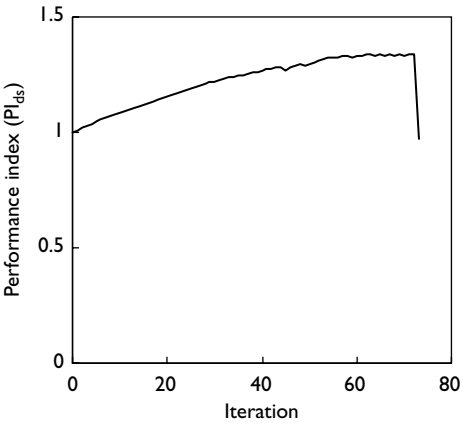

Figure 5.24 Performance index history of corbel mounted on a column.

four-node plane stress elements. A displacement constraint was imposed at the loaded point in the vertical direction. The compressive cylinder strength of concrete $f'_c = 32$ MPa, Young's modulus of concrete $E_c = 28567$MPa and Poisson's ratio $\nu = 0.15$ were specified in the FEA. The element removal ratio of 1 percent was employed in the optimization process.

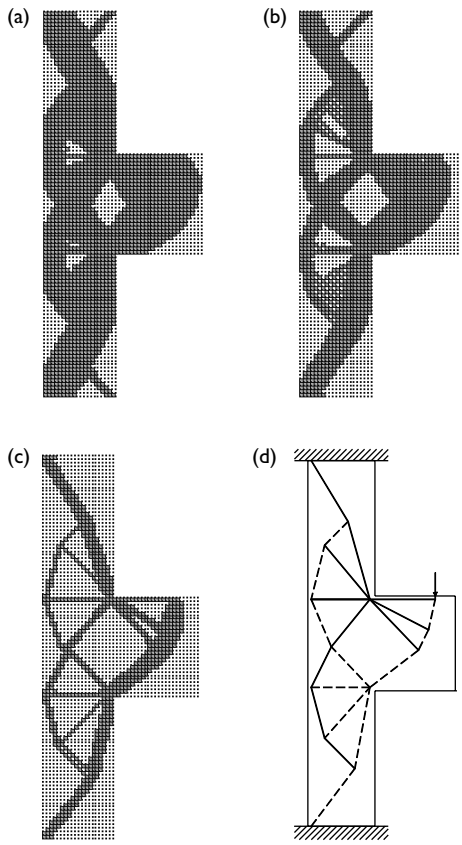

Figure 5.25 Optimization history of strut-and-tie model in the corbel mounted on a column. (a) Topology at iteration 20; (b) topology at iteration 40; (c) optimal topology; (d) optimal strut-and-tie model.

The performance index history of the structure in the optimization process is depicted in Figure 5.24, which shows that the maximum performance index is 1.34. From the optimization history of the structure presented in Figure 5.25, checkerboard patterns are observed in the topology obtained at iteration 40. The load is transferred from the corbel to the whole column along the paths of concrete struts and tension ties. The strut-and-tie model obtained is rather complicated. It is suggested that the corbel and column should be considered as a whole structure in developing the strut-and-tie model. The optimal strut-and-tie model shown in Figure 5.25(d) agrees very well with the solution obtained by Schlaich *et al.* (1987) using the load path method.

5.12.5.2 Corbel with a ledge support

A corbel with ledge support is shown in Figure 5.26(a). The ledge support is fixed. This corbel is subjected to a point load of 500 kN. The width of the corbel is 300 mm. In the finite element modeling, the corbel was discretized into 1360 four-node plane stress elements. The material properties of the concrete are the same as the previous corbel mounted on a column. The PBO technique formulated on the basis of overall stiffness performance criteria was employed to develop a strut-and-tie model for the design and detailing of the corbel. The mean compliance constraint was considered. The element deletion ratio of 2 percent was used in the optimization process. The optimal topology generated by the PBO technique is presented in Figure 5.26(b). The optimal topology was idealized to a discrete strut-and-tie model depicted in Figure 5.26(c), where straight truss members were used to idealize the struts. It can be observed that the point load is transferred to the support through the struts tied by five tension ties. These tension ties are combined to one to transfer the load to the support. The arrangement of main steel reinforcement in the corbel based on the strut-and-tie model obtained is illustrated in Figure 5.26(d).

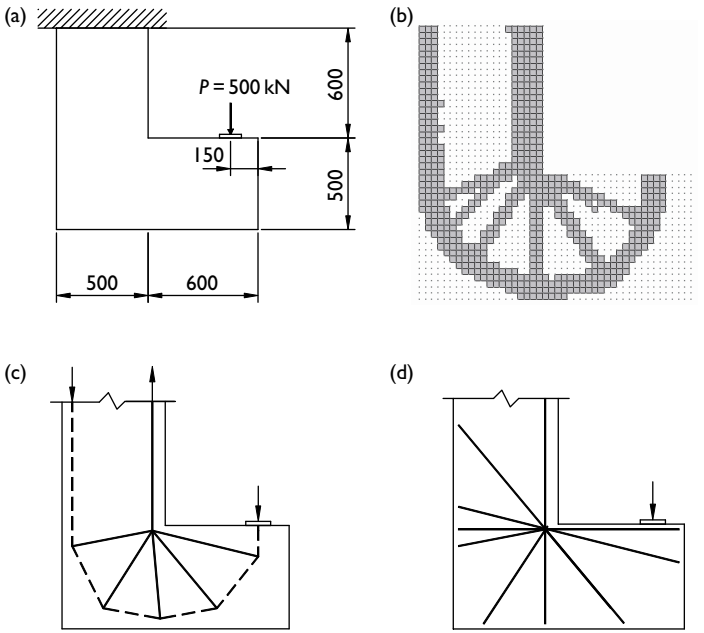

Figure 5.26 (a) Design domain; (b) optimal topology; (c) strut-and-tie model; (d) reinforcement for corbels.

It is seen that an additional horizontal bar has been provided in the corbel to control cracking.

5.12.5.3 Corbel mounted on the top of a column

Another support condition of corbels may be encountered in structural design, as shown in Figure 5.27(a). The end of the column is fixed on the foundation. The structural model illustrated in Figure 5.27(a) was developed to simulate the disturbed region of the corbel with a column whose height may be shortened. It was assumed that the height of the column had no effect on the strut-and-tie model in the corbel region. The corbel was to be designed to support a point load of 500 kN. The width of the corbel was initially assumed as 300 mm. The material properties of concrete were the same as the previous example. The PBO technique formulated on the basis of overall stiffness performance criteria was applied to the corbel, which was divided into 1360 four-node plane stress elements. The element removal ratio of 2 percent was specified in the optimization process.

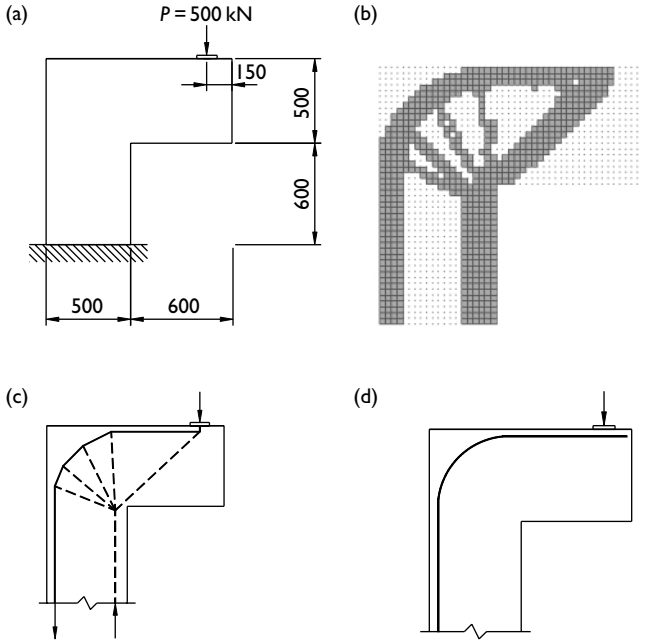

Figure 5.27 (a) Design domain; (b) optimal topology; (c) strut-and-tie model; (d) main reinforcement for corbels.

The optimal topology, strut-and-tie model and main reinforcement for the corbel are presented in Figure 5.27. It is seen from this figure that the point load induces compression and tensile forces in the corbel. The compression force is transferred to the column by a straight strut while the tensile force is transferred to the column by a curve load path. The detailing of this corbel is simple. Bent steel reinforcing bars can be provided in the corbel to resist tensile forces as shown in Figure 5.27(d). It can be observed from Figures 5.25–5.27 that strut-and-tie models in corbels vary greatly with the support conditions. As a result, the arrangements of the main steel reinforcement in corbels should adapt to their support conditions as well as geometry. The PBO technique can be applied to a wide range of the design and detailing problems of corbels.

5.12.6 Bridge pier

A bridge pier shown in Figure 5.28 is to be designed to support four concentrated loads of 2750 kN transferred from four steel-concrete composite girders. The bridge pier is fixed on the foundation. An initial thickness of 1.5 m is assumed for this bridge pier. The bridge will be constructed in a region with an exposure classification of B2. It is required to develop a strut-and-tie model for the design and detailing of this bridge pier. The automated PBO technique was employed to undertake this task. The compressive cylinder strength of concrete $f'_c = 32$ MPa, Young's modulus of concrete $E_c = 28\,600$ MPa, and Poisson's ratio $\nu = 0.15$ were specified in the FEA. The bridge pier was modeled using 125-mm square, four-node plane stress elements. Plane stress conditions and the mean compliance constraint were considered. The element removal ratio of 1 percent was used in the optimization process.

Figure 5.29 depicts the performance characteristics of the bridge pier structure in the optimization process. The performance characteristics are

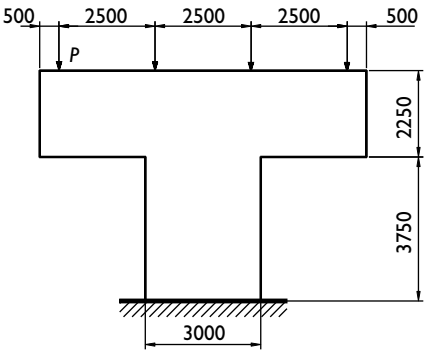

Figure 5.28 Design domain for a bridge pier.

represented by a weight-compliance curve. It can be observed from Figure 5.29 that the mean compliance of the bridge pier increased when inefficient elements were eliminated from the pier. The performance of the bridge pier in the optimization process was monitored by the performance index as shown in Figure 5.30. It appears from Figure 5.30 that by removing a small number of elements with the lowest SEDs from the bridge pier at each iteration, the performance index increased from unity to a maximum value of 1.17. After iteration 69, however, the performance index decreased because further element elimination resulted in the breakdown of the load transfer mechanism in the bridge pier.

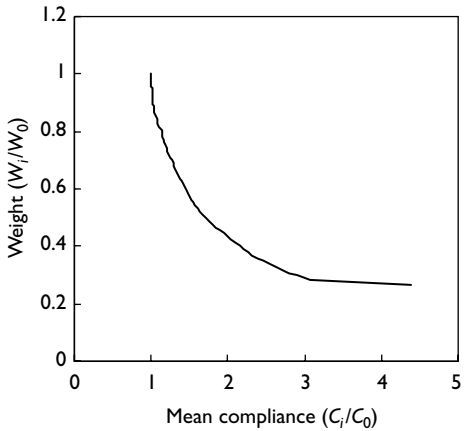

Figure 5.29 Performance characteristic curve for the bridge pier.

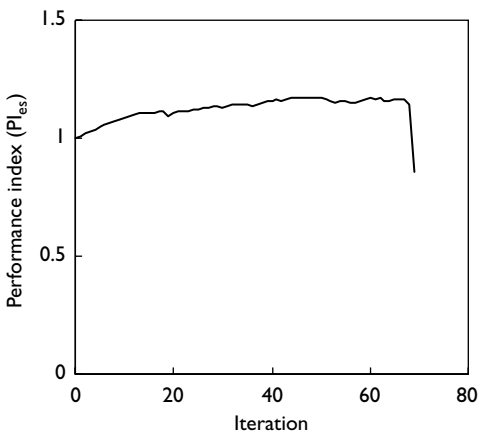

Figure 5.30 Performance index history of the bridge pier.

The optimization history of strut-and-tie model in the bridge pier is presented in Figure 5.31. It can be observed from the optimization history that the load transfer mechanism in the bridge pier became more and more clear when the portions that had no contribution to the load-carrying capacity of the structure were systematically removed from the finite element model. The optimal topology depicted in Figure 5.31(c) occurred at iteration 49. The applied loads were mainly sustained by the optimal structure, which essentially represents the most efficient load transfer mechanism in the bridge pier. The optimal topology was transformed to a discrete strut-and-tie model illustrated in Figure 5.32, where the solid lines represent tension ties and the dashed lines represent compression struts. The geometry of the design proposal depicted in Figure 5.32 has been altered in comparison with the original design to achieve a better flow of internal force within the pier structure and economical designs. It would appear from Figure 5.31(c) that the pier wall can be designed as two separated columns so that the most efficient design of the bridge pier is obtained. A detailed design of this bridge pier is provided in Section 5.14.3.

5.12.7 Shearwalls with openings

Reinforced concrete shearwalls are commonly used in buildings to resist lateral loads arising from wind or earthquakes. High-rise concrete shearwalls in tall buildings behave essentially in the same manner as flexural reinforced concrete members, which can be designed on the basis of the flexural beam theory. In contrast, low-rise concrete shearwalls in low-rise buildings more often have a height-to-length ratio of less then 1.5 and thus their behavior cannot be predicted by conventional methods for tall shearwalls. The design of low-rise shearwalls in the past practice was largely based on the findings of experimental work on low-rise shearwalls (Benjamin and Williams 1957) and on deep beams.

Low-rise reinforced concrete shearwalls are actually deep beams, which can be designed by using strut-and-tie models. Marti (1985) has used the load path method to develop strut-and-tie models in low-rise concrete shearwalls with openings. His study indicates that strut-and-tie modeling is a promising tool for the design of low-rise reinforced concrete shearwalls. However, the utility of strut-and-tie models in practice is often limited by the designer's ability to develop appropriate models for concrete structures with complex loading and geometry conditions. This is because the conventional methods employed to develop the models involve a trial-and-error iterative process. The PBO technique provides the designer with an efficient automated tool that is particularly applicable to the generation of strut-and-tie models in low-rise concrete shearwalls with complex geometry and loading conditions. An example is provided in this section to demonstrate the efficiency of the automated PBO program developed on the basis of

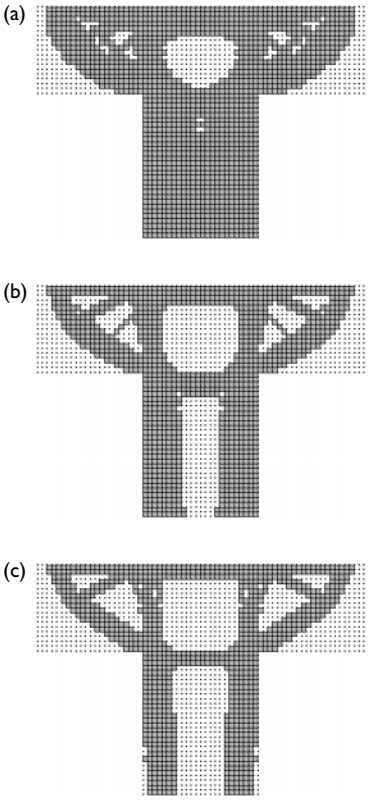

Figure 5.31 Optimization history of strut-and-tie model in the bridge pier: (a) topology at iteration 20; (b) topology at iteration 40; (c) optimal topology at iteration 49.

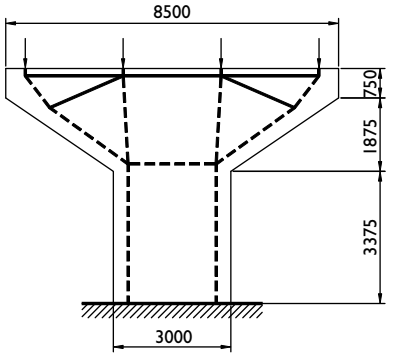

Figure 5.32 Strut-and-tie model in the bridge pier.

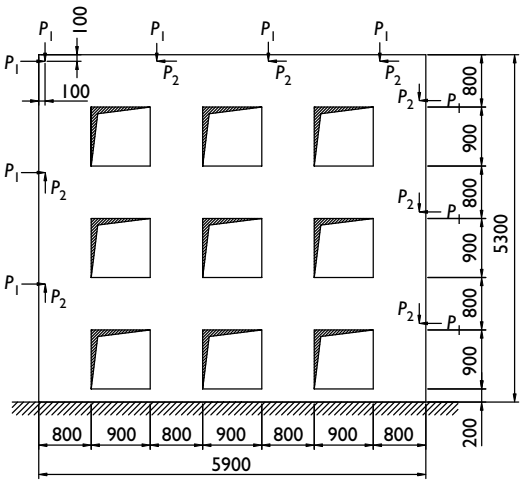

Figure 5.33 Low-rise concrete shearwall with openings.

overall stiffness performance criteria in dealing with low-rise concrete shearwalls with complex geometry and loading conditions.

Figure 5.33 shows a low-rise concrete shearwall with openings under many concentrated loads in one load case. This shearwall is based on the example presented by Marti (1985). The shearwall is fixed on the foundation. In the present study, the point loads $P_1 = 1000$ kN and $P_2 = 500$ kN were assumed. The compressive cylinder strength of concrete $f'_c = 32$ MPa, Young's modulus of concrete $E_c = 28\,600$ MPa, and Poisson's ratio $\nu = 0.15$ were specified in the FEA. The initial thickness of the shearwall was taken as 200 mm. The plain concrete shearwall was modeled using 100-mm square, four-node plane stress elements. The PBO technique for structures with mean compliance constraints was applied to the shearwall with an element removal ratio of 1 percent.

Figure 5.34 shows the performance characteristic curve for the concrete shearwall in the optimization process. It can be observed from the figure that the mean compliance of the shearwall increased with a reduction in its weight when elements with the lowest SEDs were gradually removed from the shearwall. When 35.3 percent elements compared with the original mesh were removed from the shearwall, the mean compliance of the shearwall increased by 29 percent and the performance of the shearwall was maximized. After that, further element elimination led to a significant increase in the mean compliance of the shearwall, as shown in Figure 5.34. The performance characteristic curve indicates whether a proposed design for the required performance level is feasible. Figure 5.35 presents the performance index

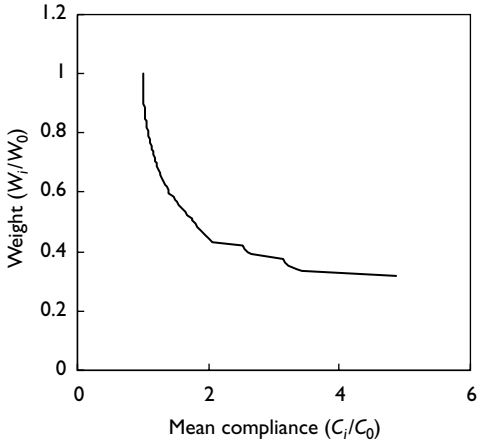

Figure 5.34 Performance characteristics of shearwall with openings.

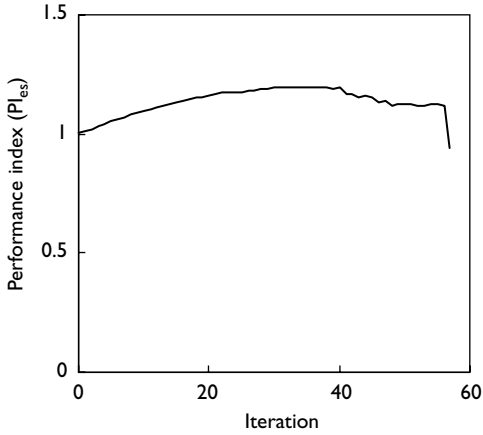

Figure 5.35 Performance index history of shearwall with openings.

history of the shearwall with openings. It appears from Figure 5.35 that the performance of the shearwall in terms of the efficiency of material usage and overall stiffness was still gradually improved by eliminating elements with the lowest SEDs from the model even if there were a large portion of openings. The maximum performance index of 1.2 occurred at iteration 35.

Figure 5.36 demonstrates the optimization history of the strut-and-tie model in the shearwall with openings. It can be observed that the resulting topology evolved toward a frame-like structure when elements with the lowest SEDs were systematically removed from the shearwall. The optimal topology produced by the PBO program is presented in Figure 5.36(d). This optimal topology represents the load

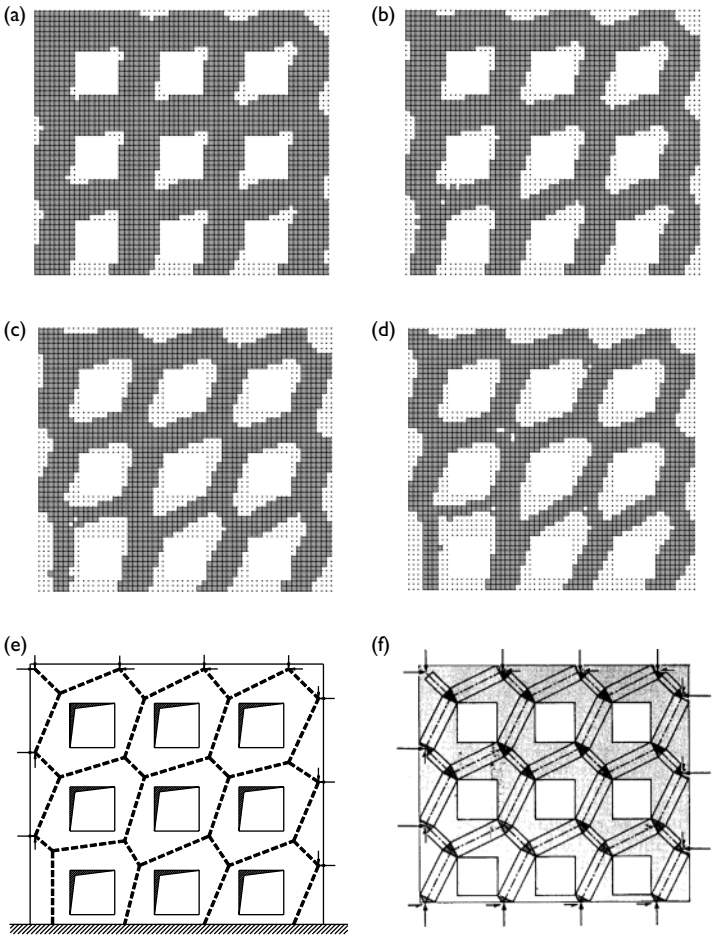

Figure 5.36 Optimization history of strut-and-tie model in shearwall with openings: (a) topology at iteration 10; (b) topology at iteration 20; (c) topology at iteration 30; (d) optimum at iteration 35; (e) optimal strut model; (f) model by Marti (1985).

transfer mechanism in the concrete shearwall with openings under the given loading and support condition. It can be idealized as a discrete strut-and-tie model depicted in Figure 5.36(e). It is interesting to note that this model consists of only struts. The optimal model generated by the PBO technique agrees extremely well with the analytical solution shown in Figure 5.36(f), which was derived by Marti (1985).

In dimensioning the strut-and-tie model, either the optimal topology presented in Figure 5.36(d) or the model given in Figure 5.36(e) can be used as

a basic for dimensioning the depths of concrete struts. The final width of concrete struts (or the thickness of the shearwall) can be determined using the effective compressive strength of concrete according to the forces they carry and bearing conditions. No main steel reinforcement is required to carry tensile forces in the shearwall because the model obtained consists of no tensile ties. However, a minimum amount of steel reinforcement in compliance with codes of practice should be provided in the concrete shearwall to control cracking. For a completed design, the strength performance of nodal zones in the model should be checked.

5.12.8 Beam–column connections

Beam–column connections in reinforced concrete frames are D-regions, which are potential weak spots that need special considerations in detailing. The connection serves as the purpose of transferring forces from the beams to the columns. The internal forces in the connection change their directions sharply. The flow of internal forces in a connection becomes more complex when more members enter the connection. Beam–column connections must be strong enough to allow the full strengths of the connected beams and columns to be developed and must have adequate ductility at the ultimate limit state. Appropriate reinforcement detailing is therefore required for beam–column connections to achieve the required strength and ductility performance. Strut-and-tie modeling can be used in the design and detailing of beam–column connections. By visualization of the beam–column connections as D-regions, the PBO technique can be employed to develop strut-and-tie models for the design and detailing of beam–column connections in framed concrete structures. The strut-and-tie models and corresponding reinforcement detailing of beam–column connections are presented in this section.

5.12.8.1 Opening knee joints

The beam–column connection under positive moment in portal frames is known as an opening knee joint, which can be visualized as the structural model shown in Figure 5.37(a). In the FEA, the positive moment was modeled using a couple forces applied to the beam. The end of the column was fixed to give the reaction forces equal to the applied couple. The thickness of the connection was assumed to be 300 mm in the finite element analysis. The compressive strength of concrete was assumed to be 32 MPa. The Young's modulus $E_c = 28\,567$ MPa and Poisson's ratio $\nu = 0.15$ were specified for the concrete material. The connection was discretized into 1360 four-node plane stress elements. The PBO method was employed to generate a strut-and-tie system with the maximum overall stiffness and minimum weight. The optimal topology produced by the PBO technique is

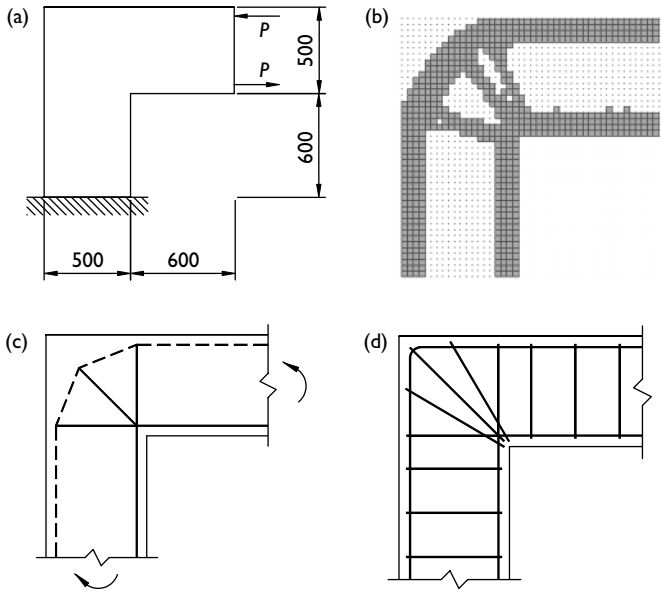

Figure 5.37 (a) Design domain; (b) optimal topology; (c) strut-and-tie model; (d) reinforcement for frame corner under positive moment.

shown in Figure 5.37(b). It is seen that the optimal topology is not symmetrical, as the initial structural model is not symmetrical. The optimal topology was idealized as the strut-and-tie model shown in Figure 5.30(c). It is noted that diagonal tensile force developed within the connection. The reinforcement detailing based on the strut-and-tie model is illustrated in Figure 5.37(d). Three stirrups fan out from the reentrant corner to control possible diagonal cracking in the connection. U-bars should be used as main tensile steel reinforcement in beam and column of the connection to achieve effective anchorage.

5.12.8.2 Closing knee joints

When the end moment in the beam is negative, the beam–column connection in a frame corner is called a closing knee joint. The design domain, optimal topology, strut-and-tie model and corresponding reinforcement for a closing knee joint are shown in Figure 5.38. The optimal topology obtained for a closing knee joint is the same as that for an opening knee joint, but not the strut-and-tie model. The strut-and-tie model indicates that tensile forces develop around the outer corner in a closing knee joint. The continuous and curved steel reinforcement has been used in the closing knee

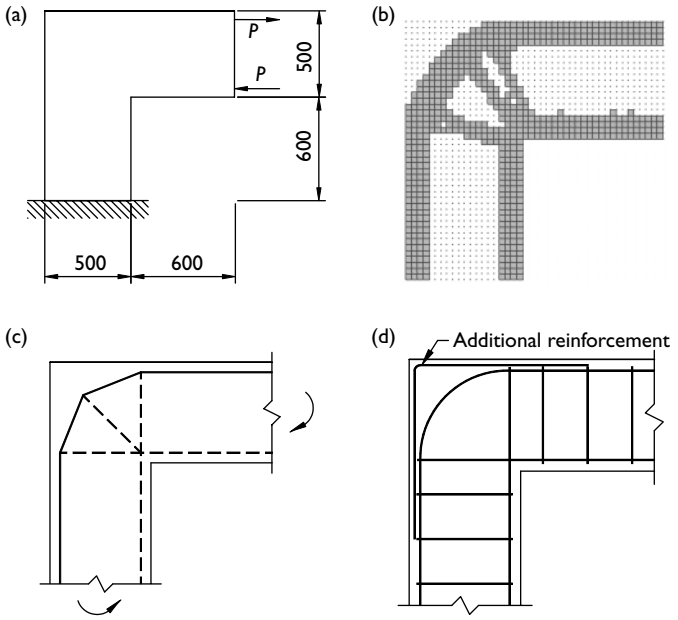

Figure 5.38 (a) Design domain; (b) optimal topology; (c) strut-and-tie model; (d) reinforcement for frame corner under negative moment.

joint to resist tensile forces based on the strut-and-tie mode obtained. Additional reinforcement may be provided in the outer corner to prevent the concrete splitting at the corner, as shown in Figure 5.38(d).

5.12.8.3 Exterior beam–column connections

An exterior beam–column connection is a region where a beam connects to an exterior continuous column. In such a connection, the bending moment in the beam is transferred to the upper column and the lower column. One corner of the connection is closing and the other is opening. The structural model shown in Figure 5.39(a) was used to simulate an exterior beam–-column connection. The beam moment was represented using a couple forces of $2P$. It was assumed that half of the beam moment was transferred to the upper column, where the moment was modeled using a couple forces of P. The bottom of the lower column was fixed. The thickness of the connection was 300 mm. The compressive strength of concrete used in the analysis was 32 MPa. The Young's modulus $E_c = 28\,567$ MPa and Poisson's ratio $\nu = 0.15$ were assumed for the concrete material. The connection was divided into 1840 four-node plane stress elements. The element removal ratio of 2 percent was used in the performance optimization process.

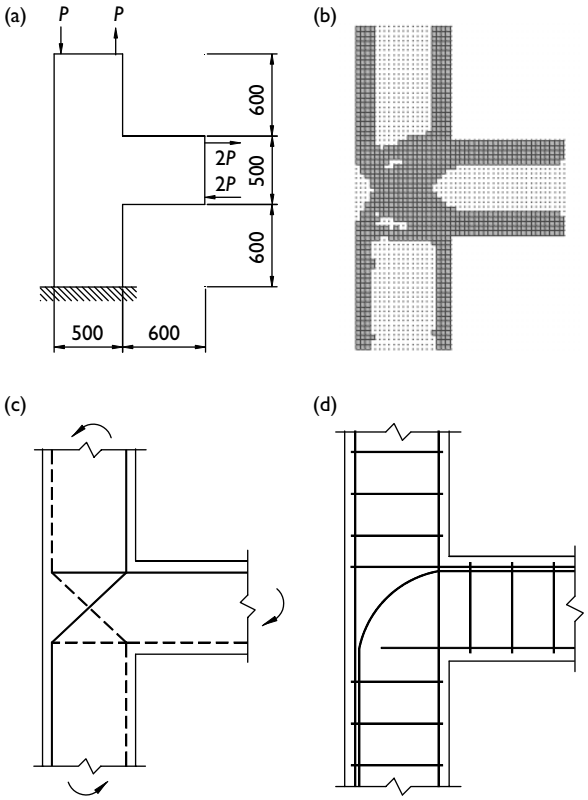

Figure 5.39 (a) Design domain; (b) optimal topology; (c) strut-and-tie model; (d) reinforcement for exterior beam–column connection.

The optimal topology, strut-and-tie model and reinforcement details are provided in Figure 5.39. It can be observed from the strut-and-tie model that tensile forces develop in the upper part of the beam, the right side of the upper column, the diagonal of the connection, and the left side of the lower column. These tensile forces in these regions can induce cracking. The steel reinforcement details based on the strut-and-tie model are shown in Figure 5.39(d). It is suggested that continuous and curved reinforcing bars should be used to resist the diagonal tensile forces in exterior beam–column connections.

5.12.8.4 Interior beam–column connections

One of the interior beam–column connections consists of a continuous beam supported on a column. Under horizontal loads, one of the beams is subjected to the positive moment and the other is in negative bending. This type of

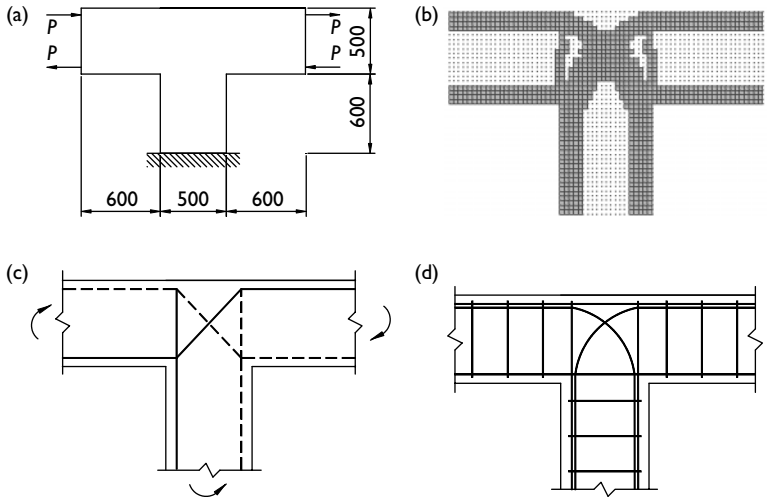

Figure 5.40 (a) Design domain; (b) optimal topology; (c) strut-and-tie model; (d) reinforcement for interior beam–column connection.

interior beam–column connections can be simulated using the structural model provided in Figure 5.40(a). In the FEA, the beam moments were represented using a couple forces. The bottom of the column was fixed. The connection was divided into 1840 four-node plane stress elements. The compressive strength of concrete was 32 MPa. The Young's modulus $E_c = 28\,567$ MPa and Poisson's ratio $\nu = 0.15$ were specified in the FEA for the concrete material. The optimal topology obtained by the PBO method is shown in Figure 5.40(b). This topology is symmetrical about the *y*-axis. The strut-and-tie idealization of the connection is presented in Figure 5.40(c). It is seen that diagonal tensile forces develop in the connection. The beam–column connection is reinforced using continuous and curved steel bars to resist diagonal tensile forces induced by two horizontal load cases, as shown in Figure 5.40(d).

5.13 Optimal strut-and-tie models in prestressed concrete

In prestressed concrete beams, compressive prestressing forces are artificially applied to the concrete beam with the help of hydraulic jacks in order to reduce or eliminate cracking due to high tensile stresses and deflection induced by the applied loads. The traditional design procedure of prestressed concrete members has been described by Gilbert and Micklborough (1990). It is noted that strut-and-tie modeling offers a better understanding of the behavior of prestressed concrete. It also simplifies the design procedure.

Choosing the appropriate tendon profile, the type and the magnitude of prestressing forces can favorably and efficiently alter the load transfer mechanism in concrete beams. A fully prestressed concrete beam has no tensile chord at its bottom whilst a partially prestressed concrete beam has a tensile chord at its bottom, which is shorter than that of a nonprestressed concrete beam. Schlaich *et al.* (1987) suggested that by treating prestressing forces as external loads, prestressed concrete beams could be analyzed and dimensioned like reinforced concrete ones with strut-and-tie systems. Ramirez (1994) has applied the strut-and-tie model approach to the design of pretensioned concrete members.

Kirsch (1993) proposed a procedure for optimizing the member size, initial prestressing force and tendon profile of a prestressed concrete system based on traditional design procedure. However, little work has been undertaken so far on optimization of strut-and-tie models in prestressed concrete beams by continuum topology optimization methods. In this section, therefore, optimal strut-and-tie models in nonprestressed, partially prestressed and fully prestressed concrete beams are investigated by using the PBO technique for structures with displacement constraints. It is proposed to optimize strut-and-tie models in prestressed concrete structures by treating prestressing forces as external loads.

5.13.1 Nonprestressed concrete beam

A simply supported prestressed concrete beam with a rectangular cross-section under two concentrated loads of $F = 500$ kN and the prestressing force P is depicted in Figure 5.41. When the prestressing force is equal to zero, the beam is a nonprestressed concrete beam, which is considered herein for comparison purposes. The depth of the beam is 1000 mm. In the FEA, the initial width of the concrete beam was taken as 300 mm. The Young's modulus of concrete $E_c = 31\,940$ MPa and Poisson's ratio $\nu = 0.15$ were specified in the FEA. This concrete beam was modeled using 160×20 four-node plane stress elements. Two displacement constraints of the same limit were imposed at the points of load F in the vertical direction. The element removal ratio of 1 percent was used in the optimization process.

Figure 5.42 depicts the performance index history of the nonprestressed concrete beam obtained by the PBO technique. It is observed from the figure that the performance index increased from unity to the maximum value of 1.38 when elements with the lowest VSEDs were removed from the model. After the performance of the beam was maximized, the performance index dropped sharply. It indicates that further element removal led to large deflections. The performance index may jump in the optimization history as depicted in Figure 5.42 because the element removal ratio used in the PBO process was still high. As discussed in Chapter 3, it is possible to achieve smoother solutions to nonprestressed members by using a smaller element removal ratio, but the computational cost will be increased considerably.

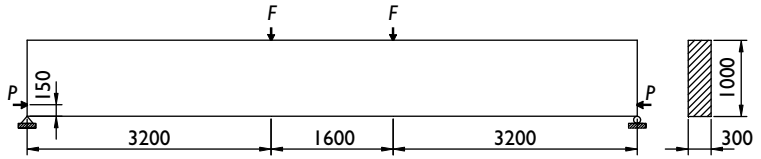

Figure 5.41 Prestressed concrete beam.

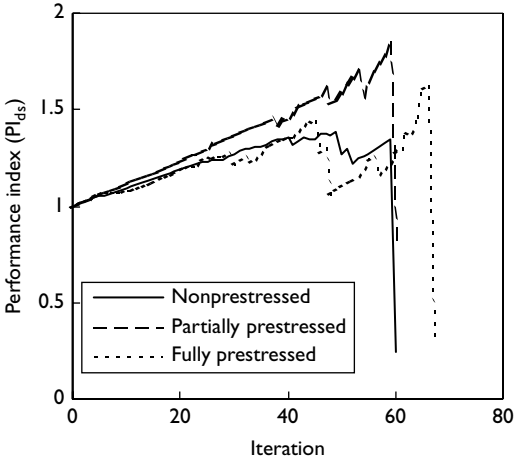

Figure 5.42 Performance index history of prestressed concrete beams.

The optimization history of the strut-and-tie model in the nonprestressed concrete beam is demonstrated in Figure 5.43, in which only half of the model is shown by taking the advantage of symmetry. It can be seen from Figure 5.43 that the strut-and-tie model was characterized by the remained elements in the beam when inefficient elements were gradually deleted from the beam. The optimal strut-and-tie model shown in Figure 5.43(d) suggests that inclined reinforcing bars bent up from the bottom reinforcement should be used to sustain inclined tensile forces developed in the shear span. Figure 5.43(e) depicts the strut-and-tie model of this reinforced concrete beam obtained by Schlaich *et al.* (1987). In their strut-and-tie model, vertical ties were assumed to form the model.

5.13.2 Partially prestressed concrete beam

Structural concrete members deigned to crack at the full service loads are called partially prestressed. Prestressing forces applied to a concrete beam result in reduced cracking and reduced deflections induced by the

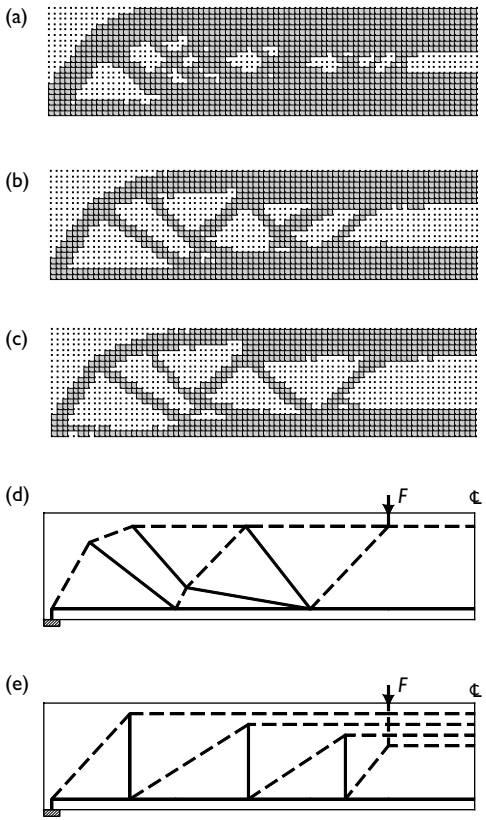

Figure 5.43 Optimization history of strut-and-tie model in nonprestressed concrete beam: (a) topology at iteration 20; (b) topology at Iteration 40; (c) optimal topology; (d) optimal strut-and-tie model; (e) strut-and-tie model by Schlaich *et al.* (1987).

applied loads. Partial prestressing shortens the length of the tension chord along the bottom of a concrete beam. By treating prestressing forces as external loads, prestressed concrete beams can be analyzed, optimized and designed with strut-and-tie models in the same manners as reinforced concrete beams.

A prestressing force of $P = 1650$ kN was applied to the concrete beam shown in Figure 5.41. The displacement constraints of the same limit were imposed at the points of loading F in the vertical direction since the deflections of the beam were to be reduced. The element removal ratio of 1 percent was used in the PBO process. The performance index history of this prestressed concrete beam is also shown in Figure 5.42. The maximum

performance index of the prestressed concrete beam is 1.85, which is higher than that of the nonprestressed concrete beam.

Figure 5.44 shows the optimization history of the prestressed concrete beam. The load transfer mechanism in the beam became more and more clear when elements were systematically eliminated from the model. It can be seen from Figure 5.44(d) that a tension tie developed at the bottom of the prestressed concrete beam. This tension chord is shorter than that of the nonprestressed concrete beam depicted in Figure 5.43(d). Thus, this concrete beam is partially prestressed. It can be observed from a comparison of Figures 5.43(d) and 5.44(d) that prestressing loads significantly alter the strut-and-tie model in the concrete beam and the loads transmit along a more direct load path. Furthermore, Figure 5.42 demonstrates that the partially prestressed concrete member has the highest performance. This suggests that the most economical design can be achieved by using partial prestressing. The strut-and-tie model of the partially prestressed concrete beam given by Schlaich *et al.* (1987) is depicted in Figure 5.44(e). In the model suggested by Schlaich *et al.*, however, the strut at the bottom of the beam is absent. It implies that the large prestressing load is transferred through the inclined strut only but not a more direct load path.

5.13.3 Fully prestressed concrete beam

Structural concrete members designed to remain uncracked at service loads are called fully prestressed. To satisfy this serviceability performance requirement, very large prestressing forces are applied to the concrete beam. The prestressing forces and the applied loads lead the entire prestressed concrete beam into a beam–column. The strut-and-tie model of a fully prestressed concrete beam has no tension chord at the bottom of the beam as demonstrated by Schlaich *et al.* (1987). By choosing the prestressing force of 2500 kN, the PBO technique was used to generate the strut-and-tie model in the prestressed concrete beam depicted in Figure 5.41. The maximum performance index obtained is 1.62, as presented in Figure 5.42. It can be observed from Figure 5.42 that the performance index increased after decreasing at a few iterations. This is because further element removal resulted in a more direct load path in the beam.

Figure 5.45 shows the strut-and-tie model optimization history. The optimal strut-and-tie model depicted in Figure 5.45(d) indicates that there is no tensile chord at the bottom of the beam because the full prestressing transformed the beam under applied loads into a beam–column. However, inclined tensile forces developed in the shear spans. Schlaich *et al.* (1987) developed a strut-and-tie model for this fully prestressed concrete beam as illustrated in Figure 5.45(e). They suggested that in a fully prestressed condition, the resultant of the prestressed force and the support force meet the line of action of the load F within the kern of the section. However, the optimal

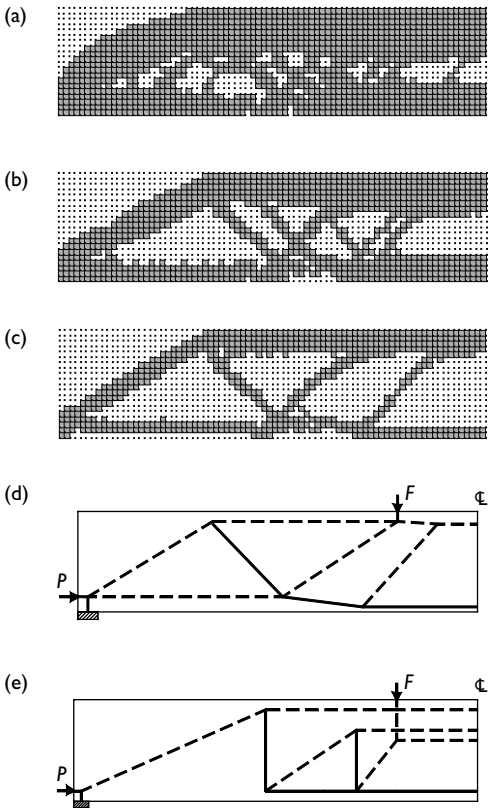

Figure 5.44 Optimization history of strut-and-tie model in partially prestressed concrete beam: (a) topology at iteration 20; (b) topology at iteration 40; (c) optimal topology; (d) optimal strut-and-tie model; (e) strut-and-tie model by Schlaich *et al.* (1987).

strut-and-tie model shown in Figure 5.45(d) indicates that a full prestressing condition may be fulfilled, without that the resultant meets the action line of the load *F*. In fact, a fully prestressed concrete beam is characterized by the absence of a tension chord along the bottom of the beam, as shown in Figure 5.45(d).

5.14 Worked design examples

As demonstrated in the preceding sections, the automated PBO technique is capable of generating optimal strut-and-tie models in any types of reinforced and prestressed concrete structures. The optimal strut-and-tie model produced by the PBO technique indicates the locations of struts, ties and

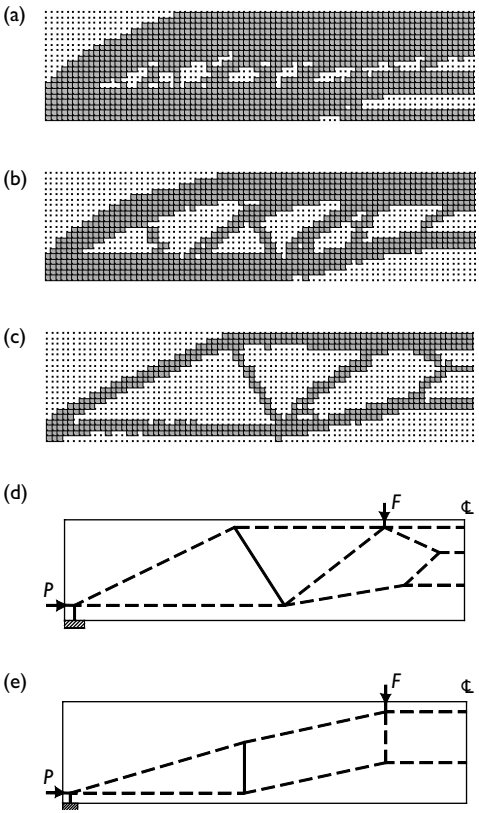

Figure 5.45 Optimization history of strut-and-tie model in fully prestressed concrete beam: (a) topology at iteration 20; (b) topology at iteration 40; (c) optimal topology; (d) optimal strut-and-tie model; (e) strut-and-tie model by Schlaich *et al.* (1987).

nodal zones in a structural concrete member so that the load-carrying capacity and the likely failure modes of the member can be predicted accurately. The optimal strut-and-tie model in a structural concrete member represents the load transfer mechanism of the cracked concrete member at its ultimate limit state. It appears that the design of a structural concrete member is mainly to strengthen the load transfer mechanism of the member. Three worked design examples are presented in this section. A shortened design and optimization procedure is proposed as follows.

1 Develop a strut-and-tie model for the concrete member using PBO.
2 Calculate axial forces in struts and ties.
3 Check the bearing capacity of loading points and supports.

4 Determine steel reinforcement for tension ties.
5 Check the capacity of struts and nodal zones.
6 Determine minimum steel reinforcement for crack control.
7 Detail the layout of steel reinforcement based on the strut-and-tie model.

5.14.1 Deep beam under two-point loads

Figure 5.46 provides the geometric and loading configurations of a simply supported deep beam that is to be designed and detailed. The factored point load is 2050 kN. The width of the deep beam is 350 mm.

(1) *Develop a strut-and-tie model using the PBO technique.* It is assumed that 32 MPa concrete is used. The Young's modulus $E_c = 28\,567$ MPa and Poisson's ratio $\nu = 0.15$ were specified for the concrete material in the FEA. The deep beam was modeled using 78×36 plane stress elements. The PBO technique based on the system performance criteria was applied with an element removal ratio of 2 percent in the optimization process. The optimal topology produced by PBO technique is presented in Figure 5.47(a). The discrete strut-and-tie model transformed from the optimal topology is depicted in Figure 5.47(b).

(2) *Calculate axial forces in struts and ties.* The angles of the inclined struts are calculated as

$$\tan \theta_{AD} = 3200/2400 = 1.333, \quad \theta_{AD} = 53.13^\circ$$

The reaction forces can be determined as

$$R_A = R_B = 2050\,\text{kN}$$

Due to symmetry, only half of the model needs to be considered. By considering vertical and horizontal equilibrium at nodes A and D, we can obtain the axial forces in struts and ties as

$$F_{AB} = 1538\ \text{kN}, \qquad F_{AD} = 2563\ \text{kN}, \qquad F_{DC} = 1538\ \text{kN}$$

(3) *Check the bearing capacity of loading points and supports.* It is assumed that the bearing plates of 400×350 mm are used in the loaded point and supports.

The bearing strength at loading point:

Since the nodal zone under the loading point is bounded by struts and bearing plate, β_n is equal to 1.0. The bearing strength at loading point is

$$F_{un} = \phi 0.85 f'_c \beta_n A_n = 0.75 \times 0.85 \times 32 \times 1.0 \times 400 \times 350/1000$$
$$= 2856\ \text{kN} > 2050\ \text{kN}$$

Therefore, the bearing capacity at loading point is adequate.

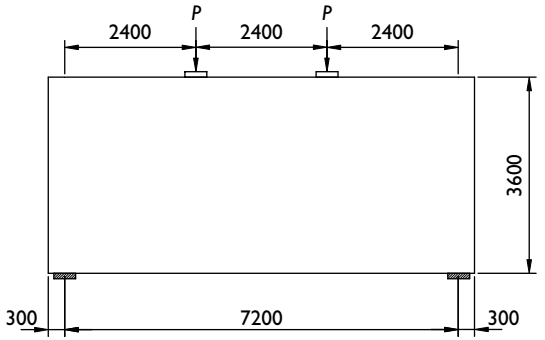

Figure 5.46 Simply supported deep beam under two-point loads.

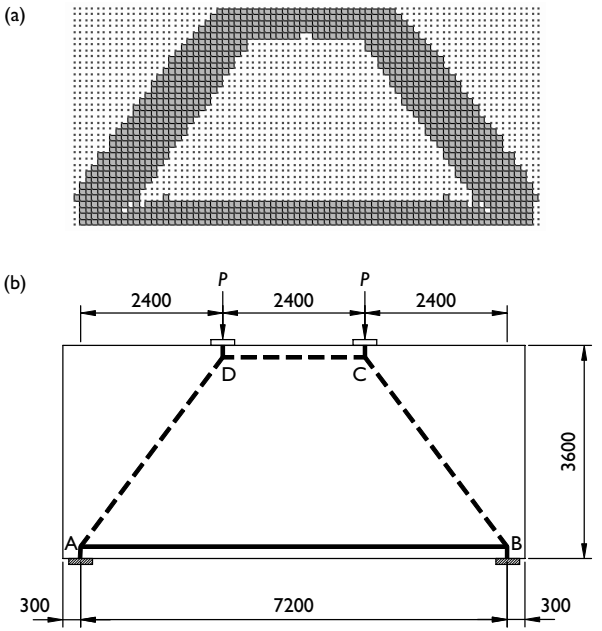

Figure 5.47 (a) Optimal topology and (b) strut-and-tie model in the deep beam under two-point loads.

The bearing strength at the supports:

The nodal zone A anchored one tie, β_n is taken as 0.8. The bearing strength at the supports is

$$F_{un} = \phi 0.85 f'_c \beta_n A_n = 0.75 \times 0.85 \times 32 \times 0.8 \times 400 \times 350/1000$$
$$= 2284.8 \text{ kN} > 2050 \text{ kN}$$

Therefore, the bearing strength at the supports is adequate.

(4) *Determine steel reinforcement for tension ties.* The cross-sectional area of steel reinforcement sustaining the tension force F_{AB} in tie AB when using Y400 steel is

$$A_{st} = F^*/\phi f_{yr} = 1538 \times 10^3/(0.75 \times 400) = 5127 \text{ mm}^2$$

Use 12Y24 bars ($A_{st} = 5400\,\text{mm}^2$) in four layers.

It is noted that the force in strut AD is equal to the force in tie AB. The topology shown in Figure 5.47(a) indicates that the depth of strut AD is approximately the same as that of the tie. The anchorage depth of the tie is taken as 400 mm.

(5) *Check the capacity of struts and nodal zones.* The depth of strut AD can be calculated as

$$d_{AD} = l_b \sin\theta + d_a \cos\theta = 400 \sin 53.13° + 400 \cos 53.13° = 560 \text{ mm}$$

The capacity of strut AD:

The factor β_s can be taken as 0.75, provided that sufficient web reinforcement is provided for crack control. The capacity of strut AD is

$$\phi F_{uc} = \phi 0.85\, \beta_s f'_c A_c = 0.75 \times 0.85 \times 0.75 \times 32 \times 560 \times 350/1000$$
$$= 2998.8 \text{ kN} > 2563 \text{ kN}$$

The capacity of strut DC:

Since strut DC is a prismatic strut in the compression zone, β_s can be taken as 1.0. The capacity of strut DC is:

$$\phi F_{uc} = \phi 0.85\, \beta_s f'_c A_c = 0.75 \times 0.85 \times 1.0 \times 32 \times 400 \times 350/1000$$
$$= 2856 \text{ kN} > 1538 \text{ kN}$$

The capacity of nodal zone A:

The nodal zone anchors one tie, β_s is equal to 0.8. The capacity of the nodal zone A can be determined as

$$\phi 0.85\, \beta_n f'_c A_n = 0.75 \times 0.85 \times 0.8 \times 32 \times 560 \times 350/1000$$
$$= 3198.7 \text{ kN} > 2563 \text{ kN}$$

The capacity of nodal zone D:

Since the nodal zone D is bounded by struts AD, DC and bearing area, β_s is equal to 1.0. The capacity of the nodal zone is

$$\phi 0.85 \beta_n f'_c A_n = 0.75 \times 0.85 \times 1.0 \times 32 \times 400 \times 350/1000$$
$$= 2856 \text{ kN} > 1538 \text{ kN}$$

(6) *Determine minimum steel reinforcement for crack control.* Horizontal web reinforcement:

Use Y12@300 on each face over the entire height of the deep beam,

$$A_{sh} = 110 \text{ mm}^2$$

Vertical web reinforcement:

Use Y12@250 on each face over the entire length of the deep beam,

$$A_{sv} = 110 \text{ mm}^2$$

The total web reinforcement ratio:

$$\sum \frac{A_{si}}{bs_i} \sin \theta_i = \frac{2 \times 110}{350 \times 300} \sin 53.13^\circ + \frac{2 \times 110}{350 \times 250} \sin 36.87^\circ$$
$$= 0.00318 > 0.003$$

The minimum web steel reinforcement for crack control is adequate.

(7) *Detail the layout of steel reinforcement.* The clear cover to the reinforcing bar is taken as 40 mm. The tensile development length for the deformed bar Y24 is 600 mm from table 13.1.2.2(a) of AS 3600 (1994). The anchorage space in this deep beam is not adequate. Anchor plates are thus used to anchor reinforcing bars in tension ties. The main steel reinforcement in the deep beam is depicted in Figure 5.48.

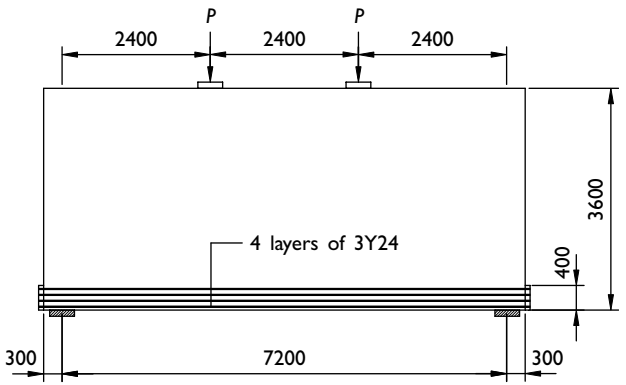

Figure 5.48 Layout of main steel reinforcement with anchor plates in the deep beam under two-point loads.

5.14.2 Deep beam under one-point load

A simply supported deep beam under one-point load is shown in Figure 5.49. The factored point load is 3000 kN. The width of the beam is 400 mm. It is required to design and detail the deep beam using the strut-and-tie model approach.

(1) *Develop a strut-and-tie model using the PBO technique.* The compressive strength of concrete is assumed to be 32 MPa. In the FEA, the Young's modulus $E_c = 28\,567$ MPa and Poisson's ratio $\nu = 0.15$ were specified for the concrete material. The deep beam was discretized into 66×30 four-node plane stress elements. The PBO technique based on the system performance criteria was applied with an element removal ratio of 2 percent in the optimization process. Figure 5.50(a) shows the optimal topology generated by the PBO technique. It can be observed from the figure that the member size of the model is proportional to the member force. The discrete strut-and-tie model transformed from the optimal topology is depicted in Figure 5.50(b).

(2) *Calculate axial forces in struts and ties.* The angles of struts AE, BE, CD and DE, and tie BD are calculated as

$$\begin{aligned}
\tan\theta_{AE} &= 2800/2000 = 1.4, & \theta_{AE} &= 54.46^\circ \\
\tan\theta_{BE} &= 2800/2100 = 1.333, & \theta_{BE} &= 53.13^\circ \\
\tan\theta_{CD} &= 1300/900 = 1.444, & \theta_{CD} &= 55.3^\circ \\
\tan\theta_{DE} &= 1500/3100 = 0.484, & \theta_{DE} &= 25.82^\circ \\
\tan\theta_{BD} &= 1300/1000 = 1.3, & \theta_{DE} &= 52.43^\circ
\end{aligned}$$

By considering the static equilibrium, the forces in struts and ties, and the reactions can be determined as follows:

$$R_A = 2000 \text{ kN}, \quad R_C = 1000 \text{ kN}$$
$$F_{AB} = 1428.7 \text{ kN}, \quad F_{AE} = 2457.9 \text{ kN}, \quad F_{BE} = 605.8 \text{ kN}$$

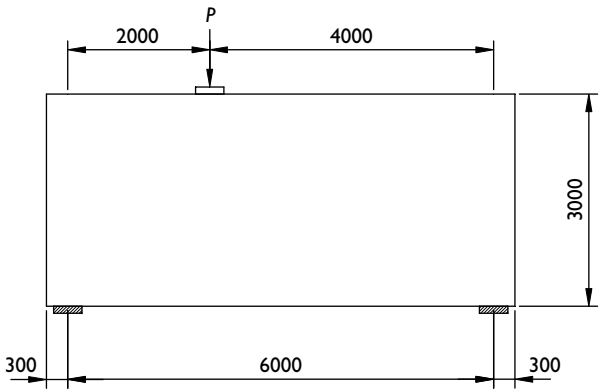

Figure 5.49 Deep beam under one-point load.

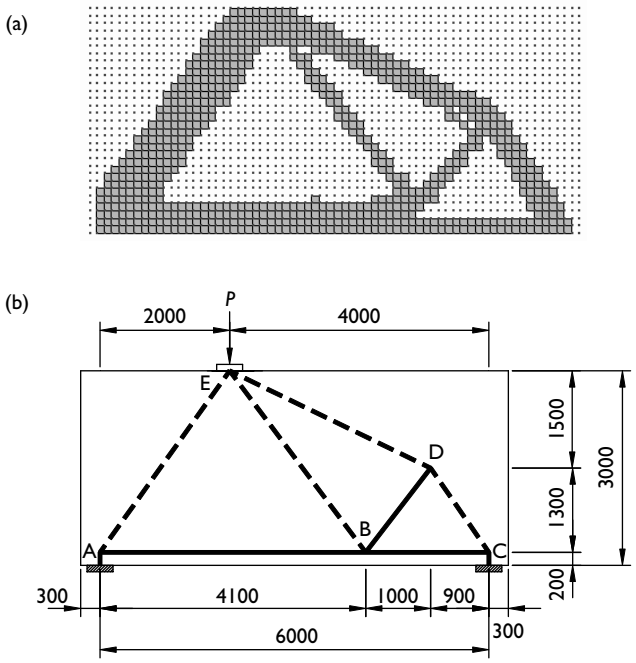

Figure 5.50 (a) Optimal topology and (b) strut-and-tie model under one-point load.

$F_{BC} = 692.4$ kN, $F_{BD} = 611.6$ kN, $F_{CD} = 1216.3$ kN,
$F_{CD} = 1216.3$ kN, $F_{DE} = 1183.3$ kN

(3) *Check the bearing capacity of loading points and supports.* It is assumed that the bearing plates of 400 × 400 mm are used in the loaded point and supports.

The bearing strength at loading point:

Since the nodal zone under the loading point is bounded by struts and bearing plate, β_n is taken as 1.0. The bearing strength at loading point is

$$F_{un} = \phi 0.85 f'_c \beta_n A_n = 0.75 \times 0.85 \times 32 \times 1.0 \times 400 \times 400/1000$$
$$= 3264\ kN > 3000\ \text{kN}$$

The bearing strength at loading point is adequate.

The bearing strength at the supports:

It is noted that the reaction at the support A is greater than that at the support C. It only needs to check the bearing strength at the support A.

Since the node A anchored one tie, β_n is equal to 0.8. The bearing strength at the supports is determined as

$$F_{un} = \phi 0.85 f'_c \beta_n A_n = 0.75 \times 0.85 \times 32 \times 0.8 \times 400 \times 400/1000 = 2611.2\ kN > 2000\ \text{kN}$$

Therefore, the bearing strength at the supports is adequate.

(4) *Determine steel reinforcement for tension ties.* Using Y400 steel, the cross-sectional area of steel reinforcement sustaining tensile force in tie AB is

$$A_{st} = F^*/\phi f_{yr} = 1425.7 \times 10^3/(0.75 \times 400) = 4762\ \text{mm}^2$$

Use 16Y20 bars ($A_{st} = 4960\ \text{mm}^2$) in four layers for tie AB.

The steel reinforcement for tie BC is

$$A_{st} = F^*/\phi f_{yr} = 692.4 \times 10^3/(0.75 \times 400) = 2380\ \text{mm}^2$$

Use 8Y20 bars ($A_{st} = 2480\ \text{mm}^2$) in two layers for tie BC.

The steel reinforcement for tie BD is

$$A_{st} = F^*/\phi f_{yr} = 611.5 \times 10^3/(0.75 \times 400) = 2038\ \text{mm}^2$$

Use 8Y20 bars ($A_{st} = 2480\ \text{mm}^2$) in two layers for tie BD. These reinforcing bars can be bent up from the reinforcement for tie AB.

(5) *Check the capacity of struts and nodal zones.* The anchored depths of the ties AB and BC are taken as 400 and 200 mm, respectively.

The depth of strut AE is determined as

$$d_{AE} = l_b \sin\theta + d_a \cos\theta = 400 \sin 54.46° + 400 \cos 54.46° = 558\,\text{mm}$$

Thus, take $d_{AE} = 558$ mm

The capacity of strut AE:

The factor β_s is taken as 0.75, provided that sufficient web reinforcement is provided for crack control. The capacity of the strut AE can be determined as

$$\phi F_{uc} = \phi 0.85 \beta_s f'_c A_c = 0.75 \times 0.85 \times 0.75 \times 32 \times 558 \times 400/1000 = 3415\ \text{kN} > 2457.9\ \text{kN}$$

The depth of strut CD:

$$d_{CD} = l_b \sin\theta + d_a \cos\theta = 400 \sin 55.3° + 200 \cos 55.3° = 442.7\,\text{mm}$$

Take d_{CD} = 440 mm

The capacity of strut CD:

Providing sufficient web reinforcement β_s can be taken as 0.75. The capacity of strut CD is calculated as

$$\phi F_{uc} = \phi 0.85\,\beta_s f'_c A_c = 0.75 \times 0.85 \times 0.75 \times 32 \times 440 \times 400/1000$$
$$= 2692.8\ \text{kN} > 1216.3\ \text{kN}$$

It can be seen from Figure 5.50(a) that the depth of strut CD is equal to that of strut DE.

The depth of strut BE can be taken approximately as 150 mm according to Figure 5.50(a).

The capacity of strut BE:

Strut BE is a prismatic strut, β_s can be taken as 1.0. The capacity of the strut is

$$\phi F_{uc} = \phi 0.85\,\beta_s f'_c A_c = 0.75 \times 0.85 \times 1.0 \times 32 \times 150 \times 400/1000$$
$$= 1224\ \text{kN} > 605.8\ \text{kN}$$

By considering the geometry of struts AE, BE and DE, the length of the top face of the nodal zone E can be determined as 849 mm. This length is greater than that of the bearing plate (400 mm) and less than that of the optimal topology shown in Figure 5.50(a).

The capacity of nodal zone A:

The nodal zone A anchors one tie, β_s is equal to 0.8. The capacity of the nodal zone can be calculated as

$$\phi 0.85\,\beta_n f'_c A_n = 0.75 \times 0.85 \times 0.8 \times 32 \times 558 \times 400/1000$$
$$= 3642.6\ \text{kN} > 2457.9\ \text{kN}$$

The capacity of nodal zone B:

The nodal zone B anchors three ties, β_s is taken as 0.6. This nodal zone is the critical one. The capacity of the nodal zone is

$$\phi 0.85\,\beta_n f'_c A_n = 0.75 \times 0.85 \times 0.6 \times 32 \times 150 \times 400/1000$$
$$= 734.4\ \text{kN} > 605.8\ \text{kN}$$

The capacity of nodal zones C and D:

Both nodal zones anchor one tie, the factor β_s can be taken as 0.8. The capacity of the nodal zones is

$$\phi 0.85\beta_n f'_c A_n = 0.75 \times 0.85 \times 0.83 \times 32 \times 440 \times 400/1000$$
$$= 2872.3\ \text{kN} > 1216.3\ \text{kN}$$

The capacity of nodal zone E:

The nodal zone E is bounded by three struts and bearing plate, β_s is equal to 1.0. The capacity of the nodal zone can be determined as

$$\phi 0.85\beta_n f'_c A_n = 0.75 \times 0.85 \times 1.0 \times 32 \times 558 \times 400/1000$$
$$= 4553.3\,\text{kN} > 2457.9\,\text{kN}$$

(6) *Determine minimum steel reinforcement for crack control.* Horizontal web reinforcement:

Use Y12@250 on each face over the entire height of the deep beam,

$$A_{sh} = 110\,\text{mm}^2$$

Vertical web reinforcement:

Use Y12@250 on each face over the entire length of the deep beam,

$$A_{sv} = 110\,\text{mm}^2$$

The total web reinforcement ratio:

$$\sum \frac{A_{si}}{bs_i} \sin\theta_i = \frac{2\times 110}{400\times 250}\sin 54.46^\circ + \frac{2\times 110}{400\times 250}\sin 35.54^\circ$$
$$= 0.00307 > 0.003$$

The minimum steel reinforcement for crack control is adequate.

(7) *Detail the layout of steel reinforcement.* From table 13.1.2.2(a) of AS 3600 (1994), the tensile development length for a Y20 bar is 500 mm. The clear cover to the reinforcing bars is taken as 40 mm. The anchorage lengths for straight Y24 bars are 597 mm at nodal zone A and 508 mm at nodal zone B according to ACI 318-02 (2002). Thus, the anchorage length is adequate. The layout of main steel reinforcement in the deep beam is provided in Figure 5.51.

5.14.3 Bridge pier

The bridge pier presented in Section 5.12.6 is to be designed and detailed using the strut-and-tie model approach.

(1) *Develop a strut-and-tie model using the PBO technique.* The detail strut-and-tie model is depicted in Figure 5.52.

(2) *Calculate axial forces in struts and ties.* The angles of struts AB, BC and CD are calculated as

$$\tan\theta_{AB} = 812.5/625 = 1.3, \qquad \theta_{AB} = 52.43^\circ$$

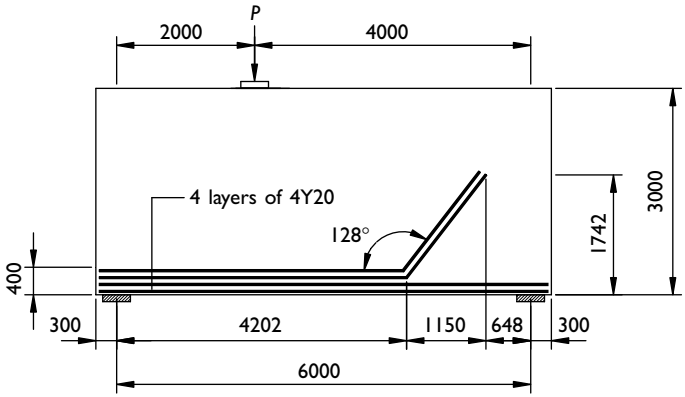

Figure 5.51 Layout of main steel reinforcement in the deep beam under one-point load.

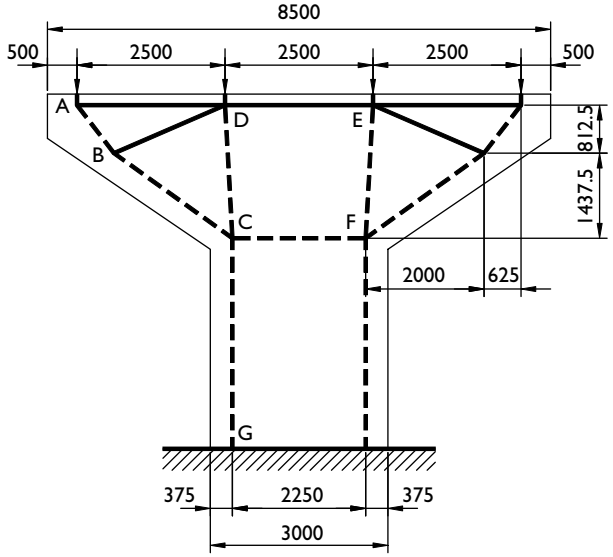

Figure 5.52 Strut-and-tie model in the bridge pier.

$$\tan\theta_{BC} = 1437.5/2000 = 0.718, \quad \theta_{BC} = 35.71^\circ$$
$$\tan\theta_{CD} = 2250/125 = 18.0, \quad \theta_{CD} = 86.82^\circ$$

The angle of tie BD is

$$\tan\theta_{BD} = 812.5/1875 = 0.433, \quad \theta_{BD} = 23.43^\circ$$

The forces in struts and ties are calculated on the basis of static:

$$F_{AD} = 2114 \text{ kN}, \quad F_{BD} = 1162 \text{ kN}, \quad F_{DE} = 3363 \text{ kN}$$
$$F_{AB} = 3470 \text{ kN}, \quad F_{BC} = 3919 \text{ kN}, \quad F_{CD} = 3219 \text{ kN}$$
$$F_{CF} = 3363 \text{ kN}, \quad F_{CG} = 5500 \text{ kN}$$

(3) *Check the bearing capacity of loading points.* The bearing plate of 350 × 800 mm is used at the loading point.

Since the nodal zone under the loading point anchors more than one tie, β_n is taken as 0.6. The bearing strength at loading point is calculated as

$$F_{un} = \phi\, 0.85\, f'_c \beta_n A_n = 0.75 \times 0.85 \times 32 \times 0.6 \times 350 \times 800/1000$$
$$= 3427 \text{ kN} > 2750 \text{ kN}$$

(4) *Determine steel reinforcement for tension ties.* Using Y400 steel, the steel reinforcement for tie DE is determined as

$$A_{st} = F^*/\phi f_{yr} = 3363 \times 10^3/(0.75 \times 400) = 11\,210 \text{ mm}^2$$

Use 19Y28 bars (A_{st} = 11 700 mm^2) in three layers for tie DE. The top layer of 6Y28 bars is placed with their centroid at a depth of 80 mm. The second layer of 6Y28 bars is placed at a depth of 170 mm. The third layer of 7Y28 bars is placed with their centroid at a depth of 295 mm.

The steel reinforcement for tie AD is

$$A_{st} = F^*/\phi f_{yr} = 2114 \times 10^3/(0.75 \times 400) = 7047 \text{ mm}^2$$

Use 12Y28 bars (A_{st} = 7440 mm^2) in two layers for tie AB.

The steel reinforcement for tie BD is

$$A_{st} = F^*/\phi f_{yr} = 1162 \times 10^3/(0.75 \times 400) = 3874 \text{ mm}^2$$

Use 7Y28 bars (A_{st} = 4340 mm^2) in tie BC. These bars are bent down from the third layer reinforcing bars in tie DE to resist tensile force in tie BD.

(5) *Check the capacity of struts and nodal zones.* According to the optimal topology shown in Figure 5.31(c), the anchored depth of tie AD can be taken as 250 mm. The depth of strut AB is

$$d_{AB} = l_b \sin\theta + d_a \cos\theta = 350 \sin 52.43° + 250 \cos 52.43° = 429 \text{ mm}$$

Take d_{AB} = 425 mm

The depths of struts connected at the nodal zone C can be proportioned to the forces that they sustain. Taking $d_{BC} = d_{AB} = 425$ mm for the compressive load path, the depths of these struts can be determined as

$$d_{CD} = 345 \text{ mm}, \quad d_{CF} = 365 \text{ mm}, \quad d_{CG} = 600 \text{ mm}$$

It can be seen that these dimensions are slightly smaller than those indicated in Figure 5.31(c).

The capacity of struts BC and AB:

Providing sufficient reinforcement for crack control β_s can be taken as 0.75. The capacity of struts BC and AB can be calculated as

$$\begin{aligned}\phi F_{uc} &= \phi 0.85\, \beta_s f'_c A_c = 0.75 \times 0.85 \times 0.75 \times 32 \times 425 \times 800/1000 \\ &= 5202 \text{ kN} > 3919 \text{ kN}\end{aligned}$$

The capacity of strut CD:

The factor β_s can be taken as 0.75, provided that sufficient reinforcement is provided to control cracking. The capacity of strut CD is determined as

$$\begin{aligned}\phi F_{uc} &= \phi 0.85\, \beta_s f'_c A_c = 0.75 \times 0.85 \times 0.75 \times 32 \times 345 \times 800/1000 \\ &= 4223 \text{ kN} > 3470 \text{ kN}\end{aligned}$$

The capacity of strut CF:

Strut CF is a prismatic strut in compression zone, β_s can be taken as 1.0. The capacity of the strut is

$$\begin{aligned}\phi F_{uc} &= \phi 0.85\, \beta_s f'_c A_c = 0.75 \times 0.85 \times 1.0 \times 32 \times 365 \times 800/1000 \\ &= 5957 \text{ kN} > 3363 \text{ kN}\end{aligned}$$

The capacity of strut CG:

Strut CG can be treated as a prismatic strut in compression zone, β_s is equal to 1.0. The capacity of strut CG can be calculated as

$$\begin{aligned}\phi F_{uc} &= \phi 0.85\, \beta_s f'_c A_c = 0.75 \times 0.85 \times 1.0 \times 32 \times 600 \times 800/1000 \\ &= 9792 \text{ kN} > 5500 \text{ kN}\end{aligned}$$

The capacity of nodal zones A and B:

Since the both nodal zones anchor one tie, β_n is taken as 0.8. The capacity of nodal zones can be determined as

$$\begin{aligned}\phi 0.85\, \beta_n f'_c A_n &= 0.75 \times 0.85 \times 0.8 \times 32 \times 425 \times 800/1000 \\ &= 6936 \text{ kN} > 3919 \text{ kN}\end{aligned}$$

The capacity of nodal zone C:

Since nodal zone C is bounded by four struts, β_n is equal to 1.0.

The capacity of strut CF is calculated as

$$\phi 0.85\,\beta_n f'_c A_n = 0.75 \times 0.85 \times 1.0 \times 32 \times 365 \times 800/1000 = 5957\,\text{kN} > 3363\,\text{kN}$$

The capacity of nodal zone D:

Since nodal zone D anchors three ties, β_n is taken as 0.6. The capacity of the nodal zone is

$$\phi\,0.85\,\beta_n\,f'_c\,A_n = 0.75 \times 0.85 \times 0.6 \times 32 \times 345 \times 800/1000 = 3378\,\text{kN} > 3219\,\text{kN}$$

(6) *Determine minimum steel reinforcement for crack control.*

Horizontal web reinforcement:

Use Y16@200 on each face over the entire height of the bridge pier,

$$A_{sh} = 200\ \text{mm}^2$$

Vertical web reinforcement:

Use Y16@200 on each face over the entire length of the bridge pier,

$$A_{sv} = 200\,\text{mm}^2$$

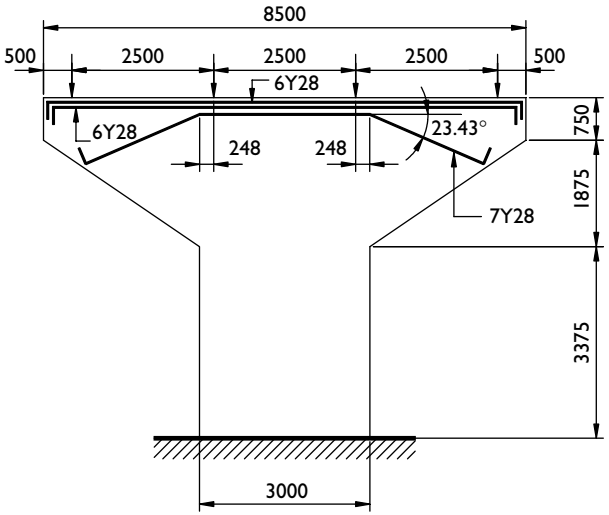

Figure 5.53 Layout of main steel reinforcement in the bridge pier.

The total web reinforcement ratio for strut BC:

$$\sum \frac{A_{si}}{bs_i} \sin\theta_i = \frac{2\times200}{800\times200}\sin 52.43^\circ + \frac{2\times200}{800\times200}\sin 35.57^\circ$$
$$= 0.0035 > 0.003$$

The web reinforcement provided is also adequate for struts BC and CD.

(7) *Detail the layout of steel reinforcement.* From table 13.1.2.2(a) in AS 3600, the tensile development length for a Y28 bar is $L_{sy.t} = 700$ mm. The clear cover to the bars is 65 mm. Since the anchorage space is not adequate for the Y28 bars, a cog is used to provide adequate anchorage length. The layout of main steel reinforcement is provided in Figure 5.53.

5.15 Conclusion

This chapter has presented the PBO techniques formulated on the basis of stiffness performance criteria for automatically generating optimal strut-and-tie models in reinforced and prestressed concrete structures. In the proposed methodology, the development of strut-and-tie models in structural concrete is transformed to an optimal topology design problem of continuum structures. The optimal topology of a concrete structure produced by the PBO technique is treated as the optimal strut-and-tie model for the design and detailing of the concrete structure. An integrated design optimization procedure has been proposed for optimizing and dimensioning structural concrete with strut-and-tie systems. The automated PBO techniques have been used to develop strut-and-tie models in reinforced concrete members and prestressed concrete beams. Optimal strut-and-tie models generated by the proposed design optimization procedure have been verified by existing analytical solutions and experimental observations.

Based on the work presented in this chapter, the following conclusions are drawn:

- The automated PBO technique is a rational, efficient and reliable design tool that can be used to generate optimal strut-and-tie models for the design and detailing of structural concrete, which includes reinforced and prestressed concrete structures, especially for complex concrete structures where no previous experience is available.
- The PBO technique is also a useful tool for concrete researchers in quantifying the shear transfer mechanism in structural concrete.
- It has been proved to be appropriate to develop strut-and-tie systems in structural concrete based on the linear elastic theory of cracked concrete for system performance criteria (overall stiffness) and to design the concrete structures based on the theory of plasticity for component performance criteria (strength).

- The load transfer mechanism in a structural concrete member adapts to its geometry, loading and support condition. Without modification, a strut-and-tie model developed for a specific member cannot be used for the design of other members.
- By treating prestressed forces as external loads, prestressed concrete beams can be analyzed, optimized and dimensioned with strut-and-tie systems like reinforced concrete.
- For a structural concrete member under multiple loading cases, multiple strut-and-tie models must be developed for the member for multiple load cases. The design must be checked for all load cases. Reinforcing steel must be provided to carry tensile forces in tension members under each load case.
- For very slender concrete beams, optimal topologies obtained by the PBO method are continuum-like structures in which strut-and-tie actions are difficult to be identified. For such cases, standard truss models with vertical ties or sectional methods can be used to design these concrete beams. The PBO technique is most appropriately used for developing strut-and-tie models in complex non-flexural concrete members, where standard truss models are not applicable.
- Optimal strut-and-tie models developed for concrete beams suggest that the angles of inclined struts with respect to the longitudinal axis of the tie should not be less than 45° to be efficient in transferring the loads.
- In developing strut-and-tie models for corbels, the support conditions of the corbels must be taken into account. Different support conditions lead to different strut-and-tie models and different steel reinforcement layouts in the corbels.
- Optimal strut-and-tie models generated by the PBO method indicate the location of struts, ties and nodes, but not necessarily the exact dimensions. Dimensioning the strut-and-tie model should be based on the strength performance criteria.
- Strut-and-tie modeling corresponds to the lower-bound limit analysis. It is of significant importance to ensure that the load transfer mechanism predicted by the PBO technique can be realized at its ultimate limit state. The adequate anchorage of steel reinforcement in tension ties must be provided together with minimum web reinforcement in both longitudinal and transverse directions.
- PBO concepts are consistent with the performance-based design concepts being adopted in current building codes of practice in many countries.
- The automated PBO technique overcomes the limitations of traditional trial-and-error methods for developing strut-and-tie models in structural concrete. The use of the advanced PBO technology in the design of structural concrete will result in not only significant reductions in the design time and costs but also high performance concrete structures. Thus, the PBO technology is appropriate to be adopted in concrete model codes to achieve economical designs of structural concrete.

5.16 References

ACI 318-02 (2002) *Building Code Requirements for Structural Concrete*, Farmington Hills, MI, USA: American Concrete Institute.

Ali, M. A. and White, R. N. (2001) "Automatic generation of truss model for optimal design of reinforced concrete structures," *ACI Structural Journal*, 98(4): 431–442.

Alshegeir, A. and Ramirez, J. (1992) "Computer graphics in detailing strut-tie models," *Journal of Computing in Civil Engineering*, ASCE, 6(2): 220–232.

AS 3600 (1994) *Concrete Structures*, Sydney: Standards Australia.

ASCE-ACI Committee 445 on Shear and Torsion (1998) "Recent approaches to shear design of structural concrete," *Journal of Structural Engineering*, ASCE, 124(12): 1375–1417.

Benjamin, J. R. and Williams, H. A. (1957) "The behavior of one-story reinforced concrete shear walls," *Journal of Structural Division*, ASCE, 83(ST3): 1254(1–49).

Biondini, F., Bontempi, F. and Malerba, P. G. (1998) "Optimization of strut-and-tie models in reinforced concrete structures," Paper presented at the Australasian Conference on Structural Optimization, Sydney, Australia, pp.115–122.

CEB (1987) *CEB-FIP Model Code for Concrete Structures*, Comité Euro-International du Béton (CEB).

Cohn, M. Z. and Dinovitzer, A. S. (1994) "Application of structural optimization," *Journal of Structural Engineering*, ASCE, 120(2): 617–650.

Collins, M. P. and Mitchell, D. (1980) "Shear and torsion design of prestressed and non-prestressed concrete beams," *PCI Journal*, 25(5): 32–100.

Foster, S. J. and Gilbert, R. I. (1996) "The design of nonflexural members with normal and high-strength concrete," *ACI Structural Journal*, 93(1): 3–10.

Gilbert, R. I. and Micklborough, N. C. (1990) *Design of Prestressed Concrete*, London: Unwin Hyman.

IABSE (1979) *IABSE Colloquium on Plasticity in Reinforced Concrete*, Copenhagen, Final Report, IABSE V. 29, International Association for Bridge and Structural Engineering (IABSE).

Kirsch, U. (1993) *Structural Optimization: Fundamentals and Applications*, Berlin: Springer-Verlag.

Kong, F. K. and Sharp, G. R. (1973) "Shear strength of lightweight reinforced concrete deep beams with web openings," *The Structural Engineer*, 51(8): 267–275.

Kong, F. K. and Sharp, G. R. (1977) "Structural idealization for deep beams with web openings," *Magazine of Concrete Research*, 29(99): 81–91.

Kumar, P. (1978) "Optimal force transmission in reinforced concrete deep beams," *Computers and Structures*, 8(2): 223–229.

Kupfer, H. (1964) "Generalization of Mörsch's truss analogy using principle of minimum strain energy," *CEB Bulletin d'information*, No. 40, Comite Ero-International du Beton, No. 40, 44–57.

Lampert, P. and Thürlimann, B. (1971) "Ultimate strength and design of reinforced concrete beams in torsion and bending," *Publication* No. 31-I, Zurich: IABSE, pp. 107–131.

Leonhardt, F. (1965) "Reducing the shear reinforcement in reinforced concrete beams and slabs," *Magazine of Concrete Research*, 17(53): 187.

Liang, Q. Q. (2001a) *Performance-Based Optimization Method for Structural Topology and Shape Design*, Ph.D. thesis, Victoria University of Technology, Australia.

Liang, Q. Q. (2001b) "Performance-based optimization method in civil and structural engineering," paper presented at the Australasian Structural Engineering Conference, Gold Coast, Australia, pp. 37–44.

Liang, Q. Q., Uy, B. and Steven, G. P. (2002) "Performance-based optimization for strut–tie modeling of structural concrete," *Journal of Structural Engineering*, ASCE, 128(6): 815–823.

Liang, Q. Q., Xie, Y. M. and Steven, G. P. (1999a) "Optimal strut-and-tie models in structural concrete members," in Topping, B. H. V. and Kumar, B. (eds) *Optimization and Control in Civil and Structural Engineering, Proceedings of the Seventh International Conference on Civil and Structural Engineering Computing*, Oxford, England: Civil-Comp Press, pp. 1–8.

Liang, Q. Q., Xie, Y. M. and Steven, G. P. (2000) "Topology optimization of strut-and-tie models in reinforced concrete structures using an evolutionary procedure," *ACI Structural Journal*, 97(2): 322–330.

Liang, Q. Q., Xie, Y. M. and Steven, G. P. (2001) "Generating optimal strut-and-tie models in prestressed concrete beams by performance-based optimization," *ACI Structural Journal*, 98(2): 226–232.

Liang, Q. Q., Xie, Y. M., Steven, G. P. and Schmidt, L. C. (1999b) "Topology optimization of strut-and-tie models in non-flexural reinforced concrete members," paper presented at the International Conference on Mechanics of Structures, Materials and Systems, Wollongong, Australia, February, pp. 309–315.

Marti, P. (1985) "Basic tools of reinforced concrete beam design," *ACI Structural Journal*, 82(1): 46–56.

Marti, P. (1999) "A simple, consistent approach to structural concrete," *The Structural Engineer*, 77(9): 20–26.

Mish, K. D. (1994) "Strut-and-tie modeling of reinforced concrete: a case study in interactive visualization," paper presented at the National Science Foundation Workshop on Visualization Applications in Earthquake Engineering, Chico, California.

Mörsch, E. (1920, 1922) *Der Eisenbetonbau-Seine Theorie und Anwendung (Reinforced concrete Construction – Theory and Application)*, 5th edn, Stuttgart: Wittwer, 1(Part 1), 2(Part 2).

Nielsen, M. P. (1984) *Limit Analysis and Concrete Plasticity*, Englewood Cliffs, NJ: Prentice-Hall.

Ramirez, J. A. (1994) "Strut-and-tie design of pretensioned concrete members," *ACI Structural Journal*, 91(4): 572–578.

Ramirez, J. A. and Breen, J. E. (1991) "Evaluation of a modified truss-model approach for beams in shear," *ACI Structural Journal*, 88(5): 562–571.

Ramm, E. and Maute, K. (1994) "Topology optimization – a general tool in structural design," in Mang, H., Bicanic, N. and de Borst, R. (eds) *Computational Modelling of Concrete Structures*, Swansea: Pineridge Press, pp. 805–824.

Ramm, E., Beltzinger, K.-U. and Maute, K. (1997) "Structural optimization," in Abel, J., Astudillo, R. and Sricastava, N. K. (eds) *Current and Emerging Technologies of Shell and Spatial Structures, Proceedings of the IASS Colloquium*, Madrid, pp. 201–216.

Ritter, W. (1899) "Die bauweise henebique," *Schweizerische Bauzeitung*, 33(7), Zürich, 59–61.

Sanders, D. H. and Breen, J. E. (1997) "Post-tensioned anchorage zone with single straight concentric anchorages," *ACI Structural Journal*, 94(2): 146–158.

Schlaich, J. and Schäfer, K. (1991) "Design and detailing of structural concrete using strut-and-tie models," *The Structural Engineer*, 69(6): 113–125.

Schlaich, J., Schäfer, K. and Jennewein, M. (1987) "Toward a consistent design of structural concrete," *PCI Journal*, 32(3): 74–150.

Thürlimann, B., Marti, P., Pralong, J., Ritz, P. and Zimmerli, B. (1983) "Vorlesung zum Fortbildungskurs für Bauingenieure," Institut für Baustatik und Konstruktion ETH Zürich.

Yun, Y. M. (2000) "Nonlinear strut-and-tie model approach for structural concrete," *ACI Structural Journal*, 97(4): 581–590.

Chapter 6

Optimization of lateral load resisting systems

6.1 Introduction

Multistory buildings are designed not only for gravity loads but also for lateral loads. In the performance-based design of a multistory building, four major performance requirements such as strength, stiffness, stability and cost must be considered. In the design for vertical loads, the floor system in a building must be strong enough to transfer the loads to the columns or walls and stiff enough not to deflect excessively. Moreover, the floor system must be designed to have sufficient strength and stiffness to brace all columns and walls so that they will not buckle under the design loads. In the design for lateral loads, the structural system must be adequate stiff to resist wind and seismic forces. The strength performance requirement is the dominant factor in the design of low-rise buildings. The effects of lateral loads on buildings increase rapidly with increases in the height of the buildings. The stiffness and stability performance requirements are often dominant criteria in the design of tall buildings. There are two methods to satisfy the stiffness and stability performance criteria. The first is to increase the sizes of the members. However, increasing the sizes of structural members results in either impractical or uneconomical designs of tall buildings. The second is to select a more rigid and stable lateral load resisting system to reduce the deflections and to increase the stability. The first step in the structural design process of a tall building is to select a lateral load resisting system for wind and seismic forces. The selected lateral load resisting system is then sized. The final step is to ensure that the lateral resisting system is adequate for the stability bracing of the building.

The design of tall steel and steel–concrete composite buildings under lateral loads is usually governed by system performance criteria (overall stiffness) rather than by component performance criteria (strength). An important task in the design of a tall building for the structural designer is to select a cost-efficient lateral system for resisting wind and seismic forces. Pure rigid frame systems alone are not efficient in resisting lateral loads for tall buildings since the shear-racking component of deflections induced by

the bending of columns and girders will cause the building drift too large (Taranath 1988). Braced frameworks can significantly improve the performance of pure rigid frame actions by eliminating the bending effects of columns and girders. This can be achieved by using truss members such as diagonals to brace the frames so that those diagonals absorb the shear. The braced frame is an efficient lateral load resistance system as all members are subjected to axial forces only. In the absence of an efficient optimization technique, the selection of lateral load resisting systems for multistory frames is usually undertaken by the designer based on the trial-and-error process and past experience. Traditional design methods for lateral resisting systems in a tall building are highly iterative and time-consuming. The optimal design of lateral load resisting systems is a challenging task for structural designers as it involves a large number of possibilities for the arrangement of bracing members. Figure 6.1 shows the possible layouts of bracing systems for a six-story steel building frame.

Stiffness-based sizing techniques for the minimum-weight design of lateral load resisting systems in multistory buildings have been developed. Baker (1990) presented a sizing technique based on energy methods for lateral load resisting systems in multistory steel buildings. The technique

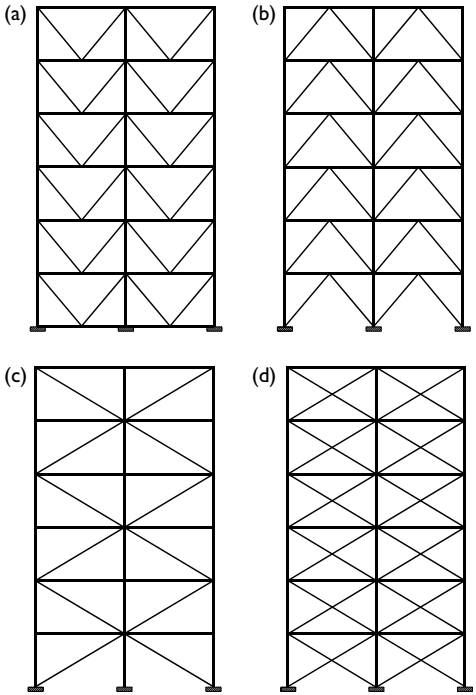

Figure 6.1 Possible layout of bracing systems for multistory frames.

can be applied to the sizing of both axial and flexural members of lateral systems. The discretized optimality criteria (OC) method proposed by Zhou and Rozvany (1992) is shown to be efficient in sizing large structural systems subject to stress and displacement constraints under multiple loading conditions. Grierson and Chan (1993) and Chan *et al*. (1995) developed an automatic resizing technique for the optimal design of tall steel building frames under lateral loads. The OC method is employed to solve the minimum-weight design problem of a tall steel building frame subject to constraints on overall and interstory drifts. In these approaches mentioned above, all members of a lateral load resisting system are resized on the basis of uniform strain energy density (SED) criteria. Kim *et al*. (1998) presented a method for the design of tall steel buildings where steel frameworks are designed for strength criteria, and only bracing members are resized for stiffness performance criteria. They suggested that it is most efficient to increase the lateral stiffness of lower stories in a tall building to improve the performance of lateral load resisting systems. However, all of these sizing techniques can apply only to lateral resisting systems with fixed topologies. The efficiency of a resized structural system in resisting lateral loads is limited by the chosen topology of bracing systems.

The homogenization-based optimization method has been used by Díaz and Kikuchi (1992) to find optimal reinforcement layouts, which modify the natural frequency of a plane stress continuum structure. Walther and Mattheck (1993) used the soft kill option method to generate efficient frameworks for supporting floor systems in construction engineering. The layout design of bracing systems for multistory steel building frames under lateral loads has been presented by Mijar *et al*. (1998) using a topology optimization method based on the classical Voigt–Resuss mixing rules. In this method, the objective is to minimize the compliance of a steel frame braced by a continuum design domain under the given loading and boundary condition. The constraint is imposed on an amount of solid material used for the bracing system. Obviously, the bracing system produced by this method depends largely on the material volume constraint, which is arbitrarily specified by the designer.

In this chapter, the performance-based optimization (PBO) method formulated on the basis of system performance criteria is extended to the optimal design of lateral load resisting systems for multistory building frames under multiple lateral loading conditions. Various lateral load resisting systems are introduced. In the PBO method described in preceding chapters, either plane stress elements or plate elements are used to model a structure for optimization. However, in dealing with practical design problems, different types of elements have to be used to model a structure. The capacity of the PBO method is extended to include both beam and plane stress elements in one model. In the proposed design optimization procedure, unbraced frames are first designed for component performance criteria by selecting

standard sections from databases. The optimal topology of a bracing system is generated by gradually removing underutilized plane stress elements from a continuum design domain that braces the frame. Sizing optimization of lateral resisting systems for tall building frames are also described. Design examples are provided to demonstrate the effectiveness and validity of the PBO technique for achieving efficient and economical designs of lateral load resisting systems for multistory frames. Some of the results have been reported by Liang *et al.* (2000a).

6.2 Lateral load resisting systems

The design of tall buildings is usually governed by the lateral loads such as wind and seismic forces. The most important design task for tall buildings is to identify a proper structural system to resist lateral loads. The lateral load resisting system must be not only economical but also satisfy the design criteria of other disciplines. The selection of lateral systems for tall buildings is one of the most challenging and rewarding tasks in structural design. There are innumerable structural systems that can be used for resisting lateral loads. The following lateral load resisting systems are commonly used in the design of tall steel and composite steel–concrete buildings:

- Rigid frames
- Semirigid frames
- Braced frames
- Framed tubes
- Exterior braced tubes
- Shearwalls.

These lateral load resisting systems for tall buildings are introduced in this section. The emphasis is on the strength design methods of steel–concrete composite elements resulting from the most recent research work of the author and his co-researchers.

6.2.1 Rigid frames

Portal frames consisting of beams and columns have been extensively used as lateral load resisting systems in tall buildings. This system has the advantage of the minimum obstruction to architectural layouts. A rigid frame is defined as the framing system with rigid connections that are sufficiently stiff to hold the angles between members unchanged under the design loads. Rigid frames resist lateral loads primarily through the bending of beams and columns. The lateral deflections of a rigid frame are induced by the cantilever bending and shear-racking components. The wind load acting on

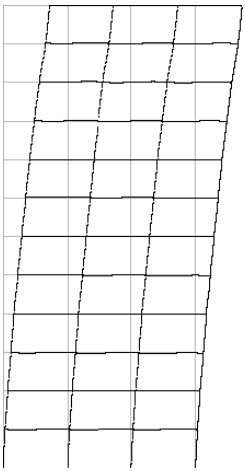

Figure 6.2 Response of a 12-story rigid frame to lateral loads.

the vertical face of a building induces an overall bending moment on any horizontal cross-sections of the building. The maximum moment at the base of the building caused by the wind load is known as the overturning moment. The frame under the overturning moment behaves as a vertical cantilever characterized by the axial deformation of the columns, which results in the chord drift component of the lateral deflection. This phenomenon contributes to about 20 percent of the total drift of the building (Taranath 1988). The shear-racking component is similar to the shear deflection in a beam. The lateral load causes horizontal and vertical shear forces on columns and beams, and in turn induces bending moments in members. The entire frame is distorted by the bending of the columns and beams. This deformation accounts for about 80 percent of the total deflection of the building. Figure 6.2 shows the responses of a 12-story rigid steel frame to lateral loads.

6.2.2 Semirigid frames

Heavy connection elements are usually used in rigid frames to achieve the desired fixity. The advantage of reduced beam-bending requirements may be offset by the gravity moment induced in the external columns. As a result, rigid frames may not be the optimal lateral load resisting systems for building of less than 30 stories. Semirigid frames with semirigid connections have been found to be economical for the design of buildings of less than 30 stories. The behavior of semirigid connections is intermediate between

fully rigid and simple connections. Semirigid connections provide substantial restraint to the end moment and sufficient reduction in the midspan moment of a beam under gravity loads. However, they are not rigid enough to suppress the formation of all rotations at the beam end. Semirigid frames are sometimes called partially restrained frames. The behavior of semirigid connections is complex. The design of semirigid connections is usually based on experimental data.

6.2.3 Braced frames

Pure rigid frames are not efficient in resisting lateral loads for buildings with more than 30 stories. This is because the shear racking component of deflection induced by the bending of beams and columns causes the building drift to be too large. To reduce the building drift, the bending factors of beams and columns must be eliminated. This can be achieved by adding truss members such as diagonals between the floor systems. Braced frames resist lateral loads primarily through axial actions in members. This lateral load resisting mechanism generally offers excellent lateral stiffness characteristics. Braced frames are generally more economical than pure rigid frames.

There are many types of braces that can be used for the design of tall buildings. Any pattern of bracing systems can be designed, provided that the shear is resisted at every story and the stiffness performance is maintained within the acceptable limit. The most comment types are the concentric K or X brace between columns and eccentric bracing. Figure 6.1 shows some of the possible bracing systems for a building frame. In a concentrically braced frame, the centerlines of the various members that frame into a joint meet at a single point. The ductility of concentric bracing systems is limited because they rely on the inelastic buckling of the bracing members to resist large overloads. Eccentrically braced frames combine the excellent ductility of moment-resisting frames with the high stiffness of concentrically braced frames. An eccentrically braced frame consists of bracing members that are deliberately offset from the centerline of the beam–column connections. The short portion of the beam between the brace and the column is called the link beam. The link beam is designed to act as ductile fuses that can dissipate large amounts of energy during earthquakes. Bracing elements can be either steel members or smaller-diameter concrete-filled steel tubes. The in-filled concrete improves the local buckling resistance of the steel tube walls.

6.2.4 Framed tubes

A framed tubular system is constructed using closely spaced columns and deep spandrel beams placed around the entire perimeter of a high-rise

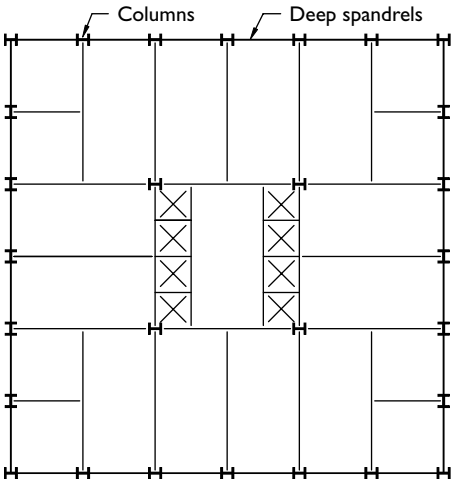

Figure 6.3 Schematic floor plan of a framed tube building.

building. The entire lateral loads are resisted by the perimeter frame, which acts as a hollow cantilever tube. In practice, the tubular behavior is achieved by placing columns 1.5–4.5 m apart and spandrel beams with depths varying from 0.9 to 1.5 m. The tubular system can be constructed using reinforced concrete, structural steel or composite steel–concrete structures. Figure 6.3 depicts the typical floor plan of a tall building with a framed tubular system.

Framed tubes are efficient lateral load resisting systems for tall buildings. In most cases, the amount of structural material used in tubular systems is only half of that used in conventionally framed buildings. Some of the world's tallest buildings are framed tubes, such as the 110-story Sears Tower, the 100-story John Hancock Building in Chicago and the formerly 110-story World Trade Center towers in New York. The World Trade Center towers were collapsed due to the event of September 11, 2001. It would appear from the collapse mode of the World Trade Center towers that the buildings could have performed better if the tubular systems were braced using diagonals. Nevertheless, the concept of the tubular system for resisting lateral loads has lead to a revolution in the design of tall buildings. This concept has been employed in the design of many high-rise buildings in excess of 50 stories.

6.2.5 Exterior braced tubes

In reality, the response of a framed tubular system to lateral loads combines the overall action of the cantilever bending due to the elongation of windward

columns and shortening of leeward columns and the shear deformation due to the local bending of columns and spandrel beams. The shear lag effect associated with this system significantly reduces the structural performance of framed tubes. The efficiency of a tubular system can be improved by eliminating the shear lag effect. This can be achieved by strengthening the perimeter frame with diagonals. The resulting system is an efficient exterior braced tube, which exhibits a nearly pure cantilever behavior when subjected to lateral loads. In an exterior braced tube, the perimeter columns can be spaced apart but are braced by the widely spaced diagonals to act as a tube. Figure 6.4 shows a 50-story exterior braced tube office building, where the X brace is used to brace 10 stories on each of the four sides. The diagonals in braced tubes sustain the lateral loads through primarily axial actions. The diagonals are multifunctional elements, which resist most of the shear forces induced by lateral loads, carry some of the gravity loads, and stiffen the framed tubular system. The braced tube works as a wall-like system with high stiffness to resist lateral loads.

The exterior braced tube system has been used in the 100-story John Hancock Tower in Chicago. The project indicates that significant savings in steel can be achieved by using the exterior braced tubes as lateral load resisting systems for tall buildings compared with other structural systems. Another notable example of the braced tube system is the Bank of China Tower in Hong Kong. The Bank of China Tower is a steel–concrete composite structure with exterior braced space truss. It should be noted that the patterns of bracing systems in tall buildings built in the past might not be

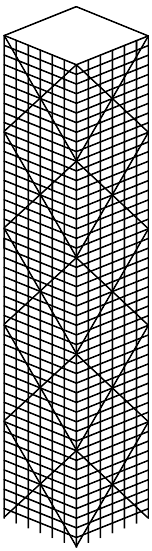

Figure 6.4 A 50-story building with exterior braced tube systems.

the optimal ones since no topology optimization techniques have been employed in the design. It is believed that the optimization of lateral load resisting systems for tall buildings will result in not only significant savings in materials but also high performance structural systems for resisting lateral loads.

6.2.6 *Shearwalls*

Shearwalls enclosing building services have been used as lateral load resisting systems for high-rise steel and composite steel–concrete buildings. They are usually designed as C or I shapes interconnected with coupling beams. In composite construction, the coupling beam is made of structural steel. Erection steel columns are usually used in the intersections of the shearwall. The entire lateral loads are resisted by the core shearwall. If the shearwall cores are not sufficiently large to resist the total lateral loads, other moment-resisting frames are designed to interact with the shearwall and to supplement the lateral stiffness of the shearwall. Figure 6.5 shows a typical floor plan of a composite building with shearwall–frame interaction systems.

The most common composite shearwall consists of a reinforced concrete shearwall with structural steel columns and beams as boundary elements. Stud shear connectors are usually welded to the structural steel elements to transfer shear between the concrete and structural steel. Another form of composite shearwalls is the double skin composite panel, which is constructed by placing concrete between two steel plates welded with headed

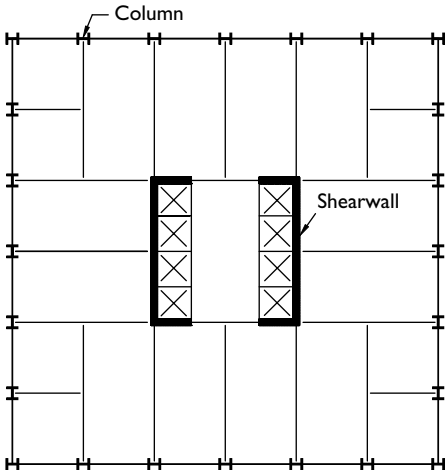

Figure 6.5 Typical floor plan of a composite building with shearwall–frame interaction system.

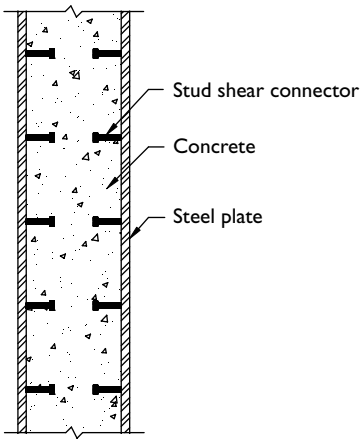

Figure 6.6 Cross-section of double skin composite shearwall.

stud shear connectors at a regular spacing (Liang *et al.* 2003, 2004a). A typical cross-section of a double skin composite shearwall is depicted in Figure 6.6. In this composite system, steel plates act as permanent formwork and biaxial steel reinforcement for the concrete core. The need for plywood formwork and the detailing of steel reinforcing bars are eliminated. This significantly reduces the construction time and cost. Double skin composite shearwalls generally provide very high strength, stiffness and ductility characteristics and are efficient lateral load resisting systems for high-rise buildings.

One of the failure modes associated with double skin composite shearwalls is the local buckling of steel plates between stud shear connectors when subjected to biaxial compression and shear. Liang *et al.* (2003, 2004a) has proposed design models for the buckling interaction and strength interaction of steel plates in double skin composite shearwall in biaxial compression and shear. The limiting width-to-thickness ratios for steel plates in biaxial compression in double skin composite shearwalls based on the von Mises yield criterion are determined by (Liang *et al.* 2003)

$$\frac{b}{t}\sqrt{\frac{\sigma_o}{250}} = 26.89\left(k_x^2 - \frac{k_x k_y}{\varphi^2} + \frac{k_y^2}{\varphi^4}\right)^{1/4} \tag{6.1}$$

where b is the width of the steel plate between stud shear connectors; t, the thickness of the plate; σ_o, the proof or yield stress of the steel plate; k_x, the critical buckling coefficient in the x direction; k_y, the critical buckling coefficient in the y direction and φ, the aspect ratio of the plate ($\varphi = a/b$). It should be noted that the Young's modulus $E = 200$ GPa, Poisson's ratio

Table 6.1 Parameters of strength interaction formulas for square plates in biaxial compression

b/t	α_c	η	γ
100	2.0	1.4	0.14
80	2.0	1.47	0.211
60	2.0	1.45	0.353
40	2.0	0.8	0.65
20	2.0	0.0	0.846

Source: Adapted from Liang *et al.* (2003).

$\nu = 0.3$ have been used in the derivation of Eq. (6.1). The critical buckling coefficients for plates with various aspect ratios and compressive stresses are given in the work of Liang *et al.* (2003). For square steel plates subjected to equal biaxial compression, the local buckling coefficient k_x and k_y are 2.404.

The design formula given by Liang *et al.* (2003) for the ultimate strength interaction of steel plates in biaxial compression is expressed by

$$\left(\frac{\sigma_{xu}}{\sigma_o}\right)^{\alpha_c} + \eta\left(\frac{\sigma_{xu}\sigma_{yu}}{\sigma_o^2}\right) + \left(\frac{\sigma_{yu}}{\sigma_o}\right)^2 = \gamma \quad (\gamma \leq 1) \tag{6.2}$$

where σ_{xu} and σ_{yu} are the ultimate strengths of the steel plate in biaxial compression in the x and y directions, respectively; α_c, the strength shape factor of the interaction curve; η, a function of the plate slenderness and γ, the uniaxial strength factor. The parameters of strength interaction equation for square steel plates are provided in Table 6.1.

Steel plates in double skin composite shearwalls under lateral loads may be subjected to the combined actions of biaxial compression and in-plane shear. The design formulas for critical buckling interactions of square steel plates in combined biaxial compression and shear are given as follows (Liang *et al.* 2004a)

$$\left(\frac{k_x}{k_{xo}}\right)^{\alpha_b} + \left(\frac{k_{xy}}{k_{xyo}}\right)^2 = 1 \tag{6.3}$$

where k_{xo} is the buckling coefficient in the x direction in the absence of shear stresses; k_{xyo}, the shear buckling coefficient of the plate under pure shear only and α_b, the buckling shape factor that defines the shape of a buckling interaction curve. The buckling coefficients and shape factor for steel plates with different boundary conditions are provided in Table 6.2 for design. The limiting width-to-thickness ratio for plates in combined biaxial

Table 6.2 Parameters of buckling interaction formulas for plates in biaxial compression and shear

Boundary condition	k_{xo}					k_{xyo}	α_b
	$\alpha = 1.5$	$\alpha = 1.0$	$\alpha = 0.5$	$\alpha = 0.25$	$\alpha = 0$		
C − C − S − S + SC	3.362	4.216	5.514	6.56	7.797	18.596	2
C − S − S − S + SC	2.589	3.168	4.06	4.705	5.552	14.249	1.7
S − S − S − S + SC	1.923	2.404	3.204	3.84	4.782	10.838	1.1

Source: Adapted from Liang *et al.* (2004a).

Table 6.3 Parameters of strength interaction formulas for plates in biaxial compression and shear

b/t	α_s	σ_{xuo}/σ_o	τ_{xyuo}/τ_o
100	0.8	0.205	0.875
80	1.1	0.248	0.984
60	1.3	0.321	1.0
40	1.6	0.481	1.0
20	2.0	0.658	0.927

Source: Adapted from Liang *et al.* (2004).

compression and shear can be determined as (Liang *et al.* 2004a)

$$\frac{b}{t}\sqrt{\frac{\sigma_o}{250}} = 26.89\left(k_x^2 - \frac{k_x k_y}{\varphi^2} + \frac{k_y^2}{\varphi^4} + 3k_{xy}^2\right)^{1/4} \tag{6.4}$$

The ultimate strength interaction formula for steel plates under combined biaxial compression and shear is expressed by (Liang *et al.* 2004a)

$$\left(\frac{\sigma_{xu}}{\sigma_{xuo}}\right)^{\alpha_s} + \left(\frac{\tau_{xyu}}{\tau_{xyuo}}\right)^2 = 1 \tag{6.5}$$

where σ_{xuo} is the ultimate strength of the plate in the x direction under biaxial compression only; τ_{xyu}, the ultimate shear strength of the plate and τ_{xyuo}, the ultimate strength of the plate under pure shear; α_s, the strength shape factor of interaction curves for plates under combined biaxial compression and shear. The ultimate strength of square steel plates under either biaxial compression or shear and the strength shape factor are given in Table 6.3.

6.3 Steel–concrete composite systems

The most important characteristics of structural steel are high strength, high modulus of elasticity and high ductility. The main advantages of steel

structures are the speed of construction, high strength-to-weight ratio, and ease of fabrication. On the other hand, structural concrete possesses the characteristics of excellent fire-resistance, high inherent mass and relatively low material cost. It can be molded into any shape to provide complex structural forms. Structural concrete is an economical material in carrying axial and shear forces. Composite construction utilizes the best characteristics of both materials of steel and concrete. Composite elements and structures combine the advantages of both steel and concrete construction, and provide very high strength, stiffness and ductility performance. As a result, steel–concrete composite structures are generally more economical than either all steel or all concrete structures. Composite systems have been widely used in high-rise buildings to resist gravity and lateral loads.

6.3.1 Composite beams

Composite beams have been widely used in multistory building and bridge construction. A composite beam comprises a concrete slab attached to the top flange of a steel beam. The composite action in a composite beam is achieved by welding shear connectors to the top flange of the steel beam. Through the shear connection, the steel beam and the concrete slab work together as one structural member to resist applied loads. The composite action significantly improves the strength and stiffness of the composite beam. The cross-section of a composite beam with profiled steel sheeting placed parallel to the steel beam is shown in Figure 6.7.

6.3.1.1 Shear connection

The strength and stiffness performance of a composite beam depends on the shear connection provided between the concrete slab and the steel member. Shear connectors are used in composite beams to resist the longitudinal slip at the interface and the vertical separation between the steel member and the concrete slab. The shear connection of a composite beam consists of

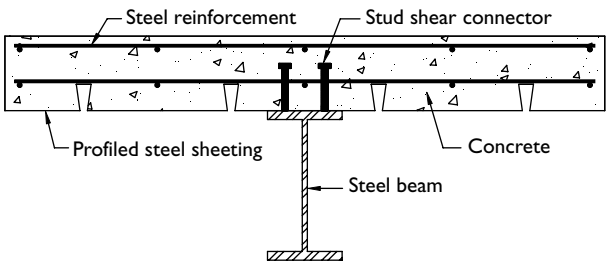

Figure 6.7 Cross-section of composite beam.

several components such as the top flange of the steel member, shear connectors, concrete slab, profiled steel sheeting and slab reinforcement, as shown in Figure 6.7. The behavior of shear connection is influenced by these components. The behavior and design of the shear connection of simply supported composite beams to Australian Standard AS 2327.1 (1996) have been described by Liang and Patrick (2001). A new approach to the design of the shear connection of composite beams was proposed. Computer software called COMPSHEAR has been developed by Liang *et al.* (2001) for the design and detailing of the shear connection of simply supported composite beams to AS 2327.1.

There are many types of steel members that can be used in the design of composite beams, including hot-rolled steel I-beams, built-up beams, steel boxes, tapered girders, stub girders, joists and trusses (Viest *et al.* 1997; Liang and Patrick 2001). However, the top flange of the steel member must satisfy the minimum thickness requirement in order to attach the shear connectors without significant reductions in the strength. The common types of mechanical shear connectors are headed studs, channels and high-strength structural bolts. Among these, the welded stud is the most widely used shear connector in composite construction. The behavior of headed stud shear connectors is usually expressed by the shear–slip curve, which can be determined from push-out tests. It should be noted that the responses of stud shear connectors in a real composite beam under loads are complex. The shear–slip curve obtained from push-out tests only approximately describes the actual behavior of stud shear connectors in composite beams.

The concrete slab used to form a composite beam can be either a solid slab or composite slab incorporating profiled steel sheeting. In a composite slab, profiled steel sheeting acts as permanent formwork and bottom steel reinforcement for the concrete slab. Profiled steel sheeting has an adverse effect on the behavior of the shear connection of composite beams. AS 2327.1 (1996) imposes restrictions on the geometry of profiled steel sheeting to allow composite slabs incorporating profiled steel sheeting to be treated as solid slabs in the determination of the design shear capacity of shear connectors. When a composite slab incorporating narrow rib profiled steel sheeting orientated parallel to the steel beam, the slab is treated as solid in the calculation of the nominal moment capacity of the composite section. However, the composite slab with parallel steel sheeting is not treated as solid in determining the longitudinal shear reinforcement because the open ribs significantly reduce the longitudinal shear surface. On the other hand, composite slabs with profiled steel sheeting orientated deemed perpendicular to the steel beams are regarded as solid slabs when designing steel reinforcement against longitudinal shear failures.

Shear connectors transfer longitudinal shear from the steel beam to the concrete slab. The shear transfer mechanism in the concrete slab of a composite beam can be represented by either the strut-and-tie model

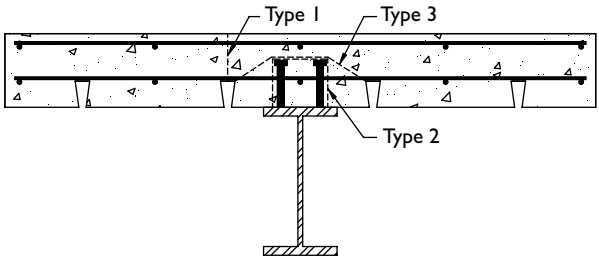

Figure 6.8 Types 1, 2 and 3 longitudinal shear failure surfaces.

(Liang *et al.* 2000b) or the shear-friction model. The longitudinal shear transferred by shear connectors is resisted by the concrete and slab reinforcement. Longitudinal shear reinforcement must be provided in the concrete slab to sustain tensile forces induced by the longitudinal shear transfer. AS 2327.1 (1996) identifies four types of longitudinal shear failures. The Types 1, 2 and 3 longitudinal shear failure surfaces are illustrated in Figure 6.8. The Type 4 longitudinal shear failure may occur in composite edge beams with profiled steel sheeting placed deemed perpendicular to the steel beam when the outstand of the composite beam is less than 600 mm and stud shear connectors are welded through the sheeting. Special steel reinforcing components have been developed in Australia for use in composite beams as longitudinal shear reinforcement (Liang and Patrick 2001; Liang *et al.* 2001). These new reinforcing products complement the new design approach to the longitudinal shear in composite beams and have been incorporated in the computer software COMPSHEAR for the design of the shear connection of composite beams (Liang *et al.* 2001).

The design procedure for determining Types 1, 2 and 3 longitudinal shear reinforcement in the concrete slab of a composite beam is summarized as follows:

1 Calculate the design shear capacity of shear connectors, which requires the minimum number of shear connectors to be determined.
2 Calculate total design longitudinal shear force per unit length.
3 Calculate the perimeter lengths of Types 1, 2 and 3 longitudinal shear surfaces.
4 Check for the concrete shear capacity of Types 1, 2 and 3 longitudinal shear surfaces, such that $\phi 0.32 f'_c u_p \geq V^*_L$. If this condition is not satisfied, either the perimeter lengths or the concrete compressive strength should be increased and then go back to step 1.
5 Calculate the cross-sectional areas and lengths of additional longitudinal shear reinforcement for Types 2 and 3 shear surfaces. The

cross-sectional area of any fully anchored bottom reinforcement in the concrete slab placed transverse to the longitudinal axis of the steel beam is taken into account.

6 Calculate the design longitudinal shear force per unit length for Type 1 surface at any distance from the extremity of the slab effective width.
7 Calculate the cross-sectional areas and lengths of additional reinforcement for Type 1 shear surface for every V_{L}^{*}. The cross-sectional area of any fully anchored transverse reinforcement, and the additional Types 2 and 3 reinforcement are taken into consideration.
8 Determine the maximum cross-sectional area and lengths of additional reinforcement for Type 1 shear surface, which is treated as top reinforcement in the concrete slab.

The total cross-sectional area of longitudinal shear reinforcement for resisting Types 1, 2 and 3 shear surfaces can be determined by using the following equation, respectively:

$$A_{\mathrm{sv}}=\left(\frac{V_L^*}{\phi}-0.36u_{\mathrm{p}}\sqrt{f_c'}\right)\Big/\,0.9f_{\mathrm{yr}} \tag{6.6}$$

where u_{p} is the perimeter length of the longitudinal shear surface. The lesser of the perimeter lengths u_2 and u_3 of Types 2 and 3 shear surfaces should be used in Eq. (6.6). However, the larger of the perimeter lengths u_2 and u_3 should be used to calculate the minimum cross-sectional area of shear reinforcement for Types 2 and 3 shear surfaces. Any existing flexural and shrinkage reinforcement placed transverse to the steel beam in the concrete slab can be treated as the effective longitudinal shear reinforcement if they satisfy the anchorage requirement of Clause 9.7.3 of AS 2327.1 (1996). It is noted that the additional reinforcement for Type 1 shear surface depends on the Types 2 and 3 shear reinforcement as well as existing reinforcement in the concrete slab.

6.3.1.2 Composite beams in combined bending and shear

The ultimate strength of a composite beam depends on the degree of shear connection provided at the interface between the steel beam and the concrete slab. When no shear connection is provided at the interface, the steel beam and the concrete slab will work independently to resist the loading. It is conservatively assumed that the ultimate strength of the non-composite beam is taken as the plastic capacity of the steel beam alone, ignoring any contribution from the concrete slab. Perfect connection requires a connection with infinite shear, bending and axial stiffness. It is difficult to achieve perfect connection since no mechanical shear connectors can provide this degree of shear connection. In practice, the shear connectors are designed

to transfer the longitudinal shear force, which is the smaller of either the tensile capacity of the steel beam or the effective compressive capacity of the concrete slab. The connection so designed is called complete interaction or full shear connection, which results in the maximum possible capacity of a composite section. The incomplete interaction or partial shear connection is between no connection and complete interaction. In partial shear connection, the total shear transferred by the shear connectors is less than the smaller of the tensile capacity of the steel beam and the effective compressive capacity of the concrete slab. The partial shear connection offers economical designs of simply supported composite beams.

The moment capacity of a composite section under positive bending can be determined by assuming that either the structural steel section is fully yielded or the concrete slab is stressed to $0.85 f'_c$ through its full depth (Oehlers and Bradford 1999). The partial shear connection theory is adopted in AS 2327.1 (1996) and Eurocode 4 (1994) for the design of simply supported composite beams. On the other hand, the codes allow only full shear connection to be considered in the design of composite beams in negative moment regions. The design of composite beams with partial shear connection is so complex that computer software should be employed in practice (Liang *et al.* 2001).

Composite beams under applied loads are often subjected to combined actions of bending and vertical shear. Despite experimental evidence, the contributions of the concrete slab and composite action to the vertical shear strength of composite beams are ignored in current design codes, such as AS 2327.1 (1996), Eurocode 4 (1994) and LRFD (1999). The design codes assume that the web of the steel section resists the entire vertical shear. This assumption obviously leads to conservative designs of composite beams. The effects of the concrete slab and composite action on the flexural and vertical shear strengths of simply supported and continuous composite beams have been investigated by Liang *et al.* (2004a,b) using the finite element analysis (FEA) method. Their investigations indicate that the concrete slab and composite action contribute significantly to the flexural and vertical shear strengths of composite beams.

When no shear connection is provided between the steel beam and the concrete slab, the vertical shear capacity of the non-composite section can be determined by (Liang *et al.* 2004b,c)

$$V_o = V_c + V_s \tag{6.7}$$

where V_c is the contribution of the concrete slab and V_s, the shear capacity of the web of the steel beam. Tests indicated that the pullout failure of stud shear connectors in composite beams might occur. This failure mode limits the vertical shear capacity of the concrete slab. As a result, the contribution of the concrete slab V_c should be taken as the lesser of the shear strength of the concrete slab V_{slab} and the pullout capacity of stud shear connectors T_p. The shear strength of the concrete slab proposed by Liang *et al.* (2004b,c) is expressed by

$$V_{slab} = \beta_1 \left(f'_c \right)^{1/3} A_{ec} \tag{6.8}$$

where β_1 is equal to 1.16 for simply supported composite beams and 1.31 for continuous composite beams; f'_c, the compressive strength of the concrete (MPa) and A_{ec}, the effective shear area of the concrete slab. The effective shear area of a solid slab can be taken as $A_{ec} = (b_f + D_c)D_c$, in which b_f is the width of the top flange of the steel beam and D_c, the total depth of the concrete slab. For a composite slab incorporating profiled steel sheeting placed perpendicular to the steel beam, A_{ec} can be taken as $(b_f + h_r + D_c)(D_c - h_r)$, in which h_r is the rib height of the profiled steel sheeting.

The pullout capacity of stud shear connectors in a composite beam comprising a solid slab can be calculated by

$$T_p = [\pi(d_s + h_c) + 2(n_s - 1)s]h_c f_{ct} \tag{6.9}$$

in which d_s is the head diameter of the headed stud; h_c, the total height of the stud; n_s, the number of studs per cross-section; s, the transverse spacing of studs and f_{ct}, tensile strength of concrete (MPa). The pullout capacity of stud shear connectors in composite slabs incorporating profiled steel sheeting should be determined using the effective pullout failure surfaces in the above equations. It should be noted that the transverse spacing of stud shear connectors should not be greater than two times of the stud height.

The shear capacity of the web of the steel beam can be calculated by (Trahair and Bradford 1991)

$$V_s = 0.6\alpha_w f_{yw} d_w t_w \tag{6.10}$$

where f_{yw} is the yield strength of the steel web (MPa); d_w, the depth of the steel web; t_w, the thickness of the steel web and α_w, the reduction factor for slender webs in shear buckling. For stocky steel webs without shear buckling, the reduction factor α_w is equal to 1.0.

Equation (6.7) can be used to determine the vertical shear capacity of non-composite sections. To take advantage of composite actions, Liang *et al.* (2004b,c) proposed design models for the vertical shear strength of composite beams with any degree of shear connection as

$$V_{uo} = V_o \left(1 + \beta_2 \sqrt{\beta} \right) \quad (0 \le \beta \le 1) \tag{6.11}$$

where V_{uo} is the ultimate shear strength of the composite section in pure shear, β_2 can be taken as 0.295 for simply supported composite beams and sagging moment regions in continuous composite beams and 0.092 for hogging moment regions in continuous composite beams and β is the degree of shear connection. It should also be noted that the pullout failure of stud

shear connectors leads to the damage of composite action. If this occurs, the ultimate shear strength of the damaged composite beam (V_{uo}) should be taken as V_o for safety.

Interaction equations are used in AS 2327.1 (1996) and Eurocode 4 (1994) to account for the effect of vertical shear on the ultimate moment capacity of composite beams. However, the design codes allow only the shear strength of the steel web to be considered in the interaction equations. Liang *et al.* (2004b,c) has proposed design formulas, which take account of the effects of the concrete slab and composite action, for strength interaction as

$$\left(\frac{M_u}{M_{uo}}\right)^{\alpha_m} + \left(\frac{V_u}{V_{uo}}\right)^{\alpha_v} = 1 \tag{6.12}$$

where M_u and V_u are the ultimate moment and shear capacities of the composite beam in combined bending and shear, respectively and M_{uo}, the ultimate moment capacity of the composite section in pure bending. The exponents α_m and α_v are equal to 6.0 for simply supported composite beams and 5.0 for sagging moment regions in continuous composite beams. For hogging moment regions in continuous composite beams, α_m and α_v are equal to 0.6 and 6.0, respectively. The ultimate moment capacity of the composite section (M_{uo}) can be determined using the rigid plastic analysis method in accordance with the codes of practice such as AS 237.1 (1996) and Eurocode 4 (1994). It should be noted that the ultimate moment to shear ratio is equal to the applied moment to shear ratio. If the applied moment and vertical shear are known, the ultimate strengths of a composite beam in combined actions of bending and shear can be determined using Eq. (6.12).

6.3.1.3 Modeling of composite beams

In the optimization process of bracing systems for composite frames, the linear elastic FEA is usually undertaken to obtain the responses of the systems to lateral loads. In the linear elastic analysis, the stress–strain relationship of concrete in compression is assumed to be linear while the material properties of composite beams are adjusted to reflect the reduction in stiffness due to the cracking of concrete in tension. The modification of the composite beam stiffness can be based on the effective areas and the moment of inertia or the transform section method. The effect of slip between the structural steel and the concrete slab can be neglected in the overall analysis of composite frames.

The moments of inertia of continuous composite beams are significantly different for positive and negative bending. Under reverse lateral loads, the bending moment diagram of the beam will change. As a result, the stiffness of the beam will also change. Neither the positive nor negative composite

beam moment of inertia alone can be used in the frame analysis since it will result in significant errors. Ammerman and Leon (1990) suggested that a weighted average approach could be used to calculate the composite beam moment of inertia for the frame stiffness analysis. The modified moment of inertia of a composite section is determined by

$$I_c = 0.6I_p + 0.4I_n \tag{6.13}$$

where I_p is the lower bound moment of inertia of the composite section in positive bending and I_n, the lower bound moment of inertia of the composite section in negative bending. The lower bound values can be calculated in accordance with AS 2327.1 (1996).

6.3.2 *Composite columns*

Composite columns are used to support either heavy axial loads as compression members or gravity and lateral loads as beam–columns in moment-resisting tall buildings. The most commonly used composite columns in buildings are encased composite columns, concrete-filled rectangular steel box columns and concrete-filled circular steel tubes, as shown in Figure 6.9. An encased composite column usually consists of a structural steel I-section encased in a reinforced concrete column. Stud shear connectors may be welded to the structural steel section to transfer forces between the steel section and the concrete. In concrete-filled steel tubes, the steel tubes act as permanent formwork for the concrete core and increase the strength and stiffness of the columns. Concrete-filled steel tubes exhibit a very ductile behavior due to the confinement provided by the steel tubes to the concrete core. On the other hand, the concrete core provides restraints to the steel tube so that the resistance of the steel tube with filled concrete to local buckling is much higher than that of the hollow steel tube.

The ultimate strength of composite columns under axial compression depends on the cross-sectional properties and slenderness of the columns.

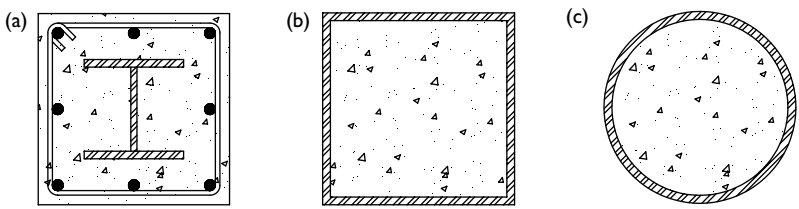

Figure 6.9 Typical composite columns: (a) encased composite column; (b) concrete-filled steel box column; (c) concrete-filled circular steel tube.

The strength of stocky composite columns is governed by the capacities of the cross sections. The strength of very slender columns is governed by the elastic overall buckling. The ultimate strength of short composite columns under axial compression can be calculated by combining the ultimate strength of the concrete core and the steel (Liang and Uy 1998, 2000), and is expressed by

$$N_u = 0.85f'_c A_c + f_{sy}A_{se} + f_{yr}A_{st} \tag{6.14}$$

where A_c is the area of concrete in the cross-section; f_{sy}, the yield strength of structural steel section; A_{se}, the total effective structural steel area of the cross-section; f_{yr}, the yield strength of longitudinal steel reinforcement and A_{st}, the total cross-sectional area of longitudinal steel reinforcement. For concrete-filled rectangular steel box columns, the total effective steel area of the cross-section can be calculated using the effective width models proposed by Liang and Uy (1998, 2000). The effective width models are expressed by

$$\frac{b_e}{b} = 0.675\left(\frac{\sigma_{cr}}{f_{sy}}\right)^{1/3} \tag{6.15}$$

when $\sigma_{cr} \leq f_{sy}$, and

$$\frac{b_e}{b} = 0.915\left(\frac{\sigma_{cr}}{\sigma_{cr} + f_{sy}}\right)^{1/3} \tag{6.16}$$

when $\sigma_{cr} > f_{sy}$.

In the above equations, b_e is the effective width of the plate and σ_{cr}, the critical local buckling stress, which can be calculated using the minimum elastic-buckling coefficient of 9.81 (Liang and Uy 1998).

In the modeling of composite columns for optimization, the gross transformed properties of the columns can be used if the axial compressive loads are large enough to ensure that the cracking of concrete does not occur.

6.4 Semirigid connections

Simple and rigid connections in frame structures are highly idealized cases. In reality, most of the beam–column connections are semirigid. In composite construction, a simple connection can be transformed into a rather stiff semirigid joint by adding only a small amount of slab reinforcing bars, shear connectors and seat angles in the negative moment regions. The semirigid connections offer significant additional strength and stiffness to the composite frame thereby greatly reduce the lateral deflections.

The flexibility of beam–column connections has a significantly effect on the analysis of lateral load resisting systems. It should be taken into account in the FEA of braced frames for structural optimization. Semirigid connections

are generally nonlinear. The inelastic behavior of semirigid connections is usually described by the moment–rotation relationship. In the analysis of lateral load resisting systems, semirigid connections can be modeled using linear springs with an effective stiffness reduced from the initial elastic stiffness to incorporate the inelastic behavior of the connections, as suggested by Bjorhovde (1984). This will affect the lateral deflections and the distribution of member forces.

6.5 Optimization of bracing systems

Multistory buildings are usually braced by vertical and horizontal elements. Vertical elements consist of moment-resisting frames, diagonally braced frames and shearwalls while horizontal elements comprise floor and roof diaphragms. Only the optimization of bracing systems for multistory frames in the vertical direction is considered here.

6.5.1 Optimization problem formulation

Bracing systems are used to reinforce multistory building frames so that the lateral drifts of the frames are maintained within acceptable performance levels. In the proposed PBO method, a continuum structure under plane stress conditions is used to stiffen a multistory frame. The continuum structure is modeled using plane stress finite elements. The frame itself with a fixed topology is treated as a nondesign domain, which is modeled by using beam elements. Beam elements are not removed during the optimization process. A building frame fully braced by a continuum structure is used as a starting point for deriving the optimal bracing system for the frame. This is achieved by removing underutilized elements from the continuum structure. Since lateral loads such as wind and seismic forces are usually reversible, tall building frames are subjected to multiple load cases.

The performance objective of the layout design for bracing systems is to minimize the weight of the continuum design domain while maintaining the overall stiffness of the braced frame within an acceptable limit. The performance objective can be expressed as follows:

$$\text{minimize } W = \sum_{e=1}^{n} w_e \tag{6.17}$$

$$\text{subject to } C^p \leq C^* \quad (p = 1, 2, 3, \ldots \text{NL}) \tag{6.18}$$

where W is the total weight of the continuum structure; w_e, the weight of the eth element in the continuum structure; C^p, the absolute value of the mean compliance of a braced frame under the load case p; C^*, the prescribed limit of the mean compliance and n, the total number of elements in the discretized continuum design domain. It is noted that the mean compliance of a structure is used as an inverse measure of its overall stiffness.

The maximization of the overall stiffness of a braced frame is equivalent to minimizing its mean compliance.

6.5.2 Element removal criteria

The FEA indicates that some regions of a continuum structure used to stiffen a multistory frame are not effective in resisting lateral loads. These underutilized regions can be removed from the continuum design domain to improve the performance of the lateral load resisting system. Element removal criteria are used to identify these underutilized regions in the optimization algorithm, and can be derived by undertaking a sensitivity analysis. The sensitivity analysis is to investigate the effects of element removal on the change in the mean compliance of a braced frame.

In FEA, the equilibrium equation of a braced frame can be expressed by

$$[K]\{u\} = \{P\} \tag{6.19}$$

where $[K]$ is the stiffness matrix of a braced frame structure; $\{u\}$, nodal displacement vector of the braced frame and $\{P\}$, load vector. When the eth element is removed from a discretized continuum design domain, the stiffness and displacements of the whole structure will change accordingly, and Eq. (6.19) can be rewritten as

$$[K + \Delta K]\{u + \Delta u\} = \{P\} \tag{6.20}$$

in which ΔK is the changes in the stiffness matrix and $\{\Delta u\}$, the change in nodal displacement vector of the braced frame. When only the eth element is removed from the continuum design domain, the change in the stiffness matrix can be derived as

$$[\Delta K] = [K_r] - [K] = -[k_e] \tag{6.21}$$

where $[K_r]$ is the stiffness matrix of the resulting structure and $[k_e]$, the stiffness matrix of the eth element in the continuum design domain. The change in the displacement vector can be obtained approximately by neglecting the higher order terms as

$$\{\Delta u\} = -[K]^{-1}[\Delta K]\{u\} \tag{6.22}$$

The mean compliance or strain energy of a braced frame structure is calculated by

$$C = \tfrac{1}{2}\{P\}^{T}\{u\} \tag{6.23}$$

The change in the strain energy of the braced frame due to the elimination of the eth element from the continuum design domain can be derived

approximately as

$$\Delta C = \tfrac{1}{2}\{P\}^{\mathrm{T}}\{\Delta u\} = -\tfrac{1}{2}\{P\}^{\mathrm{T}}[K^{-1}][\Delta K]\{u\} = -\tfrac{1}{2}\{u\}^{\mathrm{T}}[\Delta K]\{u\} = -\tfrac{1}{2}\{u_e\}^{\mathrm{T}}[k_e]\{u_e\} \tag{6.24}$$

in which $\{u_e\}$ is the displacement vector of the eth element in the continuum design domain. It appears from Eq. (6.24) that the change in the strain energy of a braced frame structure due to the removal of the eth element can be approximately evaluated by the strain energy of the eth element. This implies that the element strain energy is a measure of the efficiency of an element in contribution to the overall stiffness performance of a lateral bracing system and is denoted as

$$c_e = \tfrac{1}{2}\{u_e\}^{\mathrm{T}}[k_e]\{u_e\} \tag{6.25}$$

To achieve the maximum stiffness and minimum weight design of lateral bracing systems, elements with the lowest strain energy should be gradually removed from the continuum design domain. If a continuum design domain is modeled by different size elements, the lowest SED of elements should be used as element removal criteria. The SED of the eth element is calculated as $\gamma_e = |c_e|/w_e$.

To eliminate the formation of checkerboard patterns in optimal bracing systems, the redistribution method can be employed to recalculate the SEDs of elements before any element removal, as presented in Chapter 4.

Multistory buildings are often subjected to reverse wind loads, which can be treated as multiple load cases. For a braced frame structure subject to multiple loading cases, a logical AND scheme is employed in the proposed method to take account of the effect of different loading cases, as described in Chapter 4. In the logical AND scheme, an element is removed from the continuum design domain only if its SED is the lowest for all load cases. The resulting bracing system will be the most efficient in resisting lateral loads. Elements with the lowest SEDs are counted by a loop until they make up the specified amount, which is the element removal ratio times the number of elements in the initial design domain. The element removal ratio (R) for each iteration is defined by the ratio of the number of elements to be removed to the total number of elements in the initial continuum structure.

6.5.3 Performance-based optimality criteria

In an optimization process, braced systems are gradually modified by eliminating elements with the lowest SEDs from a continuum design domain that braces a multistory frame. To obtain the optimal bracing system, the performance of the resulting bracing system at each iteration must be evaluated using some sorts of performance indicators. Performance-based

optimization criteria (PBOC) in terms of performance indices have been proposed in previous chapters using the scaling design concept for assisting the selection of optimal designs from the optimization history. These performance indices are also useful tools for ranking the performance of structural topologies and shapes generated by different optimization methods.

Since the continuum structure under plane stress conditions is structurally connected to a multistory frame, the overall stiffness of the braced frame is not a linear function of the thickness of the continuum structure. As a result, the element thickness of the continuum structure cannot be linearly scaled to keep the mean compliance constraint active at each iteration. However, it is known that the best structure is the one that has the maximum stiffness at minimum weight, as pointed out by Hemp (1973). Therefore, the energy-based performance index (PI_{es}) derived using the scaling design procedure can still be used to evaluate the performance of bracing systems for building frames with mean compliance constraints. The performance index is expressed by

$$PI_{es} = \frac{C_0 W_0}{C_i W_i} \tag{6.26}$$

in which C_0 and C_i are the absolute values of the mean compliance of the initial braced frame and the current braced frame at the ith iteration, respectively; W_0, the weight of the initial continuum structure and W_i, the weight of the current continuum structure. The weight of the frame is not included in the calculation of the performance index since the beam elements of the frame are not removed in the optimization process. The performance index can indicate the efficiency of a lateral bracing system in terms of the material usage and the overall stiffness. The performance of a bracing system is improved when elements with the lowest SEDs are gradually removed from the continuum design domain.

To achieve optimal bracing systems for tall building frames, the PBOC can be stated as

$$\text{maximize} \quad PI_{es} = \frac{C_0 W_0}{C_i W_i} \tag{6.27}$$

The PBOC means that the best bracing systems can be achieved by maximizing the stiffness-to-weight ratio of a braced frame. The performance index is used in the optimization algorithm to monitor the optimization process, from which the optimal topology can be identified.

6.5.4 Design optimization procedure

The design optimization process of bracing systems for multistory building frames is divided into two main stages. In the first stage, a FEA is undertaken on the unbraced frame under gravity and lateral loads and its

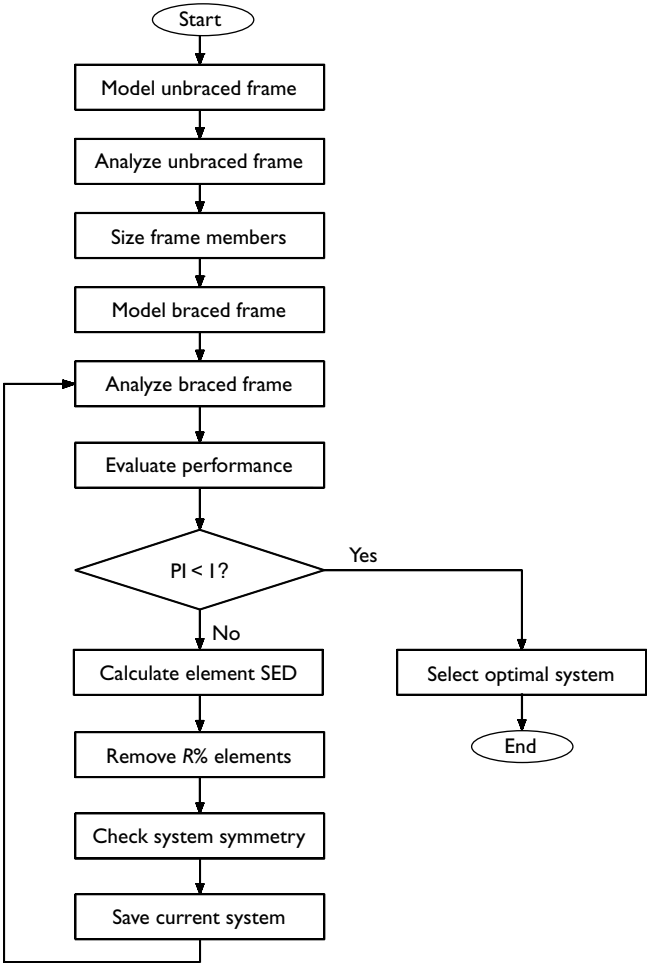

Figure 6.10 Flowchart of design optimization procedure for bracing systems in multistory frames.

members are then sized for strength performance criteria by selecting commercial standard sections from databases. In the second stage, a repeated FEA and topology optimization cycle is undertaken for the frame braced by a continuum structure until the performance of the braced frame is maximized. The main steps of the design optimization procedure are illustrated in Figure 6.10, and summarized as follows:

1 Model the unbraced frame with beam elements. The loads, support conditions and material properties of the assumed sections are specified.

2 Perform a linear elastic FEA on the unbraced frame structure.
3 Size the members of the unbraced frame based on the results of the FEA for strength performance criteria by selecting commercial standard sections from databases.
4 Add a continuum structure modeled with plane stress elements to the frame. The discretization of the continuum structure must be consistent with that of the frame.
5 Perform a linear elastic FEA on the braced frame.
6 Evaluate the performance of the resulting bracing system using the energy-based performance index. For a braced frame under multiple load cases, the strain energy of the braced frame under the most critical load case should be used in calculating the performance index.
7 Calculate the SEDs of elements in the continuum structure for each loading case.
8 Remove a small number of elements with the lowest SEDs from the continuum design domain.
9 Check the symmetry of the bracing system under an initially symmetrical condition.
10 Save model data for the current braced frame structure.
11 Repeat steps 5–11 until the performance index is less than unity.
12 Plot the performance index history and select the optimal bracing system.

It is desirable that the mean compliance constraint in terms of the lateral drifts of the building is active at the optimum. However, because the thickness of the continuum structure significantly influences the efficiency of resulting systems, the mean compliance constraint may not always be active at the optimum. To deal with this problem, shape and sizing optimization techniques can be employed to further optimize the bracing system until lateral drifts reach prescribed limits. Another way to handle this is to uniformly change the element thickness of the optimal systems obtained so that the required system performance is satisfied. This can also be done by uniformly changing the thickness of the continuum design domain to keep the mean compliance constraint active in the optimization process. However, the derivatives of the mean compliance constraint with respect to the thickness have to be calculated.

For practical purposes, some modifications to the optimal bracing system obtained may be necessary. It is also possible to select a bracing system that meets the construction and architectural requirements from the optimization history as the final design proposal. However, the performance of the selected bracing system must be within an acceptable level. The performance index is a useful tool in the selection of bracing systems for the design of multistory steel building frames.

6.6 Sizing optimization of lateral load resisting systems

Sizing optimization of lateral load resisting systems is to find the optimal cross sections of members in a lateral system with the maximum stiffness and minimum weight. The topology of the lateral load resisting system is fixed. The design variables of sizing optimization are the cross-sections of the members. The topology of lateral bracing systems for tall buildings can be generated using the PBO technique presented in the preceding section. The design of composite members for strength has been presented in preceding sections. The strength design methods of other structural members can be found in other textbooks and are not discussed here. Only the stiffness-based sizing techniques are described in this section.

6.6.1 Sizing problem formulation

The performance objective of the sizing optimization of a lateral load resisting system is to find a minimum weight design of the system for the required stiffness performance level. The stiffness performance level is characterized by the lateral drift constraints. This can be stated as

$$\text{minimize} \quad W = \sum_{i=1}^{n} \rho_i l_i A_i \tag{6.28}$$

$$\text{subject to} \quad C^p \leq \mathrm{C}^* \quad (p = 1, 2, \ldots, \mathrm{NL}) \tag{6.29}$$

$$A_i^{\mathrm{L}} \leq A_i \leq A_i^{\mathrm{U}} \tag{6.30}$$

where ρ_i, l_i and A_i are the material density, length and cross-sectional area of the ith member, respectively; A_i^{L} and A_i^{U}, the lower and upper bounds for A_i and n, the total number of members in the lateral load resisting system.

6.6.2 Member sizing criteria

To achieve the minimum weight design for a frame structure under lateral loads and overall stiffness constraints, the underutilized material can be removed from the members by changing the member cross-sectional areas. This can be done by assigning the members to the smaller available sections. The effect of member cross-section reduction on the mean compliance of a frame structure can be evaluated by the design sensitivity analysis, as demonstrated in the preceding section.

When the cross-sectional area of the ith member is reduced from A_i to $(A_i - \Delta A_i)$, the stiffness matrix and the mean compliance of the frame structure will change accordingly. The change in the stiffness matrix of the structure is

$$[\Delta K] = [\Delta K_i] = [K_i(A_i - \Delta A_i) - K_i(\mathrm{A}_i)] \tag{6.31}$$

where $K_i(A_i - \Delta A_i)$ and $K_i(A_i)$ are the stiffness matrices of the ith member for the cross-sectional areas $(A_i - \Delta A_i)$ and A_i, respectively. The change in the mean compliance of the lateral system can be evaluated by

$$\Delta C = -\tfrac{1}{2}\{u_i\}^{\mathrm{T}}[\Delta K_i]\{u_i\} \tag{6.32}$$

The above equation indicates that the change in the strain energy of a lateral load resisting system due to reduction in the cross-sectional area of the ith member is equal to the change in the strain energy of that member. The change in strain energy per unit weight is defined as the change in SED, which is calculated by

$$\gamma_i^{\mathrm{s}} = \frac{|\Delta C|}{|\rho_i l_i \Delta A_i|} \tag{6.33}$$

It is obvious that reducing the size of a member whose γ_i^{s} is the lowest will result in the minimum change in the mean compliance of the lateral load resisting system. In other words, the maximum stiffness design for lateral load systems can be obtained by resizing the members that have the minimum changes in their strain energy due to resizing.

The member sizing criteria can also be derived using the Lagrange multiplier method. The Lagrangian function for the sizing optimization problem with the mean compliance constraint is written as

$$\mathrm{L}(A_i, \lambda) = \sum_{i=1}^{n} \rho_i l_i A_i + \lambda(C - C^*) \tag{6.34}$$

where λ is the Lagrange multiplier. The optimality condition for the problem is

$$\frac{\partial \mathrm{L}(A_i, \lambda)}{\partial A_i} = \frac{\partial\left(\sum_{i=1}^{n} \rho_i l_i A_i\right)}{\partial A_i} - \lambda \left|\frac{\partial C}{\partial A_i}\right| = \rho_i l_i - \lambda \left|\frac{\partial C}{\partial A_i}\right| = 0 \quad (i = 1, n) \tag{6.35}$$

Equation (6.35) can be approximated by

$$\rho_i l_i - \lambda \left|\frac{\Delta C}{\Delta A_i}\right| = 0 \quad (i = 1, n) \tag{6.36}$$

The optimality condition becomes

$$\gamma_i^{\mathrm{s}} = \frac{|\Delta C|}{|\rho_i l_i \Delta A_i|} = \frac{1}{\lambda} = \text{constant} \quad (i = 1, n) \tag{6.37}$$

Equation (6.37) represents the OC, which states that at the optimum the absolute ratio of the change in the member strain energy and the change in the member weight is equal for all members. This will lead to uniform SED distribution of structural members within a frame.

6.6.3 Optimization algorithm

The performance-based sizing optimization procedure for lateral load resisting systems under multiple load cases can be summarized as follows:

1 Model the lateral load resisting system using finite elements with maximum available sizes.
2 Perform a linear elastic FEA on the structure.
3 Evaluate the performance of the resulting system using the energy-based performance index.
4 Calculate the changes in the SEDs of elements due to resizing.
5 Reduce the cross-sectional areas of a small number of members with the smallest changes in SEDs.
6 Repeat steps 2–5 until the performance index is maximized.
7 Plot the performance index history and select the optimal design.

6.7 Design examples

Several examples are presented in this section to demonstrate the effectiveness of the PBO technique for optimal design of bracing systems for multi-story building frames under multiple lateral load cases. The effects of nondesign domains on the layouts and performance of bracing systems are also investigated. For simplicity, only steel frames with rigid connections are considered here.

6.7.1 Six-story steel frame

A six-story steel building frame under two lateral load cases is shown in Figure 6.11. It is required to design a bracing system for this steel frame in order to control the lateral drifts. The PBO technique was employed to generate an optimal bracing system for the frame and the result obtained is compared with the solution given by Mijar *et al.* (1998). The unbraced frame as shown in Figure 6.12 was initially designed by Huang (1995) using standard steel sections under stress constraints according to the American Institute of Steel Construction design code. In Huang's design, the uniformly distributed load applied to floor beams was 14.59 kN/m and the wind loads of 40.05 kN were applied as horizontal point loads at each floor level. The wide flange sections used for the 14 members indicated in Figure 6.11(a) are given in Table 6.4. The lateral wind loads shown in Figure 6.11(a) were used

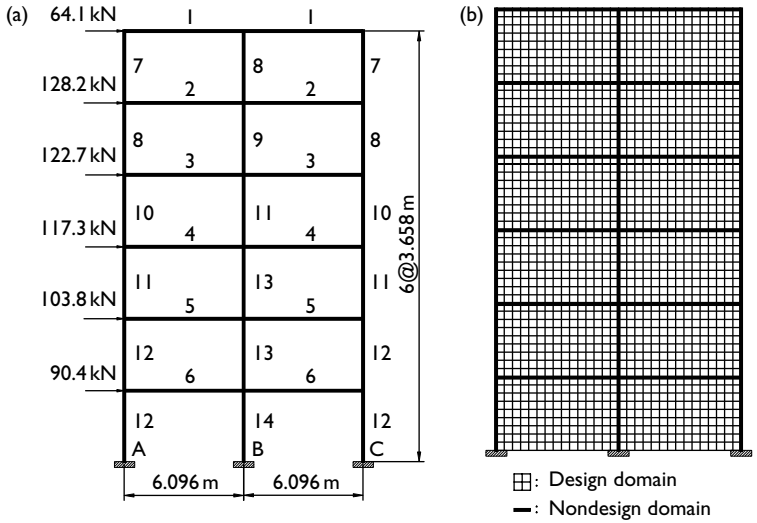

Figure 6.11 Two-bay, six-story steel frame: (a) unbraced; (b) braced.

by Mijar *et al.* (1998) to find the bracing systems for this frame. Under this lateral loading condition, stresses in the members of the unbraced frame may exceed the allowable stress.

Two lateral load cases were considered in the present study to take account of the effect of reversed wind loads. It should be noted that lateral bracing systems in multistory steel buildings are mainly designed to resist lateral loads. It was assumed that the effect of floor loads that were carried by beams and columns on the layout of bracing systems could be neglected. Floor loads were thus not included in the analysis. In the present study, the steel frame itself was modeled using 342 linear beam elements with rigid connections. In the optimization process, the frame itself was treated as a nondesign domain in which beam elements were not eliminated. The steel frame was fully braced by a continuum structure, which was discretized using 1620 four-node plane stress elements as shown in Figure 6.11(b). The discretization of the steel frame was consistent with that of the continuum structure. The continuum structure was structurally connected to the beams and columns of the frame. The continuum structure was treated as design domain where elements could be removed according to the element removal criteria. The supports of the frame at points A, B and C were fixed. The Young's modulus of material $E = 200$ GPa, Poisson's ratio $\nu = 0.3$ and a uniform thickness $t = 25.4$ mm were specified for the continuum design domain. The element removal ratio of 1 percent was used in the optimization process.

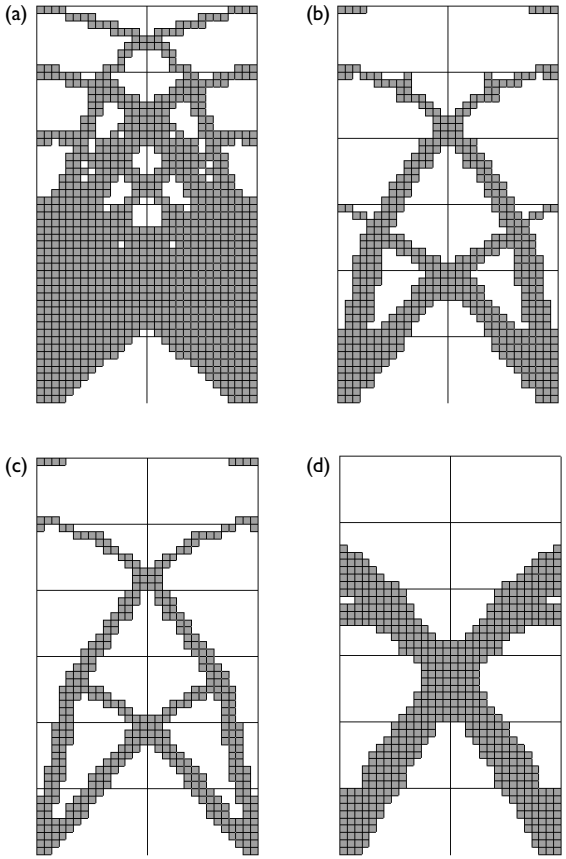

Figure 6.12 Optimization history of bracing system for the six-story steel frame: (a) topology with $V = 0.63V_0$; (b) topology with $V = 0.3V_0$; (c) topology with $V = 0.22V_0$; (d) topology with $V = 0.3V_0$ (Mijar *et al.* 1998).

Table 6.4 Member sizes of the six-story steel frame

Member	*Section*	*Member*	*Section*
1	W8 × 21	8	W8 × 10
2	W8 × 28	9	W12 × 19
3	W10 × 26	10	W12 × 14
4	W12 × 26	11	W14 × 22
5	W14 × 26	12	W16 × 26
6	W14 × 19	13	W16 × 31
7	W10 × 17	14	W24 × 62

The maximum lateral displacement of the unbraced steel frame was 560 mm. Figure 6.12 depicts the optimization history of the bracing system for the six-story steel frame. It can be observed from Figure 6.12 that the continuum structure evolved toward a truss-like bracing system when elements with the lowest SEDs were gradually eliminated from the continuum design domain. All topologies obtained are symmetrical about the vertical axis of the frame as expected under the reversible wind loading conditions. It appears from the optimization history of bracing systems presented in Figure 6.12 that the bracing system needs more material in the lower stories to resist the lateral loads.

Figure 6.12(d) shows the optimized topology of the bracing system for the steel frame given by Mijar *et al.* (1998) using a continuum topology optimization method based on the Voigt–Resuss mixed rules. The figure was regenerated here for comparison. This topology was obtained by minimizing the mean compliance of the braced frame subject to a volume constraint that was 30 percent of the initial continuum design domain. The maximum lateral displacement of the bracing system presented in Figure 6.12(d) was 70 mm. The maximum lateral displacement of the bracing system depicted in Figure 6.12(c) is only 24 mm while its material volume is 22 percent of the initial continuum structure. The performance index of the bracing system shown in Figure 6.12(c) is 1.15 while it is only 0.32 for the topology presented in Figure 6.12(d). This indicates that the structural performance of lateral load resisting systems is significantly affected by the layout of bracing systems. The PBO technique is an efficient design tool that can be used to achieve minimum-weight designs for bracing systems while lateral drifts are maintained within acceptable limits.

The topology shown in Figure 6.12(b) can be used in the design of the bracing system for the six-story steel frame. The layout arrangement of bracing members is illustrated in Figure 6.13. This bracing system can be constructed by using available standard steel sections from databases. It should be noted that the bracing members must be connected to the beams if they cross the beams of the frame.

6.7.2 The 3-bay, 12-story steel frame

The automated PBO technique was employed to generate an optimal bracing system for a 3-bay, 12-story tall steel building frame shown in Figure 6.14. The tall steel frame was subjected to two lateral wind-loading cases, that is, one from the left and the other from the right. Gravity loads were not considered in the optimization of the lateral bracing system. The frame structure was fixed at points A, B, C and D as shown in Figure 6.14. Rigid beam–column connections were assumed for the frame. Beams and columns were modeled using linear beam elements. The beam and column were divided into 15 and 9 elements, respectively, with a total of 684 elements for the whole

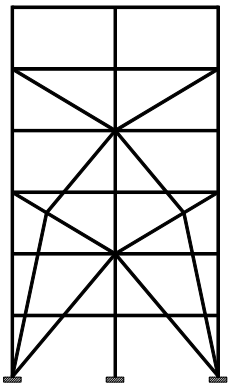

Figure 6.13 Layout of bracing system for the six-story steel frame.

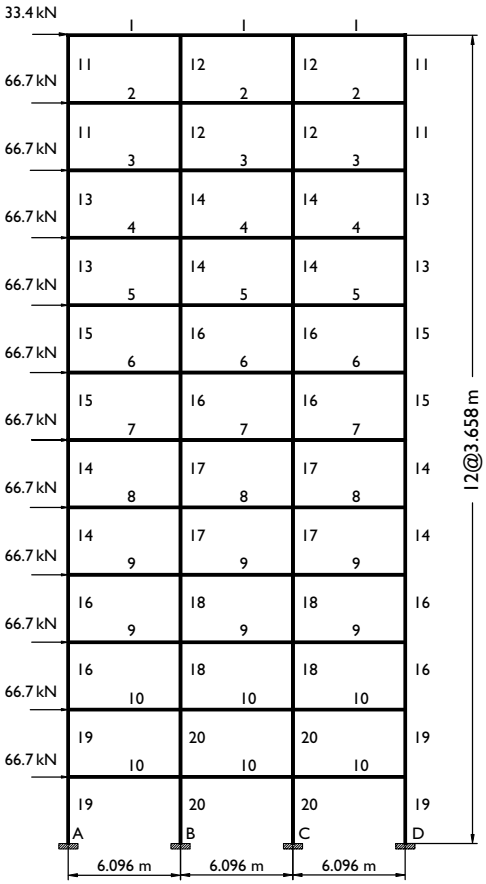

Figure 6.14 A 3-bay, 12-story steel frame.

Table 6.5 Member sizes of the 12-story steel frame

Member	*Section*	*Member*	*Section*
1	150UB18.0	11	150UC23.7
2	180UB18.1	12	150UC37.2
3	200UB29.8	13	200UC46.2
4	250UB27.3	14	200UC59.5
5	310UB40.4	15	200UC52.2
6	360UB50.7	16	250UC72.9
7	360UB56.7	17	250UC89.5
8	410UB53.7	18	310UC96.8
9	460UB67.1	19	310UC118
10	460UB74.6	20	310UC137

frame structure. The Young's modulus $E = 200$ GPa, shear modulus $G = 7690$ MPa, and the material density $\rho = 7850$ kg/m^3 were specified for steel sections. A linear elastic FEA was undertaken on the unbraced frame structure. The BHP hot rolled standard steel sections were then selected from databases to size the members of the frame based on strength performance criteria. For practical purposes, beams were grouped together as having a common section for each floor while columns were grouped for every two stories. Steel sections selected for frame members are given in Table 6.5.

A continuum structure with a uniform thickness of 25 mm was used to fully brace the frame. The continuum structure was treated as a design domain, which was divided into a 45×108 mesh using four-node plane stress elements. The discretization of the continuum design domain was consistent with that of the steel frame. The steel frame and the continuum structure were connected together at the locations of beams and columns with compatible degree of freedoms. The Young's modulus $E = 200$ GPa and Poisson's ratio $\nu = 0.3$ were used for the continuum design domain. The element removal ratio of 2 percent was adopted in the optimization process.

The maximum lateral displacement of the unbraced frame obtained was 618 mm, which exceeds the drift limit of $H/400$, where H is the total height of the frame. Figure 6.15 shows the performance index history of the bracing system obtained by the PBO technique. It can be seen that the performance index of the bracing system increased from unity to the maximum value when elements with the lowest SEDs were gradually eliminated from the continuum design domain in the optimization process. After reaching the peak, the performance index decreased if further elements were removed from the continuum design domain. The maximum performance index obtained is 1.51. The performance characteristic curve predicted by the PBO technique for the braced frame structure is depicted in Figure 6.16. The weight of the continuum structure and the mean compliance of the braced frame were used in the performance characteristic curve. It appears

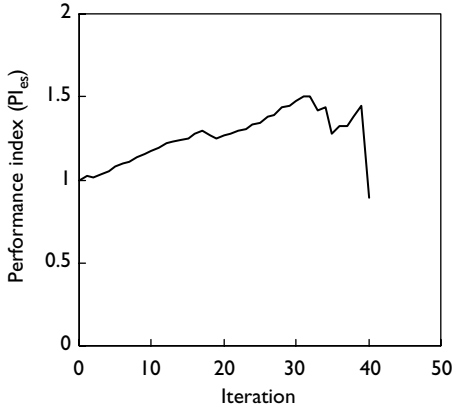

Figure 6.15 Performance index history of bracing system.

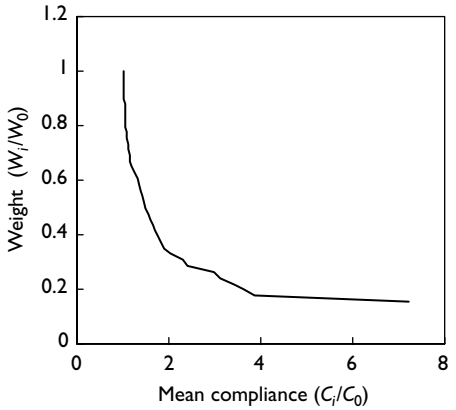

Figure 6.16 Performance characteristics of bracing system.

from Figure 6.16 that the element removal resulted in a significant reduction in the weight of the continuum structure and the increase in the mean compliance of the braced frame.

The optimal topology of the bracing system for the 12-story steel frame under multiple lateral loads is shown in Figure 6.17(a). The optimal bracing system displays a large-scale discrete structure. The optimal topology provides very useful information for the structural designer on which member of the steel frame should be stiffened by resizing. It is seen from Figure 6.17(a) that exterior columns from the ground level up to the fifth level need to be resized. The optimal topology of the bracing system for the

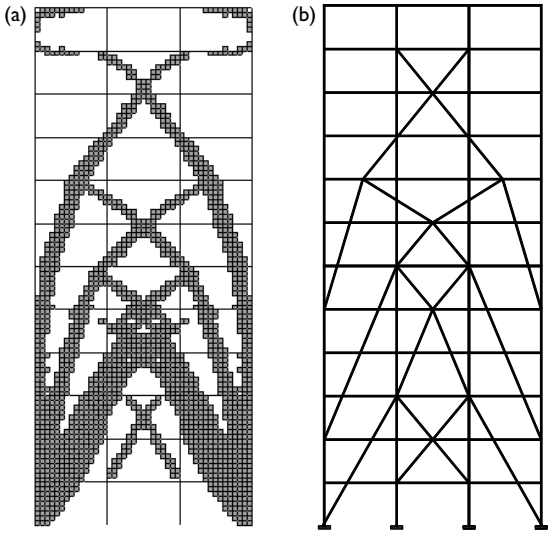

Figure 6.17 (a) Optimal topology and (b) discrete bracing system for the 12-story steel frame.

12-story steel building frame can be transformed to the bracing layout depicted in Figure 6.17(b), where columns that need to be resized are not shown. Since the mean compliance constraint in terms of the lateral drift has not reached the actual limit at the optimum, sizing techniques can be employed to further optimize the braced frame using available standard steel sections. It should be noted that the exact dimensions of bracing members as well as columns that need to be resized are not shown Figure 6.17(b), which only illustrates the basic layout of the bracing system for the frame structure. Sizing the braced frame should be based on the optimal topology presented in Figure 6.17(a), which shows the dimensions of the bracing system and the lateral stiffness distribution within the frame structure under lateral loads. Bracing members are rigidly connected to the frame members.

6.7.3 *Effect of regions without bracing on the 12-story braced frame*

Although full-width braced frames are economical lateral load resisting systems for tall buildings as discussed in preceding sections, they have a disadvantage of interference with architectural requirements. In practical design of tall buildings, it is sometimes required to free certain bays or stories from any obstacle that may prevent outside views. This implies that

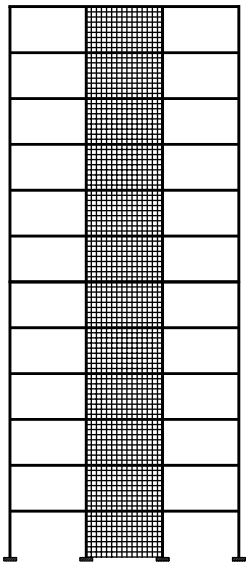

Figure 6.18 A 12-story steel frame with 1-bay braced by a continuum structure.

the efficiency of the lateral bracing system in resisting lateral loads may be reduced. This example is to investigate the effect of regions without bracing on the optimal bracing systems and their performance.

Only the middle bay in the 3-bay, 12-story steel frame presented in the preceding section allows to be braced for lateral drift control, as shown in Figure 6.18. The loading condition, material properties and steel sections of the frame are the same as those used in the preceding example. The continuum structure was modeled using 15×108 four-node plane stress elements. The thickness of the continuum structure was 50 mm. The Young's modulus $E = 200$ GPa and Poisson's ratio $\nu = 0.3$ were used for the continuum design domain. The element removal ratio of 2 percent was adopted in the optimization process.

The performance index history of the bracing system for the 12-story steel frame is presented in Figure 6.19. Despite that only one bay in the steel frame was braced by a continuum structure, the performance of the bracing system was still improved by eliminating underutilized material from the continuum structure, as indicated by the performance index. The performance of the bracing system was maximized at iteration 28 corresponding to the maximum performance index of 1.66. Figure 6.20 shows the performance characteristics of the braced frame in the optimization process. It is observed from the figure that at the optimum the weight of the continuum structure was reduced to 41 percent while the mean compliance of the braced frame increased by 47 percent in comparison with the initial braced frame.

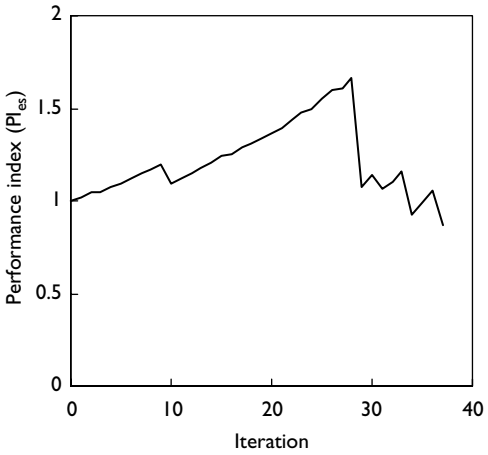

Figure 6.19 Performance index history of the 12-story steel frame with 1-bay braced.

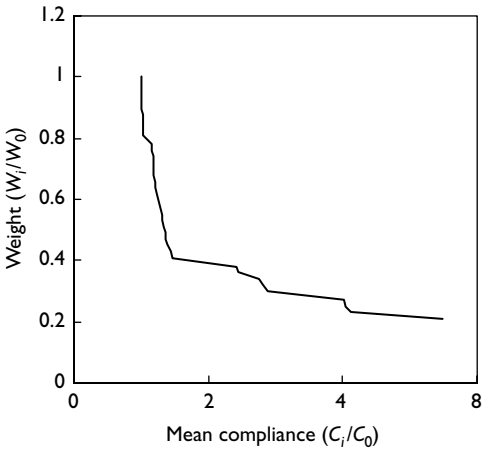

Figure 6.20 Performance characteristics of bracing system.

The optimal topology produced by the PBO technique is shown in Figure 6.21(a). The optimal topology indicates that the sizes of the columns in the lower stories in the braced bay need to be increased to provide sufficient lateral stiffness to control lateral deflections. This implies that the efficient design for the lateral load resisting system discussed here can be achieved by resizing these columns and using diagonal bracing as demonstrated in Figure 6.21(a). A discrete bracing system based on the optimal topology obtained is presented in Figure 6.21(b). It should be noted that the vertical bracing members represented by the columns are not shown in Figure 6.21(b).

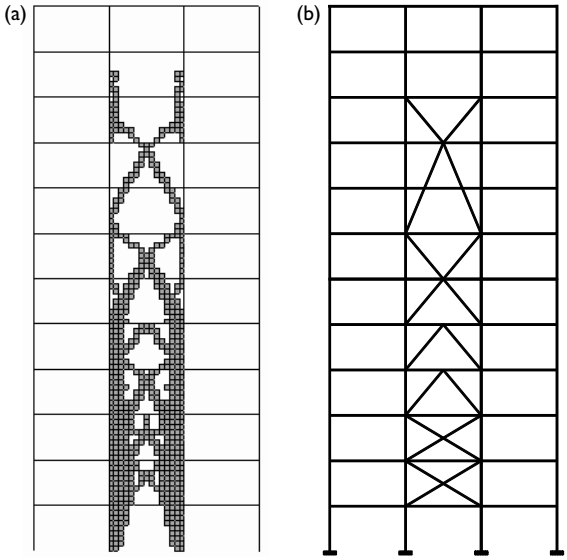

Figure 6.21 (a) Optimal topology and (b) discrete bracing system for the 12-story steel frame with 1-bay braced.

It appears from the figure that the braces are the typical X and K bracing, which is shown to be efficient in resisting lateral loads.

It has been pointed out that extending the bracing to the full width of the frame results in more efficient lateral load resisting system for tall buildings. To compare the efficiency of the optimal bracing system shown in Figure 6.21(a) with that presented in Figure 6.15(a), the performance index of the braced frame shown in Figure 6.18 was recalculated with respective to the frame with 3-bays braced by a continuum structure. The recalculated performance index is shown in Figure 6.22. It can be seen from the figure that the performance of the frame with 1-bay braced is significantly lower than that of the frame with 3-bays braced. The maximum performance of the 1-bay braced frame is only 0.33. This suggests that significant savings in material costs can be achieved using large-scale bracing systems for tall buildings to resist lateral loads.

6.7.4 The 4-bay, 12-story steel frame

A 4-bay, 12-story rigid steel frame modified from the one presented in Section 6.7.2 is depicted in Figure 6.23, which indicates the numbering of members. This frame is subjected to two reversible wind load cases as shown in Figure 6.23. The sizes of beams and columns are also provided in Table 6.5. The material properties of steel sections are the same as those

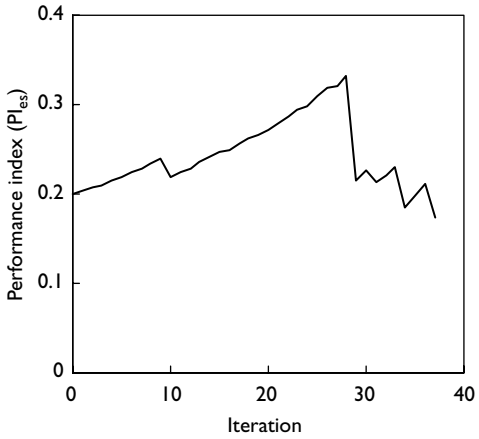

Figure 6.22 Performance index with respect to the 12-story fully braced frame.

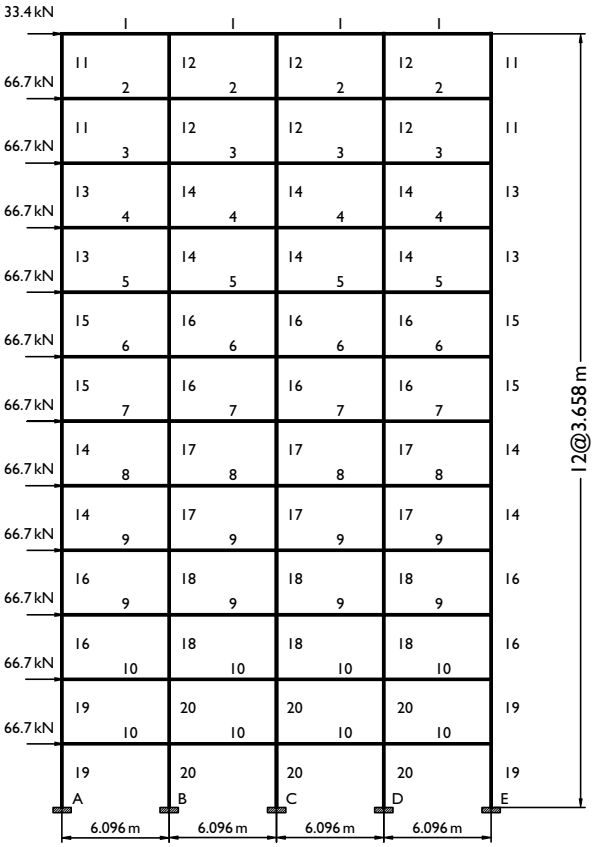

Figure 6.23 A 4-bay, 12-story steel frame.

used for the 3-bay frame. Bracing systems are to be designed to stiff the frame structure to maintain the lateral drifts within prescribed limits. The PBO technique was employed to carry out this task. In the FEA, beam elements were used to simulate the frame members. Each beam was divided into 15 elements and each column was divided into 9 elements. The steel frame was fully braced by a continuum structure, which was discretized into 60×108 four-node plane stress elements. The continuum structure was specified a thickness of 40 mm. The Young's modulus $E = 200$ GPa and Poisson's ratio $\nu = 0.3$ were used for the continuum design domain in the FEA. The element removal ratio of 2 percent was specified in the optimization phase.

Figure 6.24 demonstrates the performance index history of the bracing system in the optimization process. It is observed from the figure that the performance index of the bracing system increased from 1.0 to 1.24 and then decreased to 1.05 at iteration 17. After iteration 17, the performance index increased again when elements were removed from the continuum structure. The performance index reached its maximum value of 1.26 at iteration 36. The bracing system with a performance index of 1.24 can be seen as a local optimum. After iteration 36, the element removal led to a significant increase in the mean compliance (lateral deflections) of the braced frame structure as indicated by the performance characteristic curve presented in Figure 6.25. The optimal bracing system results in a reduction in the material volume by 76 percent in comparison with the initial continuum structure.

The optimal topology of the bracing system for the 4-bay 12-story steel frame is shown in Figure 6.26(a). It can be observed from the optimum that

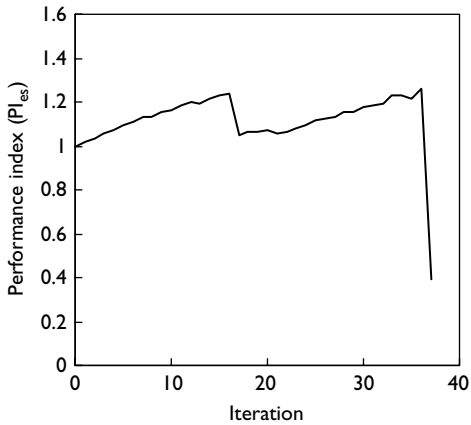

Figure 6.24 Performance index history of bracing system for the 4-bay, 12-story steel frame.

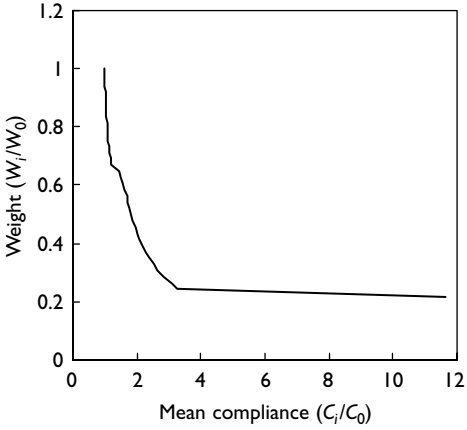

Figure 6.25 Performance characteristics of bracing systems.

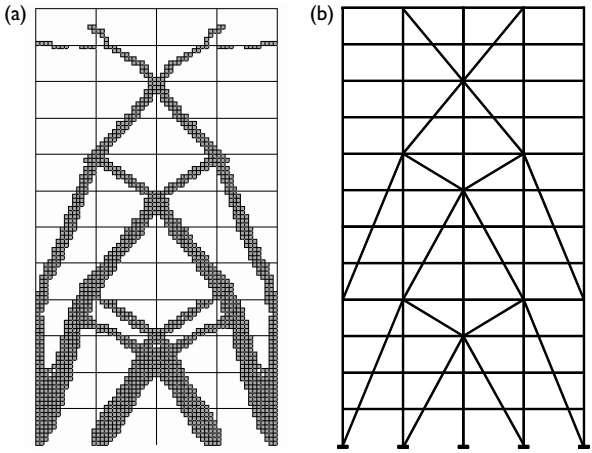

Figure 6.26 (a) Optimal topology and (b) discrete bracing system for the 4-bay, 12-story steel frame.

the bracing system is a large-scale discrete-like structure, which is symmetrical about the central columns in the frame. The bracing system is optimal in the sense that it can effectively resist the two wind loads. The optimal bracing system also indicates the relative dimensions of bracing members, which are proportional to the forces they sustain. The discrete bracing system for the 4-bay, 12-story steel frame is depicted in Figure 6.26(b), which shows an innovative and efficient lateral load resisting systems for tall

buildings. It is worth noting that dimensioning the discrete bracing system should be based on the optimal topology presented in Figure 6.26(a). Stiffness-based sizing techniques can also be used to resize the lateral load resisting system.

6.7.5 The 4-bay steel frame with 2-bays braced

The 4-bay, 12-story steel frame presented in the preceding section now allows only two bays to be braced, as shown in Figure 6.27. The thickness of the continuum structure used to stiff the frame is 40 mm. The element removal ratio of 2 percent was specified in the PBO process.

The performance index history of the bracing system in the optimization process is shown in Figure 6.28. The maximum performance index is 1.54. The performance of the bracing system was maximized when 66 percent material was removed from the continuum structure with an increase in its mean compliance by 92 percent compared with the initial continuum structure.

The optimal topology generated by the PBO technique is presented in Figure 6.29(a). It can be seen from the figure that some of the lower story columns need to be resized to have sufficient lateral stiffness to resist lateral loads. The discrete bracing system for this 4-bay, 12-story steel building frame is depicted in Figure 6.29(b). It is observed that the PBO technique can generate innovative and efficient lateral bracing systems for tall buildings under multiple lateral loading condtions.

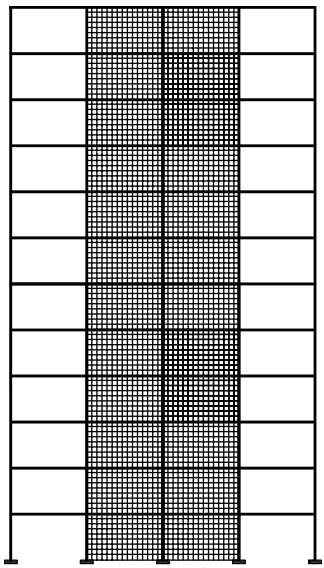

Figure 6.27 The 12-story steel frame with 2-bays braced by a continuum structure.

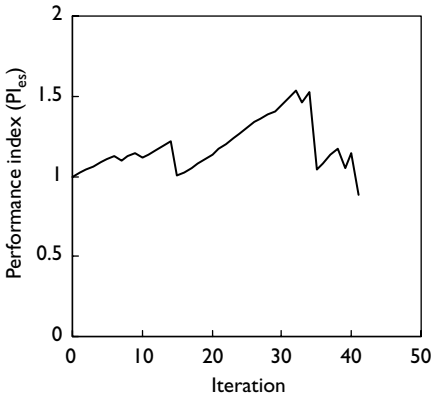

Figure 6.28 Performance index history of bracing system for the 12-story steel frame with 2-bay braced.

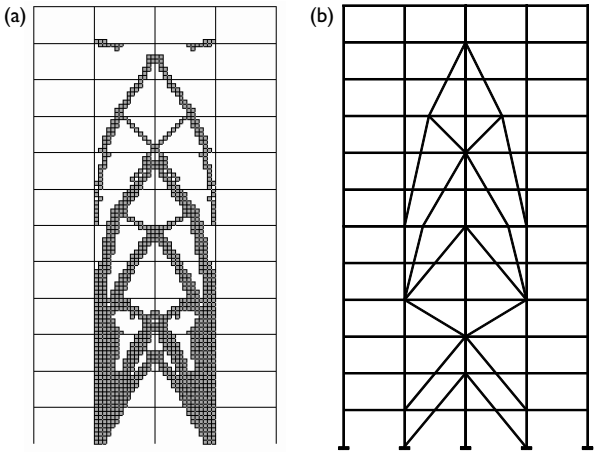

Figure 6.29 Bracing system for the 4-bay, 12-story steel frame with 2-bays braced: (a) optimal topology; (b) bracing system.

6.8 Conclusion

In this chapter, the optimal design of lateral load resisting systems has been presented. Lateral load resisting systems have been introduced with emphasis on the strength design methods of steel–concrete composite elements. The PBO method tailored for the minimum-weight topology design of bracing systems for multistory building frames under multiple lateral loading conditions has been presented. The proposed method allows for an unbraced steel

building framework to be initially sized for strength performance criteria by selecting commercially available standard steel sections from databases. Bracing systems for multistory steel frames are developed on the basis of system performance criteria. The optimal topology of the bracing system is generated by systematically removing elements with the lowest SEDs from a continuum structure that is used to stiffen the frame until the performance of the braced frame is maximized.

The performance-based sizing optimization of lateral load resisting systems for tall building frames has also been described. Member sizing criteria have been derived on the basis of sensitivity analysis on the mean compliance with respect to cross-sectional area reduction. Numerical examples have been presented to demonstrate the capability of the PBO technique in generating optimal designs of lateral resisting systems for tall buildings under multiple load cases. Examples presented have demonstrated that the design method can produce efficient bracing systems, which provide the structural designer with useful information on bracing and stiffening multistory steel building frames. It is shown that the full-width bracing of the building frame is the most efficient in resisting lateral loads.

6.9 References

Ammerman, D. J. and Leon, R. T. (1990) "Unbraced frames with semi-rigid connections," *AISC Engineering Journal*, April: 12–21.

AS 2327.1 (1996) *Composite Structures, Part I: Simply Supported Beams*, Sydney: Standards Australia.

Baker, W. (1990) "Sizing technique for lateral systems in multi-story steel buildings," in *Proceedings of the 4th World Congress on Tall Buildings*, Council on Tall Buildings and Urban Habitat, Hong Kong, pp. 868–875.

Bjorhovde, R. (1984) "Effects of end restraint on column strength – practical applications," *AISC Engineering Journal*, 1–13.

Chan, C.-M., Grierson, D. E. and Sherbourne, A. N. (1995) "Automatic optimal design of tall steel building frameworks," *Journal of Structural Engineering*, ASCE, 121(*5*): 838–847.

Díaz, A. R. and Kikuchi, N. (1992) "Solution to shape and topology eigenvalue optimization problems using a homogenization method," *International Journal of Numerical Methods in Engineering*, 35: 1487–1502.

Eurocode 4 (1994) *Design of Composite Steel and Concrete Structures, Part 1.1, General Rules and Rules for Buildings*.

Grierson, D. E. and Chan, C.-M. (1993) "An optimality criteria design method for tall steel buildings," *Advances in Engineering Software*, 16: 119–125.

Hemp, W. S. (1973) *Optimum Structures*, Oxford: Clarendon Press.

Huang, M.-W. (1995) *Algorithms for Mixed Continuous–Discrete Variable Problems in Structural Optimization*, PhD dissertation, University of Iowa, USA.

Kim, C. K., Kim, H. S., Hwang, J. S. and Hong, S. M. (1998) "Stiffness-based optimal design of tall steel frameworks subject to lateral loads," *Structural Optimization*, 15: 180–186.

Liang, Q. Q. and Patrick, M. (2001) *Design of the Shear Connection of Simply Supported Composite Beams, Design Booklet DB1.2, Composite Structures Design Manual*, Sydney, Australia: OneSteel Manufacturing Pty Limited.

Liang, Q. Q. and Uy, B. (1998) "Parametric study on the structural behaviour of steel plates in concrete-filled fabricated thin-walled box columns," *Advances in Structural Engineering*, 2(1): 57–71.

Liang, Q. Q. and Uy, B. (2000) "Theoretical study on the post-local buckling of steel plates in concrete-filled box columns," *Computers and Structures*, 75(5): 479–490.

Liang, Q. Q., Patrick, M. and Bridge, R. Q. (2001) "Computer software for longitudinal shear design of steel–concrete composite beams," paper presented at the Australasian Structural Engineering Conference, Gold Coast, Australia, pp. 515–522.

Liang, Q. Q., Uy, B., Wright, H. D. and Bradford, M. A. (2003) "Local and post-local buckling of double skin composite panels," *Proceedings of the Institution of Civil Engineers Structures and Buildings*, 156(2): 111–119.

Liang, Q. Q., Uy, B., Wright, H. D. and Bradford, M. A. (2004a) "Local buckling of steel plates in double skin composite panels under biaxial compression and shear," *Journal of Structural Engineering*, ASCE, 130(3): 443–451.

Liang, Q. Q., Uy, B., Bradford, M. A. and Ronagh, H. R. (2004b) "Ultimate strength of continuous composite beams in combined bending and shear," *Journal of Constructional Steel Research*, 60(8): 1109–1128.

Liang, Q. Q., Uy, B., Bradford, M. A. and Ronagh, H. R. (2004c) "Strength analysis of steel–concrete composite beams in combined bending and shear," *Journal of Structural Engineering*, ASCE. (Accepted for publication.)

Liang, Q. Q., Xie, Y. M. and Steven, G. P. (2000a) "Optimal topology design of bracing systems for multistory steel frames," *Journal of Structural Engineering*, ASCE, 126(7): 823–829.

Liang, Q. Q., Xie, Y. M. and Steven, G. P. (2000b) "Topology optimization of strut-and-tie models in reinforced concrete structures using an evolutionary procedure," *ACI Structural Journal*, 97(2): 322–330.

LRFD (1999) *Load and Resistance Factor Design Specification for Steel Buildings*, American Institution of Steel Construction.

Mijar, A. R., Swan, C. C., Arora, J. S. and Kosaka, I. (1998) "Continuum topology optimization for concept design of frame bracing systems," *Journal of Structural Engineering*, ASCE, 124(5): 541–550.

Oehlers D. J. and Bradford, M. A. (1999) *Elementary Behaviour of Composite Steel and Concrete Structural Members*, Oxford: Butterworth-Heinemann.

Taranath, B. S. (1988) *Structural Analysis and Design of Tall Buildings*, New York: McGraw-Hill, Inc.

Trahair, N. S. and Bradford, M. A. (1991) *The Behaviour and Design of Steel Structures*, London: Chapman & Hall.

Viest, I. M., Colaco, J. P., Furlong, R. W., Griffis, L. G., Leon, R. T. and Wyllie, L. A. Jr. (1997) *Composite Construction Design for Buildings*, New York: ASCE and McGraw-Hill.

Walther, F. and Mattheck, C. (1993) "Local stiffening and sustaining of shell and plate structures by SKO and CAO," in *Proceedings of the Institution of Conference on Structural Optimization, Computational Mechanics*, Southampton, UK, pp. 181–188.

Zhou, M. and Rozvany, G. I. N. (1992) "DCOC: an optimality criteria method for large systems. I: Theory," *Structural Optimization*, 5: 12–25.

Author index

Subject index